Neural and molecular mechanisms of sensory signal integration in *Caenorhabditis elegans*.

A Dissertation

Presented to

The Faculty of the Graduate School of Arts and Sciences
Brandeis University

Molecular and Cell Biology Program

Professor Piali Sengupta, Advisor

In Partial Fulfillment
of the Requirements for the Degree
Doctor of Philosophy

by

Scott Jeffrey Neal

May 2015

The signed version of this form is on file in the Graduate School of Arts and Sciences.

This dissertation, directed and approved by Scott Jeffrey Neal's Committee, has been accepted and approved by the Faculty of Brandeis University in partial fulfillment of the requirements for the degree of:

DOCTOR OF PHILOSOPHY

Eric Chasalow, Dean
Graduate School of Arts and Sciences

Dissertation Committee:

Piali Sengupta, Biology Department
James Haber, Biology Department
Leslie Griffith, Biology Department
Yun Zhang, Organismic and Evolutionary Biology Department, Harvard University

ACKNOWLEDGEMENTS

First, and foremost, I would like to acknowledge the mentorship of Piali Sengupta. She has patiently guided my development into a neuroscience-leaning molecular biologist. I am a better scientist as a result of her consistently high expectations and emphasis on focus. I would also like to thank my committee members, Jim Haber and Leslie Griffith, whom embody the selfless and nurturing environment that is Biology at Brandeis. I appreciate the independent perspective given to my work by my external examiner, Yun Zhang.

To all the Senguptlets, past and present, thank you for making the lab feel like home; yes, even you Cilia Squad! Science is hard, but being in a supportive environment filled with enthusiastic, independently motivated and forward thinking individuals makes doing the tedious experiments possible; 4pm on Thursdays doesn't hurt either. The group has been, let's say, dynamic in my time at Brandeis, but has always pulled together. Piali deserves a second acknowledgement for assembling such a great group of people.

I would like to acknowledge generous funding support from the Natural Sciences and Engineering Research Council of Canada and from the Brandeis National Committee. Tremendous administrative support provided by the Division of Life Sciences and the International Students and Scholars Office has allowed me to focus on my research. Marcia, Maryanna, Jessica and now Jennifer have made sure that I have been kept on track in my program and Heather somehow manages to keep everything and everyone in line. Over at the ISSO, Emily, Gillian, Ruth, David and Souad made for a smooth immigration process and have ensured that I never got stuck on the wrong (right?) side of the border.

In a Doctoral program, as with any long term commitment, family plays a pivotal role in establishing perspective and balancing work and life. My parents Jeff and Mary, despite

being uncertain at times as to why I might want to be in school for so long, have always been incredibly supportive and proud; thank you. Finally, Jessica has led me across the continent and back and has inspired me to explore new opportunities. Her companionship of many years and her recent flurry of baking have really made this all possible.

ABSTRACT

Neural and molecular mechanisms of sensory signal integration in *Caenorhabditis elegans*.

A dissertation presented to the Faculty of the
Graduate School of Arts and Sciences of Brandeis University
Waltham, Massachusetts

By Scott Jeffrey Neal

Life exists in complex environments, requiring organisms to have adaptive developmental strategies in order to survive. The nematode *Caenorhabditis elegans* has evolved a developmental polyphenism whereby it may arrest development in the dauer diapause state when environmental conditions are not suitable for reproductive growth. The relative simplicity of the *C. elegans* nervous system, together with its robust molecular and genetic tool set, make it an ideal system in which to study how environmental stimuli are sensed and integrated to drive developmental plasticity. Food availability, temperature and the presence of dauer pheromone each inform the dauer fate decision. I have taken molecular and genetic approaches to study the mechanism by which pheromone signals are transduced *by C. elegans* sensory neurons and also to understand how food and pheromone signals are integrated to drive an adaptive developmental choice. I have identified roles in dauer formation for the protein scaffold QUI-1, the rough endoplasmic reticulum protein MACO-1 and a putative Tau tubulin kinase, which we have named PHD-1. I have also identified a critical role for the calcium/calmodulin-dependent protein kinase 1 CMK-1 in encoding the food signal and integrating this information in the dauer fate decision. Furthermore, these studies have led to the previously unrecognized roles for the ASH and AWC neurons in the regulation of dauer formation.

PREFACE

The primary focus of this dissertation is the study of the mechanisms by which environmental stimuli are perceived, encoded and integrated to regulate development. Such processes are carried out across diverse phyla, from simple prokaryotes to complex metazoans. Nutrition is a major environmental factor that exerts robust effects on growth and developmental processes. Examples include the expression of metabolic pathway genes with respect to the carbon source in bacteria(Opienska-Blauth et al., 1952), and the development of giant ornamental structures in dung beetles that are regulated by a maternally-provided food source(Emlen, 1994). While there are myriad descriptive studies of these phenomena in metazoans, there are relatively few which examine the neural and molecular processes that govern them(Nylin, 2013).

In order to uncover basic principles of the sensory signal transduction processes which govern developmental polyphenism, I have studied the dauer developmental fate decision in the genetically-tractable model nematode *Caenorhabditis elegans*. This decision is dictated via integration of environmental cues, including the availability of food(Golden and Riddle, 1984b). This paradigm has allowed me to discover the molecular and cellular signaling cascades for specific stimuli, as well as to explore the mechanisms by which the developmental outcome is regulated by the integration of external signals. The sections below will provide a brief introduction to the concepts and mechanisms underlying developmental plasticity, and to the advantages of studying this phenomenon in *C. elegans*(Brenner, 2009).

TABLE OF CONTENTS

LIST OF TABLES

LIST OF FIGURES

CHAPTER 3

CHAPTER 1

General Introduction

1.1 Developmental Plasticity

Most organisms inhabit a niche to which they are well adapted. However, seasonal changes in the environment may affect food availability and/or the risk of predation rendering some traits potentially maladaptive (Morehouse et al., 2013; Nylin, 2013; Simpson et al., 2011; Stearns, 1989). Thus, many species have the potential to exhibit a range of possible phenotypes for any given trait, a phenomenon known as polymorphism (Stearns, 1989). The expression of developmental plasticity represents a mechanism by which organisms may uncouple their genotype and phenotype (Stearns, 1989), to better exploit their current or near-future environments (Beldade et al., 2011). In contrast, evolutionary adaptation happens over a much longer time scale. In this regard, the expression of polymorphic traits is a reflection of a gene by environment interaction, a substrate upon which natural selection can act in the long term (Nijhout, 2003; Stearns, 1989). Thus, animal may choose to express beneficial traits and conceal maladaptive ones such that their fitness is optimal in fluctuating environments (Beldade et al., 2011; Morehouse et al., 2013; Nylin, 2013; Stearns, 1989).

Polymorphic traits which are expressed over a continuum are referred to as ‘reaction norms’, whereas the expression of distinct traits is known as polyphenism (Beldade et al., 2011; Stearns, 1989). The term polyphenism was first proposed by Michener (Michener, 1961), and the concept was highlighted by Mayr (Mayr, 1963). Polyphenism has also been referred to as a ‘developmental switch’ in regards to the fact that exhibition of polyphenic traits often follows either embryogenesis, metamorphosis or an inter-stage molt (Nijhout, 2003; Stearns, 1989). Examples of polyphenism include sex-determination in reptiles, the seasonal morphs of butterflies, the exhibition of wings on locusts and aphids, and the complex caste determination

system in eusocial insects like ants, bees and termites (Evans and Wheeler, 2001; Morehouse et al., 2013; Nijhout, 2003; Nylin, 2013; Simpson et al., 2011; Stearns, 1989).

The expression of polyphenism is triggered by environmental stimuli. Both 'top down' factors such as the risk of predation and 'bottom up' factors such as nutrition, are known to regulate polyphenism (Evans and Wheeler, 2001; Morehouse et al., 2013). These factors typically act during a defined sensitive period, after which the trait can no longer be expressed. Examples of polyphenism are abundant in invertebrates, particularly insects (Simpson et al., 2011). Whereas homeostatic processes function to buffer against environmental variation, small organisms with reduced buffering capacity may have had the need to evolve alternate adaptive strategies (Kodama-Namba et al., 2013; Nijhout, 2003). The evolutionary success of holometabolous insects may be attributed to such strategies. Their normal development features distinct morphs for feeding and growth (larvae) as for dispersal and reproduction (adults). Furthermore, their ability to integrate environmental cues during larval stages to express polyphenism in the adult stage is highly adaptive. Adaptations may include crypsis or predator avoidance (Greene, 1989; Tanaka et al., 2012), mating and dispersal strategies (Castaneda et al., 2010), and other feeding adaptations (Ogawa et al., 2011); several examples are discussed in detail below. To date, most research has focused on these ecological functions and the selective pressures that have shaped the evolution of polyphenism within species. Consequently, there are beautiful examples of polyphenism throughout nature but our understanding of the molecular processes by which they arise are quite limited.

1.2 Examples of Polyphenism

One well-studied example of polyphenism is the expression of seasonal morphs in bivoltine *Lepidoptera*. In temperate regions, seasonal changes in the environment may reduce the potential adaptive value of traits linked to a particular food source and the physiological requirements for survival in the summer and winter are distinct (Morehouse et al., 2013). Spring brood butterflies of the genus *Arashnia* exhibit bright wing coloration whereas the summer brood exhibits wings that are essentially black (Morehouse et al., 2013). One potential advantage of such coloration is crypsis, whereby the animals are able to blend with the predominant colors of the flowers on which they feed. Striking examples of such adaptation are also observed in the larval stages of other genera, such as *Nemoria* (Figure 1.1A) (Greene, 1989). An alternate, and non-mutually exclusive hypothesis is that the melanization of wings in summer brood confers the ability to harvest more warmth during the cool season, a trait which may be maladaptive in the warm season (Morehouse et al., 2013). Together, these adaptations allow *Arashnia* to support two broods per year (Morehouse et al., 2013).

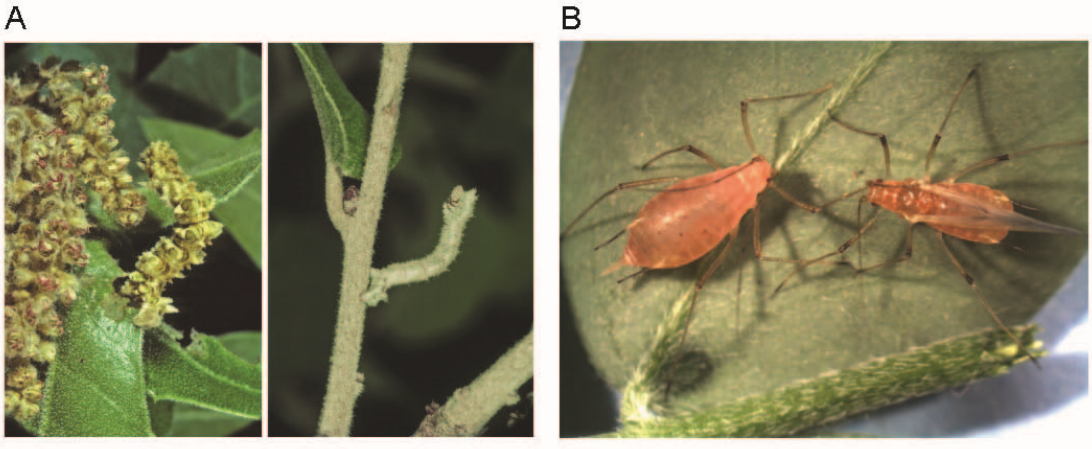

Figure 1.1. (A) Examples of the catkin and twig morphs of Nemoria. (B) Examples of the wingless and winged morphs of aphids. Images adapted from Simpson, 2011 (Figures 1 and 4, respectively).

A second example of polyphenism in insects is the selective expression of a winged morph. Aphids employ two reproductive strategies, such that in a resource-rich environment they reproduce by parthenogenesis but as resources diminish or when predators are present they may form a sexually reproductive winged morph (Figure 1.1B) (Castaneda et al., 2010; Nylin, 2013; Simpson et al., 2011). Locusts also selectively express a winged morph (Simpson et al., 2011). In both cases the exhibition of wings facilitates dispersal, but comes at a relative cost to fecundity (Castaneda et al., 2010; Simpson et al., 2011; Stearns, 1989).

A final example of polyphenism comes from the study of bees, where the dichotomy between the queen and the worker castes is perhaps the best known example of such a phenomenon (Maisonnasse et al., 2010; Wilson, 1971). Morphologically the queen has a greatly enlarged abdomen and highly developed ovaries, but her size severely limits her motility (Holman, 2010; Kamakura, 2011; Maisonnasse et al., 2010). Thus, workers must procure food and perform tasks related to the maintenance of the hive. Development of the queen morph is determined solely by nutrition during the larval stages (Mutti et al., 2011; Wheeler et al., 2006).

1.3 Environmental Determinants of Polyphenism

The most cited examples of environmental determinants of polyphenism include temperature, photoperiod, nutrition, and crowding, though the mechanisms by which each acts are just beginning to be understood (Evans and Wheeler, 2001). In nature, temperature and photoperiod are often linked such that a dependence for either stimulus alone can only be established in a laboratory environment. Similarly, nutrition and crowding are often correlated. Careful experimentation is thus necessary to define the role of a particular factor in inducing polyphenism as well as to define the relevant sensitive or critical periods in the host organism.

In butterflies of the genus *Bicyclus* there are wet and dry season morphs which differentially express eyespots on the underside of their wings. The expression of this polyphenism is driven by the temperature experienced during the final larval stage; those raised at 27ºC develop as the wet season morphs and those raised at 20ºC develop in to the dry season morph (Nylin, 2013; Simpson et al., 2011). Alternatively, wing color polyphenism in *Arashnia* is driven by photoperiod such that larvae reared on a long photoperiod emerge as the summer form whereas those raised on a short photoperiod develop as the spring form (Morehouse et al., 2013). In aphids, the wing polyphenism can be overridden by both long photoperiod and high temperature during the first instar (Nylin, 2013).

In *Nemoria* larvae, the spring brood feeds exclusively on oak catkins while the summer brood feeds on leaves (Greene, 1989). Consequently, spring caterpillars are bright yellow (catkin morph) and the summer caterpillars are brown (twig morph). The catkin morph develops faster and exhibits higher fecundity that the twig morph (Greene, 1989). However, the twig morph must survive the winter and thus rapid development in this morph is maladaptive. In a laboratory setting it was discovered that morph expression in *Nemoria* is determined by tannin levels in the food, and not by either temperature or photoperiod (Greene, 1989). Thus, despite being characterized as a seasonal polyphenism, *Nemoria* development is in fact driven by food.

Competition for resources may also result in crowding within a population. In gregarious locusts both the smell and physical contact with other locusts produces changes in behavior and, ultimately, changes in development (Simpson et al., 2011). Along with the wing polyphenism, juveniles born to crowded parents exhibit a color polyphenism such that they are all share similar patterning (Simpson et al., 2011; Tanaka et al., 2012). Crowding has also been observed to regulate the dauer polyphenism in *C. elegans* (Albert et al., 1981; Golden and Riddle, 1982).

1.4 Endocrine Regulation of Polyphenism

Juvenile Hormone (JH) and 20-hydroxyecdysone (20E) have prominent roles in the development of insects (Evans and Wheeler, 2001; Lavine et al., 2015; Mirth et al., 2014; Watanabe et al., 2014). JH is most associated with morphogenesis in larvae whereas 20E regulates molting and metamorphosis; both play roles in the expression of polyphenism. In addition, insulin signaling has been shown to provide a critical link between nutrition and development (Koyama et al., 2013; Lavine et al., 2015; Mirth et al., 2014).

Figure 1.2. Timed injections of 20-hydroxyecdysone demonstrate that the *Arashnia* wing color polyphenism is the evolved bistable product of a reaction norm. Adpated from Nijhout, 2003 (Figure 4).

In *Arashnia*, although wing color is polyphenic in nature, it can be induced to be polymorphic in the lab simply by timed injections of 20E (Figure 1.2) (Nijhout, 2003). Thus, the environmental determinants of wing color polyphenism are integrated by the timing of 20E

pulses in this organism, and some aspect of this integration has evolved to be bistable. A similar case is observed in *Bicyclus*, where rearing at temperatures above 21°C result in an earlier 20E peak and drives formation of the alternate morph (Simpson et al., 2011).

In the honey bee, the queen fate is determined between the L2 and L4 larval stages, based on continuous feeding with royal jelly (Mutti et al., 2011; Wheeler et al., 2006), or its active ingredient, royalactin (Kamakura, 2011). Larvae that are not fed continuously with royal jelly become workers. Royalactin signals via the epidermal growth factor receptor to control growth via the target of rapamycin (TOR) pathway (Kamakura, 2011; Mutti et al., 2011). Feeding with royal jelly also results in the differential expression of two insulin-like peptides (ILPs), ILP1 and ILP2, in the two castes (Wheeler et al., 2006). ILP1 is expressed more highly in larvae destined to become queens, and in the L4 stage, so is JH (Wheeler et al., 2006). ILP1 may induce the expression of JH, which is supported by the fact that knockdown of the insulin receptor (InR) results in a diminished JH response (Mutti et al., 2011). Queen fate can be rescued by the application of exogenous JH, suggesting that its action falls downstream of nutritional regulation (Mutti et al., 2011).

1.5 Diapause

The culmination of many of the above regulatory pathways is often the induction of diapause (Beldade et al., 2011; Nylin, 2013). Diapause is a hibernation like state that is linked with many seasonal polyphenisms, especially in over-wintering animals (Nylin, 2013). The three defining features of diapause are that it occurs at a characteristic developmental stage, that both entry to and exit from diapause are determined by environmental factors and, finally, that the organism exhibits preemptive metabolic changes prior to diapause (Kostal, 2006). In some

ants, only queens that have undergone diapause are able to produce new queens (Libbrecht et al., 2013). Exposure to cold alters the maternal deposition of vitellogenin in eggs, representing a rich source of nutrition in the developing embryo which may act through the insulin pathway (Libbrecht et al., 2013). Vitellogenin production is regulated by JH in queens, as in mosquitos, and is thus thought to also be downstream of insulin signaling in the parental generation (Hansen et al., 2014; Libbrecht et al., 2013; Sim et al., 2015).

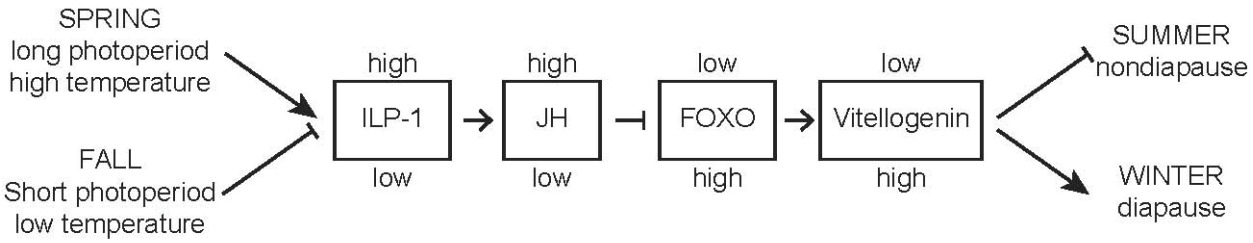

Figure 1.3. Schematic of the integration of environmental stimuli by insulin (ILP-1) and juvenile hormone (JH) signaling in the regulation of diapause in mosquito. Adapted from Sim et al., 2015 (Figure 1).

Environmental factors which regulate diapause entry include many of the same stimuli that regulate polyphenism (Nylin, 2013). For instance, low temperature and short photoperiods promote diapause entry in *Drosophila* and in mosquitoes (Hahn and Denlinger, 2011; Sim and Denlinger, 2013). In the silk-worm moth diapause entry is regulated transgenerationally, such that warm temperatures experienced by the mother prepare embryos for their over-winter diapause (Sato et al., 2014). Larval and puparial diapauses are characterized by the failure to molt, and are thus likely to be regulated in some way by 20E (Nylin, 2013). Additional diapause hormones are produced in some species (Yamashita, 1996), and roles for JH have been suggested as well (Nylin, 2013; Sim and Denlinger, 2013). Animals may also undergo an adult stage, or reproductive diapause. In mosquitoes the blood meal regulates insulin signaling, which is

critical to the regulation of reproductive diapause (Hansen et al., 2014; Sim et al., 2015). In this example, knockdown of the InR is sufficient to induce a diapause like state (Sim et al., 2015), but as seen in the bee, it can be overcome by administration of exogenous JH (Sim and Denlinger, 2013).

1.6 Rationale for Dissertation Research

It is clear from the above examples that environmental factors regulate development across taxa. Furthermore, many of the examples have highlighted the convergence of these signals on conserved endocrine networks, such as the insulin signaling pathway. Unfortunately, few of the organisms discussed are well suited to study in the laboratory. Many exhibit long generation times, and the molecular and genetic tools available to study them are scarce. The advent of low cost genome sequencing has opened some of these systems to further study, and significant progress has been made, particularly in the study of bees. Nonetheless, studies to date have been heavily focused on either descriptive analysis or on the biology at the organismal level. The methods to study molecular signal transduction mechanisms and the process of sensory signal integration in the regulation of endocrine signaling networks simply do not exist in these species at this time.

C. elegans is an ideal system in which to study the sensory processes, neural mechanisms and effects of environmental regulation of development. *C. elegans* develops quickly, is amenable to genetic manipulation, and the connectivity of every cell in its nervous system is known (Bargmann, 2012; Brenner, 1974; Mello et al., 1991; White et al., 1986). In addition, *C. elegans* exhibits a polyphenic developmental trait - entry into the dauer diapause - which already benefits from decades of prior study. Thus, this organism provides an ideal system in which to

identify and characterize the mechanisms by which diverse environmental stimuli are sensed and integrated to modulate hormonal signaling and a developmental polyphenic trait. Below I will introduce what is known about dauer diapause and its regulation, and highlight salient aspects of *C. elegans* biology, including its chemosensory system, and its stereotyped behaviors which have helped establish how sensory signals are integrated by this organism.

1.7 Food-Regulation of Development in *C. elegans*

C. elegans embryos hatch, even under non-ideal conditions, but development beyond the first larval stage requires food (Baugh, 2013). Given that L1 arrest occurs due to the lack of nutrients, unsurprisingly it is regulated by a complex insulin signaling pathway (Baugh, 2013; Baugh and Sternberg, 2006; Chen and Baugh, 2014; Kasuga et al., 2013; Schindler et al., 2014). Once arrested, L1 larvae exhibit increased stress resistance and may survive up to one month while maintaining the ability to fulfill a normal lifespan if conditions improve (Baugh, 2013; Cui et al., 2013). Unlike the L1 arrest, *C. elegans* may also enter a true diapause, termed dauer (Cassada and Russell, 1975). The dauer stage is an alternative 3rd larval stage that *C. elegans* may enter when environmental conditions are unfavorable, including the unavailability of food (Figure 1.4) (Cassada and Russell, 1975; Golden and Riddle, 1984a, b). In wild-collected strains, animals are generally found in either the starved or dauer state (Barriere and Felix, 2005; Felix and Duveau, 2012). Dauer larvae are non-feeding and exhibit a special, thicker cuticle compared to L3 larvae (Cassada and Russell, 1975; Riddle et al., 1981). Dauers are radially constricted, elongated, and denser that non-dauer larvae (Hu, 2007). Dauers formed by starvation alone are pale, but those formed in the presence of food are more retractile and have increased lipid stores (Hu, 2007). These adaptations render dauer larva resistant to desiccation

and even to detergent (Cassada and Russell, 1975; Erkut et al., 2012; Erkut et al., 2011). It has also been proposed that dauer-specific nictation behavior is a mechanism to facilitate dispersal (Schroeder et al., 2013); they also respond to mechanosensory stimuli with a burst of rapid movement (Golden and Riddle, 1984b). Upon return to favorable environmental conditions dauer larvae molt, resume development and exhibit a normal lifespan and reproductive capabilities, regardless of the total time spent in dauer (Klass and Hirsh, 1976). For a thorough review of the *C. elegans* dauer larva please refer to Hu (2007).

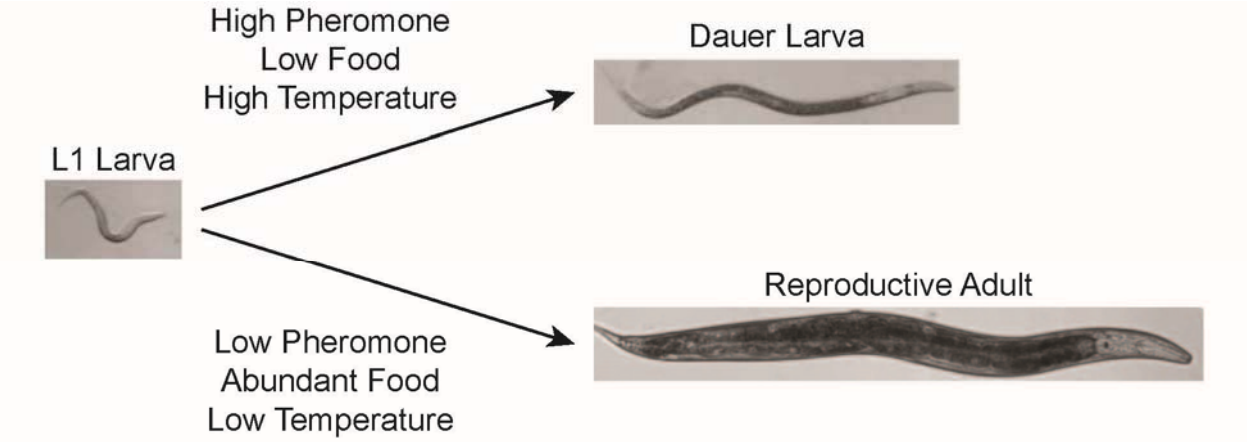

Figure 1.4. The integration of environental stimuli by L1 larvae of *C. elegans* drives a polyphenic developmental choice. Adapted from McGrath et al., 2011 (Figure 1).

Dauer formation is also an example of a polyphenism, as animals may elect to enter dauer or to continue directly in the reproductive cycle. Pioneering studies identified the environmental factors which govern the dauer polyphenism as food availability, temperature and crowding (Golden and Riddle, 1982, 1984a, b, c). As opposed to the mechanosensory perception of crowding by locusts (Simpson et al., 2011), *C. elegans* assess population density via a secreted substance called dauer pheromone (Golden and Riddle, 1982). The critical period for dauer entry begins midway through the L1 stage during which a linear relationship between food and

pheromone controls the fate decision (Schaedel et al., 2012; Swanson and Riddle, 1981). Temperatures above 20°C appear to function additively with the other factors to increase the probability of dauer formation (Golden and Riddle, 1984b). Interestingly, animals which undergo L1 arrest are less likely to enter dauer than those that are fed continuously until the critical period (Rechavi et al., 2014). Regardless of whether or not they ultimately become dauers, all animals raised in the presence of high concentrations of pheromone exhibit a prolonged predauer stage called L2d (Avery, 2014; Golden and Riddle, 1984b), which is larger than L2, likely due to increased feeding before the molt (Golden and Riddle, 1984b). Addition of food, removal of pheromone or decreasing the temperature midway through L2d allows some, but not all animals to bypass dauer completely (Avery, 2014; Golden and Riddle, 1984b). Though advances in the genetic basis for dauer formation have been made (summarized below), the mechanisms by which dauer-inducing environmental signals are integrated to drive this polyphenism remain unclear.

1.8 Endocrine Control of Dauer Formation

A number of genetic screens have been carried out to identify molecular determinants of dauer formation (*daf*) (Albert et al., 1981; Riddle et al., 1981; Swanson and Riddle, 1981). These screens yielded two broad classes of mutants, those that form dauers constitutively (*daf-c*) and those that are defective at forming dauers under dauer-inducing conditions (*daf-d*) (Riddle et al., 1981). Categorization of *daf* genes by epistasis revealed four signal transduction cascades, including three endocrine pathways (Hu, 2007).

Several components of a transforming growth factor β (TGF-β) signaling pathway were identified including those encoding a ligand (*daf-7*) (Ren et al., 1996; Schackwitz et al., 1996),

receptors (*daf-1*, *daf-4*) (Estevez et al., 1993; Georgi et al., 1990), and downstream transcription factors (*daf-3*, *daf-5*, *daf-8*, *daf-14*) (da Graca et al., 2004; Inoue and Thomas, 2000a, b; Liu et al., 2004; Massague et al., 2005; Park et al., 2010; Patterson et al., 1997; Thatcher et al., 1999). TGF-β pathway mutants are *daf-c* with the exception of *daf-5*, and *daf-3* (context-dependent) which are *daf-d* and suppress the upstream mutations (Ailion and Thomas, 2000; Gerisch et al., 2001; Park et al., 2010; Thomas et al., 1993). In parallel to the TGF-β pathway exists an insulin signaling pathway (Figure 1.5) (Murphy and Hu, 2013). Initially this pathway was defined by

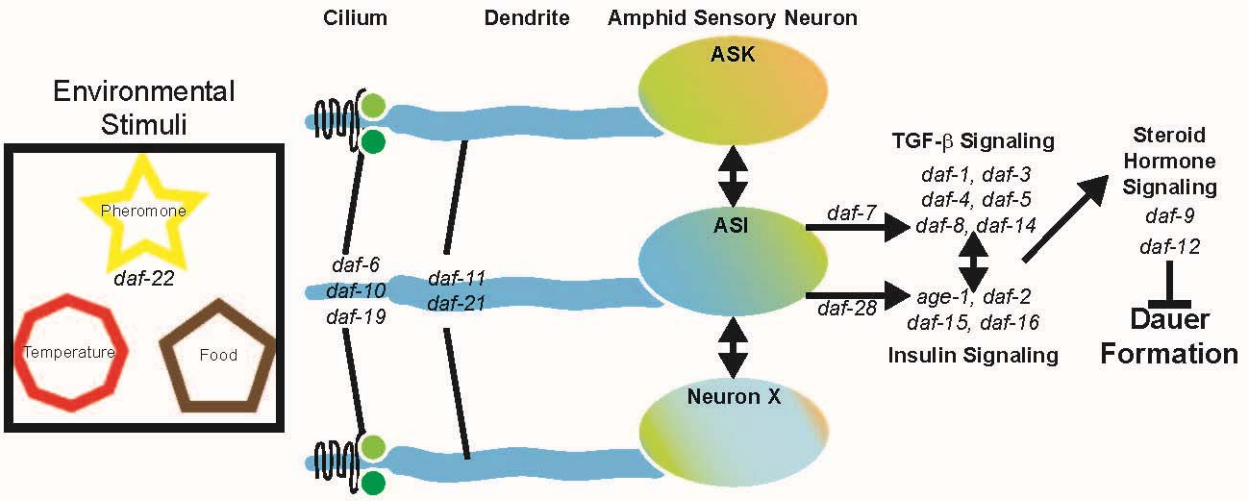

Figure 1.5. Schematic of the genetic pathways regulating dauer formation in *C. elegans*.

the *daf-c* mutations in the InR encoded by *daf-2* and the phosphoinositide 3-kinase encoded by *age-1*, and the suppressor mutation in *daf-16*, which encodes the FOXO transcription factor (Gems et al., 1998; Gottlieb and Ruvkun, 1994; Morris et al., 1996; Ogg et al., 1997). Other factors in this pathway include *akt-1*, *akt-2* (Kimura et al., 1997; Morris et al., 1996; Paradis and Ruvkun, 1998), a regulator of TOR (*daf-15)* (Albert and Riddle, 1988; Jia et al., 2004; Long et al., 2002), and PTEN (*daf-18)* (Gil et al., 1999; Mihaylova et al., 1999; Ogg and Ruvkun, 1998),

as well as 40 ILPs (eg. *ins-1*, *ins-18*, *daf-28*) that are encoded in the *C. elegans* genome (Pierce et al., 2001). A third pathway is characterized by a GC, encoded by *daf-11*, and whose function is modulated by another locus, *daf-21* (Birnby et al., 2000; Thomas et al., 1993; Vowels and Thomas, 1992, 1994). Current evidence suggests that the GC pathway lies upstream of both the TGF-β and insulin pathways, and not in parallel to them (Li et al., 2003; Murakami et al., 2001).

The final steroid hormone pathway is downstream of all the others (Albert et al., 1981; Albert and Riddle, 1988; Gerisch et al., 2001; Jia et al., 2002; Thomas et al., 1993). There are two principal components of this pathway; *daf-9* encodes an enzyme necessary for steroid hormone biosynthesis (Albert and Riddle, 1988; Gerisch and Antebi, 2004; Gerisch et al., 2007; Gerisch et al., 2001; Jia et al., 2002; Motola et al., 2006), while *daf-12* encodes a nuclear hormone receptor (Antebi et al., 1998; Antebi et al., 2000; Gems et al., 1998; Larsen et al., 1995; Snow and Larsen, 2000). In the ligand-bound state DAF-12 promotes reproductive growth whereas in the absence of ligand it promotes dauer arrest (Gerisch et al., 2007; Motola et al., 2006; Sharma et al., 2009). Mutations in *daf-12* are *daf-d* and are epistatic to all other *daf* mutations. The function of the DAF-12 ligand is similar to that of 20E in that it serves to regulate molting in *C. elegans* (Magner and Antebi, 2008; Thummel, 2001). Thus, the dauer phenotype is a coordinated state of the whole organism that is regulated by endocrine signaling.

Considerable interest has been garnered by insulin signaling networks due to their association with longevity (Alcedo and Kenyon, 2004; Dorman et al., 1995; Kenyon et al., 1993; Kimura et al., 1997; Murphy and Hu, 2013), and two recent large-scale interaction studies have made efforts to deconvolute the insulin signaling network in *C. elegans* (Fernandes de Abreu et al., 2014; Ritter et al., 2013). Together with more focused studies of specific ILPs (Chen et al., 2013; Cornils et al., 2011), these studies addressed aspects of functional redundancy among

insulins and identified ILP-to-ILP signaling cascades. Twenty-five of the 40 ILPs are expressed in sensory neurons, and most ILPs exhibit dynamic expression throughout development (Ritter et al., 2013). Interestingly, 10 ILPs have reduced expression in dauer larvae (Ritter et al., 2013). There are also inter-ILP genetic interactions with respect to expression levels, perhaps indicative of compensation (Ritter et al., 2013). Overall, the architecture of the ILP network has been described as 'functionally diverse rather than globally redundant' (Fernandes de Abreu et al., 2014), with many sub-networks functioning in parallel to govern development, behavior and reproduction. Several ILPs appear to regulate dauer entry or exit, though only in sensitized backgrounds (Fernandes de Abreu et al., 2014); no pairwise deletion among ILPs was sufficient to induce dauer formation in routine culture conditions (Ritter et al., 2013). The ILP encoded by *daf-28* has the most penetrant effects on suppressing dauer entry (Li et al., 2003; Malone et al., 1996; Malone and Thomas, 1994), and is enhanced by INS-6 (Cornils et al., 2011). Alternatively, INS-1 and INS-18 function to enhance dauer entry and to suppress dauer exit (Cornils et al., 2011; Matsunaga et al., 2012; Pierce et al., 2001). For a thorough review of insulin signaling in *C. elegans* please refer to Murphy and Hu (2013).

1.9 Sensory Regulation of Dauer Formation

Several studies have addressed how environmental factors influence the established dauer genetic pathways (Golden and Riddle, 1984a, b). The expression of *daf-7* is regulated by food, pheromone and temperature (Ren et al., 1996; Schackwitz et al., 1996). Dauer pheromone strongly suppresses *daf-7* expression whereas increasing cultivation temperature also reduces it (Gallo and Riddle, 2009; Schackwitz et al., 1996); bacterial food upregulates *daf-7* expression (Ren et al., 1996). The ILP encoded by *daf-28* is also regulated by sensory signaling, it exhibits

reduced expression in pheromone and starvation-induced dauers (Li et al., 2003). In contrast to *daf-7*, *daf-28* expression is not positively regulated by environmental signals as it is in fact increased in sensory mutants (Li et al., 2003). Mutations in *daf-11* result in reduced expression of both *daf-7* and *daf-28*, and *daf-11* functions cell-autonomously in ASI to regulate *daf-7* (Gallagher et al., 2013; Li et al., 2003; Murakami et al., 2001). Sensory mutations suppress the effects of mutation in *daf-11*, providing evidence of its critical role in translating environmental cues into both the TGF-β and insulin pathways (Vowels and Thomas, 1992).

Crosstalk between the TGF-β and insulin pathways has been implied by microarray studies of gene expression in different *daf* mutants (Liu et al., 2004; Shaw et al., 2007), and by more focused genetic experiments (Narasimhan et al., 2011; Park et al., 2012a). In particular, the expression of several ILP genes is reduced in *daf-7* mutant, including *daf-28* (Li et al., 2003; Liu et al., 2004). Further support for crosstalk was established by the identification of the phosphatase PDP-1. PDP-1 is a positive regulator of DAF-16 target genes, affecting ILP expression, and yet genetically it falls into the TGF-β pathway where it suppresses *daf-7* mutations, but not those in *daf-8* or *daf-14* (Narasimhan et al., 2011). A hypothesis derived from these data is that insulin signaling is downstream of TGF-β signaling, and is supported by slightly offset sensitive periods in the relevant pathways.

Consistent with the environmental regulation of dauer formation the above genetic screens identified mutants in which the structure of specialized sensory organelles called cilia were affected (*daf-6*, *daf-10*, and *daf-19)* (Albert et al., 1981; Bell et al., 2006; Perens and Shaham, 2005; Perkins et al., 1986; Swoboda et al., 2000). Mutations of these genes results in a *daf-d* phenotype. In contrast, laser ablation of subsets of the ADF, ADL, ASG, ASI, ASJ and ASK sensory neurons recapitulates the *daf-c* class of mutants (Bargmann and Horvitz, 1991;

Schackwitz et al., 1996). Either ADF or ASI, the primary site of *daf-7* expression, is necessary to promote development to adulthood (Bargmann and Horvitz, 1991). An interesting observation from this study was the fact that sensory mutants fail to enter dauer whereas ablating sensory neurons induces dauer formation (Bargmann and Horvitz, 1991). Thus, in the normal context, sensory signals must induce dauer formation by down-regulating a signal that is intrinsic to sensory neurons, such as what has been observed for *daf-7* and *daf-28* (Li et al., 2003; Ren et al., 1996; Schackwitz et al., 1996). This is consistent with dauer pheromone having an instructive role in dauer entry (Swanson and Riddle, 1981).

1.10 Dauer Pheromone (Ascarosides)

Pheromones are small molecules that, by definition, act as intraspecific signals and form the basis for chemical communication in almost all animals (Karlson and Luscher, 1959; Touhara and Vosshall, 2009; Wyatt, 2003). They may exhibit both primer and releaser effects; the former referring to an immediate chemotactic signal, while the latter refers to longer-term developmental effects (Wilson, 1971; Wyatt, 2003). Honeybee brood pheromone and queen mandibular pheromone (QMP) are examples of such pheromones (Grozinger et al., 2007; Le Conte et al., 2001). QMP releases a retinue response and is attractive to young bees but also exhibits a primer effect in which it down-regulates the expression of foraging-related genes in the brains of young bees (Grozinger et al., 2007; Vergoz et al., 2009). Pheromone action is also typically context- and concentration-dependent (He et al., 2010). At low concentration the *Drosophila* male-specific pheromone 11-*cis*-vaccenyl acetate suppresses male-male courtship and promotes aggression whereas at high concentration it is sufficient to suppress male-female courtship (Bartelt et al., 1985; Wang and Anderson, 2010; Wang et al., 2011).

The first demonstrations of the presence of a *C. elegans* pheromone were in 1982 (Golden and Riddle, 1982; Ohba and Ishibashi, 1982), but it was not until 2005 that the chemical structure of a dauer pheromone component was first elucidated (Jeong et al., 2005). The structure of ascr#1 (originally "daumone"; C7) revealed a derivative of the pentose sugar ascarylose with an aliphatic side chain (Jeong et al., 2005). Subsequent efforts have identified a family of related molecules (Butcher et al., 2007; Butcher et al., 2009a; Butcher et al., 2008; Butcher et al., 2009b; Pungaliya et al., 2009; Schroeder, 2006; Srinivasan et al., 2008), collectively termed ascarosides, which has been described as a modular chemical language (Schroeder, 2015). In referring to these compounds I will use the small molecule identifier (SMID, www.smid-db.org), and will indicate prominent alternative names in parentheses. When produced synthetically several ascarosides are sufficient to induce dauer formation under conditions which would normally promoter reproductive growth (Figure 1.6) (Butcher et al.,

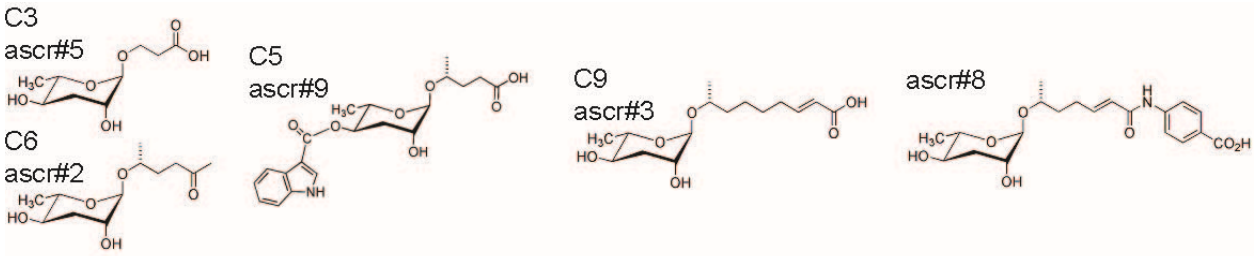

Figure 1.6. Chemical structures of several ascarosides which are sufficient to induce dauer formation. Structures are from the Small Molecule Identifier Database (www.smid-db.org).

2009a; Kim et al., 2009). Ascarosides also exhibit releaser effects on *C. elegans* behavior, for instance, ascr#8 (PABA-C7) is a potent male attractant (Chute and Srinivasan, 2014; Srinivasan et al., 2008). As do pheromones in other organisms, ascarosides exhibit emergent properties when used as blends. A combination of ascr#2 (C6) and ascr#3 (C9, ΔC9) is attractive to males

at concentration at which neither alone is attractive (Jang et al., 2012). It is likely that the specific blend activates a distributed set of sensory neurons in a precise manner to yield the resulting behavior, although it is also possible that individual components compete for binding to specific receptors. How and where are pheromone signals detected by *C. elegans*?

1.11 Chemosensation in *C. elegans*

Roughly one third of the somatic cells in *C. elegans* are neurons, and 60 of the 302 neurons are ciliated (Perkins et al., 1986; Ward et al., 1975; Ware et al., 1975). Mutations affecting cilia structure and function result in broad sensory deficits, including the failure to detect dauer pheromone (Collet et al., 1998; Dusenbery, 1980; Perkins et al., 1986; Starich et al., 1995). Ciliary signaling compartments are known to house diverse sensory molecules which serve to transduce environmental signals into patterns of neuronal activity (Nechipurenko et al., 2013). Molecules such as G protein-coupled receptors (GPCRs), GCs, and cyclic nucleotide-gated ion channels (CNGs) are all capable of transducing environmental signals (Bargmann, 2006; Coburn and Bargmann, 1996; Komatsu et al., 1996; Ortiz et al., 2006; Thomas and Robertson, 2008; Touhara and Vosshall, 2009; Yu et al., 1997). Importantly, at the outermost level of detection a stimulus is either present or absent; additional cellular and molecular mechanisms are required to assess stimulus concentration and its valence (neutral, attractive or repulsive) with respect to the organism (Kato et al., 2014; Li and Liberles, 2015). These downstream processes are plastic, and can thus be modulated by context and experience, further refining the ability of the animal to mount the appropriate response to the stimulus (Luo et al., 2014; Satoh et al., 2014). Please refer to Bargmann (2006) for a comprehensive review of chemosensation in *C. elegans*.

The first dauer pheromone GPCRs, SRBC-64 and SRBC-66, were identified in our lab (Kim et al., 2009; Thomas and Robertson, 2008). The receptors are localized to the sensory cilia of ASK neurons and mediate responses to acsr#2, ascr#3 and icas#9 (C5) via the G_α proteins GPA-2 and GPA-3 (Kim et al., 2009). Subsequently, SRG-36 and SRG-37 were identified as ascr#5 (C3) receptors and these are expressed in the ASI neurons (McGrath et al., 2011). Two more receptors, DAF-37 and DAF-38, also appear to mediate some aspects of dauer pheromone signaling (Park et al., 2012b). Interestingly, despite being expressed throughout life, these receptors are dispensable for adult pheromone-mediated behavior; with the possible exception of DAF-37 (Jang et al., 2012; Kim et al., 2009; Park et al., 2012b). Thus, the cellular and molecular basis of action for many ascarosides remains to be discovered. In addition, much remains to be learned about how ascaroside signals are processed and integrated by the nervous system.

1.12 Neural Control of Sensory Behaviors

Although the focus of this work is on sensory integration during development, we have learned a great deal about how sensory information is processed by the nervous system by observing highly stereotyped behaviors. In particular, *C. elegans* exhibits robust avoidance of and attraction to exogenous chemicals, leading to the identification of the primary sensory neurons which detect these cues and those that modulate the response as a function of context (Bargmann, 2006).

The ASH, ADL and AWB neurons are all involved in avoiding aversive cues (Bargmann, 2006; de Bono et al., 2002). ASH has been described as a polymodal nociceptor as it mediates responses to solutions of high osmolarity (glycerol, octanol), metal ions (Cu^{2+}, Cd^{2+}), and also to mechanosensory stimuli (Hart et al., 1999; Hilliard et al., 2005; Kaplan and Horvitz, 1993;

Sambongi et al., 1999). Together with the ADL neurons, ASH also drives aversion to bitter compounds such as quinine and to high concentrations of O_2 (Chang et al., 2006; Hilliard et al., 2004; Rogers et al., 2006). The ASE, AWA and AWC neurons are those primarily responsible for detecting attractive cues (Bargmann, 2006). The ASE mediate salt chemotaxis behaviors (Iino and Yoshida, 2009; Leinwand and Chalasani, 2013; Suzuki et al., 2008), while the AWA and AWC neurons are responsive to food-related volatile odorants such as diacetyl and isoamyl alcohol, respectively (Bargmann et al., 1993). AWC neurons track olfactory stimuli with high temporal precision and have also been implicated in thermotaxis behaviors (Beverly et al., 2011; Kato et al., 2014; Ohnishi et al., 2011).

When presented with a mixture of cues of opposing valence a decision must be made (Li and Liberles, 2015). In behavior, as in development, the wrong choice may be maladaptive. Primary sensory neurons responses are unaffected by training in an associative learning paradigm (Ha et al., 2010), and thus resolution must occur downstream in the circuit (Gordus et al., 2015). The valence of the cue is likely encoded at the level of the first synapse. In a contrast between Cu^{2+} and diacetyl, integration was already apparent in the shared first-order interneuron AIA (Shinkai et al., 2011). Motor output is already encoded at the level of the first interneuron (Luo et al., 2014; Shinkai et al., 2011), thus giving rise to two possible outcomes for conflict resolution: the behavior of the organism may represent a graded response to the two stimuli; alternatively, one stimulus may prove to be epistatic to the other. In the case of the RMG hub-and-spoke circuit which features push-pull circuit motifs, behaviors are more likely to represent a graded response to opposing stimuli (Jang et al., 2012; Macosko et al., 2009). However, with respect to a feeding behavior, a flip-flop circuit motif was identified such that the motor output was reversibly controlled by the dominant input and did not exhibit intermediate phenotypes (Li

et al., 2012). The dauer fate decision is likely to be regulated by a similar bistable flip-flop mechanism, yet one which integrates information over a longer time scale.

1.13 Sensory Signal Integration in the *C. elegans* Dauer Fate Decision

Although the stimuli (temperature, food, and pheromone), many sensory neurons (ADF, ADL, ASG, ASI, ASJ and ASK) and several signaling pathways (GC, TGF-β, insulin and steroid-hormone) have been implicated in the regulation of dauer formation, very little is known about how the various sensory stimuli are integrated to inform the all-or-none polyphenic decision. If animals fail to enter dauer in a harsh environment that may die before being able to reproduce. Alternatively, inappropriate entry into the dauer state is metabolically costly and retards reproductive development by at least 24 hours, which may yield an acceptable niche to a competitor (Avery, 2014). Moreover, all animals continuously assess their environments and process the information to make adaptive decisions. **By studying the small sensory circuit regulating dauer formation in *C. elegans* we hope to gain insight into the general principles of the cellular and molecular mechanisms of polymodal sensory integration.**

In the subsequent chapters I have explored the molecular mechanisms underlying signal transduction of specific pheromone cues (Chapter 2) and also the cellular and molecular basis for food signal integration into the dauer fate decision (Chapter 3). In the course of my studies I authored a book chapter on the methodology for the quantitative assessment of dauer formation (Appendix 1) (Neal et al., 2013). I also took part in two collaborative studies that examined different aspects of sexual dimorphism in sensory perception and integration. In the first study we identified a push-pull circuit involving the ADL, ASK and RMG neurons which regulates the relative attractiveness of ascr#3 in males and hermaphrodites (Appendix 2) (Jang et al., 2012).

Finally, in the second study we determined how age, sex and feeding-state contribute to the dynamic regulation of a chemoreceptor that functions in food-odor taxis (Appendix 3) (Ryan et al., 2014).

CHAPTER 2

A genetic screen to identify components of the dauer pheromone molecular signal transduction machinery in *Caenorhabditis elegans*

This chapter is a work in progress, and has been formatted as a manuscript for submission to Genetics.

A genetic screen to identify components of the dauer pheromone molecular signal transduction machinery in *Caenorhabditis elegans*

Scott J. Neal[1], JiSoo Park[2], Jason Yoon[1], Michelle L. Wang[1], Mayumi Shibuya[1], Kyuhyung Kim[2] and Piali Sengupta[1]

[1]Department of Biology and National Center for Behavioral Genomics, Brandeis University, Waltham, MA 02454

[2] Department of Brain Science, Daegu Gyeongbuk Institute of Science and Technology (DGIST), Daegu 711-873, Korea

2.1 Contributions to this work

SJN performed the dauer phenotype screen, genome sequence analysis and preliminary rescue experiments for all mutants. JY and MLW, undergrads under the supervision of SJN, contributed to the cell-specific rescue experiments for *oy107* and, *oy104* and *oy106*, respectively. JSP is currently conducting cell-specific rescue experiments for *oy105* and *oy108* under the supervision of KK. The forward genetic screens were conducted by KK and MS. KK performed the 3-factor mapping of *oy108* and *oy109*. PS served as the advisor for all work contained herein. SJN wrote the manuscript.

2.2 Abstract

Pheromones are small molecule cues that constitute a diverse chemical language used for intraspecific communication in most organisms. The study of pheromone action is most advanced in non-traditional model organisms which lack the superior genetic resources of more traditional models, such as *Caenorhabditis elegans*. *C. elegans* produces a blend of ascarosides collectively referred to as dauer pheromone, and whose chemical nature is known. Ascarosides regulate diverse adult behaviors and are instructive cues for entry into dauer diapause. The convergent genetic pathways regulating dauer formation are well established but the molecular signal transduction pathways through which specific pheromones act are less clear. Given that pheromones typically act as blends with distinct modes of action it is important to understand how individual components signal so that the combinatorial logic can be deciphered. Here we identify new neuronal sites of action and new molecules that function in pheromone signal transduction in the nematode *C. elegans* to regulate dauer formation.

2.3 Introduction

Animals typically react to harsh environments by avoiding them, although some animals have evolved additional mechanisms to survive adverse conditions. During specific developmental periods these animals may enter diapause, a hibernation like state in which metabolic activity is reduced, feeding ceases, and stress resistance is increased (Avery, 2014; Emerson et al., 2009; Hahn and Denlinger, 2011; Kostal, 2006; Nylin, 2013). In all cases, entry into diapause is regulated by factors in the environment, which must be properly integrated to make a robust and adaptive developmental decision (Emerson et al., 2009; Hahn and Denlinger, 2011; Morehouse et al., 2013; Nylin, 2013; Sato et al., 2014; Schaedel et al., 2012; Sim and Denlinger, 2009, 2013; Sim et al., 2015; Tennessen et al., 2010). Despite its prevalence, especially among invertebrates, cellular and molecular processes governing diapause entry are not well understood.

A particularly well-studied diapause is the formation of dauer larvae in *Caenorhabditis elegans.* Early in development *C. elegans* senses its environment, ultimately choosing whether to continue in the reproductive cycle or to arrest as a dauer larva (Avery, 2014; Cassada and Russell, 1975; Golden and Riddle, 1982, 1984b). Thus, dauer formation is also an example of polyphenism in which an individual can adopt one or more distinct morphs. Decades of study have resolved that dauer formation is regulated by temperature, food availability and population density (Albert et al., 1981; Golden and Riddle, 1982, 1984a, b; Hu, 2007; Swanson and Riddle, 1981), the latter assessed by pheromone levels (Golden and Riddle, 1982). Furthermore, the genetic tractability of *C. elegans* has permitted the discovery of multiple pathways that coordinately regulate dauer formation, defining a class of genes resulting in abnormal dauer formation (*daf*) (Albert et al., 1981; Riddle et al., 1981; Swanson and Riddle, 1981).

Insulins and transforming growth factor β (TGF-β) signal along parallel pathways that ultimately converge to regulate a steroid hormone pathway which governs the decision between the reproductive or dauer developmental pathways (Hu, 2007). Mutations affecting the TGF-β ligand (*daf-7*) (Ren et al., 1996; Schackwitz et al., 1996), its receptors (*daf-1*, *daf-4*) (Estevez et al., 1993; Georgi et al., 1990), and specific downstream SMAD transcription factors (*daf-8*, *daf-14*) (Inoue and Thomas, 2000; Park et al., 2010; Thomas et al., 1993),result in constitutive dauer formation (*daf-c*), but can be suppressed by mutations in two other transcription factors (*daf-3*, *daf-5*) (da Graca et al., 2004; Liu et al., 2004; Patterson et al., 1997; Thatcher et al., 1999; Vowels and Thomas, 1992), which result in the dauer defective (*daf-d*) phenotype. The penetrance of dauer phenotypes when any one of the 40 insulin-like peptides (ILPs; eg. *ins-1*, *ins-18*, *daf-28*) expressed by *C. elegans* is low (Li et al., 2003; Malone et al., 1996; Malone and Thomas, 1994; Matsunaga et al., 2012; Pierce et al., 2001), though mutation of the single insulin receptor (*daf-2*) results in a highly penetrant *daf-c* phenotype (Gems et al., 1998; Gottlieb and Ruvkun, 1994). All insulin pathway mutants are suppressed by mutation of the FOXO transcription factor gene (*daf-16*) (Gottlieb and Ruvkun, 1994; Vowels and Thomas, 1992). *Daf-c* mutants in both pathways remain temperature and pheromone sensitive (Golden and Riddle, 1984b; Malone and Thomas, 1994; Swanson and Riddle, 1981). Under favorable conditions TGF-β and insulin signals promote the DAF-9-dependent synthesis of the steroid hormone dafachronic acid (Albert and Riddle, 1988; Gerisch and Antebi, 2004; Gerisch et al., 2007; Gerisch et al., 2001; Jia et al., 2002; Motola et al., 2006), which binds to the nuclear hormone receptor DAF-12 to promote reproductive growth (Antebi et al., 1998; Antebi et al., 2000; Gems et al., 1998; Larsen et al., 1995; Snow and Larsen, 2000). Collectively these pathways integrate environmental signals and drive the execution of a binary developmental decision (Figure 2.1A).

Though the TGF-β and insulin signaling pathways are well characterized, relatively little is known about how and where environmental cues are processed in the nervous system to regulate endocrine signaling. Laser ablation studies defined six sensory neurons (ADF, ADL, ASG, ASI, ASJ, and ASK) whose functions are necessary to regulate dauer formation (Bargmann and Horvitz, 1991; Schackwitz et al., 1996). However, many sensory signaling mutants are *daf-d*, including those with defects in the ciliated ending of sensory neurons (*daf-6*, *daf-10*, *daf-19*) (Albert et al., 1981; Bell et al., 2006; Perens and Shaham, 2005; Perkins et al., 1986; Swoboda et al., 2000). This result led to the conclusion that sensory neurons detect signals which normally serve to downregulate insulin and TGF-β signaling (Bargmann and Horvitz, 1991). Importantly, no pheromone receptors or other pathway-specific sensory molecules were identified in the comprehensive genetic screens for *daf* genes.

Recent studies have begun to uncover the regulators which govern the endogenous production of dauer pheromone (Joo et al., 2010; Zhang et al., 2015). Advances have also been made in our understanding of the chemical composition of dauer pheromone, resulting in the discovery of daumone (Jeong et al., 2005), and a multitude of related molecules collectively called ascarosides (Butcher et al., 2007; Butcher et al., 2009a; Butcher et al., 2008; Butcher et al., 2009b; Pungaliya et al., 2009; Srinivasan et al., 2008). This information has enabled us to revisit the mechanisms by which specific ascarosides act, and has led to the identification of three pairs of receptors and their sites of action. The SRBC-64 and SRBC-66 G protein-coupled receptors are expressed in the ciliated endings of the ASK neurons and mediate dauer formation in response to ascr#2 (C6), ascr#3 (C9, ΔC9) and icas#9 (C5) (Kim et al., 2009); these pheromone signals are in turn transduced by the G_α proteins GPA-2 and GPA-3 (Kim et al., 2009; Zwaal et al., 1997). Ablation of the ASK neurons yields a more penetrant defect in dauer formation,

suggesting that this cell type may express additional receptors (Kim et al., 2009). SRG-36 and SRG-37 mediate dauer formation to ascr#5 (C3), and are expressed in the ASI neurons (McGrath et al., 2011). Finally, the narrowly-tuned ascr#2 receptor DAF-37 and the more broadly-tuned putative co-receptor DAF-38 were isolated, though this latter study defines the site of action of ascr#2 as ASI (Park et al., 2012). However, the intracellular and intercellular mechanisms by which ascaroside signals are transduced downstream of these receptors remain largely unknown (Figure 2.1B). Furthermore, the cellular and molecular processes which integrate pheromone cues with other environmental determinants of dauer formation have not been identified.

We undertook a forward genetic screen to identify additional pheromone-response defective (*phd*) mutants (Figure 2.1C). Dauer-inducing conditions, including high temperature and the presence of pheromone down-regulate the expression of the *daf-7* and *str-3* promoters in the ASI neurons (Nolan et al., 2002; Peckol et al., 2001; Ren et al., 1996; Schackwitz et al., 1996). Our hypothesis was that the failure to repress expression from the *str-3* promoter in the presence of pheromone would identify mutants that are *daf-d*, and that such mutants might help to define molecules involved in the direct environmental regulation of the TGF-β pathway, or in the context-dependent integration of pheromone signals. We isolated more than 100 putative *phd* mutants and characterized the ability of 28 of these to form dauers in the presence of multiple ascarosides at multiple concentrations. We further characterized seven mutants and sequenced their genomes to identify the causative lesions. Functional rescue of these genes has highlighted emergent roles for the ADL and ASH neurons (*qui-1*), as well as cell-autonomous roles for a family of Tau-tubulin kinases (*F32B6.10*, *W01B6.2*) in dauer formation.

2.4 Results

2.4.1 Forward genetic screen for mutants defective in pheromone-mediated repression of *str-3*p::GFP expression

A screen of approximately 38,500 haploid genomes yielded 129 putative *phd* mutants which were identified by their failure to repress *str-3*p::GFP expression when grown on plates containing crude pheromone and plentiful food. Of these, 4 were *daf-c* and 75 exhibited either fully or partially penetrant defects in lipophilic dye uptake; the latter class was anticipated based on prior work (Nolan et al., 2002; Peckol et al., 2001).

2.4.2 Dauer formation in putative *phd* mutants

Following the identification of mutants with defects in pheromone-mediated repression of *str-3*p::*gfp* expression, we next analyzed their defects in dauer formation. To learn more about the signal transduction pathways used by specific pheromone components we used quantitative assessment of dauer formation to further characterize 28 mutants (Table S2.1) (Lee et al., 2011; Neal et al., 2013). Notably, the *str-3*p::GFP parent strain that was mutagenized exhibits wild-type dauer formation under all conditions tested - in a multivariate analysis of variance neither the effect of genotype nor of genotype by pheromone interaction were significant in comparison to the wild-type N2 strain. As expected, mutants which were defective in lipophilic dye uptake (K17, K26, K28, K33) were generally defective in pheromone-induced dauer formation (Table S2.1) (Perkins et al., 1986). General defects in dauer formation were also observed in two mutants which produced mostly unfertilized embryos under assay conditions (K16, m10) and in two which exhibited a non-dauer larval arrest (K17, K21) (Table S2.1). Of the strains that consistently laid sufficient eggs for accurate assessment of dauer formation it was interesting to

note that most exhibited wild-type dauer formation to ascr#5 (Table S2.1); ascr#5 acts directly on ASI neurons via the SRG-36 and SRG-37 receptors and exhibits distinct pharmacokinetics and temperature dependence relative to the other compounds tested (McGrath et al., 2011). Instead, more penetrant defects in dauer formation were observed for the ASK-sensed ascarosides ascr#2, ascr#3 and icas#9 (Table S2.1), suggesting that the isolated mutants define loci that act upstream of the ASI neurons (Kim et al., 2009).

To determine if we could further sub-categorize the mutants, we tested dauer formation to ascr#8 for which the site of action is unknown. Ascr#8 has mainly been studied with respect to adult behaviors, such as male attraction (Pungaliya et al., 2009; Srinivasan et al., 2008). Nonetheless, ascr#8 is a potent inducer of dauer formation in wild-type animals (Table S2.2). Dauer formation in response to ascr#8 was only moderately affected in the putative *phd* mutants (Table S2.1), thus we also examined mutants in the various G_{α}-encoding genes in *C. elegans* (Table S2.2) (Jansen et al., 1999; Lochrie et al., 1991; Zwaal et al., 1997). Mutations affecting GPA-2 and GPA-3 largely abrogate dauer formation in response to ASK-sensed pheromones (Kim et al., 2009), while constitutive activation of GPA-3 results in a *daf-c* phenotype (Zwaal et al., 1997). Overexpression of *gpa-2* and mutation of either or both *gpa-2* and *gpa-3* partially suppressed ascr#8-mediated dauer formation, while mutations in either *gpa-4* or *gpa-5* slightly enhanced it. Together with the moderate effect of ASK-ablation on ascr#8 dauer formation, these data suggest that ascr#8 may partially induce dauer formation via the ASK neurons but that the complete integration of the signal may occur over a distributed set of neurons. Enhanced responses to the other tested pheromones were also observed in *gpa-4* mutants, suggesting that GPA-4 may mediate transduction of an ascaroside-independent dauer-suppressing cue.

We proceeded with the in-depth characterization of 7 putative *phd* mutants (Table 2.1). In addition, we further characterized dauer formation in mutants known to affect ascaroside signaling in ASK neurons (*srbc-64*; *srbc-66* and *gpa-2*; *gpa-3*) as well as the strain in which ASK neurons are genetically ablated (*qrIs2*) (Kim et al., 2009). The selected *phd* candidates generally exhibited strong *str-3*p::GFP expression in the repression assay and had selective deficits in ascaroside-induced dauer formation, with the exception of K15 (*oy105*) which exhibited similar moderately-reduced sensitivity to all compounds (Table 2.1).

2.4.3 Complementation Analysis and Genetic Mapping

Since there was a qualitative correlation between *str-3*p::GFP repression defects and dauer formation defects (Table S2.1), our first mapping strategy was to examine *str-3*p::GFP repression in the F2 progeny of mutants mated to strains that have recessive phenotypic markers on each chromosome (Fay, 2006a); results are summarized in Table 2.2. We did not observe any evidence of X-linkage. As a second approach, we scored dauer formation in the F2 progeny of mutants mated to strains expressing dominant markers; results are summarized in Table 2.2. Finally, 3-factor mapping was used for the two strains that had the brightest *str-3*p::GFP expression on crude pheromone plates, resulting in the probable linkage of *oy108* to LGI (to the right of *unc-5*, near to the left of *unc-29*) and of *oy109* to the end of LGII (Table 2.2).

2.4.4 Whole-Genome Resequencing

Genome data were aligned and compared to the N2 reference genome using MAQgene/CloudMap analysis (Table 2.3) (Bigelow et al., 2009; Minevich et al., 2012; Sarin et al., 2010). Since all of the alleles were derived from the same parental strain any mutation

common to at least three of the strains was eliminated from consideration (Sarin et al., 2010). A prioritized list of candidate genes for each strain was constructed, guiding our efforts to clone the affected loci (Table 2.4).

2.4.5 *oy103*

The *oy103* allele was associated with highly penetrant defects in dauer formation to all compounds, except for ascr#5, similar to the phenotype of ASK-ablated animals (Figure 2.2A). There are four predicted PTCs in the *oy103* strain, affecting *cec-3*, *T05C1.1*, *C01G12.7* and a locus (*C06G3.4*) now considered to be a pseudogene. In addition, the *nhr-142* and *col-43* loci are predicted to harbor splice site mutations. An independent allele of *cec-3* failed to recapitulate the *oy103* phenotype, while a strain bearing a deletion allele of the *nhr-142* locus exhibited partial defects in dauer formation to ascr#3 (Figure 2.2B). However, expression of wild-type *nhr-142* sequences in *oy103* failed to rescue dauer formation under the conditions tested, as did expression of transgenes encoding the remaining candidate genes (Figure 2.2C). It is possible that we have not yet tested our rescue constructs under the appropriate conditions, that one of the numerous missense mutations we have yet to consider encodes *oy103*, or that *oy103* is compounded by a second mutation.

2.4.6 *oy104*

The *oy104* allele was particularly interesting because of its selective and highly penetrant effects on dauer formation in response to icas#9 and ascr#3 (Figure 2.3A). There are putative PTCs in *mks-6*, *obr-1* and *lgc-36* in the *oy104* strain; independent alleles of *mks-6* and *obr-1* exhibited wild-type dauer formation (Figure 2.3B), while expression of wild-type *lgc-36*

sequences failed to rescue (Figure 2.3C). There was a trend towards decreased dauer formation in the *mks-6* mutant, but expression of wild-type *mks-6* sequences in *oy104* failed to rescue (Figure 2.3C). The *oy104* strain also harbors a potential deletion in the putative neuropeptide receptor-encoding gene *B0034.5* and missense mutations in the ion channel gene *asic-1* and an uncharacterized gene *F28H1.1*. An independent allele of *asic-1* failed to recapitulate the *oy104* phenotype (Figure 2.3B) and expression of *B0034.5* sequence in *oy104* also failed to rescue (Figure 2.3C). We have confirmed the missense mutation in the remaining candidate, *F28H1.1* (Figure 2.3D), which encodes a *Caenorhabditis*-specific 221 amino acid protein with no conserved domains, and will determine whether this mutation is causal to the phenotypes of *oy104* mutants.

2.4.7 *oy105*

The *oy105* allele is associated with slightly reduced dauer formation, especially to lower concentrations of ASK-sensed ascarosides (Figure 2.4A). The *oy105* strain harbors putative PTCs in *Y57A10A.31*, *R10E4.6*, *R13A5.7* and *qui-1*, the latter mapping to the expected chromosome. Expression of wild-type sequences of *R10E4.6* and *R13A5.7* did not rescue whereas partial rescue was achieved with a fosmid encoding *qui-1* when tested with ascr#3 (Figure 2.4B). QUI-1 is a large WD40 repeat protein with a putative coronin-like domain at its C-terminus (Figure 2.4C). It mediates avoidance of bitter compounds, such as quinine, and is expressed in the ASH and ADL neurons, but not in ASK (Hilliard et al., 2004). We obtained an independent allele of *qui-1*, harboring the *gb404* nonsense mutation and it phenocopied *oy105* with respect to dauer formation (Figure 2.4D).

Cell-specific rescue experiments using the *qui-1* coding sequences suggest that QUI-1 function is necessary in both ASH and ADL to restore wild-type dauer formation to *qui-1* mutants (Figure 2.4E). Neither neuron has previously been implicated in the regulation of dauer formation.

2.4.8 *oy106*

The *oy106* allele was associated with slightly reduced dauer formation to ascr#8, icas#9 and ascr#2, though the icas#9 results were distinct from ASK-ablated animals and from other putative *phd* mutants (Figure 2.5A). Responses to icas#9 were greatly reduced at 60 nM but nearly wild-type at 600 nM, whereas the other tested strains were highly defective to both concentrations. We noted a putative nonsense mutation in *che-12*, which encodes a HEAT domain protein that is necessary for the structural maintenance of cilia (Figure 2.5B) (Bacaj et al., 2008). However, putative null mutations in *che-12* result in defects in lipophilic dye uptake, which we did not observe in *oy106*, and unlike *oy106*, *che-12*(*e1812*) mutants are also completely *daf-d* (data not shown). Closer examination reveals that two shorter isoforms of CHE-12 are unlikely to be affected by the *oy105* PTC, whereas the *e1812* polymorphism occurs in the 5' splice site of a common exon (Figure 2.5B). Expression of wild-type *che-12* genomic sequences in *oy106* mutants provided partial rescue of dauer formation to icas#9 and ascr#3 and exhibited a rescuing trend to ascr#8 (Figure 2.5C). Work in progress is aimed at determining whether the short isoforms of CHE-12 are sufficient for dye-filling and whether the long isoforms are necessary and sufficient for dauer formation in the null background.

2.4.9 *oy107*

The *oy107* allele was associated with mild defects in dauer formation to most ascarosides, but with highly penetrant defects in icas#9-mediated dauer formation (Figure 2.6A). Expression of wild-type sequences of the putative Tau tubulin kinase (TTBK) encoding gene *F32B6.10* partially restored dauer formation to *oy107* mutants in response to ascr#8 and exhibited a rescuing trend in response to icas#9 and ascr#3 (Figure 2.6B). *oy107* generates an early stop codon in the *F32B6.10* coding sequence, upstream of the putative kinase active site (Figure 2.6C), representing the only PTC on the mapped chromosome. There are 93 potential paralogs of F32B6.10 encoded by the *C. elegans* genome including 86 members of the broad casein kinase I (CK1) superfamily and 32 TTBK or TTBK-like proteins (Manning, 2005), genes for two of which are located within 200kb of *F32B6.10* on LGIV. W01B6.2 is more similar to F32B6.10 than is C04G2.2. Reciprocally, C45G9.1 is most similar to W01B6.2, but is unlinked. We obtained an independent deletion allele, *F32B6.10*(*tm4006*), as well as alleles of *W01B6.2*(*tm4134*) (Figure 2.6C), *C04G2.2*(*tm3814*) and *C45G9.1*(*gk1235*) and tested them in dauer formation (Figure 2.6D). Interestingly, each of the alleles from the linked loci on LGIV exhibited defects in dauer formation to ascr#3 while the unlinked gene *C45G9.1* was dispensable for dauer formation under these conditions; *F32B6.10*(*tm4006*) phenocopied *oy107* (compare Figure 2.6A and D). Linkage prevented us from assessing the potential for redundancy among the LGIV genes.

Preliminary expression patterns for F32B6.10 and W01B6.2 were obtained by fusing their upstream regulatory sequences to GFP coding sequences (Figure S2.1) (Hobert, 2002). We observed GFP expression in a small number of sensory neurons in both cases; these appeared to include ASK and ASI and a few cells with distinct expression between the two constructs. We

therefore conducted cell-specific rescue experiments whereby the respective cDNA sequences were expressed in the mutant background (Figure 2.6E). Expression of F32B6.10 in ASI completely restored dauer formation to *F32B6.10*(*tm4006*) mutants, while expression in ASK produced a weak effect in response to ascr#2 (Figure 2.6E). Rescue of W01B6.2 function in ASI or ASE+AWC neurons exhibited a strong trend towards rescue of *W01B6.2*(*tm4134*) mutants, particularly in response to ascr#3. The expression profiles and rescue data will need to be confirmed, especially given some preliminary evidence that ectopic expression of W01B6.2 in *F32B6.10*(*tm4006*) may also rescue dauer formation (data not shown).

2.4.10 *oy108*

The *oy108* allele was associated with strong defects in icas#9- and ascr#2-mediated dauer formation (Figure 2.7A). The re-sequenced genome of the *oy108* strain did not contain any unique PTCs, and otherwise contained the least unique variants of all the strains examined. There was, however, a large deletion that fell within the mapped interval on LGI. This deletion affects two genes; *maco-1* and the upstream gene *D2092.4* (Figure 2.7B). An independent allele which uniquely disrupts the macoilin encoding gene *maco-1* (*ok3165*, Figure 2.7B) phenocopied *oy108* (Figure 2.7C). However, expression of *maco-1* wild-type sequences in *oy108* did not yield strong rescue. Expression of *T08B2.3* wild-type sequences, in which an independent deletion exists in the *oy108* strain, also failed to rescue (Figure 2.7D). We have obtained a *maco-1* cDNA clone and are in the process of repeating rescue experiments.

2.4.11 *oy109*

The *oy109* strain is non-*dyf*, but is almost completely *daf-d* (Figure 2.8A). However, some dauers were observed, suggesting that *oy109* retains the ability to commit to the dauer fate. Only one PTC, affecting the sorting nexin gene *snx-14*, is present on the chromosome to which linkage was established (Figure 2.8B). The PTC falls within the putative regulator of G protein signaling (RGS) domain of the long isoform of *snx-14*, but in the 3'UTR of the short isoform, and thus it may not represent a complete loss of function of the *snx-14* locus. Attempts to rescue to the *oy109* dauer formation phenotype with wild-type *snx-14* coding sequences encompassing both predicted isoforms failed (Figure 2.8C). In order to confirm that *snx-14* is indeed the gene affected by the *oy109* mutation it will be necessary to obtain an independent allele for testing and/or to achieve rescue.

2.5 Discussion

We conducted a forward genetic screen and isolated a series of mutants which displayed defects in their ability to repress expression of *str-3*p::GFP when grown on crude pheromone plates, and which also exhibited various defects in pheromone-mediated dauer formation. We performed a quantitative analysis of dauer formation in 28 strains, selecting 7 for whole-genome re-sequencing. We have preliminary evidence supporting the identification of 3 previously characterized genes (*qui-1(oy105)*, *che-12(oy106)*, and *maco-1(oy108)*) and one uncharacterized gene (formerly *F32B6.10*) for their roles in ascaroside-mediated dauer formation. We have named the latter *phd-1(oy107)*. The causal loci affected in the remaining 3 mutants are not yet identified.

2.5.1 Possible roles for QUI-1 in dauer formation

An independent allele of *qui-1* was originally isolated in a forward genetic screen for defects in avoidance of aqueous bitter substances (Hilliard et al., 2004). Although laser ablation and cilia-defect rescue experiments were used to support the role of ASK, ADL and ASH neurons in quinine avoidance, expression of *qui-1* was not detected in ASK (Hilliard et al., 2004). ASH was proposed as the primary neuron conferring quinine avoidance and this behavior requires the function of the G_{α} proteins GPA-3, and ODR-3; the former functioning in the primary role (Hilliard et al., 2005; Hilliard et al., 2004). We also observe a role for the ASH neuron, in combination with ADL, for QUI-1 in dauer formation.

QUI-1 is a large protein with 12 predicted WD40 domains, having weak similarity to *Drosophila* and mammalian proteins of unknown function. One proposed role for QUI-1 is in lipid signaling (Hilliard et al., 2004), and lipid signals are known to gate the activity of transient receptor potential channels of which two (*ocr-2*, *osm-9*) are expressed in ADL and ASH (Colbert et al., 1997; de Bono et al., 2002; Jang et al., 2012; Sokolchik et al., 2005). A slight defect in quinine avoidance was observed in *osm-9* mutants but *ocr-2* mutants were not tested (Hilliard et al., 2004). ADL and ASH neurons have previously been implicated in the regulation of social feeding behaviors (de Bono et al., 2002). One interesting possibility it that QUI-1 is involved in the activity of the RMG hub-and-spoke circuit which integrates sensory behaviors (Jang et al., 2012; Macosko et al., 2009). QUI-1 may serve to establish the appropriate state in the avoidance spoke neurons and thereby exert its effects via RMG state changes on other sensory responses such as those to pheromone.

2.5.2 Possible roles for CHE-12 in dye-filling and dauer formation

CHE-12 is a 7 HEAT repeat protein that is selectively expressed in the subset of ciliated neurons with simple channel cilia and functions in the maintenance of the ciliary distal segment, but not in intraflagellar transport in general (Bacaj et al., 2008). It has been proposed to act as a scaffolding protein that is necessary for cilium structure and function. In a dye-filling assay, correlated with cilia integrity, *che-12* mutants do not take up fluorescein isothiocyanate (FITC), but do concentrate a second lipophilic dye (DiI) (Bacaj et al., 2008). Notably, the *mn399* allele exhibits a partial defect in the latter, suggesting that different protein isoforms encoded by *che-12* may have distinct functions (Bacaj et al., 2008). The *oy106* allele we isolated has a low penetrance *dyf* phenotype to DiI and a slightly higher penetrance *dyf* phenotype to FITC (data not shown), and the mutation is positioned such that only the two long isoforms of CHE-12 are likely to be disrupted. Given that CHE-12 functions cell-autonomously (Bacaj et al., 2008), this allele will allow us to further study the roles for specific neurons and for specific isoforms of CHE-12 in dauer formation and in the structure and function of channel cilia.

2.5.3 *phd-1* encodes a putative TTBK involved in ascaroside signal transduction

TTBKs are so-named for their ability to phosphorylate the microtubule associated protein Tau (Sato et al., 2006; Takahashi et al., 1995). TTBKs also phosphorylate tubulin and are part of the larger CK1 superfamily of proteins (Manning, 2005). A *Drosophila* TTBK homolog, Asator, interacts with spindle microtubules during cell division and is encoded by an essential gene (Qi et al., 2009). Mammalian TTBK1 is neuronally expressed and has been implicated in Alzheimer's disease (Sato et al., 2006), while the more broadly expressed TTBK2 has been implicated in spinocerebellar ataxia type 11 (SCA11) (Goetz et al., 2012). Rodent TTBK2 is

also involved in the regulation of ciliogenesis by its phosphorylation of and removal of the CP110 cap from the mother centriole (Goetz et al., 2012). Truncated TTBK2 isoforms associated with SCA11 in humans block cilia formation in a semi-dominant fashion, though it is unclear whether this is related to SCA11 pathogenesis (Goetz et al., 2012).

It is unlikely that PHD-1 is involved in mitosis or ciliogenesis in *C. elegans*. First, *phd-1* mutants are viable and develop normally. Second, *phd-1* mutants are non-*dyf*, and furthermore, preliminary examination of cilia integrity using fluorescent markers in the ASE, ASI, ASK and AWC neurons did not reveal any gross defects in length or shape (data not shown). Instead, two to other *C. elegans* genes encoding putative TTBKs, *C55B7.10* and *H05L14.1*, have been identified in a screen for proteins which can directly phosphorylate TDP-43 in a nematode model of neurodegenerative disease (Liachko et al., 2013; Liachko et al., 2014), and may represent the true orthologs of mammalian TTBK1 and TTBK2. Overall the CK1 kinase family has expanded from 12 members in humans to 86 members in *C. elegans*, providing opportunity for both redundancy and specialization of function in this class of proteins (Manning, 2005). Given that we have implicated a second putative TTBK, W01B6.2, in dauer formation, the entire TTBK gene family in *C. elegans* merits further study. It will also be necessary to affirm the cellular sites of action of PHD-1 and W01B6.2, their potential for functional redundancy, and also their subcellular localization and molecular function(s).

2.5.4 Possible role of MACO-1 in dauer formation

Analysis of the *oy108* mutation suggests that the endosomal trafficking system may be involved in regulating dauer formation. MACO-1 function is likely to be disrupted by the *oy108* deletion, given that the dauer phenotype is recapitulated by the independent *ok3165* deletion.

MACO-1 is the sole *C. elegans* macoilin, a 5-transmembrane domain protein that localizes to the rough endoplasmic reticulum and that is expressed only in neurons (Arellano-Carbajal et al., 2011). A previous study has proposed that MACO-1 functions in the sorting, folding or delivery of ion channels to synaptic terminals (Arellano-Carbajal et al., 2011). Localization of MACO-1 function with respect to dauer formation may be challenging due to its pan-neuronal expression.

2.5.5 General and specific mechanisms of ascaroside-induced dauer formation

Based on the molecular functions of the proteins encoded by the genes cloned in this study we have proposed their mechanistic sites of action in a model neuron (Figure 2.9). This work has contributed to the identification of novel classes of signaling molecules and additional neurons which function in ascaroside-mediated dauer formation. Future efforts will focus on using the resources described here to establish the necessity and sufficiency for these molecules in specific neurons and in the transduction of specific ascaroside signals. Given that individual ascarosides are sufficient to induce dauer formation, it is reasonable to hypothesize that these molecules function in a small sensory circuit which integrates pheromone and other environmental signals to regulate the expression of dauer polyphenism.

2.6 Acknowledgements

We are grateful for the assistance provided by Alex Boyanov and Gregory Minevich (Columbia University) in whole-genome resequencing and data analysis. Critical reagents were kindly provided by Elia di Schiavi and Paolo Bazzicalupo, Shai Shaham, and Mario de Bono. Synthetic pheromones were generously provided by Rebecca Butcher (U. Florida) and Frank

Schroeder (Cornell University). Some strains used in this study were obtained from the *Caenorhabditis* Genetics Center (USA) and from the National BioResource Project (Japan).

2.7 Materials and Methods

2.7.1 Strains and Genetics

C. elegans were maintained on nematode growth medium (NGM) agar plates at 20°C, with *E. coli* OP50 as a food source (Brenner, 1974). Transgenic strains were constructed using standard germline transformation procedures (Mello et al., 1991). The wild-type strain is N2 (Bristol).

2.7.2 Ethylmethanesulfonate Mutagenesis

Mutagenesis was performed according to standard *C. elegans* protocols (Brenner, 1974). Briefly, L4 stage worms of the strain CX3596 (*kyIs128* [*str-3*p::*gfp lin-15*+) were collected and washed in M9 buffer and were treated with a solution of ethylmethanesulfonate (EMS) at a final concentration of 50 mM for 4 hours at room temperature. Following mutagenesis worms were washed extensively in M9 buffer and transferred to a NGM agar plate seeded with *E. coli* OP50. Mutagenized P0 worms were transferred onto individual plates after 2 hours. After 3 days F1 progeny were distributed to individual plates for clonal screening. F1 individuals or pools of individuals were allowed to lay eggs on plates with crude pheromone; young adults F2s were scored. F2 clones with bright GFP expression in the ASI neurons were collected and retested on plates with and without pheromone, and were observed for additional phenotypes. In total, 38,500 haploid genomes were screened resulting in the isolation of 129 mutants. Of these, 75 exhibited defects in lipophilic dye uptake (*dyf*) and 4 were *daf-c*.

2.7.3 Dauer Formation Screen

Animals were maintained under standard culture conditions at either 20°C or 25°C for at least three generations before testing. Since accurate quantification of dauer formation is dependent on the ability of a population of parent worms to lay sufficient eggs in a defined time period (Neal et al., 2013), only 28 mutants which were sufficiently fertile could be characterized in this assay. Dauer formation assays were preformed according to published methods (Neal et al., 2013), and were scored after 84 hours from the midpoint of the egg lay to account for delayed growth rates in some mutants. Wild-type and *gpa-2; gpa-3* mutants were tested in every assay, to account for variation in dauer formation. Mutants were initially screened for concentration-dependent dauer formation responses to ascr#2, ascr#5 and ascr#8, while 11 mutants were further characterized for their responses to ascr#3 and icas#9.

2.7.4 Complementation Testing

Complementation testing was performed by injecting strains with a fluorescent marker (coelomocyte::dsRed) such that F1 cross progeny could be clearly identified. Mating of a males from a marked strain to an unmarked hermaphrodite produced labelled F1 hermaphrodites which were immediately used as egg-layers in the dauer formation assay. If the alleles are able to complement one another then 50% of progeny are expected to exhibit wild-type probability of dauer formation, whereas if they fail to complement all animals will exhibit the mutant probability of dauer formation. Complementation with wild-type was used to determine if the mutations were dominant or recessive.

2.7.5 Genetic Mapping

Several mapping strategies were followed. First, we examined *str-3*p::GFP repression in the F2 progeny of mutants mated to strains that have recessive phenotypic markers (*dpy*, *unc*, *rol*) on each chromosome (Fay, 2006a). Mutations linked to the recessive markers result in the given phenotypic class exhibiting repressed *str-3*p::GFP when grown on pheromone plates. Mutants mated to wild-type males were also placed on pheromone plates such that *str-3*p::GFP could be scored in F1 males. As a second approach, we crossed putative *phd* mutants to strains with dominant integrated markers on the candidate chromosomes and scored dauer formation in the marked (homozygous and heterozygous for wild-type chromosome) versus unmarked F2s (homozygous mutant chromosome); candidate marked strains exhibited wild-type dauer formation. Attempts to use single-nucleotide polymorphism mapping by crossing to the Hawaiian isolate of *C. elegans* failed due to the fact that this strain proved to be *daf-d* under all conditions tested. Finally, standard 3-factor mapping was used for two strains based on *str-3*p::GFP repression on crude pheromone plates (Fay, 2006b).

2.7.6 Whole-Genome Resequencing

We selected 7 mutants for whole-genome resequencing based on the qualitative "profile" of their responses to the tested ascarosides. Genomic DNA was isolated from each mutant strain using standard molecular biology techniques, and was analyzed for integrity by agarose gel electrophoresis. Sequencing libraries and sequencing on the Illumina HiSeq platform were prepared and performed by Alex Boyanov in the Hobert Lab at Columbia University according to published methods (Sarin et al., 2010). De-multiplexing, alignment and preliminary analysis of the data with the MAQgene analysis pipeline were performed by Alex Boyanov and Gregory

Minevich (Bigelow et al., 2009). Original data were confirmed with an independent analysis using the CloudMap pipeline and default parameters in the published workflow (Minevich et al., 2012). Shared polymorphisms among strains were excluded from analysis (Sarin et al., 2010). Strain-specific polymorphisms were identified by putative effect, consistency with the mode of action of EMS (G>A, C>T) and multiple consensus reads. For each strain a prioritized list of affected loci was generated, including all unique premature termination codons (PTCs), and mutations affecting splice sites or genes of potential relevance on the chromosome to which linkage was established. Gene models are derived from information in WormBase (www.wormbase.org) and were plotted using WormWeb Tools generated by Nikhil Bhatla (www.wormweb.org).

2.7.7 Rescue of Mutant Phenotypes

PCR was used to amplify wild-type genomic sequences for each locus. Upstream regulatory sequences - defined as the lesser of 3 kb and the distance to the upstream gene, downstream regulatory sequences - defined as the lesser of 500 bp and the distance to the downstream gene, and the entire intervening coding sequence constituted the rescuing fragment. Standard methods for germline transformation were used (Mello et al., 1991). Products were column-purified (Qiagen) and injected at 50 ng/µL along with 30 ng/µL or 50 ng/µL of the co-injection markers *unc-122*p::*gfp* or *unc-122*p::*dsRed*, respectively. PCR products of the expected size were pooled from multiple reactions but were not otherwise verified. At least two transgenic lines were considered for each potential rescue.

Complementary DNA sequences were reverse transcribed from a library derived from the RNA of mixed stage wild-type animals. cDNAs were cloned into the pGEM-T Easy vector

(Promega) and were confirmed by sequencing. The *qui-1* cDNA was the generous gift of Paolo Bazzicalupo and Elia di Schiavi, the *che-12* cDNA was the generous gift of Shai Shaham and the *maco-1* cDNA was the generous gift of Mario de Bono. cDNAs were sub-cloned under the expression of cell-specific promoters: ADL (*sre-1Δ*p), ASH (*sra-6*p; also weak expression in ASI), ASI (*srg-47*p), ASK (*sra-9*p), AWC+ASE (*ceh-36*p). Cell-specific rescues were injected at 30 ng/µL or less, if viability was affected, along with 30 ng/µL *unc-122*p::*gfp*. At least two transgenic lines were examined for each potential rescue.

2.7.8 Statistical Analysis

Much of the data in this chapter are in preliminary form, with insufficient replication to be appropriate for statistical analysis. Where presented, data were analyzed by one-factor ANOVA (genotype) using the Games-Howell *post-hoc* test, as implemented in SPSS edition 22.

2.8 Figure Legends

Figure 2.1. Description of known and potential pheromone signal transduction pathways and design of the *str-3*p::GFP repression screen.

(A) A schematic outlining the cellular and genetic pathways known to regulate dauer formation. See text for details. (B) Expected classes of molecules that may function in ascaroside signal transduction, and thus be isolated in the screen. (C) A schematic outlining the forward genetic screen for putative *phd* mutant based on *str-3*p::GFP repression. Putative *phd* mutants fail to repress *str-3*p::GFP expression when grown on plates containing crude pheromone. See text for details.

Figure 2.2. Summary of findings related to the *oy103* allele.

(A) Dauer formation profile of *oy103* mutants in comparison to wild-type and ASK-ablated animals. Each bar represents the average of at least two independent trials and each assay plate contained >65 worms. This is the graphical representation of data found in Table 2.1; error bars are omitted for clarity. (B) Dauer formation in the indicated strains, in the presence of the indicated pheromones at 25ºC with 160 µg heat-killed OP50. ** and *** represent different from wild-type at $P<0.01$ and <0.001, respectively (one-way ANOVA with Games-Howell *post-hoc* test for genotype). ND, not determined. N.S., not significantly different. Error bars are the standard error of the mean. (C) Dauer formation in the indicated strains in the presence of the indicated pheromones at 25ºC with 160 µg heat-killed OP50. The indicated transgenes were amplified from wild-type genomic DNA and injected into *oy103* mutants. *** represents different from wild-type at $P<0.001$ (one-way ANOVA with Games-Howell *post-hoc* test for genotype). ND, not determined. Error bars are the standard error of the mean.

Figure 2.3. Summary of findings related to the *oy104* allele.

(A) Dauer formation profile of *oy104* mutants in comparison to wild-type and ASK-ablated animals. Each bar represents the average of at least two independent trials and each assay plate contained >65 worms. This is the graphical representation of data found in Table 2.1; error bars are omitted for clarity. ND, not determined. (B) Dauer formation in the indicated strains, in the presence of the indicated pheromones at 25ºC with 160 μg heat-killed OP50. *** represents different from wild-type at $P<0.001$ (one-way ANOVA with Games-Howell *post-hoc* test for genotype). ND, not determined. Error bars are the standard error of the mean. (C) Dauer formation in the indicated strains in the presence of the indicated pheromones at 25ºC with 160 μg heat-killed OP50. The indicated transgenes were amplified from wild-type genomic DNA and injected into *oy104* mutants. *** represents different from wild-type at $P<0.001$ (one-way ANOVA with Games-Howell *post-hoc* test for genotype). ND, not determined. N.S., not significantly different. Error bars are the standard error of the mean. (D) Diagram of the *F28H1.1* genomic locus; black bars represent the coding sequence and white bars indicate untranslated regions. A missense mutation results in a serine to glycine codon conversion at the indicated positon, in the *oy104* strain.

Figure 2.4. The *oy105* mutation is a premature stop codon in *qui-1*.

(A) Dauer formation profile of *oy105* mutants in comparison to wild-type and ASK-ablated animals. Each bar represents the average of at least two independent trials and each assay plate contained >65 worms. This is the graphical representation of data found in Table 2.1; error bars are omitted for clarity. (B) Dauer formation in the indicated strains, in the presence of the

indicated pheromones at 25ºC with 160 μg heat-killed OP50. The indicated transgenes were amplified from wild-type genomic DNA and injected into *oy105* mutants, with the exception of *qui-1* which was injected as a fosmid. *, ** and *** represent different from wild-type at $P<0.05$, 0.01 and 0.001, respectively; $^{\#\#}$ represents different from *oy105* at $P<0.01$ (one-way ANOVA with Games-Howell *post-hoc* test for genotype). N.S., not significantly different. Error bars are the standard error of the mean. (C) Diagram of the *qui-1* genomic locus; thick bars are exons, thin lines are introns, black bars represent the coding sequence and white bars indicate untranslated regions. The region shaded in grey indicates the conserved WB40 repeats. A nonsense mutation in the *oy105* strain lies upstream of these repeats, as does the independent *gb404* nonsense mutation that was obtained for comparison. (D) Dauer formation in the indicated strains in the presence of the indicated pheromones at 25ºC with 160 μg heat-killed OP50. *, ** and *** represent different from wild-type at $P<0.05$, 0.01 and 0.001, respectively (one-way ANOVA with Games-Howell *post-hoc* test for genotype). N.S. not significantly different. Error bars are the standard error of the mean. (E) Dauer formation in the indicated strains, in the presence of the indicated pheromone at 25ºC with 160 μg heat-killed OP50. The *qui-1* cDNA was subcloned into cell specific expression vectors (ASK: *sra-9*p; ASH: *sra-6*p; ADL: *sre-1*Δp) and injected into *oy105* mutants; ASH+ADL was achieved by injecting both plasmids. ** and *** represent different from wild-type at $P<0.01$ and 0.001, respectively; $^{\#}$ represents different from *oy105* at $P<0.05$ (one-way ANOVA with Games-Howell *post-hoc* test for genotype). Error bars are the standard error of the mean.

Figure 2.5. The *oy106* mutation may be a premature stop codon in *che-12*.

(A) Dauer formation profile of *oy106* mutants in comparison to wild-type and ASK-ablated animals. Each bar represents the average of at least two independent trials and each assay plate contained >65 worms. This is the graphical representation of data found in Table 2.1; error bars are omitted for clarity. (B) Diagram of the *che-12* genomic locus including the four annotated splice variants (a-d); thick bars are exons, thin lines are introns, black bars represent the coding sequence and white bars indicate untranslated regions. The region shaded in grey indicates the conserved HEAT repeats. A nonsense mutation in the *oy106* strain lies upstream of these repeats but is predicted to only affect the a and b isoforms. The *e1812* reference allele mutation causes a G to A substitution in a conserved splice donor (SD) site, affecting all isoforms. (C) Dauer formation in the indicated strains, in the presence of the indicated pheromones at 25ºC with 160 µg heat-killed OP50. The *che-12* genomic locus was amplified from wild-type genomic DNA and injected into *oy106* mutants. *, ** and *** represent different from wild-type at $P<0.05$, 0.01 and 0.001, respectively; $^{###}$ represents different from *oy106* at $P<0.001$ (one-way ANOVA with Games-Howell *post-hoc* test for genotype). N.S., not significantly different. Error bars are the standard error of the mean.

Figure 2.6. The *oy107* mutation is a premature stop codon in *phd-1* (formerly *F32B6.10*).

(A) Dauer formation profile of *oy107* mutants in comparison to wild-type and ASK-ablated animals. Each bar represents the average of at least two independent trials and each assay plate contained >65 worms. This is the graphical representation of data found in Table 2.1; error bars are omitted for clarity. (B) Dauer formation in the indicated strains, in the presence of the indicated pheromones at 25ºC with 160 µg heat-killed OP50. The *F32B6.10* genomic locus was

amplified from wild-type genomic DNA and injected into *oy107* mutants. ** and *** represent different from wild-type at $P<0.01$ and 0.001, respectively; # represents different from *oy107* at $P<0.05$ (one-way ANOVA with Games-Howell *post-hoc* test for genotype). N.S., not significantly different. Error bars are the standard error of the mean. (C) Diagram of the *F32B6.10* genomic locus, depicting the a and b isoforms, and the *W01B6.2* genomic locus; thick bars are exons, thin lines are introns, black bars represent the coding sequence and white bars indicate untranslated regions. The region shaded in grey indicates the conserved casein kinase I-family kinase domain and the predicted active site is marked in orange with an asterisk. A nonsense mutation in the *oy107* strain lies upstream of the kinase active site; regions affected by independent deletion alleles are also illustrated. (D) Dauer formation in the indicated strains in the presence of the indicated pheromones at 25ºC with 160 μg heat-killed OP50. *, ** and *** represent different from wild-type at $P<0.05$, 0.01 and 0.001, respectively (one-way ANOVA with Games-Howell *post-hoc* test for genotype). N.S. not significantly different. Error bars are the standard error of the mean. (E) Dauer formation in the indicated strains, in the presence of the indicated pheromone at 25ºC with 160 μg heat-killed OP50. The *F32B6.10* and *W10B6.2* cDNAs were subcloned into cell specific expression vectors (ASK: *sra-9*p; ASI: *srg-47*p; ASE+AWC: *ceh-36*p) and injected into the respective mutants. * and ** represent different from wild-type at $P<0.05$ and 0.01, respectively (one-way ANOVA with Games-Howell *post-hoc* test for genotype). Error bars are the standard error of the mean.

Figure 2.7. The *oy108* mutation may represent a deletion in *maco-1*.

(A) Dauer formation profile of *oy108* mutants in comparison to wild-type and ASK-ablated animals. Each bar represents the average of at least two independent trials and each assay plate

contained >65 worms. This is the graphical representation of data found in Table 2.1; error bars are omitted for clarity. (B) Diagram of the *maco-1* genomic locus; thick bars are exons, thin lines are introns, black bars represent the coding sequence and white bars indicate untranslated regions. The region shaded in grey indicates the conserved macoilin domain. A deletion in the *oy108* strain removes the upstream portion of the gene, while the *ok3165* internal deletion allele was obtained for comparison. (C) Dauer formation in the indicated strains, in the presence of the indicated pheromones at 25ºC with 160 μg heat-killed OP50. ** and *** represent different from wild-type at $P<0.01$ and 0.001, respectively (one-way ANOVA with Games-Howell *post-hoc* test for genotype). N.S., not significantly different. Error bars are the standard error of the mean. (D) Dauer formation in the indicated strains in the presence of the indicated pheromones at 25ºC with 160 μg heat-killed OP50. The indicated transgenes were amplified from wild-type genomic DNA and injected into *oy108* mutants. ** represents different from wild-type at $P<0.01$; ## represents different from *oy108* at $P<0.01$ (one-way ANOVA with Games-Howell *post-hoc* test for genotype). ND, not determined. N.S., not significantly different. Error bars are the standard error of the mean.

Figure 2.8. Summary of findings related to the *oy109* allele.

(A) Dauer formation profile of *oy109* mutants in comparison to wild-type and ASK-ablated animals. Each bar represents the average of at least two independent trials and each assay plate contained >65 worms. This is the graphical representation of data found in Table 2.1; error bars are omitted for clarity. (B) Diagram of the *snx-14* genomic locus including the two annotated splice variants (a and b); thick bars are exons, thin lines are introns, black bars represent the coding sequence and white bars indicate untranslated regions. The region shaded in grey

indicates the conserved PXA (PHOX-associated) domain, the area shaded in green indicates the RGS (regulator of G protein signaling) domain and the region shaded in yellow indicates the PHOX (phosphoinositide binding) domain. A nonsense mutation in the *oy108* strain is likely to affect only the a isoform. (C) Dauer formation in the indicated strains, in the presence of the indicated pheromones at 25ºC with 160 μg heat-killed OP50. The *snx-14* genomic locus was amplified from wild-type genomic DNA and injected into *oy108* mutants. *, ** and *** represent different from wild-type at $P<0.05$, 0.01 and 0.001, respectively (one-way ANOVA with Games-Howell *post-hoc* test for genotype). N.S., not significantly different. Error bars are the standard error of the mean.

Figure 2.9. A model with the proposed sites of action of the cloned genes.

Based on their putative molecular functions, each of the cloned genes has been inserted into our model of ascaroside signal transduction. The precise roles for these molecules and their cellular sites of action with respect to ascaroside signaling are currently under study.

Table 2.1. Dauer Formation in Focus Strains

Mutant[a]	isolate[b]/ *allele*	pheno[c]	EtOH[d]	ascr#8 (nM)			ascr#5 (nM)			icas#9 (nM)			ascr#2 (nM)			ascr#3 (nM)		
			0	6	60	600	60	600	6000	6	60	600	60	600	6000	60	600	6000
N2	Bristol		0.05 ±0.02	0.29 ±0.05	0.63 ±0.05	0.89 ±0.02	0.16 ±0.07	0.96 ±0.02	0.97 ±0.02	0.68 ±0.12	0.87 ±0.07	0.71 ±0.07	0.49 ±0.08	0.73 ±0.1	0.8 ±0.04	0.39 ±0.1	0.7 ±0.16	0.95 ±0.01
*str-3*p:: *gfp*	*kyIs128*	early hatch	0.03 ±0.01	0.34 ±0.06	0.58 ±0.06	0.83 ±0.04	0.17 ±0.04	0.88 ±0.03	0.91 ±0.04	0.6 ±0.09	0.71 ±0.11	0.8 ±0.06	0.45 ±0.06	0.68 ±0.05	0.79 ±0.03	0.49 ±0.1	0.75 ±0.07	0.95 ±0.02
srbc-64; srbc-66	*tm1946; tm2943*		0.01 ±0	0.09 ±0.06	0.26 ±0.08	0.53 ±0.08	0.03 ±0	0.64 ±0.06	0.87 ±0	0.01 ±0.02	0.1 ±0.06	0.1 ±0.07	0.21 ±0.04	0.42 ±0.06	0.46 ±0.05	0.04 ±0.02	0.16 ±0.04	0.51 ±0.06
gpa-2; gpa-3	*pk16; pk35*		0.05 ±0.01	0.12 ±0.04	0.26 ±0.06	0.64 ±0.06	0.28 ±0.09	0.33 ±0.07	0.39 ±0.08	0.4 ±0.27	0.46 ±0.28	0.43 ±0.33	0.15 ±0.03	0.4 ±0.05	0.44 ±0.06	0.16 ±0.12	0.19 ±0.08	0.54 ±0.18
ASK-ablated	*qrIs2*		0	0.08 ±0.03	0.16 ±0.04	0.48 ±0.07	0.1 ±0.03	0.71 ±0.08	0.74 ±0.04	0.04 ±0.02	0.1 ±0.06	0.04 ±0.02	0.01 ±0.01	0.11 ±0.02	0.22 ±0.04	0.03 ±0.01	0.14 ±0.01	0.33 ±0.02
K3	5-1/ *oy103*		0	0.02 ±0.01	0.07 ±0.09	0.23 ±0.06	0.03 ±0.02	0.63 ±0.02	0.93 ±0.06	0.02 ±0.01	0.05 ±0.01	0.02 ±0.01	0.03 ±0.01	0.19 ±0.04	0.36 ±0.06	0	0.02 ±0.01	0.24 ±0.02
K10	24-3/ *oy104*		0	0.05 ±0.04	0.39 ±0.15	0.66 ±0.1	0.01 ±0.01	0.4 ±0.2	0.66 ±0.18	-	0.23 ±0.05	-	0.22 ±0.09	0.47 ±0.06	0.35 ±0.05	0	0	0.03 ±0.02
K15	8-1/ *oy105*		0.12 ±0.08	0.33 ±0.17	0.52 ±0.17	0.58 ±0.15	0.01 ±0.01	0.67 ±0.02	0.66 ±0.03	0.15 ±0.03	0.29 ±0.03	0.49 ±0.12	0.23 ±0.14	0.49 ±0.08	0.44 ±0.1	0.09 ±0.1	0.23 ±0.01	0.66 ±0.07
K18	14-3/ *oy106*		0.03 ±0.03	0.02 ±0.02	0.21 ±0.11	0.54 ±0.18	0.06 ±0.06	0.72 ±0.21	0.78 ±0.1	0.03 ±0.01	0.21 ±0.14	0.7 ±0.02	0.01 ±0	0.11 ±0.02	0.4 ±0.08	0.31 ±0.14	0.55 ±0.16	0.76 ±0.11
K23	10-3/ *oy107*		0	0.21 ±0.06	0.37 ±0.11	0.67 ±0.06	0.01 ±0.02	0.47 ±0.19	0.49 ±0.09	0.08 ±0	0.14 ±0.06	0.11 ±0.01	0.31 ±0.05	0.43 ±0.05	0.55 ±0.29	0.05 ±0.07	0.2 ±0.29	0.45 ±0.08
K1	1-6/ *oy108*	*lon*, early hatch	0.03 ±0.02	0.03 ±0.03	0.27 ±0.2	0.53 ±0.15	0.31 ±0.05	0.53 ±0.11	0.68 ±0.07	0.04 ±0.02	0.27 ±0.04	0.06 ±0.08	0.17 ±0.08	0.24 ±0.07	0.36 ±0.1	0.1 ±0.03	0.32 ±0.2	0.84 ±0.04
K6	14-1/ *oy109*	social	0.05 ±0.03	0.02 ±0.02	0.04 ±0.04	0.14 ±0.05	0.16 ±0.04	0.05 ±0.01	0.13 ±0.01	-	0.02 ±0.01	-	0.06 ±0.06	0.02 ±0.02	0.1 ±0.06	-	-	-

[a] Dauer formation was assessed under the listed conditions and data are presented as the mean +/- standard error of the mean. At least two independent assays were scored. (-) not determined.

[b] The isolate number corresponds to the original frozen isolate from the screen.

[c] Potentially pleiotropic and/or independent phenotypes observed in the given strain. early hatch - embryos hatch less than 6 hours after egg lay; social - worms aggregate, also known as clumpy.

[d] Ethanol is the diluent used for the various ascarosides and is used as a negative control.

Table 2.2. Summary of Linkage Mapping

Mutant	*str-3*p::GFP Repression trial 1	*str-3*p::GFP Repression trial 2	Dauer Formation/ Balancer Chromosome trial 1	Dauer Formation/ Balancer Chromosome trial 2	3-Factor Mapping trial 1	Probable Linkage [a]
oy103	II/III	II/IV/V	II/V	II	-	II
oy104	I/V	V	I/II	I/II	-	I
oy105	II/III/IV	IV	III/IV	IV	-	IV
oy106	III/IV	IV/V	IV/V	IV/V	-	V
oy107	III/IV	IV	III/IV	V	-	IV
oy108	-	-	-	-	right of *dpy-5* left of *unc-29*	I
oy109	-	-	-	-	end of II	II

[a] Linkage was assessed as defined in Methods. (-) not determined. Probable linkage is based on quantitative and qualitative weighting of results from each trial and method.

Table 2.3. Whole-genome Resequencing Metrics

Mutant	*oy103*	*oy104*	*oy105*	*oy106*	*oy107*	*oy108*	*oy109*
Average Genome Coverage[a]	29.7X	33.2X	23.1X	23.3X	32.6X	33.8X	36.8X
Variants[b]	3659	3783	3783	3767	3735	3670	7190
Coding Variants[c]	317	345	341	312	370	244	356
Unique Variants[d]	102	118	129	97	148	31	132
High Quality Variants (G>A)[e]	71(66)	77(74)	88(79)	47(41)	92(87)	2(1)	78(73)
Unique Nonsense Mutations[f]	4	3	8	3	3	0	4
Unique Uncovered Regions[g]	1	2	13	12	14	18	230

[a] Average depth of read coverage across unique regions in the genome.

[b] Total number of variants detected with respect to the N2 reference genome.

[c] Total number of variants affecting coding regions of the genome.

[d] Variants common to three or more strains were considered to be inherent to the parent strain.

[e] Variants supported by at least five overlapping consensus reads. In parentheses are the number of such variants that are G>A substitutions, which are characteristic of the mechanism of action of EMS mutagenesis.

[f] Variants which are predicted to induce a premature termination codon in at least one isoform of a given coding locus.

[g] Genic regions for which there is no sequence coverage in the given strain, but which are not explained by the general lack of sequence coverage in all strains due to problems mapping reads to that region.

Table 2.4. Candidate Mutant Loci

Mutant	Candidate Gene	Mutation[a]	Mapped LG[b]	Conservation[c]	Function(domains)[d]	Notes[e]
oy103	*cec-3*	PTC (W>Stop)	Y	broad	(chomodomain)	regulation of motor neuron fate
	T05C1.1	PTC (Q>Stop)	Y	*Caenorhabditis*		
	C01G12.7	PTC (W>Stop)	Y	*Caenorhabditis*	purine-cytosine permease	
	C06G3.4	PTC (W>Stop)	N			pseudogene
	nhr-142	SA	N	broad	nuclear hormone receptor	increased lipid storage
	col-43	SD	N	broad	collagen	enriched in L2D
oy104	*mks-6*	PTC (W>Stop)	Y	broad	ciliary transition zone	phneotypically wt
	obr-1	PTC (R>Stop)	N	broad	oxysterol binding protein	sensitive to pore-forming toxin
	lgc-36	PTC (R>Stop)	N	broad	ligand-gated chloride channel	GABA-A-like; lethal/sterile
	F28H1.1	missense (S>G)	Y	*Caenorhabditis*		
	asic-1	missense (C>T)	Y	broad	amiloride-sensitive sodium channel	defect in starvation-paired learning
	B0034.5	deletion	Y	broad	neuropeptide receptor	7-transmembrane predicted
	noca-1	SD	N	broad	non-centrosomal microtubule array	meiosis, receptor-mediated endocytosis
oy105	*qui-1*	PTC (W>Stop)	Y	invertebrate	(WD40)(coronin)	bitter avoidance
	Y57A10A.31	PTC (Q>Stop)	N	broad	E3 ligase (ring finger)	polyubiquitylation
	R10E4.6	PTC (W>Stop)	N	*Caenorhabditis*		
	R13A5.7	PTC (Q>Stop)	N	*Caenorhabditis*		
	F52D2.6	PTC (W>Stop)	X			
	T01B6.3a	PTC (Q>Stop)	X			
	T32F2.2	PTC (Q>Stop)	X			
	C45D1.2	PTC (L>Stop)	X			
oy106	*hum-2*	PTC (Q>Stop)	Y	broad	unconventional myosin	
	che-12	PTC (W>Stop)	Y	broad	(HEAT)	channel cilia development
	F09C8.1	PTC (K>Stop)	X			
	F49C12.6	SD	N	broad	(DUF1632)	sugar transport
oy107	*F32B6.10*	PTC (Q>Stop)	Y	broad	tau-tubulin kinase	cilia development
	F32A5.3	PTC (W>Stop)	N	broad	serine carboxypeptidase	lysosomal protective protein
	T04F3.1	PTC (Q>Stop)	N	broad	aspartate-amino transferase	structural maintenance of chromosomes
oy108	*maco-1*	deletion	Y	broad	macoilin	sensory neuron function
	T08B2.3	deletion	Y			pseudogene
oy109	*snx-14*	PTC (Q>Stop)	Y	broad	sorting nexin	regulation of G-protein signaling
	Y44E3A.4	PTC (L>Stop)	N	broad	(SH3)	lethal/sterile
	unc-54	PTC (R>Stop)	N	broad	myosin heavy chain	
	T21E8.4	PTC (W>Stop)	X			

[a] The predicted effect of the mutation on the coding sequence. PTC - premature termination codon; SA - splice acceptor; SD - splice donor.

[b] Candidate loci within the predicted linkage group are indicated by "Y" and those that are not by "N". "X" identifies X-linked loci which were not considered.

[c,d,e] Characterization of the conservation, molecular function, conserved domains and other functional annotations of the proteins predicted to be encoded by the given loci. Evidence are based on BLASTP searches of the amino acid for the longest encoded isoform of the locus and on other phenotypic annotations which appear in WormBase (www.wormbase.org).

Figure 2.1

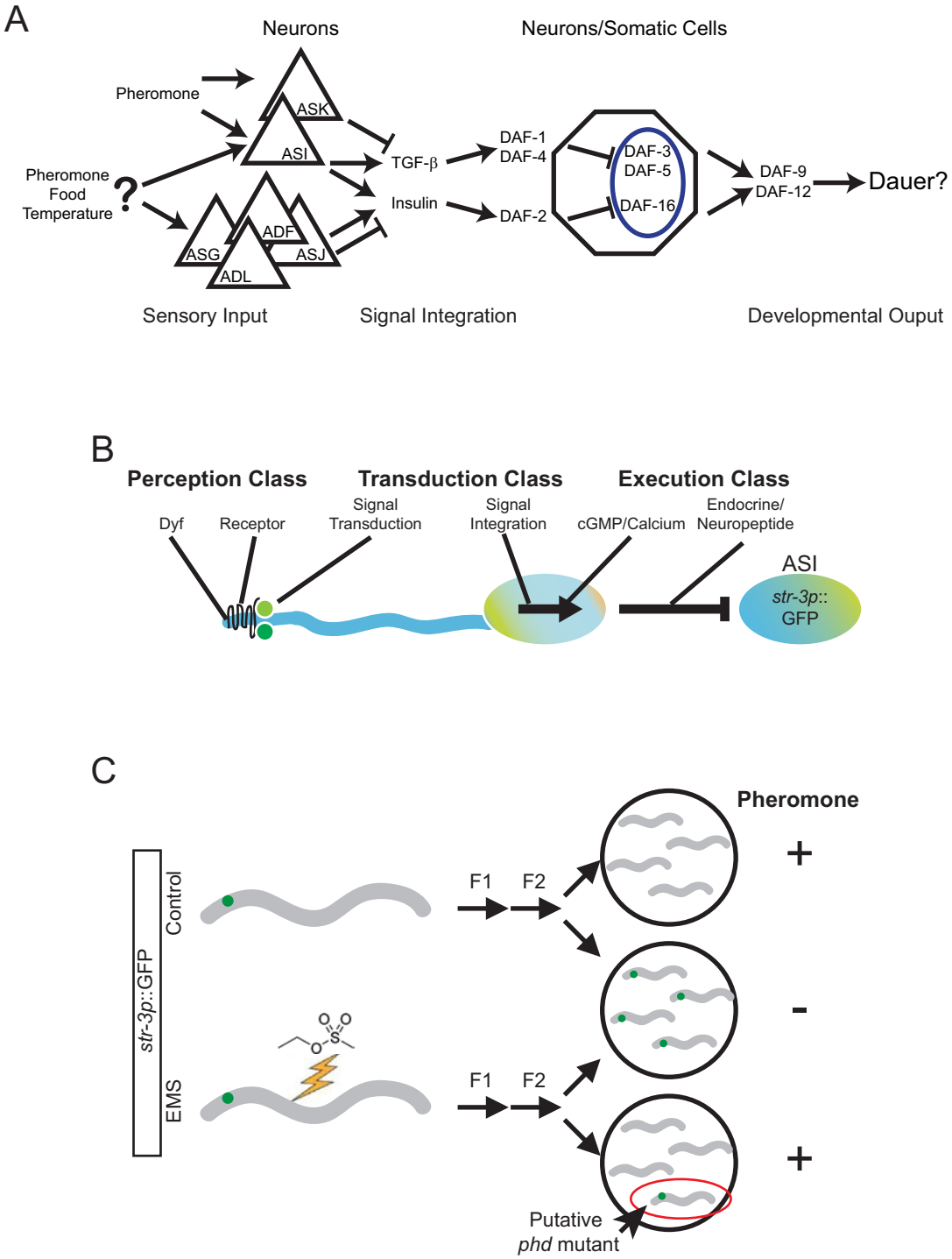
A
Neurons
Neurons/Somatic Cells
Pheromone
Pheromone
Food
Temperature
?
ASK
ASI
ADF
ASG
ASJ
ADL
TGF-β
Insulin
DAF-1
DAF-4
DAF-2
DAF-3
DAF-5
DAF-16
DAF-9
DAF-12
Dauer?
Sensory Input
Signal Integration
Developmental Ouput
B
Perception Class
Transduction Class
Execution Class
Dyf
Receptor
Signal
Transduction
Signal
Integration
cGMP/Calcium
Endocrine/
Neuropeptide
ASI
str-3p::
GFP
C
Pheromone
str-3p::GFP
Control
EMS
F1
F2
F1
F2
+
-
+
Putative
phd mutant

Figure 2.2

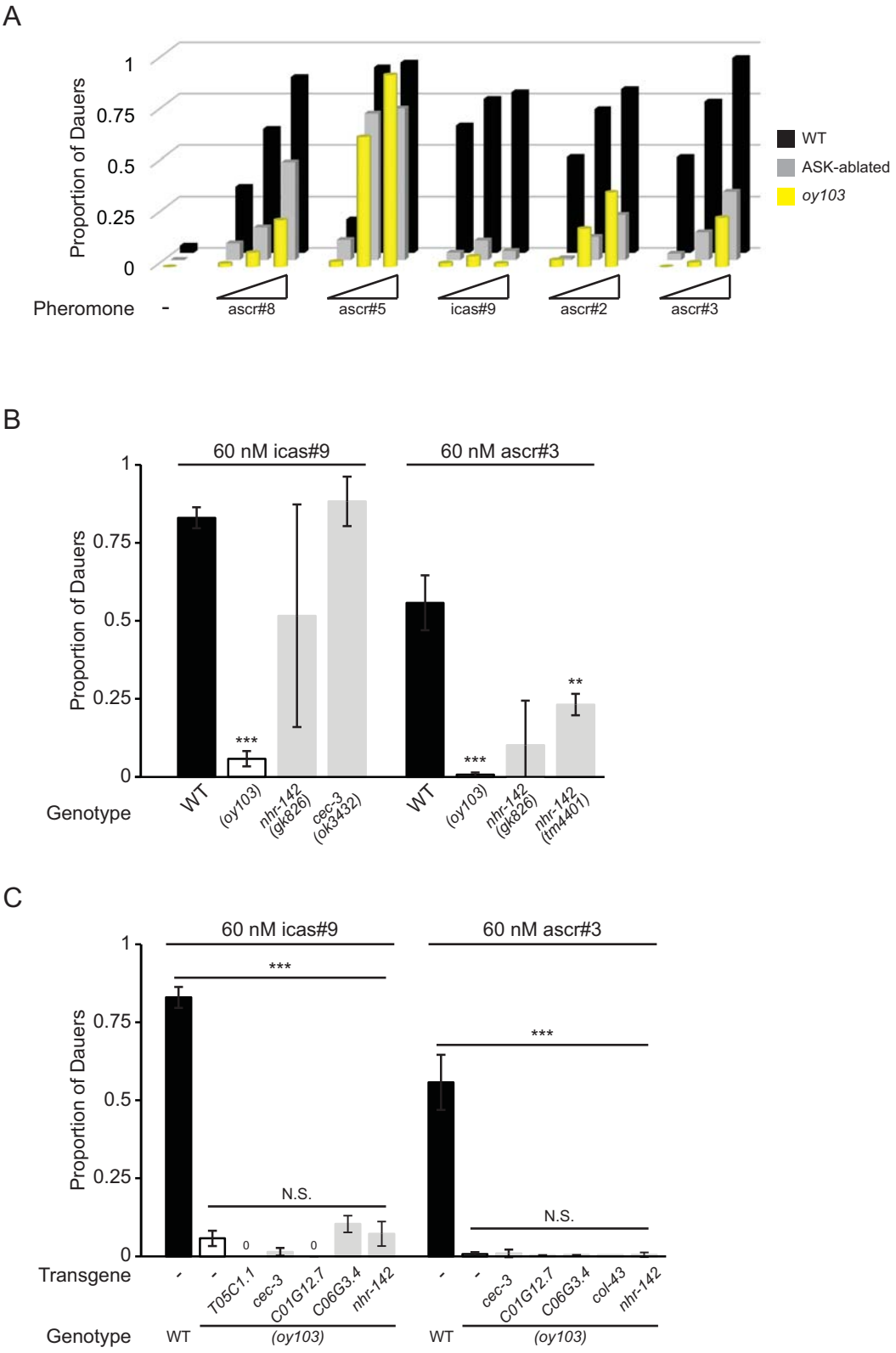
A
Proportion of Dauers
1
0.75
0.5
0.25
0
Pheromone
-
ascr#8
ascr#5
icas#9
ascr#2
ascr#3
WT
ASK-ablated
oy103
B
60 nM icas#9
60 nM ascr#3
Proportion of Dauers
***
**
Genotype
WT
(oy103)
nhr-142 (gk826)
cec-3 (ok3432)
nhr-142 (tm4401)
C
N.S.
Transgene
T05C1.1
cec-3
C01G12.7
C06G3.4
nhr-142
col-43
(oy103)

Figure 2.3

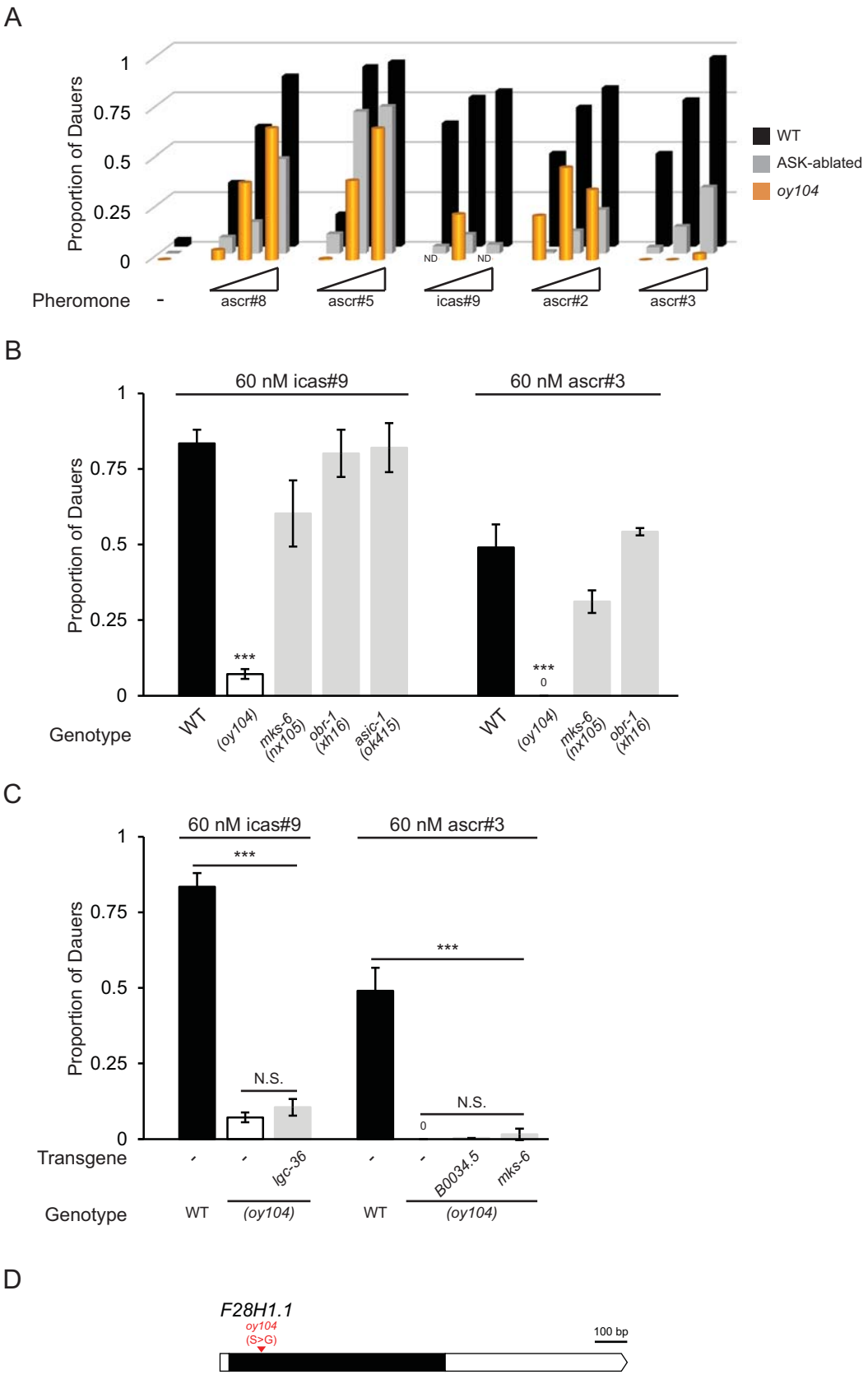
A
Proportion of Dauers
1
0.75
0.5
0.25
0
ND
ND
Pheromone
-
ascr#8
ascr#5
icas#9
ascr#2
ascr#3
WT
ASK-ablated
oy104
B
60 nM icas#9
60 nM ascr#3
Proportion of Dauers
***
***
0
Genotype
WT
(oy104)
mks-6 (nx105)
obr-1 (xh16)
asic-1 (ok415)
C
60 nM icas#9
60 nM ascr#3
***
***
N.S.
N.S.
0
Transgene
lgc-36
B0034.5
mks-6
Genotype
WT
(oy104)
D
F28H1.1
oy104
(S>G)
100 bp

Figure 2.4

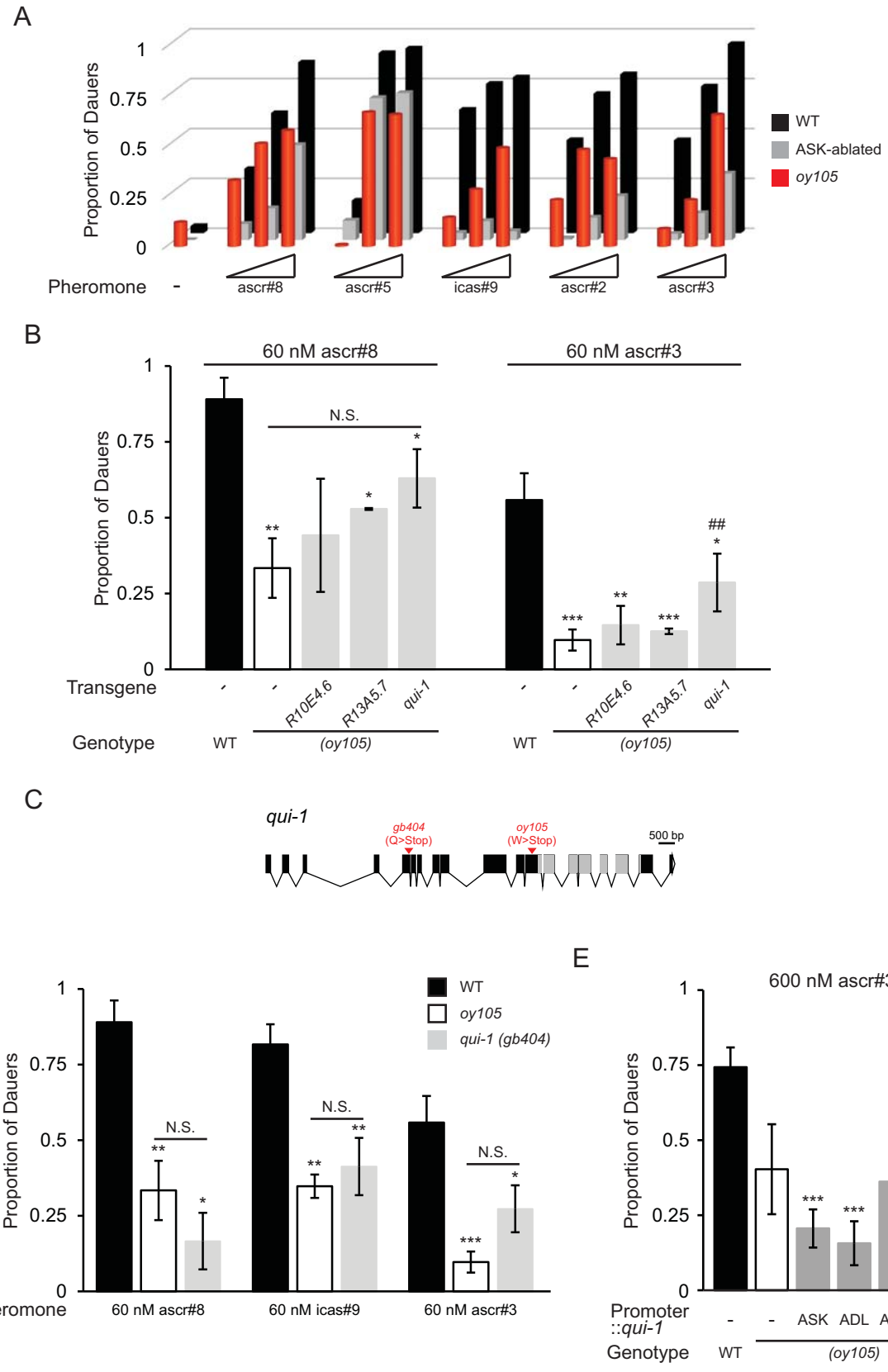
A
Proportion of Dauers
1
0.75
0.5
0.25
0
Pheromone
-
ascr#8
ascr#5
icas#9
ascr#2
ascr#3
WT
ASK-ablated
oy105
B
60 nM ascr#8
60 nM ascr#3
N.S.
Proportion of Dauers
Transgene
-
-
R10E4.6
R13A5.7
qui-1
Genotype
WT
(oy105)
C
qui-1
gb404
(Q>Stop)
oy105
(W>Stop)
500 bp
D
WT
oy105
qui-1 (gb404)
Proportion of Dauers
N.S.
Pheromone
60 nM ascr#8
60 nM icas#9
60 nM ascr#3
E
600 nM ascr#3
Proportion of Dauers
Promoter
::qui-1
-
ASK
ADL
ASH
ADL+
ASH
Genotype
WT
(oy105)

Figure 2.5

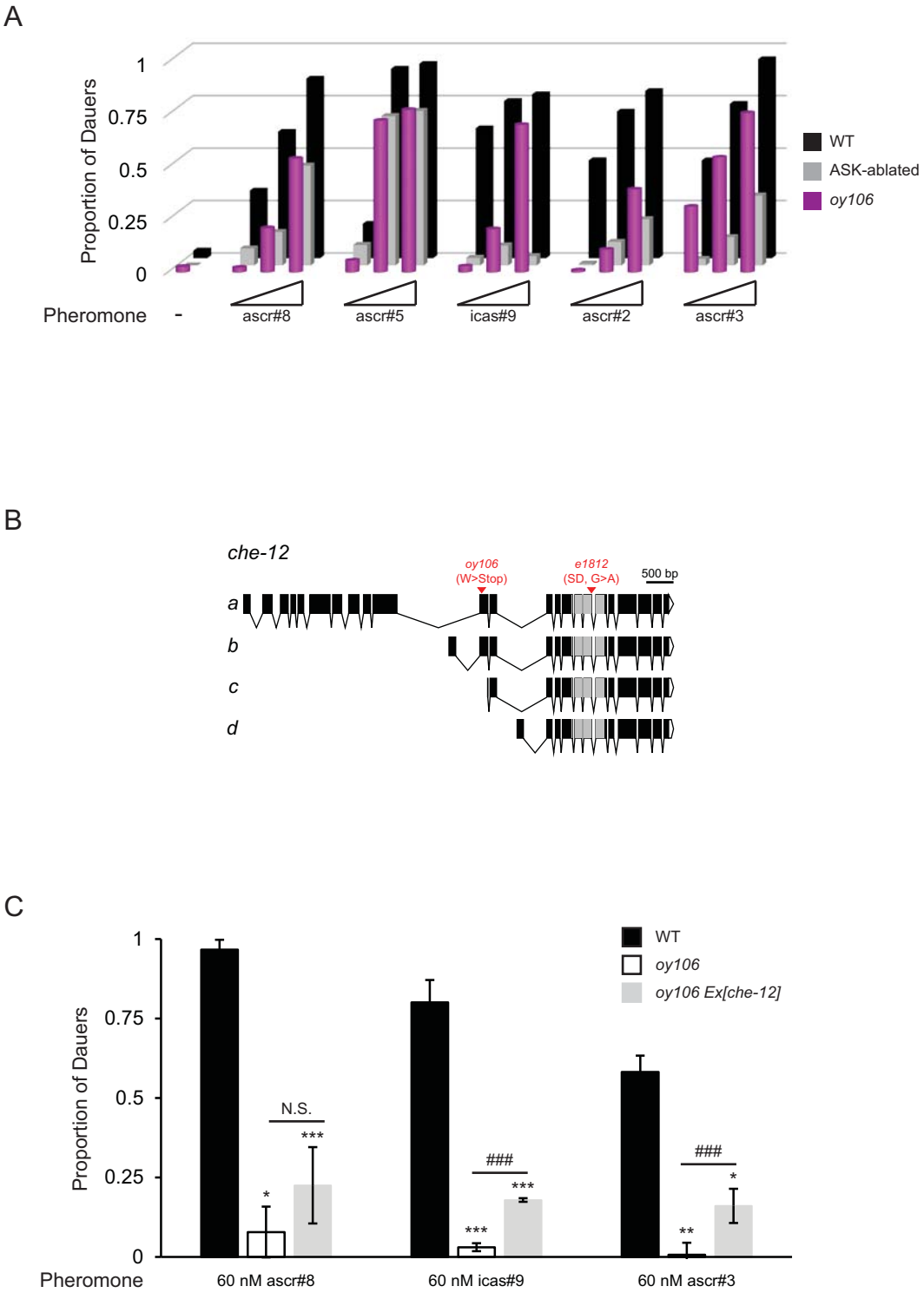
A
Proportion of Dauers
1
0.75
0.5
0.25
0
Pheromone
-
ascr#8
ascr#5
icas#9
ascr#2
ascr#3
WT
ASK-ablated
oy106
B
che-12
oy106
(W>Stop)
e1812
(SD, G>A)
500 bp
a
b
c
d
C
Proportion of Dauers
1
0.75
0.5
0.25
0
WT
oy106
oy106 Ex[che-12]
N.S.
*
***
###
***
***
###
*
**
Pheromone
60 nM ascr#8
60 nM icas#9
60 nM ascr#3

Figure 2.6

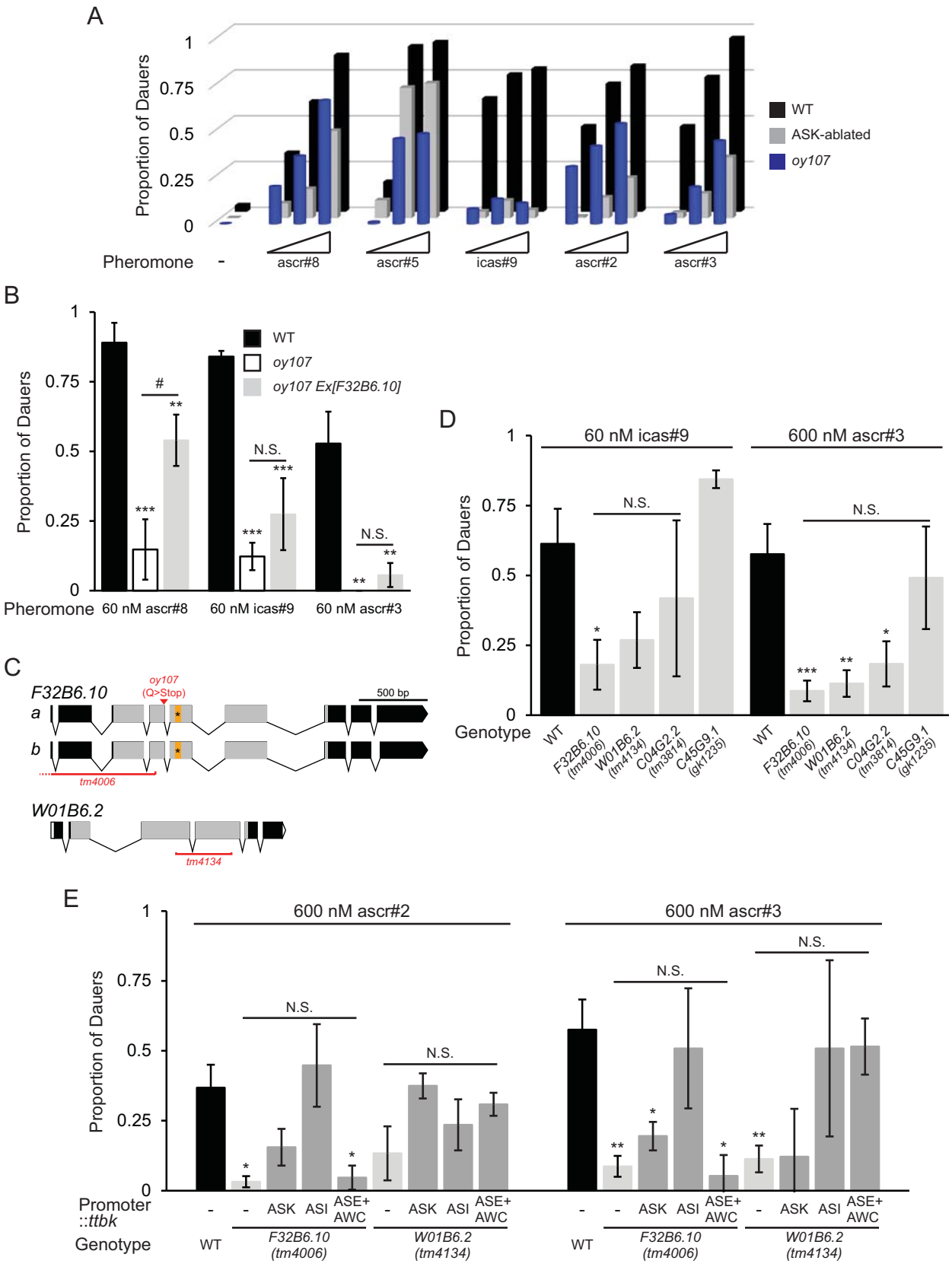
A
Proportion of Dauers
1
0.75
0.5
0.25
0
WT
ASK-ablated
oy107
Pheromone
-
ascr#8
ascr#5
icas#9
ascr#2
ascr#3
B
Proportion of Dauers
WT
oy107
oy107 Ex[F32B6.10]
#
**
***
N.S.
Pheromone
60 nM ascr#8
60 nM icas#9
60 nM ascr#3
C
F32B6.10
oy107
(Q>Stop)
500 bp
a
b
tm4006
W01B6.2
tm4134
D
60 nM icas#9
600 nM ascr#3
Proportion of Dauers
N.S.
*
**
***
Genotype
WT
F32B6.10 (tm4006)
W01B6.2 (tm4134)
C04G2.2 (tm3814)
C45G9.1 (gk1235)
E
600 nM ascr#2
600 nM ascr#3
Proportion of Dauers
N.S.
Promoter ::ttbk
-
ASK
ASI
ASE+ AWC
Genotype
WT
F32B6.10 (tm4006)
W01B6.2 (tm4134)

Figure 2.7

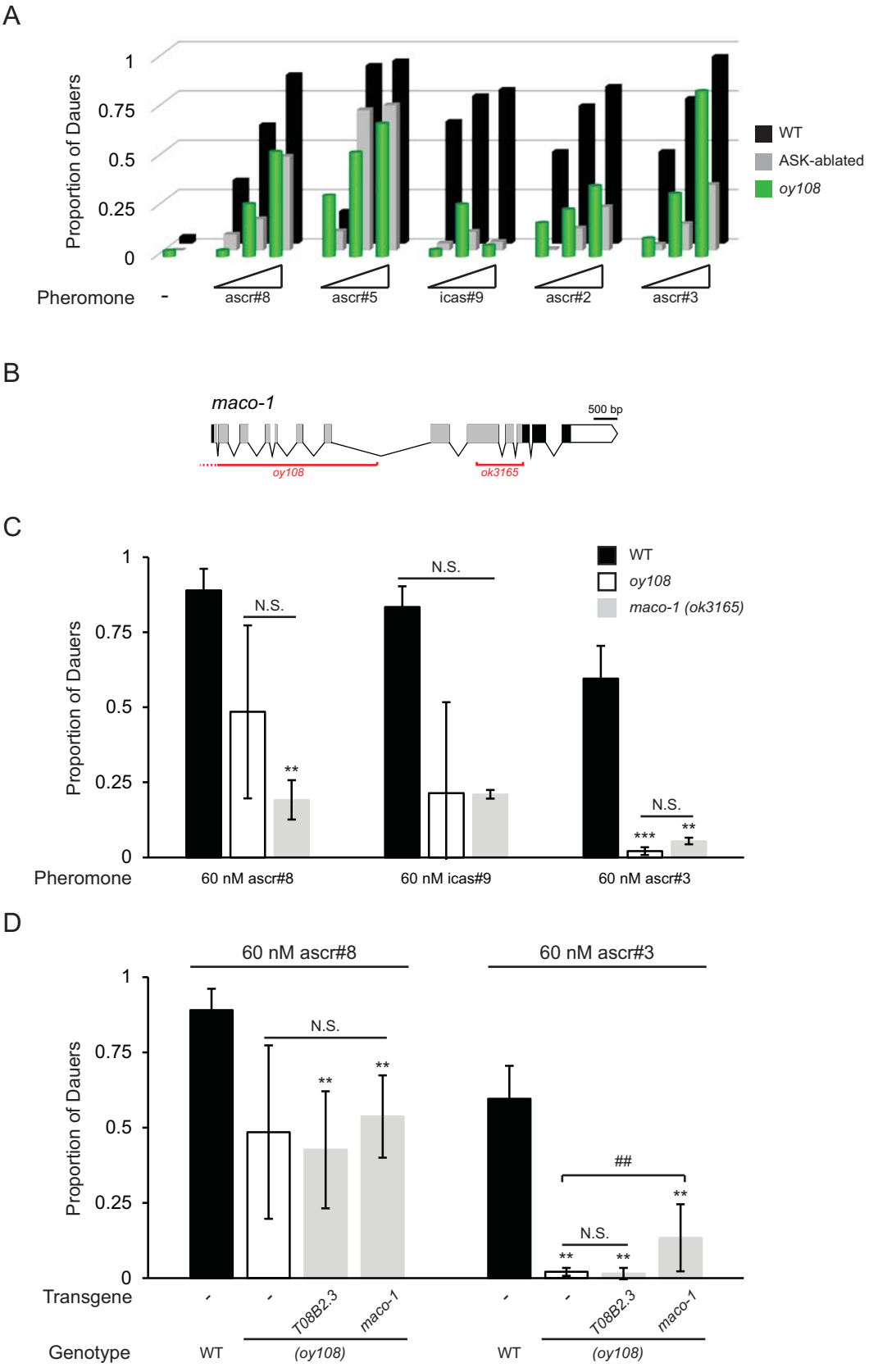
A
Proportion of Dauers
1
0.75
0.5
0.25
0
Pheromone
-
ascr#8
ascr#5
icas#9
ascr#2
ascr#3
WT
ASK-ablated
oy108
B
maco-1
500 bp
oy108
ok3165
C
Proportion of Dauers
N.S.
N.S.
**
***
**
WT
oy108
maco-1 (ok3165)
Pheromone
60 nM ascr#8
60 nM icas#9
60 nM ascr#3
D
60 nM ascr#8
60 nM ascr#3
Proportion of Dauers
N.S.
**
**
##
N.S.
**
**
Transgene
-
-
T08B2.3
maco-1
Genotype
WT
(oy108)

Figure 2.8

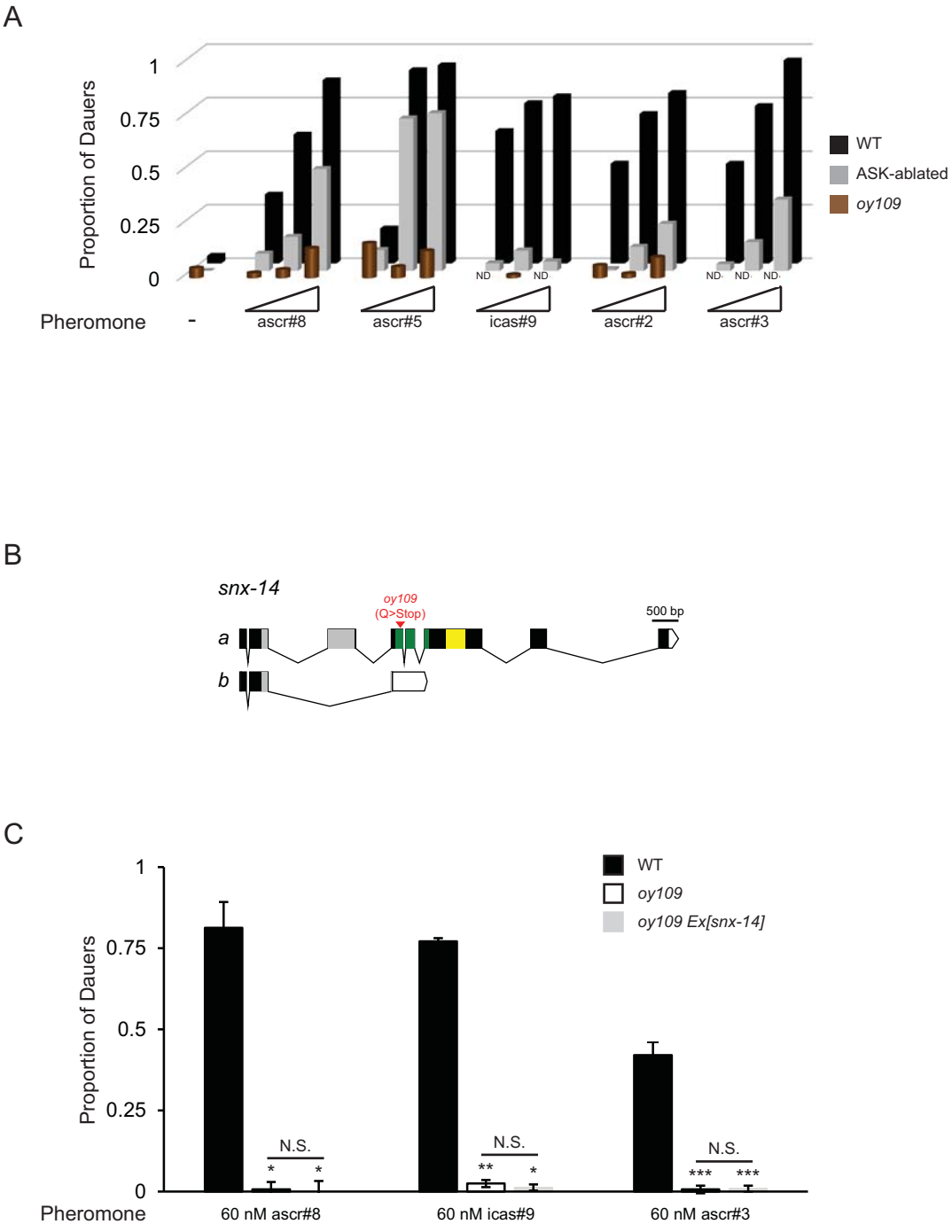
A
Proportion of Dauers
1
0.75
0.5
0.25
0
ND
ND
ND
ND
ND
Pheromone
-
ascr#8
ascr#5
icas#9
ascr#2
ascr#3
WT
ASK-ablated
oy109
B
snx-14
oy109
(Q>Stop)
500 bp
a
b
C
Proportion of Dauers
1
0.75
0.5
0.25
0
N.S.
N.S.
N.S.
*
*
**
*
***
***
Pheromone
60 nM ascr#8
60 nM icas#9
60 nM ascr#3
WT
oy109
oy109 Ex[snx-14]

Figure 2.9

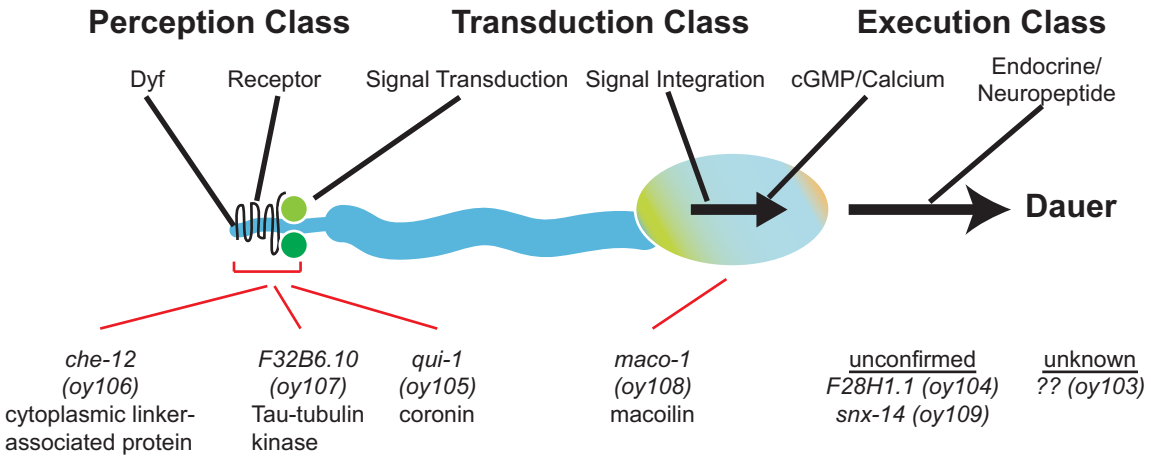
Perception Class
Transduction Class
Execution Class
Dyf
Receptor
Signal Transduction
Signal Integration
cGMP/Calcium
Endocrine/
Neuropeptide
Dauer
che-12
(oy106)
cytoplasmic linker-
associated protein
F32B6.10
(oy107)
Tau-tubulin
kinase
qui-1
(oy105)
coronin
maco-1
(oy108)
macoilin
unconfirmed
F28H1.1 (oy104)
snx-14 (oy109)
unknown
?? (oy103)

2.9 Supplemental Figure Legend

Figure S2.1. Expression patterns of putative *ttbk* genes involved in dauer formation. Transgenic strains were constructed by fusing the upstream regulatory sequence of *F32B6.10*, *W01B6.2* or *C04G2.2* to the coding sequence for green fluorescent protein. Strains were imaged on a spinning disk confocal microscope. Preliminary identification of GFP-expressing cells was made by cell body position and by overlap and/or relative position to the stereotyped cells which fill with DiI.

Table S2.1. Dauer Formation in EMS Mutants

Mutant[a]	isolate[b]/*allele*	*str-3*p ::GFP[c]	phenotype[d]	EtOH[e]	ascr#8 (nM)			ascr#5 (nM)			icas#9 (nM)			ascr#2 (nM)			ascr#3 (nM)		
				0	6	60	600	60	600	6000	6	60	600	60	600	6000	60	600	6000
*str-3*p::*gfp*	*ky1s128*	+	early hatch	<+	++	++	+++	+	+++	+++	++	+++	+++	++	++	+++	++	+++	+++
K1	1-6/*oy108*	+++	*lon*, early hatch	<+	<+	+	++	++	++	++	<+	+	<+	+	+	++	<+	++	+++
K2	4-4	++	*egl*	<+	0	-	+	<+	<+	<+	-	-	-	0	<+	0	-	-	-
K3	5-1/*oy103*	++		0	<+	<+	+	<+	++	+++	<+	<+	<+	<+	+	++	0	<+	+
K4	5-2	++	social, *egl*	0	0	-	0	0	<+	++	-	-	-	0	0	0	-	-	-
K6	14-1/*oy109*	++++	social	<+	<+	<+	+	+	<+	+	-	-	-	<+	<+	<+	-	-	-
K8	20-3	+	*egl, unc*	0	-	-	-	0	0	++	-	-	-	-	-	-	-	-	-
K9	21-1	++	*egl*	0	-	-	-	0	++	++	-	-	-	-	-	-	-	-	-
K10	24-3/*oy104*	+		0	<+	++	++	<+	++	++	-	-	-	+	++	++	0	0	<+
K11	41-1	++		<+	<+	++	++	<+	+++	+++	<+	+	++	<+	<+	+	<+	++	++
K14	7-1	+++		0	-	0	0	<+	++	+++	-	-	-	0	0	+	-	-	-
K15	8-1/*oy105*	++		+	++	++	++	<+	++	++	+	+	++	+	++	++	<+	+	++
K16	11-1	+++	*egl*	0	<+	0	+	0	<+	+++	-	-	-	0	0	+	-	-	-
K17	14-2	+++	*dyf*,, L1 arrest	0	0	+	+	-	-	++	0	0	0	+	<+	++	<+	+	+
K18	14-3/*oy106*	++		<+	<+	+	++	<+	+++	+++	<+	+	+++	<+	+	++	++	++	+++
K21	26-2	+++	L1 arrest	0	<+	0	+	<+	++	+++	<+	<+	<+	<+	+	<+	-	0	+
K23	10-3/*oy107*	++		0	+	++	++	<+	++	++	<+	+	+	++	++	++	<+	+	++
K26	56-2		amphid *dyf*	0	<+	+	++	<+	+	++	-	-	-	<+	0	+	-	-	-
K28	12-1		*p-dyf*	0	0	0	0	0	<+	++	0	<+	<+	0	<+	0	0	-	<+
K30	41-2	++		0	0	<+	+	0	<+	++	-	-	-	0	0	0	-	-	-
K33	54-1	+++	*dyf*, sheath dye-fills	0	0	0	0	<+	<+	<+	-	-	-	0	0	0	-	-	-
m8		+++	*egl*	-	-	-	-	<+	<+	++	-	-	-	-	-	-	-	-	-
m9		++++	*egl*	-	-	-	-	0	0	<+	-	-	-	-	-	-	-	-	-
m10		++++	*egl, unc*	0	-	<+	<+	0	0	0	-	-	-	0	0	0	-	-	-
m26		++++	social	<+	<+	+	++	<+	++	+++	0	<+	<+	+	+	++	0	0	+
m28		++	*unc*	0	0	<+	<+	<+	++	++	<+	<+	<+	-	<+	<+	<+	<+	++
m33				-	-	-	-	-	-	-	-	-	-	0	0	0	-	-	-
m46				0	-	0	<+	0	<+	<+	-	-	-	0	0	0	-	-	-
m47				0	<+	++	+++	++	+++	++	<+	++	++	0	<+	+	0	0	++

[a] Dauer formation was assessed under the listed conditions (0, no dauers; <+, <10%; +, 10-30%; ++, 30-70%; +++, 70-100%, (-) not determined).

[b] The isolate number corresponds to the original frozen isolate from the screen.

[c] Relative intensity of *str-3*p::GFP expression in animals grown on crude pheromone plates, from + (barely detectable) to ++++ (equivalent to expression in the absence of pheromone).

[d] Potentially pleiotropic and/or independent phenotypes observed in the given strain. early hatch - embryos hatch less than 6 hours after egg lay; social - worms aggregate, also known as clumpy.

[e] Ethanol is the diluent used for the various ascarosides and is used as a negative control.

Table S2.2. Dauer Formation in Known Mutants

Mutant[a]	*allele*	phenotype[b]	EtOH[c]	ascr#8 (nM)			ascr#5 (nM)			icas#9 (nM)			ascr#2 (nM)			ascr#3 (nM)		
			0	6	60	600	60	600	6000	6	60	600	60	600	6000	60	600	6000
N2	Bristol		<+	+	++	+++	+	+++	+++	++	+++	+++	++	+++	+++	++	+++	+++
*str-3*p::*gfp*	*kyIs128*	early hatch	<+	++	++	+++	+	+++	+++	++	+++	+++	++	++	+++	++	+++	+++
srbc-64; srbc-66	*tm1946; tm2943*		<+	<+	+	++	<+	++	+++	<+	<+	+	+	++	++	<+	+	++
gpa-2; gpa-3	*pk16; pk35*		<+	+	+	++	+	++	++	++	++	++	+	++	++	+	+	++
ASK-	*qrIs2*		0	<+	+	++	<+	+++	+++	<+	<+	<+	<+	+	+	<+	+	++
gpa-1	*pk15*		<+	+	++	+++	+	+++	+++	<+	+	+	<+	++	++	<+	++	++
gpa-2	*pk16*		<+	<+	++	++	+	++	++	+	+	++	+	++	++	<+	+	++
gpa-2(XS)	*pkIs580*		+	+	<+	<+	-	-	-	-	-	-	-	-	-	-	-	-
gpa-3	*pk35*		<+	<+	++	+++	+	++	+++	++	++	++	+	+	++	+	+	+
gpa-4	*pk381*		+	++	+++	+++	+	+++	+++	+++	+++	+++	++	+++	+++	++	+++	+++
gpa-5	*pk375*		-	++	+++	+++	-	-	-	-	-	-	-	-	-	-	-	-
gpa-6	*pk480*		-	+	++	+++	-	-	-	-	-	-	-	-	-	-	-	-
gpa-7	*pk610*		-	+	++	+++	-	-	-	-	-	-	-	-	-	-	-	-
gpa-8	*pk345*		<+	++	++	+++	-	-	-	-	-	-	-	-	-	-	-	-
gpa-9	*pk438*		<+	+	++	+++	-	-	-	-	-	-	-	-	-	-	-	-
gpa-11	*pk349*		<+	+	++	++	<+	+++	+++	<+	++	++	<+	+	+++	<+	++	+++
gpa-12	*pk322*		<+	++	++	+++	-	-	-	-	-	-	-	-	-	-	-	-
gpa-13	*pk1270*		<+	+	++	+++	-	-	-	-	-	-	-	-	-	-	-	-
gpa-14	*pk342*		<+	<+	+	+++	+	+++	+++	<+	+++	++	++	++	+++	+	++	++
gpa-15	*pk477*		<+	++	++	+++	+	+++	+++	++	+	++	++	+++	+++	<+	+	++
gpa-17	*ok2334*		<+	+	++	++	-	-	-	-	-	-	-	-	-	-	-	-

[a] Dauer formation was assessed under the listed conditions (0, no dauers; <+, <10%; +, 10-30%; ++, 30-70%; +++, 70-100%, (-) not determined).

[b] Potentially pleiotropic and/or independent phenotypes observed in the given strain. early hatch - embryos hatch less than 6 hours after egg lay; social - worms aggregate, also known as clumpy.

[c] Ethanol is the diluent used for the various ascarosides and is used as a negative control.

Figure S2.1

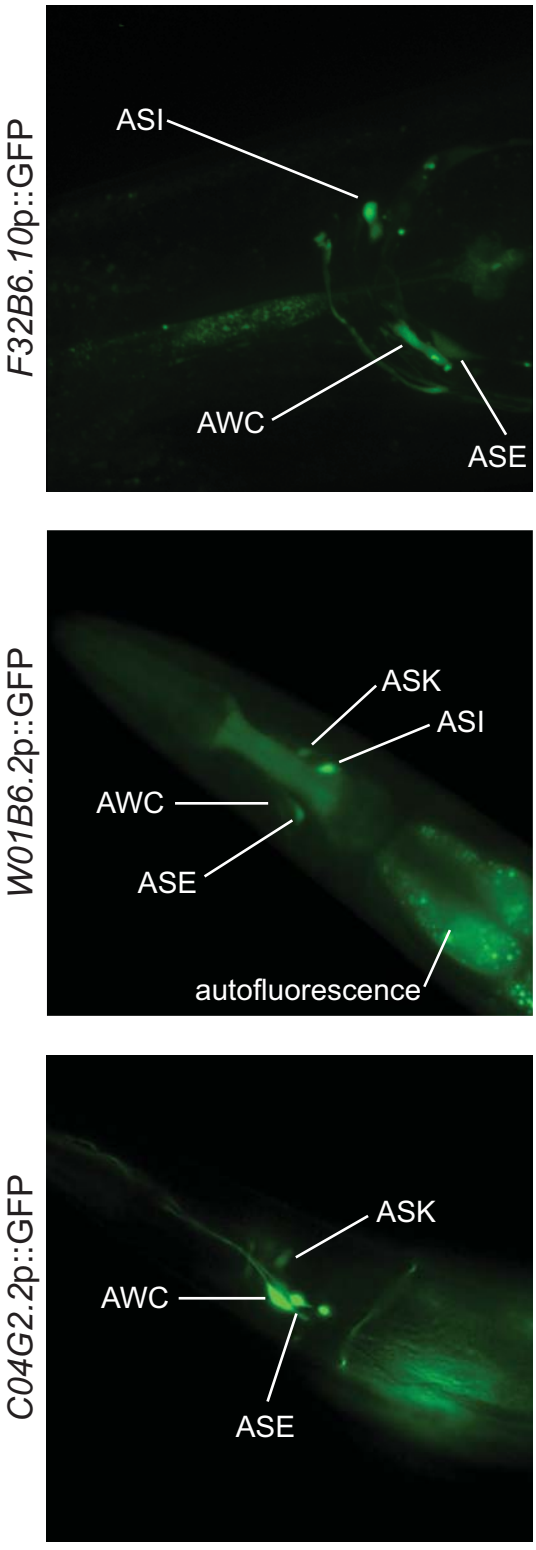
F32B6.10p::GFP
ASI
AWC
ASE
W01B6.2p::GFP
ASK
ASI
AWC
ASE
autofluorescence
C04G2.2p::GFP
ASK
AWC
ASE

CHAPTER 3

Food-dependent regulation of developmental plasticity via CaMKI and neuroendocrine signaling

This chapter has been formatted as a manuscript for eLife, where it is currently under review.

Food-dependent regulation of developmental plasticity via CaMKI and neuroendocrine signaling

Scott. J. Neal[1], Asuka Takeishi[1], Rebecca A. Butcher[2], Kyuhyung Kim[3,4] and Piali Sengupta[1,4]

[1]Department of Biology and National Center for Behavioral Genomics, Brandeis University, Waltham, MA 02454

[2]Department of Chemistry, University of Florida, Gainesville, FL 32611

[3] Department of Brain Science, Daegu Gyeongbuk Institute of Science and Technology (DGIST), Daegu 711-873, Korea

[4]Corresponding authors: sengupta@brandeis.edu; khkim@dgist.ac.kr

This work is currently under review for publication in eLife.

Running title: CaMKI regulates food integration in the dauer developmental decision

3.1 Contributions to this work

SJN generated the most strains and performed all experiments, with the exception of Figure 3.2 (A,B) which was contributed by AT. KK helped generate the hypothesis, made some strains and helped advise SJN. RAB provided essential reagents. PS oversaw the project. SJN and PS wrote the manuscript.

3.2 Abstract

Many animals integrate information about the environment, as well as internal state, to choose between alternate developmental trajectories. Environmental conditions, including food availability, inform the choice of *C. elegans* larvae to enter into the reproductive cycle or the growth arrested dauer stage. This polyphenic developmental decision is mediated via regulation of insulin and TGF-β signaling. However, the molecular and neuronal mechanisms by which food signals are assessed and integrated to regulate neuroendocrine signaling and this binary developmental decision are not well understood. Here we show that food information is integrated into the dauer pathway by the activity of the CMK-1 CaMKI enzyme in the AWC and ASI sensory neurons. AWC is hyperactive and exhibits enhanced odor responsiveness in both starved wild-type and fed *cmk-1* mutants, suggesting that the state of AWC in fed *cmk-1* larvae resembles that in starved wild-type animals. Food deprivation also regulates nuclear localization of CMK-1 in AWC in a dynamic manner, and we show that CMK-1 regulates the expression of insulin-like peptide (ILP) genes in AWC as a function of feeding state. CMK-1-regulated ILP signaling from AWC in turn regulates expression of the growth promoting *daf-28* ILP gene in the ASJ neurons. CMK-1 also acts in parallel in ASI to regulate expression of the *daf-7* TGF-β gene. Downregulation of *daf-28* and TGF-β expression in *cmk-1* mutants drives enhanced dauer formation under conditions of ample food. Together, these results identify mechanisms by which information regarding nutrient availability converges with other sensory cues in a small neuronal network to modulate neuroendocrine signaling and developmental plasticity.

3.3 Introduction

Discrete alternate phenotypes arising from a single genotype in response to varying environmental cues is referred to as polyphenism (Mayr, 1963). Well-described polyphenic traits include the exhibition of wings on locusts, caste hierarchy in social insects, and environmental sex determination in reptiles (Beldade et al., 2011; Nijhout, 2003; Simpson et al., 2011). In well-studied cases as in insects, it has been shown that animals integrate sensory cues during specific developmental stages to promote the expression of alternate phenotypic traits via regulation of endocrine and neuromodulatory signaling (Simpson et al., 2011; Watanabe et al., 2014). Environmental cues that trigger polyphenism include pheromones, temperature, mechanical stimuli, and food (Nijhout, 2003; Simpson et al., 2011). In particular, nutrient availability and quality during development is a major regulator of polyphenism in many species (Bento et al., 2010; Greene, 1989; Pfennig, 1992; Wheeler, 1986). Although the extent and adaptive value of polyphenism has been extensively discussed (Moczek et al., 2011; Pfennig et al., 2010), the underlying molecular and neuronal mechanisms that allow animals to sense and integrate signals such as food in the context of other cues to regulate phenotypic plasticity are not fully understood.

C. elegans exhibits robust phenotypic plasticity in response to environmental cues sensed during a critical period in development. Shortly following hatching, *C. elegans* larvae assess crowding in their environment via concentrations of a complex mixture of small molecules called ascarosides (collectively referred to as dauer pheromone) produced by conspecifics (Butcher et al., 2007; Edison, 2009; Golden and Riddle, 1982, 1984c; Jeong et al., 2005; Ludewig and Schroeder, 2013). High concentrations of one or more of these chemicals promote entry of larvae into the alternate stress-resistant and long-lived dauer developmental stage,

whereas in uncrowded conditions, larvae continue in the reproductive cycle (Cassada and Russell, 1975) (Figure 3.1A). Although pheromone is the instructive cue for dauer entry, additional cues such as temperature and food availability also regulate this binary decision (Ailion and Thomas, 2000; Golden and Riddle, 1984a, b, c) (Figure 3.1A). Thus, high (low) concentrations of food or low (high) temperature can efficiently inhibit (promote) pheromone-induced dauer formation, allowing animals to assess and integrate diverse sensory cues in order to make a robust developmental choice.

Decades of investigation have shown that environmental stimuli detected by sensory neurons modulate neuroendocrine signaling to regulate the choice of larval developmental trajectory in *C. elegans* (Fielenbach and Antebi, 2008). High pheromone concentrations, low food abundance and high temperature cues downregulate expression of the *daf-7* TGF-β ligand and several insulin-like peptide (ILP) genes in subsets of ciliated sensory neurons in the head amphid organs (Cornils et al., 2011; Li et al., 2003; Ren et al., 1996; Schackwitz et al., 1996) (Figure 3.1A). Downregulated TGF-β and insulin signaling in turn decrease biosynthesis of dafachronic acid steroid hormones by neuronal and non-neuronal endocrine cells (Fielenbach and Antebi, 2008) (Figure 3.1A). In the absence of these steroid hormones, the DAF-12 nuclear hormone receptor promotes dauer entry, whereas in the ligand-bound form, DAF-12 promotes reproductive development (Antebi et al., 1998; Antebi et al., 2000; Ludewig et al., 2004). Ciliated chemosensory neurons required to sense a subset of ascarosides for the regulation of dauer entry have been identified (Kim et al., 2009; McGrath et al., 2011; Park et al., 2012; Schackwitz et al., 1996). However, little is known about how food is sensed, and how food signals are integrated with pheromone signals at the level of endocrine gene expression to influence the dauer decision.

Here we show that the CMK-1 calcium/calmodulin-dependent protein kinase I (CaMKI) acts primarily in the AWC sensory neurons to regulate food input into the dauer decision pathway in *C. elegans*. *cmk-1* mutants enter into the dauer state inappropriately under food conditions that suppress dauer formation in wild-type animals. Nutrient availability is encoded in the pattern of baseline activity and odorant responsiveness of AWC. We show that AWC neuronal activity patterns in fed *cmk-1* mutants resemble those in starved wild-type larvae, and that deregulated AWC activity in fed *cmk-1* mutants may underlie their increased dauer formation phenotype. We further show that starvation results in transient nuclear localization of CMK-1 in AWC, and that CMK-1 regulates expression of the *ins-26* and *ins-35* ILP genes in AWC to transmit food information. CMK-1-dependent ILP signals from AWC in turn regulate expression of the *daf-28* ILP gene in the ASJ neurons to drive the dauer developmental decision. CMK-1 acts in parallel in the ASI neurons to regulate *daf-7* TGF-β expression. Downregulation of both insulin and TGF-β expression in *cmk-1* mutants enhances dauer formation under conditions of ample food. These results identify CMK-1 CaMKI as a key molecule that encodes information about nutrient availability within a sensory neuron network to regulate neuroendocrine signaling and a polyphenic developmental choice.

3.4 Results

3.4.1 *cmk-1* mutants form dauers inappropriately in the presence of pheromone and food

To verify that pheromone-induced dauer formation in wild-type animals is suppressed by bacterial food, we quantified dauers formed in the presence of pheromone and different concentrations of non-replicative (heat-killed) as well as replicative (live) bacteria. Heat- or antibiotic-killed bacteria provide a limited source of nutrition to *C. elegans* compared to live

bacteria (Golden and Riddle, 1982, 1984a, b). Although no dauers were observed in the absence of added pheromone (Figure S3.1A), >80% of wild-type larvae entered into the dauer stage on plates containing 6 μM ascr#3 (also referred to as asc-ΔC9 or C9) and l60 μg heat-killed OP50 bacteria (Figure 3.1B). Dauer formation decreased upon increasing the amount of heat-killed bacteria, and was fully suppressed by only 80 μg of live bacteria (Figure 3.1B). We could not reliably quantify the effects of lower concentrations of live bacteria since as reported previously, animals arrest development postembryonically when food becomes limiting (Baugh, 2013; Fukuyama et al., 2006; Hong et al., 1998). Food also inhibited dauer formation in *daf-22* mutants that are unable to produce most ascarosides (Butcher et al., 2009; Golden and Riddle, 1985) (Figure S3.1B), indicating that under these conditions, dauer formation is not increased simply due to enhanced endogenous pheromone signaling. These observations confirm that food cues modulate pheromone-induced dauer formation.

To begin to explore the mechanisms by which food signals are integrated with pheromone cues to regulate dauer entry, we sought to identify mutants that inappropriately enter into the dauer stage in the presence of pheromone and plentiful food. We excluded mutants in which dauer entry occurs in the absence of added pheromone (dauer-constitutive or Daf-c) (Hu, 2007). We focused on genes previously implicated in different aspects of nutrient sensing and/or metabolism in *C. elegans* including the *aak-1* and *aak-2* AMP-activated protein kinases (Apfeld et al., 2004; Cunningham et al., 2012; Narbonne and Roy, 2009), the *crh-1* CREB transcription factor and the *cmk-1* CaMKI kinase (Kimura et al., 2002; Suo and Ishiura, 2013; Suo et al., 2006), the *egl-4* cGMP-dependent protein kinase (Daniels et al., 2000; You et al., 2008), the *eat-4* glutamate transporter (Avery, 1993; Hills et al., 2004), the *tph-1* tryptophan hydroxylase and *cat-2* tyrosine hydroxylase enzymes (Ezcurra et al., 2011; Hills et al., 2004; Sawin et al., 2000;

Suo et al., 2009), and the *skn-1*, *hlh-30* and *mxl-3* transcription factors (O'Rourke and Ruvkun, 2013; Paek et al., 2012) (Figure 3.1C).

We found that animals carrying the *oy21* putative null and *oy20* missense mutations in the *cmk-1* CaMKI gene consistently formed dauers in the presence of 80 μg live bacteria and 6 μM ascr#3 - conditions that fully suppressed dauer formation in wild-type animals (Figure 3.1C). Few dauers were observed in the absence of added pheromone (Figure S3.1A), indicating that *cmk-1* mutants do not form dauers constitutively. *cmk-1* mutants also formed dauers in the presence of live food and ascr#2 (also referred to as asc-C6-MK or C6) and icas#9 (also referred to as IC-asc-C5 or C5) (Figure S3.1C, S1D), indicating that the response was not specific to a particular ascaroside. We could not reliably examine the effects of heat-killed bacteria in this assay since *cmk-1* mutants exited the dauer stage prematurely under these conditions (not shown), possibly due to additional metabolic defects that we have not explored further in this study. Increasing live food concentrations to 320 μg decreased but did not fully suppress dauer formation in *cmk-1* mutants (Figure 3.1D), implying that these animals are able to respond to food, but exhibit a shifted threshold of response to feeding. Consistent with the notion that *cmk-1* mutants retain the ability to respond to food cues, egg-laying was modulated by bacterial food in both wild-type and *cmk-1(oy21)* adult animals (Figure S3.1E). In addition to food and pheromone, temperature also regulates dauer formation (Golden and Riddle, 1984b), and we previously showed that *cmk-1* mutants exhibit altered thermosensory behaviors (Satterlee et al., 2004; Yu et al., 2014). *cmk-1(oy21)* mutants retained the ability to respond to temperature in the context of dauer formation, since dauer formation was fully suppressed at a lower temperature of 20°C in the presence of pheromone (Figure S3.1F). We conclude that *cmk-1* mutants are defective in correctly integrating food signals into the dauer decision pathway.

3.4.2 CMK-1 acts in the AWC and ASI/AWA sensory neurons to regulate dauer formation

cmk-1 is expressed broadly in multiple sensory and non-sensory neuron types in *C. elegans* (Kimura et al., 2002; Satterlee et al., 2004) (Figure S3.2). We first verified that expression of a *cmk-1* cDNA under its endogenous regulatory sequences rescued the dauer formation phenotype in the presence of live bacteria and exogenous ascr#3 (Figure 3.1E). We next performed cell-specific rescue experiments to identify the site(s) of CMK-1 function in the regulation of dauer entry under these conditions. Expression in the ASK pheromone-sensing, or the AFD thermosensory, neurons did not affect the dauer formation phenotype of *cmk-1* mutants (Figure 3.1E), suggesting, but not proving, that CMK-1 does not act simply by modulating pheromone or temperature sensitivity. However, expression of wild-type *cmk-1* sequences in the ASI/AWA or AWC sensory neurons resulted in partial, and nearly complete, suppression of dauer formation, respectively. Expression of *cmk-1* in both ASI/AWA and AWC suppressed dauer formation to the same extent as expression in AWC alone (Figure 3.1E). No rescue was observed upon expression in the ASJ sensory neurons which have also been previously implicated in the regulation of dauer formation (Bargmann and Horvitz, 1991; Schackwitz et al., 1996) (Figure 3.1E). Thus, CMK-1 acts primarily in AWC, but also in ASI/AWA, to regulate the effects of food on dauer formation.

3.4.3 The AWC neurons are hyperactive upon starvation and in *cmk-1* mutants

The AWC neurons have not previously been implicated in dauer formation. To further explore the role of this neuron type in the dauer decision, we examined the consequence of loss of CMK-1 on AWC function. It has previously been shown that the AWC neurons in adult

animals are silenced in the presence of food or food-related odorants, and are activated upon food/odor withdrawal (Chalasani et al., 2007). Consistent with this observation, the AWC neurons of well-fed wild-type L2 larvae expressing the GCaMP calcium indicator (Nakai et al., 2001) exhibited few, if any somatic calcium transients (Figure 3.2A, 2B). However, we found that wild-type AWC neurons became hyperactive following prolonged food deprivation. Both the frequency and amplitude of spontaneous calcium transients increased upon starvation for 2 hours, although no effects were observed after 1 hour (Figure 3.2A, 2B). Interestingly, the AWC neurons in well-fed *cmk-1* mutant larvae exhibited a high frequency and amplitude of somatic calcium transients similar to the activity pattern observed in starved wild-type larvae (Figure 3.2A, 3.2B); activity in AWC in *cmk-1* larvae was not further increased by starvation (Figure 3.2A, 3.2B). Overexpression of wild-type *cmk-1* sequences in AWC suppressed basal GCaMP expression (data not shown), implying that AWC may be silenced under these conditions, and precluded examination of cell-specific effects of CMK-1 on AWC activity.

Fed wild-type animals must be transiently starved for the AWC neurons to respond to odor/food removal following a brief exposure to the stimulus (S. Chalasani, personal communication). Confirming this observation, we found that removal of the attractive odorant isoamyl alcohol following a 1 minute exposure failed to elicit a response in the AWC neurons of wild-type adult animals transferred directly from food, but led to responses in animals starved on a food-free plate (Figure 3.2C, Table S3.1). Since the activity state of AWC in fed *cmk-1* mutants resembles that of starved wild-type animals, we asked whether AWC neurons in *cmk-1* mutant adults are able to respond to odor removal without prior starvation. Indeed, the AWC neurons in *cmk-1* adult animals responded robustly to odorant removal regardless of their feeding state (Figure 3.2C, Table S3.1). Both the number of responding cells, as well as response amplitude

were significantly increased in fed and starved *cmk-1* mutants (Table S3.1). Together, these observations imply that the basal activity state of the AWC neurons in fed *cmk-1* mutants is similar to the activity state of these neurons in starved wild-type animals, but that these neurons retain the ability to respond to food-associated odors.

We tested the notion that deregulated AWC activity and/or output in *cmk-1* mutants is causal to the increased dauer formation phenotype of these animals under fed conditions. Indeed, genetic ablation of the AWC neurons via expression of reconstituted caspases (Beverly et al., 2011; Chelur and Chalfie, 2007) fully suppressed the increased dauer formation phenotype of *cmk-1* mutants under fed conditions, but did not affect dauer formation in a wild-type background (Figure 3.2D). This result suggests that the AWC neurons may inappropriately promote, or decrease inhibition of, dauer formation, in fed *cmk-1* mutants.

If AWC were in part required to transmit information about food availability to regulate dauer formation, we would predict that dauer entry in wild-type animals lacking AWC would be less sensitive to regulation by food. We found that the ability of heat-killed bacteria to modulate dauer formation was reduced in AWC-ablated animals (Figure 3.2E) (Beverly et al., 2011), suggesting that food-mediated regulation of dauer formation acts in part via AWC. We note that AWC-ablated animals formed more dauers overall on heat-killed food than wild-type animals (Figure 3.2E), suggesting that under these conditions, AWC may also send a pro-growth signal. We conclude that CMK-1 regulates AWC activity as a function of food, and that deregulated AWC activity in fed *cmk-1* mutants promotes inappropriate entry into the dauer stage.

3.4.4 Feeding state is reflected in the temporal dynamics of CMK-1 subcellular localization in AWC

We next investigated the mechanisms by which CMK-1 acts in AWC to regulate dauer formation as a function of feeding state. We and others previously showed that CMK-1 shuttles between the nucleus and the cytoplasm in the AFD thermosensory neurons based on growth temperature, and regulates the expression of AFD-expressed thermotransduction genes (Schild et al., 2014; Yu et al., 2014). We asked whether CMK-1 subcellular localization in AWC is similarly affected by feeding status. In fed L1 larvae, a functional CMK-1::GFP fusion protein was present mostly uniformly throughout the soma of the AWC neurons (Figure 3.3A, 3.3B). Food withdrawal for 30 minutes resulted in a transient nuclear enrichment of CMK-1 that persisted for approximately one hour (Figure 3.3A, 3.3B). However, after prolonged starvation, CMK-1::GFP was enriched in the cytoplasm of AWC (Figure 3.3A, 3.3B). In contrast, food did not affect subcellular localization of CMK-1::GFP in AFD (Figure 3.3A), and we previously showed that temperature does not affect CMK-1 localization in AWC (Yu et al., 2014). As observed previously in the context of regulating thermosensory properties of AFD (Yu et al., 2014), overexpression of either a constitutively nuclear-enriched or cytoplasmically-enriched CMK-1::GFP protein in AWC rescued the dauer formation phenotype of *cmk-1* mutants (Figure 3.3C), although nuclear enriched CMK-1 consistently rescued to a greater extent (Figure 3.3C). The subcellular localization of these proteins in AWC was unaffected by genotype or feeding state (Figure S3.3). However, we note that neither the nuclear-enriched or the cytoplasmically-enriched CMK-1::GFP fusion proteins are fully excluded from the cytoplasmic or nuclear compartment, respectively, possibly due to overexpression (Figure S3.3). These results suggest that food regulates CMK-1 subcellular localization in AWC, and that CMK-1 activity in the nuclei of AWC may be important to encode food information in the dauer regulatory pathway.

3.4.5 CMK-1 regulates the expression of insulin-like peptide genes in AWC to report feeding state

The transient nuclear localization of CMK-1 in AWC suggested that CMK-1 may regulate the expression of genes in AWC to reflect feeding state. We previously described a similar role for CMK-1 in the regulation of thermosensory gene expression in AFD as a function of temperature (Yu et al., 2014). A link between nutrient availability and insulin signaling is now well established in many organisms (Erion and Sehgal, 2013; Riera and Dillin, 2015), and in *C. elegans*, the expression of several insulin-like peptide (ILP) genes has been shown to be regulated by food availability (Chen and Baugh, 2014; Cornils et al., 2011; Li et al., 2003; Ritter et al., 2013). Together with the hours-long timescale of integration of sensory cues for regulation of dauer formation (Golden and Riddle, 1984c; Schaedel et al., 2012), and the fact that AWC must signal feeding state to regulate downstream hormonal signaling, we hypothesized that CMK-1 may regulate the expression of ILP genes in AWC as a function of feeding state.

The *C. elegans* genome encodes 40 ILPs (Li and Kim, 2010; Pierce et al., 2001) (www.wormbase.org). Of the set of these genes known to be regulated by nutrient availability, the *ins-26* and *ins-35* ILP genes are expressed in AWC (as well as in additional cells) (Chen and Baugh, 2014), although whether their expression in AWC is regulated by food has not been previously determined. We asked whether *ins-26* and *ins-35* expression in AWC is regulated by food and CMK-1. Under fed conditions, *ins-26*p*::yfp* was expressed in ASI, ASE and AWC neurons in wild-type L1 larvae; expression in AWC, and to a lesser extent in ASI, was reduced upon starvation (Figure 3.4A, 3.4B). Relative to wild-type, *ins-26*p*::yfp* expression was decreased in ASE and AWC in *cmk-1* mutants grown with plentiful food, whereas expression in ASI decreased only upon starvation (Figure 3.4A, 3.4B). Similarly, *ins-35*p*::yfp* was largely

expressed in ASE and AWC in fed wild-type L1 larvae; expression in both neurons was significantly decreased upon starvation, and in fed and starved *cmk-1* mutants (Figure 3.4A, 3.4B). Weak expression of *ins-35* was also observed in the ASK neurons, particularly in *cmk-1* mutants, although expression in this neuron type was not further modulated by starvation (Figure 3.4B). We note that *ins-35*p*::yfp* was also strongly expressed in the intestine (Figure 3.4A) (Chen and Baugh, 2014); intestinal expression was not further characterized. These observations suggest that the expression of *ins-26* and *ins-35* in AWC is regulated by food availability, and that their expression pattern in AWC in fed *cmk-1* mutants resembles that of starved wild-type animals.

If reduced expression of *ins-26* and *ins-35* expression in *cmk-1* mutants is causal to the increased dauer formation phenotype under fed conditions, we would predict that *ins-26* and *ins-35* loss-of-function mutants would phenocopy the *cmk-1* dauer formation phenotype. However, neither the single mutants, or *ins-26; ins-35* double mutants exhibited increased dauer formation under conditions in which *cmk-1* mutants entered inappropriately into the dauer stage (Figure 3.4C). This result suggests that reduced expression of these ILP genes in specific cell types or tissues may lead to dauer formation phenotypes that are distinct from the phenotypes arising from complete loss of function of these genes. To test this hypothesis, we asked whether restoration of ILP gene expression specifically in AWC was sufficient to rescue the dauer formation phenotype of *cmk-1* mutants. As shown in Figure 3.4C, we found that expression of *ins-26* and *ins-35* specifically in AWC, but not in ASE or ASJ, significantly rescued the dauer formation defect of *cmk-1* mutants. Together, these results indicate that reduced *ins-26* and *ins-35* expression in the AWC neurons of *cmk-1* mutants may in part cause the increased dauer formation phenotype in this mutant under fed conditions.

Since ablation of AWC suppresses the dauer formation phenotype of fed *cmk-1* mutants, it is likely that in addition to regulating *ins-26* and *ins-35* expression in AWC, CMK-1 also regulates the expression and/or release of additional dauer-promoting signals from AWC. To explore this possibility further, we knocked down expression of the *egl-3* and *bli-4* proprotein convertases specifically in AWC. BLI-4 and EGL-3 may both regulate the processing of different subsets of ILP precursors (Hung et al., 2014; Leinwand and Chalasani, 2013). We found that knockdown of *bli-4*, but not *egl-3* suppressed dauer formation in *cmk-1* mutants (Figure S3.4), suggesting that additional BLI-4-dependent insulin signals from AWC promote dauer formation under limiting food.

3.4.6 CMK-1 acts in both the TGF-β and insulin pathways to regulate dauer formation

We next investigated the mechanisms by which food- and CMK-1-dependent ILP signaling from AWC influence the TGF-β and ILP neuroendocrine signaling pathways that act in parallel to regulate dauer formation (Fielenbach and Antebi, 2008). *daf-7* TGF-β null mutants are strongly Daf-c, and this phenotype is suppressed upon loss of DAF-3 SMAD or DAF-5 transcription factor function (Golden and Riddle, 1984c; Thomas et al., 1993; Vowels and Thomas, 1992). Despite the presence of multiple ILPs, the *C. elegans* genome encodes a single insulin receptor encoded by the *daf-2* gene. Although loss of function of single ILP genes such as *daf-28* results in only weak effects on dauer formation, likely due to redundancy (Cornils et al., 2011; Hung et al., 2014; Li et al., 2003; Ritter et al., 2013), *daf-2* insulin receptor mutants are Daf-c (Gems et al., 1998; Gottlieb and Ruvkun, 1994; Thomas et al., 1993). The Daf-c phenotype of *daf-2* mutants is suppressed by loss of *daf-16* FOXO transcription factor function (Gottlieb and Ruvkun, 1994; Riddle et al., 1981). To determine whether CMK-1 reports food

information to either, or both, the TGF-β and insulin pathways, we asked whether *daf-3, daf-5* or *daf-16* mutations suppress the dauer formation phenotype of *cmk-1* mutants. We found that mutations in *daf-3* and *daf-5* partly suppressed the dauer formation defects of *cmk-1* mutants, whereas loss of *daf-16* function fully suppressed this phenotype (Figure 3.5A). These results suggest that CMK-1 relays food information to both the TGF-β and insulin pathways to regulate dauer formation.

3.4.7 CMK-1 acts non cell-autonomously in AWC, and cell-autonomously in ASI, to mediate food-dependent regulation of insulin and TGF-β signaling, respectively

Previous work has shown that food and pheromone cues regulate the expression of both *daf-7* TGF-β and the *daf-28* ILP genes to modulate entry into the dauer stage. *daf-7* expression in ASI, and *daf-28* expression in both ASJ and ASI, are downregulated upon starvation or upon exposure to high pheromone concentrations (Li et al., 2003; Ren et al., 1996; Schackwitz et al., 1996). Since CMK-1 acts in both the TGF-β and insulin pathways to regulate dauer formation, we asked whether the inability of food to fully suppress dauer formation in *cmk-1* mutants is in part due to defects in regulation of expression of one or both ligands in *cmk-1* mutants.

A *daf-28*p::*gfp* reporter is expressed strongly in both ASI and ASJ neurons in fed wild-type larvae (Li et al., 2003) (Figure 3.5B, 3.5C). Under our conditions, addition of crude pheromone decreased expression primarily in ASI, whereas starvation resulted in decreased expression in both ASI and ASJ (Figure 3.5B). Addition of pheromone to starved wild-type larvae did not further decrease expression in either cell type (Figure 3.5B). Expression of *daf-28*p*::gfp* was unaffected by temperature (Figure S3.5). Interestingly, we observed that in fed *cmk-1* mutants grown on live bacteria without exogenous pheromone, *daf-28*p::*gfp* expression

was strongly decreased in ASJ but more weakly affected in ASI (Figure 3.5B, 3.5C). As in wild-type larvae, addition of pheromone or starvation decreased *daf-28*p*::gfp* expression in ASI; we were unable to detect whether expression in ASJ was further reduced under these conditions in *cmk-1* mutants (Figure 3.5B). The *daf-28*p::*gfp* expression defect of *cmk-1* mutants in ASJ was partly but significantly rescued upon expression of wild-type *cmk-1* sequences in AWC, but not in ASI/AWA or ASJ (Figure 3.5C). Importantly, expression of *ins-26* and *ins-35* in AWC in *cmk-1* mutants was also sufficient to partly restore *daf-28p::gfp* expression in ASJ (Figure 3.5D). These results indicate that CMK-1-mediated ILP signaling from AWC directly or indirectly regulates expression of the *daf-28* ILP gene in ASJ to modulate dauer formation as a function of feeding state. Moreover, our results suggest that while pheromone regulates *daf-28* expression primarily in ASI, food-dependent regulation of *daf-28* is observed in both ASI and ASJ.

In addition to acting in AWC, CMK-1 also acts in ASI/AWA to regulate dauer formation (Figure 3.1E), and the *cmk-1* mutant dauer phenotype is suppressed by downstream mutations in the TGF-β pathway (Figure 3.5A). We, therefore, asked whether CMK-1 also acts in parallel to insulin signaling to cell-autonomously regulate expression of the *daf-7* TGF-β ligand. As reported previously, a *daf-7*p::*gfp* reporter gene was expressed strongly and specifically in the ASI neurons of fed wild-type L1 larvae grown under conditions of low endogenous pheromone concentrations (Ren et al., 1996; Schackwitz et al., 1996) (Figure 3.6A, 3.6B). Expression was strongly decreased upon starvation, or in the presence of crude pheromone (Figure 3.6A). We found that unlike in wild-type animals, expression of *daf-7*p::*gfp* was reduced, but not abolished, in *cmk-1* mutant larvae grown on live bacteria and no exogenous pheromone (Figure 3.6A, 3.6B). The strongly reduced expression under fed conditions in *cmk-1* larvae precluded us from determining whether starvation or addition of pheromone resulted in a further decrease in *daf-*

*7*p*::gfp* expression levels in this mutant background (Figure 3.6A). Expression of *cmk-1* in ASI, but not in AWC, rescued the *daf-7*p::*gfp* expression defects of *cmk-1* mutant larvae (Figure 3.6B), indicating that CMK-1 acts cell autonomously in ASI to regulate *daf-7* expression.

If reduced expression of *daf-7* and *daf-28* in *cmk-1* mutants is causal to their dauer formation phenotypes, we would predict that increased expression of *daf-7* or *daf-28* would rescue the dauer formation defects of *cmk-1* mutants. We found that constitutive expression of *daf-28* and *daf-7* in ASJ and ASI, respectively, strongly rescued the dauer formation phenotype of *cmk-1* mutants (Figure 3.5E, 3.6C). *daf-28* expression in ASI rescued more weakly (Figure 3.5E) indicating that neuron-specific release properties or spatial diffusion constraints may require DAF-28 expression in ASJ to rescue the *cmk-1* phenotype (Chen et al., 2013; Cornils et al., 2011). Taken together, these results indicate that CMK-1 relays food information into the dauer regulatory pathway by acting non cell-autonomously in AWC to regulate *daf-28* ILP expression in ASJ, and cell-autonomously to regulate *daf-7* TGF-β expression in ASI (Figure 3.7).

We further tested the regulatory relationship between CMK-1 and the parallel TGF-β and DAF-28 ILP signaling pathways by performing genetic epistasis experiments. If CMK-1 acts in both the TGF-β and DAF-28 pathways, we predicted that *cmk-1; daf-28* double mutants would exhibit increased dauer formation defects compared to either single mutant alone in part due to reduced *daf-7* expression in *cmk-1* mutants. As shown in Figure 3.6D, we found that a significantly larger percentage of *cmk-1; daf-28* double mutant animals entered into the dauer stage as compared to *cmk-1* or *daf-28* null mutants alone in the presence of live food and no added pheromone. These results confirm that CMK-1 regulates both TGF-β and insulin signaling to modulate dauer formation.

3.5 Discussion

We have shown that CMK-1 acts in AWC to encode the feeding state of *C. elegans* larvae. Our results indicate that basal AWC neuronal activity is regulated by feeding state, and that CMK-1 transmits feeding state information via regulation of ILP gene expression in AWC to modulate the dauer decision. CMK-1-dependent INS-26 and INS-35 signals from AWC directly or indirectly regulate *daf-28* expression in ASJ. In addition, CMK-1 acts in parallel in ASI to regulate *daf-7* TGF-β expression. Downregulation of both *daf-28* and *daf-7* signaling in starved wild-type and fed *cmk-1* mutants enhances dauer formation in the presence of pheromone. Our results indicate that CMK-1 activity in the AWC and ASI sensory neurons is critical for integration of information about nutrient availability in the modulation of a key developmental decision (Figure 3.7).

Multiple lines of evidence support our hypothesis that the dauer formation phenotypes of *cmk-1* mutants arise due to defects in encoding or integrating food inputs. First, *cmk-1* mutants exhibit an increased threshold of food-mediated suppression of dauer formation. Second, both basal and odor-evoked activity patterns in AWC are similar in starved wild-type and fed *cmk-1* mutants. Third, the expression patterns of *ins-26*p*::yfp* and *ins-35*p*::yfp* in AWC are similar, although not identical, in starved wild-type and fed *cmk-1* mutants. Fourth, the expression patterns of *daf-28*p*::gfp* in ASJ and *daf-7*p*::gfp* in ASI are also similar in starved wild-type and fed *cmk-1* mutants. Together, these results suggest that *cmk-1* mutants are defective in correctly integrating food information to regulate dauer formation.

In addition to modulating basal activity, and changes in *ins-26* and *ins-35* gene expression, starvation also regulates CMK-1 subcellular localization in AWC. Nuclear localization of CMK-1 in AWC is evident within 30 mins of starvation, whereas increased AWC

activity is observed on a longer timescale. Although the causal relationship between changes in gene expression in AWC and increased activity levels in starved wild-type and fed *cmk-1* mutants is not yet clear, it is unlikely that AWC hyperactivity is solely due to the inability of this neuron type to sense bacterial cues. Addition of odorants hyperpolarizes AWC similarly in both wild-type and *cmk-1* mutants, indicating that AWC retains the ability to sense and respond to exogenous chemicals in *cmk-1* mutants. CMK-1 may instead modulate AWC activity as a function of internal state driven by the olfactory or nutritive values of food, possibly via feedback mechanisms requiring CMK-1-mediated gene expression changes in AWC. *C. elegans* larvae integrate food signals over an extended period of time to allow accurate assessment of their past, current and future environment (Avery, 2014; Schaedel et al., 2012). Increased activity of AWC following prolonged starvation may represent a consolidation of the starved state to reinforce the decision to commit to the dauer fate (Golden and Riddle, 1984c; Schaedel et al., 2012). Increased basal activity and odor-evoked responses observed in AWC in starved wild-type or fed *cmk-1* mutants may also sensitize animals to the presence of food-related odors, signaling improving environmental conditions. Similar modulation of peripheral sensory neuron responses as a function of feeding state has been suggested to underlie state-dependent plasticity in sensory behaviors in other organisms (Jyotaki et al., 2010; Palouzier-Paulignan et al., 2012; Pool and Scott, 2014; Sengupta, 2013). A goal for the future will be to determine how and why AWC activity is regulated by CMK-1 as a function of feeding state.

We have shown that CMK-1 regulates the expression of *ins-26* and *ins-35* in AWC to inhibit dauer formation under fed conditions. This model is supported by three sets of observations. First, *ins-26* and *ins-35* expression in AWC is downregulated in fed *cmk-1* and starved wild-type larvae. Second, overexpression of *ins-26* and *ins-35* specifically in AWC

suppresses the enhanced dauer formation phenotype of *cmk-1* mutants. Third, expression of *ins-26* and *ins-35* in AWC partly rescues the decreased *daf-28*p*::gfp* expression phenotype of *cmk-1* mutants. However, INS-26 and INS-35 are unlikely to be the sole mediators of the food signal from AWC. Our data suggest that additional ILP molecules from AWC, possibly processed by the BLI-4 enzyme, also regulate the dauer decision. Indeed, given the complex insulin regulatory network recently described in *C. elegans* (Fernandes de Abreu et al., 2014; Ritter et al., 2013), it is likely that multiple cues from AWC, including CMK-1-regulated dauer promoting and dauer inhibitory ILPs, transmit food information.

CMK-1-regulated ILP signaling from AWC directly or indirectly influences *daf-28* expression in ASJ to modulate dauer formation. In parallel, CMK-1 acts in ASI to regulate *daf-7* TGF-β expression. Downregulation of both pathways in starved wild-type or fed *cmk-1* mutants results in increased dauer formation. However, food information is likely to be integrated into the dauer pathway via additional CMK-1-independent mechanisms. Bacterial food is a complex cue consisting of many volatile and non-volatile compounds (Orth et al., 2011) of different nutritive value to *C. elegans*. The ability to sense different bacterial components may allow animals to accurately gauge both the presence as well as the quality of food, and thereby modulate specific behavioral or developmental decisions via distinct signaling pathways (Kang and Avery, 2009; Kaul et al., 2014; MacNeil et al., 2013; Meisel et al., 2014; Ryan et al., 2014; You et al., 2008; Zhang and Zhang, 2009). Thus, food signals are likely to be integrated into the dauer decision via multiple neurons and mechanisms. Consistent with this hypothesis, although both *daf-7* and *daf-28* expression are downregulated by starvation in ASI, CMK-1 regulates only *daf-7* expression, and appears to be dispensable for the regulation of *daf-28* expression in this neuron

type. Thus, CMK-1 function in AWC and ASI is likely to be a key, but not the sole, regulator of food input into the dauer developmental decision.

Although dauer formation and other forms of polyphenism are extreme examples of phenotypic plasticity, environmental cues experienced during defined sensitive or critical periods during development also underlie phenotypic variation in mammals (Gluckman et al., 2007). Our results describe how *C. elegans* integrates and translates environmental cues into hormonal signaling to regulate the dauer decision. We expect that continued investigation of the molecular and neuronal regulation of phenotypic plasticity by sensory cues in different species will lead to insights into the general principles underlying these critical developmental decisions, as well as provide information about the mechanisms of sensory integration that direct the choice of the appropriate developmental pathway.

3.6 Acknowledgements

We are grateful to Harry Bell and Kyle Ryan for technical assistance. We thank the *Caenorhabditis* Genetics Center and the National BioResource Project (Japan) for providing strains, and Yun Zhang, Sreekanth Chalasani and Ryan Baugh for reagents. We are also grateful to members of the Sengupta lab, Josh Meisel and Yun Zhang for critical comments on the manuscript. We acknowledge support from the Brandeis University NSF MRSEC DMR-1420382 for the production of microfluidics devices. This work was supported in part by the NSF (IOS 1256488 – P.S.), the Human Frontiers Science Program (RGY0042/2010 – P.S. and R.A.B.), the DGIST R&D Program of the Ministry of Science, ICT and Future Planning (15-BD-06 – K.K.) and the T.J. Park Science Fellowship of POSCO T.J. Park Foundation (K.K.)

3.7 Materials and Methods

3.7.1 Strains and Genetics

C. elegans were maintained on nematode growth medium (NGM) agar plates at 20°C, with *E. coli* OP50 as a food source. Strains were constructed using standard genetic procedures. The presence of mutations was confirmed by PCR-based amplification and/or sequencing. A complete list of strains used in this study is shown in Table S3.2.

3.7.2 Molecular Biology

Promoter sequences and cDNAs were amplified from genomic DNA or a cDNA library, respectively, from a population of mixed-stage wild-type animals. cDNA sequences were verified by sequencing. The promoters used in this study are as follows: *cmk-1*p (3.1 kb), *sra-9*p (ASK, 2.9 kb), *ttx-1*p (AFD, 2.7 kb), *trx-1*p (ASJ, 1.0 kb), *gpa-4*p (ASI/AWA, 2.8 kb), *ceh-36Δ*p (AWC, 0.6 kb), *srg-47*p (ASI, 1.0 kb), *ins-26*p [see (Chen and Baugh, 2014)], *ins-35*p [see (Chen and Baugh, 2014)], *che-1*p (ASE, 0.7 kb), *odr-1*p [AWC (strong), AWB (weak), 2.4 kb] and *odr-3*p [AWC (strong), AWA, AWB, ASH, ADF (weak), 2.7 kb]. Sense and antisense constructs were generated by amplifying exons 2-8 (1.5 kb; *bli-4*) and 6-8 (568 bp; *egl-3*) from cDNAs, and cloning into vectors containing cell-specific promoter sequences. Linearized vectors containing either sense or antisense sequences were injected at 100 ng/µl each.

3.7.3 Dauer Assays

Dauer assays were performed essentially as described (Neal et al., 2013), using the indicated food sources. Briefly, young adult worms were allowed to lay 65-85 eggs on an assay plate (Neal et al., 2013) containing either ethanol (control) or pheromone, and a defined amount

of bacteria. Animals were grown at 25°C unless indicated otherwise. Assays using heat-killed food or live food were examined for dauer and non-dauer larvae approximately 84 hrs or 66 hrs, respectively, after the midpoint of the egg lay. At least three independent trials were conducted for each condition with two technical replicates each.

3.7.4 Quantification of Fluorescence Intensity

Strains expressing fluorescent reporters were growth-synchronized by hypochlorite treatment, and embryos were allowed to develop for 20-24 hours at 20°C to the end of the L1 larval stage on OP50, in the presence or absence of crude pheromone (Golden and Riddle, 1984b; Zhang et al., 2013). Crude pheromone plates were prepared by spreading 20 µl of 1:4 crude pheromone (~1 unit, defined as the amount required for forming ~33% dauers on heat-killed OP50 at 25°C) on the agar surface and allowing it to dry completely prior to seeding with bacteria. For starvation conditions, worms were washed from growth plates in M9 buffer and were transferred to assay plates for 4-6 hours. Prior to imaging, worms were collected by centrifugation, transferred to a 2% agarose pad on a microscope slide, and immobilized using 10 mM levamisole (Sigma). Animals were visualized on a Zeiss Axio Imager.M2 microscope using either a 40X (NA 1.3) or 63X (NA 1.4) oil objective, and images were captured using a Hamamatsu Orca camera. Neurons were identified by position relative to the subset of neurons filled with DiI.

For quantification of fluorescence intensity, images were acquired from a single focal plane. The exposure time for each fluorescent reporter was adjusted in the wild-type background to ensure that pixel intensity in the cell of interest was in the linear range. Pixel intensities for the soma (*daf-7*p*::gfp* reporter) or the nucleus (*daf-28*p*::gfp* reporter) were measured in ImageJ

(NIH) by calculating the mean pixel intensity for the entire region of interest. All measurements within a single experiment were normalized to the median wild-type expression value (set at 1) to account for variation in conditions across trials. All imaging and subsequent quantification was performed blind to the genotype.

For shown representative images, *z*-stacks (0.5 μm per slice) were acquired through the head of the animal, and a sub-stack containing all GFP-expressing cells was rotated and maximally projected in ImageJ. All images within a panel were collected using the same exposure times. Adjustments to levels and/or contrast for optimal viewing were applied equally to images within each panel. Images used for quantification were not processed.

3.7.5 Calcium Imaging

Imaging of spontaneous calcium dynamics in AWC was performed essentially as previously described (Biron et al., 2008). Briefly, L2 larvae were glued to an NGM agar pad on a cover glass, bathed in M9, and mounted under a second cover glass for imaging. The edge of the sandwiched cover glasses was sealed with a mixture of paraffin wax (Fisher Scientific), and Vaseline, and the sample was transferred to a slide placed on a Peltier device on the microscope stage. The elapsed time from removal of the animal from the incubator to initiation of imaging was <3 min. The temperature was maintained at 20ºC via temperature-regulated feedback using LabView (National Instruments), and measured using a T-type thermocouple. Individual animals were imaged for 90 sec at a rate of 2 Hz. Images were captured using MetaMorph (Molecular Devices) and a Hamamatsu Orca digital camera. Data were analyzed using custom scripts in MATLAB (The Mathworks). A neuronal response was defined as the percent change of the relative fluorescence of the neuron from its baseline fluorescence level after background

subtraction. A fluorescence change of >5% in AWC was considered a response. The duration of calcium events was calculated as the sum of all events in each animal, and averaged for each genotype and condition.

Odor-evoked imaging was performed as described previously (Jang et al., 2012; Ryan et al., 2014) using custom microfluidics devices. Imaging was conducted on an Olympus BX52WI microscope equipped with a 40X oil objective and a Hamamatsu Orca CCD camera. Animals were exposed to a 1 min pulse of 10^{-4} isoamyl alcohol in S-basal. Recording was performed at 4 Hz during the last 10 seconds of the pulse and 50 seconds following removal of the stimulus. Starved worms were transferred to an assay plate with no food before imaging. Recorded image stacks were aligned using the StackReg plugin (Thevenaz et al., 1998) for ImageJ (rigid body option) and were cropped to a region containing the AWC cell body. Relative changes in fluorescence, following background subtraction, were calculated using custom MATLAB scripts. Individual traces were normalized to their average baseline value for the five seconds prior to odorant removal.

3.8 Figure Legends

Figure 3.1. CMK-1 acts in the AWC and ASI/AWA neurons to inhibit dauer formation in fed animals.

(A) Simplified model of sensory inputs modulating TGF-β and insulin signaling in the regulation of the dauer decision. See text for details. (B) Quantification of dauer formation in wild-type animals in the presence of 6 μM ascr#3 and the indicated amounts of heat-killed or live OP50 bacteria. Each filled circle represents one assay; n>65 animals per assay, three independent experiments. Line represents best fit to the data. ** and *** indicate different from values using 160 μg of heat-killed bacteria at $P<0.01$ and 0.001, respectively (ANOVA and Games-Howell *post-hoc* test). (C) Dauers formed by strains of the indicated genotypes in the presence of 6 μM ascr#3 and 80 μg live OP50. Each data point is the average of ≥3 independent experiments of >65 animals each. Errors are SEM. *, ** and *** indicate different from wild-type at $P<0.05$, 0.01, and 0.001, respectively (ANOVA and Games-Howell *post-hoc* test). (D) Dauer formation in *cmk-1* mutants grown with 6 μM ascr#3 and the indicated amounts of live OP50. Each data point is the average of ≥3 independent experiments of >65 animals each. Errors are SEM. ** and *** indicate different from corresponding values using 80 μg OP50 at $P<0.01$ and 0.001, respectively (Student's t-test). (E) Dauers formed by strains of the indicated genotypes grown on plates containing 6 μM ascr#3 and 80 μg live OP50. Promoters used to drive wild-type *cmk-1* cDNA expression were: *cmk-1*p – 3.1 kb of *cmk-1* upstream regulatory sequences; ASK – *sra-9*p; AFD – *ttx-1*p; ASJ – *trx-1*p; ASI/AWA – *gpa-4*p; AWC – *ceh-36*Δp. Each data point is the average of ≥3 independent experiments of >65 animals each. For transgenic strains, data are averaged from two independent lines each. Errors are SEM. *, ** and *** indicate different from

wild-type at $P<0.05$, 0.01, and 0.001, respectively; ### indicates different from *cmk-1*(*oy21*) at $P<0.001$ (ANOVA and Games-Howell *post-hoc* test).

Figure 3.2. The AWC neurons exhibit increased basal activity in fed *cmk-1*, and starved wild-type animals.

(A) Heat maps showing fluorescence intensity ($\Delta F/F_0$) in the soma of AWC neurons in fed or starved *cmk-1*(*oy21*) L2 larvae expressing GCaMP 3.0 in AWC under the *ceh-36*Δ promoter. Animals were cultured at 20°C, starved for 0, 1 or 2 hrs and imaged at 20°C. Each horizontal line shows calcium dynamics in a single AWC neuron; n=20 neurons each. (B) Box-and-whisker plots quantifying total duration of calcium responses >5% above baseline for each genotype and condition shown in A). Median is indicated by a red line. Tops and bottoms of boxes indicate 75th and 25th percentiles; whiskers indicate 5th and 95th percentiles. Outliers are indicated by + signs. ** indicates different from wild-type at 0 hr at $P<0.01$ (Kruskal-Wallis test). n.s. – not significant. n=20 neurons each. (C) Individual (colors) and averaged (black) calcium responses in the AWC soma in fed and starved wild-type and *cmk-1*(*oy21*) adult animals in the presence, or upon removal of, 10^{-4} isoamyl alcohol (IAA; light gray bar). Imaging was performed using strains expressing GCaMP3.0 specifically in AWC. Error bars (gray shading) are SEM. See Table S3.1 for quantification of responding neurons, and average response amplitudes. n>11 neurons each. (D) Dauers formed by wild-type, AWC-ablated (60), and *cmk-1*(*oy21*) with or without AWC on 80 µg live OP50 and 6 µM ascr#3. *** and ### indicate different from wild-type and *cmk-1*, respectively, at $P<0.001$ (ANOVA and Games-Howell *post-hoc* correction). Errors are SEM. For each assay: n>65 animals; 4 independent experiments. (E) Quantification of dauer formation in AWC-ablated animals in the presence of 6 µM ascr#3 and the indicated amounts of

heat-killed or live OP50 bacteria. Each filled circle represents one assay; n>65 animals per assay, 5 independent experiments. *, ** and *** indicate different from values using 160 μg of heat-killed bacteria at P<0.05, 0.01 and 0.001, respectively (ANOVA and Games-Howell *post-hoc* test). Line represents best fit to the data. Dashed line indicates the curve for wild-type animals from Figure 3.1B shown for comparison.

Figure 3.3. Subcellular localization of CMK-1 in AWC is regulated by feeding state.

(A, B) Representative images (A) and quantification (B) of subcellular localization of CMK-1::GFP in AWC neurons following removal from food for the indicated times. Representative images of CMK-1::GFP localization in AFD are also shown in A). Scale bar: 5 μm (A). n>75 AWC neurons each (B). *** indicates different from distribution at 0 min at P<0.001 (χ^2 test). (C) Dauers formed by the indicated strains on 80 μg live OP50 and 6 μM ascr#3. CMK-1::NLS::GFP and CMK-1::NES::GFP (55, 61) were expressed in AWC under the *ceh36*Δ promoter. Shown are the averages of ≥3 independent experiments with >65 animals each. For transgenic strains, data are averaged from two independent lines each. Errors are SEM. * and *** indicate different from wild-type at P<0.05 and 0.001, respectively; $^{###}$ indicates different from *cmk-1*(*oy21*) at P< 0.001 (ANOVA and Games-Howell *post-hoc* test).

Figure 3.4. CMK-1 regulates expression of a subset of ILP genes in AWC.

(A) (Top) Schematic of worm head indicating positions of sensory neuron soma. Boxed area is shown in images below. (Below) Representative images of *ins-26*p::*yfp* and *ins-35*p::*yfp* expression in fed wild-type and *cmk-1*(*oy21*) mutants. White and yellow arrowheads indicate ASI and ASE, respectively; white arrow indicates AWC; yellow asterisk marks expression in the

intestine. The location of ASK is indicated by a red arrowhead; fluorescence in ASK is weak and not visible at this exposure in shown images. Lateral view; scale bar: 10 μm. (B) Quantification of expression in each neuron type in fed and starved conditions is shown. Solid and hatched bars indicate strong and weak expression, respectively, in each cell. n>50 animals each; 3 independent experiments. (C) Dauers formed by shown strains on 6 μM ascr#3 and 80 μg live OP50. Alleles used were: *cmk-1*(*oy21*), *ins-26*(*tm1983*), and *ins-35*(*ok3297*). *ins-26* and *ins-35* cDNAs were expressed in ASE, ASJ and AWC under *che-1*, *trx-1* and *ceh-36*Δ regulatory sequences, respectively. At least two independent lines were analyzed for each transgenic strain. ** and *** indicate different from wild-type at $P<0.01$ and $P<0.001$, respectively; $^{###}$ indicates different from *cmk-1* at $P<0.001$ (ANOVA and Games-Howell *post-hoc* test). Shown are the averages of at least three independent experiments with >65 animals each.

Figure 3.5. CMK-1 acts non cell-autonomously in AWC to regulate *daf-28* ILP gene expression in ASJ.

(A) Dauers formed by the indicated strains on 80 μg live OP50 and 6 μM ascr#3. Alleles used were: *cmk-1*(*oy21*), *daf-3*(*mgDf90*), *daf-5*(*e1385*), and *daf-16*(*mgDf50*). Shown are the averages of ≥3 independent experiments with >65 animals each. Errors are SEM. *and *** indicate different from wild-type at $P<0.05$ and $P<0.001$, respectively, $^{#}$, $^{##}$ and $^{###}$ indicate different from *cmk-1* at $P<0.05$, $P<0.01$ and $P<0.001$, respectively (ANOVA and Games-Howell *post-hoc* test). (B) Representative images of *daf-28*p::*gfp* expression in L1 larvae of wild-type or *cmk-1*(*oy21*) animals under the indicated conditions. Schematic of worm head indicating positions of the ASI and ASJ sensory neuron cell bodies is shown at top; boxed region is shown in panels below. Animals were grown with plentiful live OP50 or starved for at least 6 hours in the

absence or presence of 1 unit of crude pheromone (see Materials and Methods). White arrowheads and arrows indicate cell bodies of ASI and ASJ, respectively. Yellow arrowheads indicate expression in an ectopic cell observed in ~14% of wild-type and ~50% of cmk-1 mutants under all conditions. Numbers in bottom left hand corners indicate the percentage of examined larvae that exhibit the shown expression patterns; n>50 each; 3 independent experiments. Lateral view; scale bar: 10 μm. (C) Scatter plot of fluorescence intensity of *daf-28*p::*gfp* expression in ASJ in wild-type or *cmk-1*(*oy21*) mutants. Median is indicated by red horizontal line. Animals were grown on ample live OP50 in the absence of exogenous pheromone. Each dot is the fluorescence intensity of a single neuron in a given experiment; n>60 neurons total each, at least 3 independent experiments. For transgenic strains, a representative line was selected from experiments shown in Figure 3.1E and crossed into the reporter strains. Promoters driving wild-type *cmk-1* cDNA were: ASI/AWA – *gpa-4*p; AWC – *ceh-36*Δp; ASJ – *trx-1*p. *** and $^{\#\#\#}$ indicate different from wild-type and *cmk-1*(*oy21*), respectively, at $P<0.001$ (ANOVA and Games-Howell *post-hoc* test). (D) Scatter plot of fluorescence intensity of *daf-28*p::*gfp* expression in ASJ in the indicated genetic backgrounds. The *cmk-1*(*oy21*) allele was used. *ins-26* and *ins-35*::*SL2*::*mCherry* cDNAs were expressed in AWC under *odr-1* regulatory sequences. Only animals expressing mCherry in AWC were scored. Median is indicated by red horizontal line. Each dot is the fluorescence intensity of a single neuron in a given experiment; n>60 neurons total each, 4 independent experiments. *** and $^{\#}$ indicate different from wild-type and *cmk-1*(*oy21*), respectively, at $P<0.001$ and 0.05, respectively (ANOVA and Games-Howell *post-hoc* test). (E) Dauers formed by shown strains on 80 μg live OP50 and 6 μM ascr#3. Promoters used to drive expression of wild-type *daf-28* cDNA were: ASI – *srg-47*p and ASJ – *trx-1*p. Shown are the averages of ≥3 independent experiments with >65 animals each. Errors are

SEM. * and *** indicate different from wild-type at $P<0.05$ and 0.001, respectively; ### indicates different from *cmk-1* at $P<0.001$ (ANOVA and Games-Howell *post-hoc* test).

Figure 3.6. CMK-1 acts cell-autonomously to regulate *daf-7* TGF-β expression in ASI. (A) Representative images of *daf-7*p::*gfp* expression in L1 larvae of wild-type or *cmk-1*(*oy21*) animals under the indicated conditions. Schematic at top indicates position of ASI cell body (lateral view); boxed region is shown in panels below. Occasional weak expression is observed in the ADL neurons. Animals were grown with plentiful live OP50 or starved for at least 6 hours in the absence or presence of 1 unit of crude pheromone (see Materials and Methods). White arrowheads indicate cell bodies of ASI. Numbers in bottom left hand corners indicate the percentage of examined larvae that exhibit the shown phenotype; n>50 each; 3 independent experiments. Lateral view; scale bar: 10 μm. (B) Scatter plot of fluorescence intensity of *daf-7*p::*gfp* expression in ASI in wild-type or *cmk-1*(*oy21*) mutants. Median is indicated by a red horizontal line. Animals were grown on ample live OP50 in the absence of exogenous pheromone. Each dot is the fluorescence intensity of a single neuron in a given experiment; n>60 neurons total each, at least 3 independent experiments. Promoters driving wild-type *cmk-1* cDNA were: ASI – *srg-47*p; AWC – *ceh-36*Δp. *** and ### indicate different from wild-type and *cmk-1*(*oy21*), respectively, at $P<0.001$ (ANOVA and Games-Howell *post-hoc* test). (C) Dauers formed by shown strains on 80 μg live OP50 and 6 μM ascr#3. The *srg-47*p promoter was used to drive expression of wild-type *daf-7* cDNA in ASI. Shown are the averages of ≥3 independent experiments with >65 animals each. Errors are SEM. *** indicates different from wild-type at $P<0.001$; ### indicates different from *cmk-1* at $P<0.001$ (ANOVA and Games-Howell *post-hoc* test). (D) Dauers formed by the indicated strains on 80 μg OP50 at 20°C in the absence of

exogenous pheromone. Alleles used were: *cmk-1*(*oy21*) and *daf-28*(*tm2308*). Shown are the averages of ≥3 independent experiments with >65 animals each. Errors are SEM. $^{\#}$ and $^{\#\#\#}$ indicate different from *cmk-1* at $P<0.05$ and <0.001, respectively, $^{\&\&\&}$ indicates different from *daf-28* at $P<0.001$ (ANOVA and Games-Howell *post-hoc* test).

Figure 3.7. Model for the role of CMK-1 and AWC in the integration of food information into the dauer decision.

In fed wild-type animals, CMK-1 functions in ASI and AWC to regulate the expression of *daf-7* TGF-β in ASI, and *daf-28* ILP in ASJ, and promote reproductive development. In starved wild-type animals, AWC activity is upregulated, and *daf-7* and *daf-28* expression is downregulated to promote dauer formation in the presence of pheromone. Pheromone is sensed by ASI as well as other neuron types including ASK. In fed *cmk-1* mutants, loss of *cmk-1* activity increases basal activity of AWC, and downregulates *daf-7* expression in ASI and *daf-28* expression in ASJ to enhance dauer formation in the presence of pheromone. Dauer formation in starved wild-type and fed *cmk-1* mutants is mediated by CMK-1-dependent downregulation of the *ins-26*/*ins-35* dauer-inhibitory, and upregulation of as yet unidentified dauer-promoting, ILP signals from AWC. *ins-26* and *ins-35* signaling from AWC promotes *daf-28* ILP expression in ASJ. TGF-β and ILP signals are integrated in neurons and somatic cells to regulate the dauer decision.

Figure 3.1

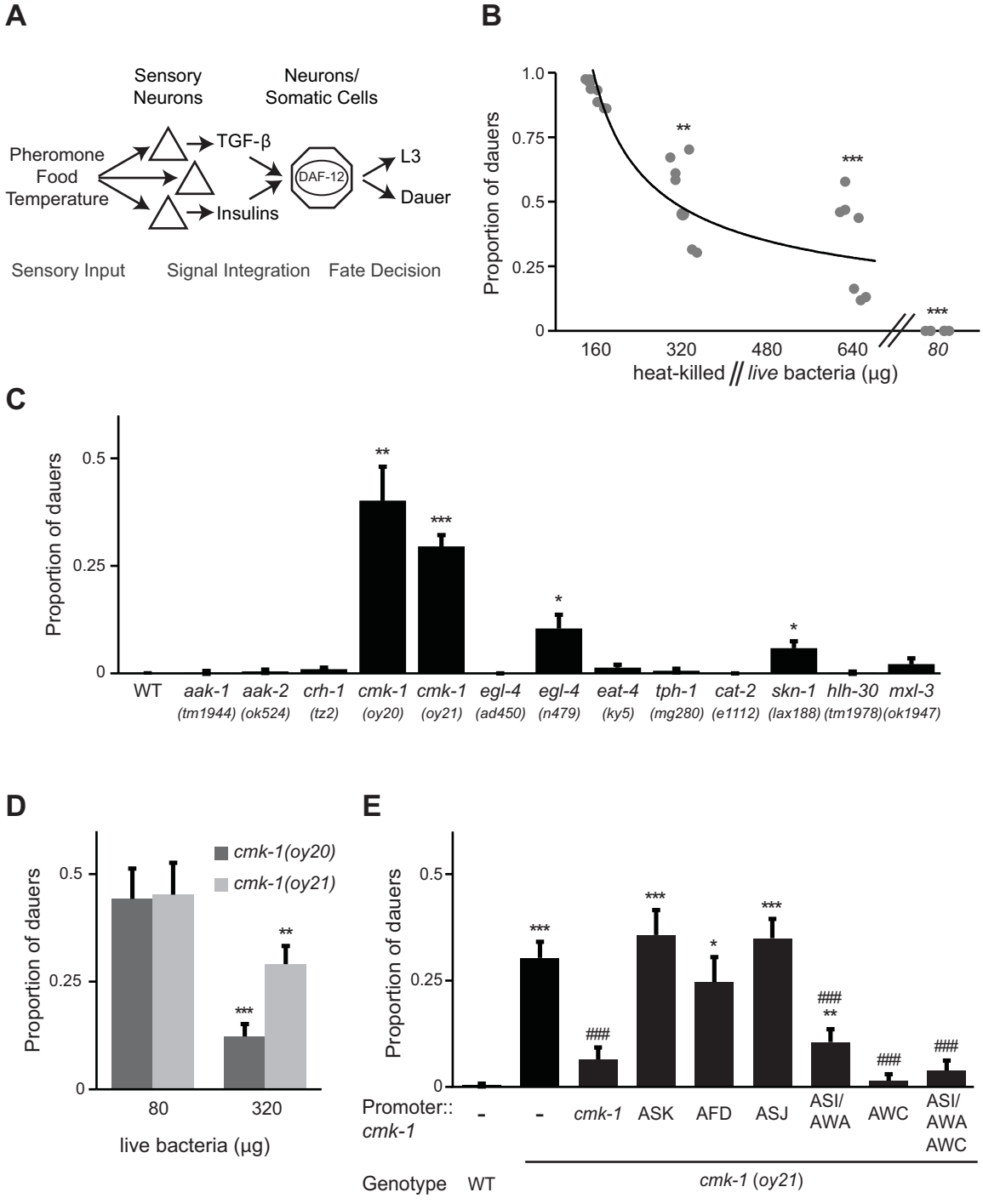
A
Sensory Neurons
Neurons/ Somatic Cells
Pheromone
Food
Temperature
TGF-β
Insulins
DAF-12
L3
Dauer
Sensory Input
Signal Integration
Fate Decision
B
Proportion of dauers
heat-killed // live bacteria (μg)
C
Proportion of dauers
WT
aak-1 (tm1944)
aak-2 (ok524)
crh-1 (tz2)
cmk-1 (oy20)
cmk-1 (oy21)
egl-4 (ad450)
egl-4 (n479)
eat-4 (ky5)
tph-1 (mg280)
cat-2 (e1112)
skn-1 (lax188)
hlh-30 (tm1978)
mxl-3 (ok1947)
D
cmk-1(oy20)
cmk-1(oy21)
Proportion of dauers
live bacteria (μg)
E
Proportion of dauers
Promoter:: cmk-1
ASK
AFD
ASJ
ASI/ AWA
AWC
ASI/ AWA AWC
Genotype
WT
cmk-1 (oy21)

Figure 3.2

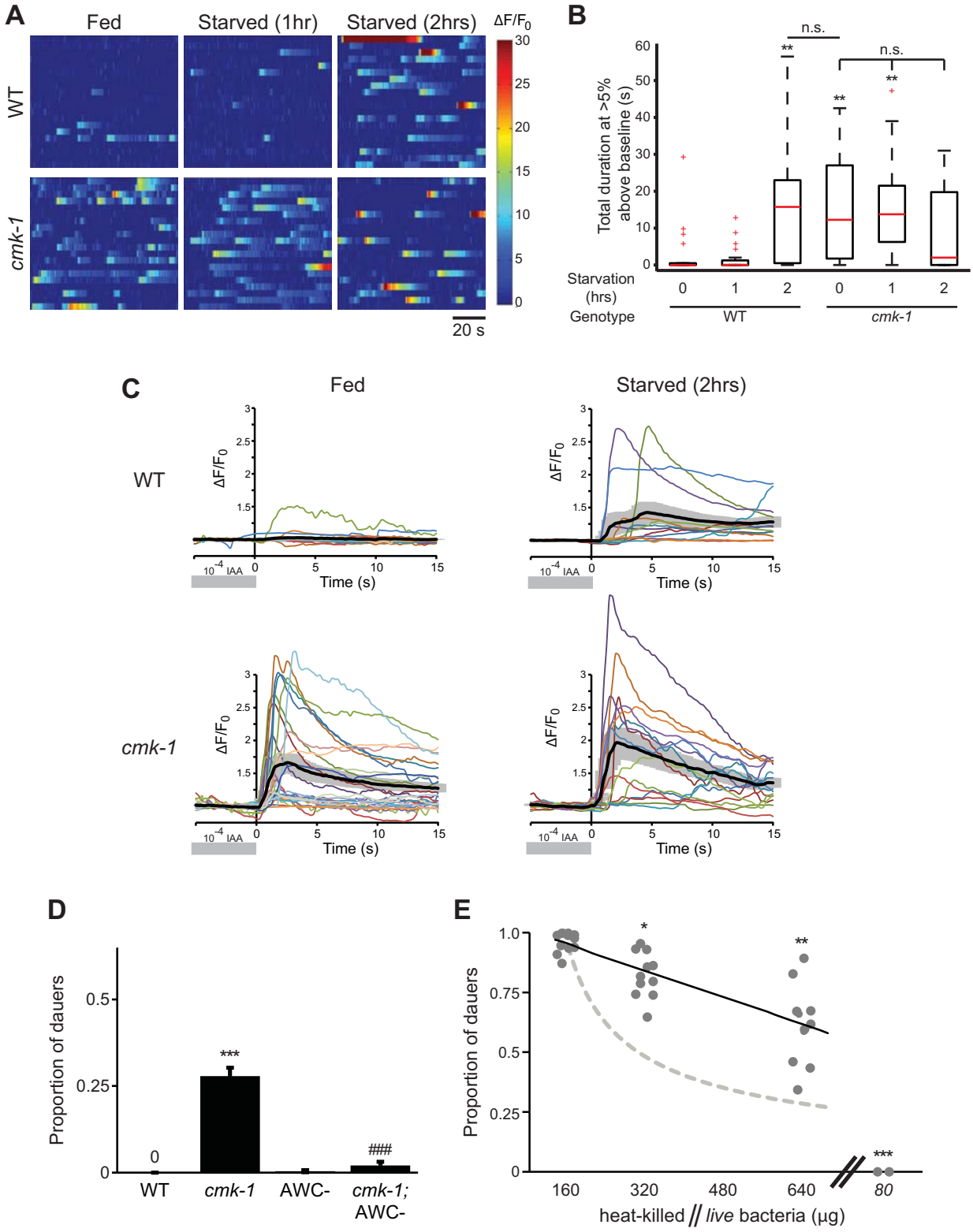
A
Fed
Starved (1hr)
Starved (2hrs)
ΔF/F0
WT
cmk-1
20 s
B
Total duration at >5% above baseline (s)
n.s.
**
Starvation (hrs)
Genotype
WT
cmk-1
C
Fed
Starved (2hrs)
WT
cmk-1
ΔF/F0
10-4 IAA
Time (s)
D
Proportion of dauers
***
###
WT
cmk-1
AWC-
cmk-1; AWC-
E
Proportion of dauers
heat-killed // live bacteria (µg)

Figure 3.3

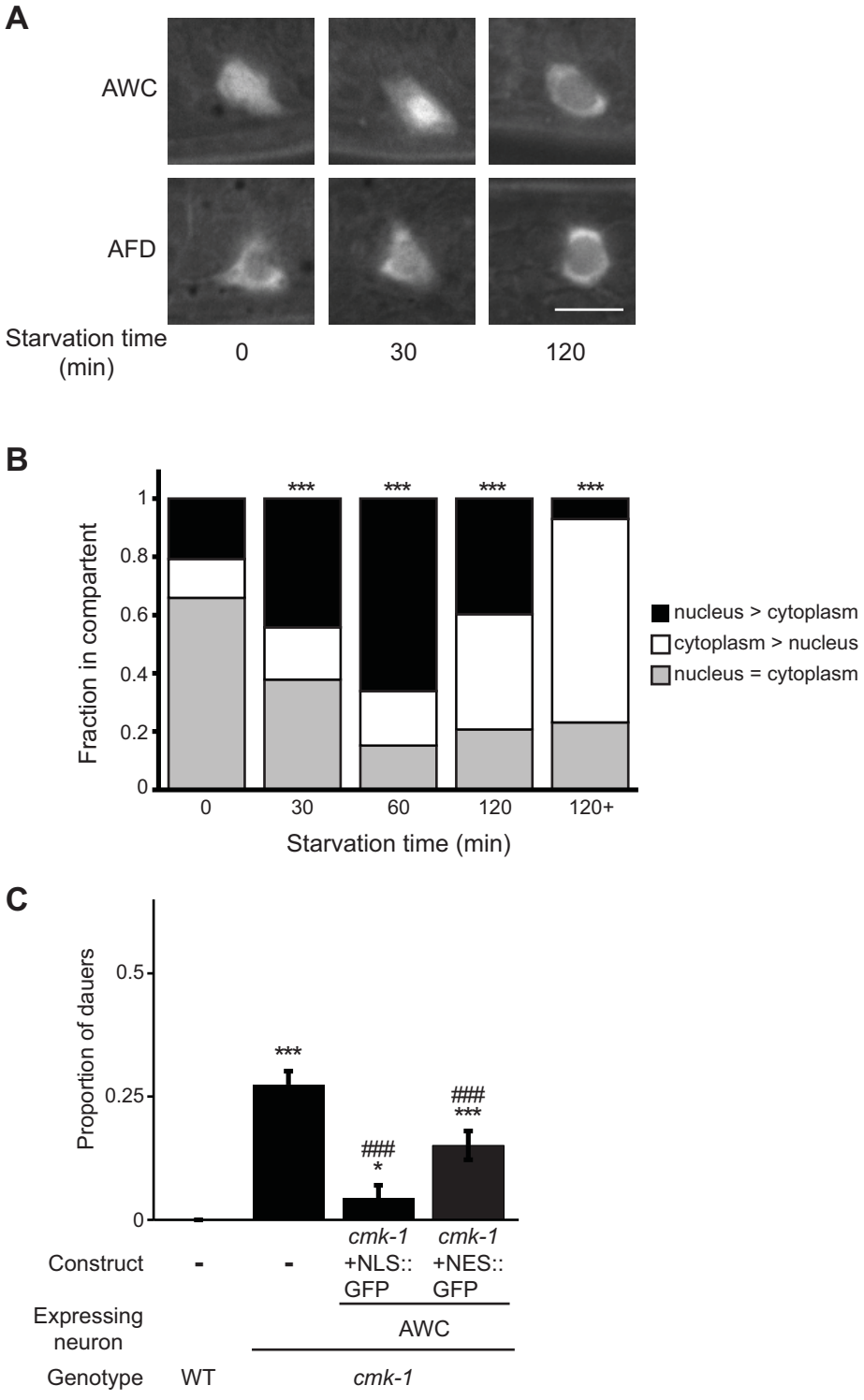
A
AWC
AFD
Starvation time (min)
0
30
120
B
Fraction in compartent
1
0.8
0.6
0.4
0.2
0
***
0
30
60
120
120+
Starvation time (min)
nucleus > cytoplasm
cytoplasm > nucleus
nucleus = cytoplasm
C
Proportion of dauers
0.5
0.25
0
***
###
*
###
***
Construct
-
-
cmk-1 +NLS:: GFP
cmk-1 +NES:: GFP
Expressing neuron
AWC
Genotype
WT
cmk-1

Figure 3.4

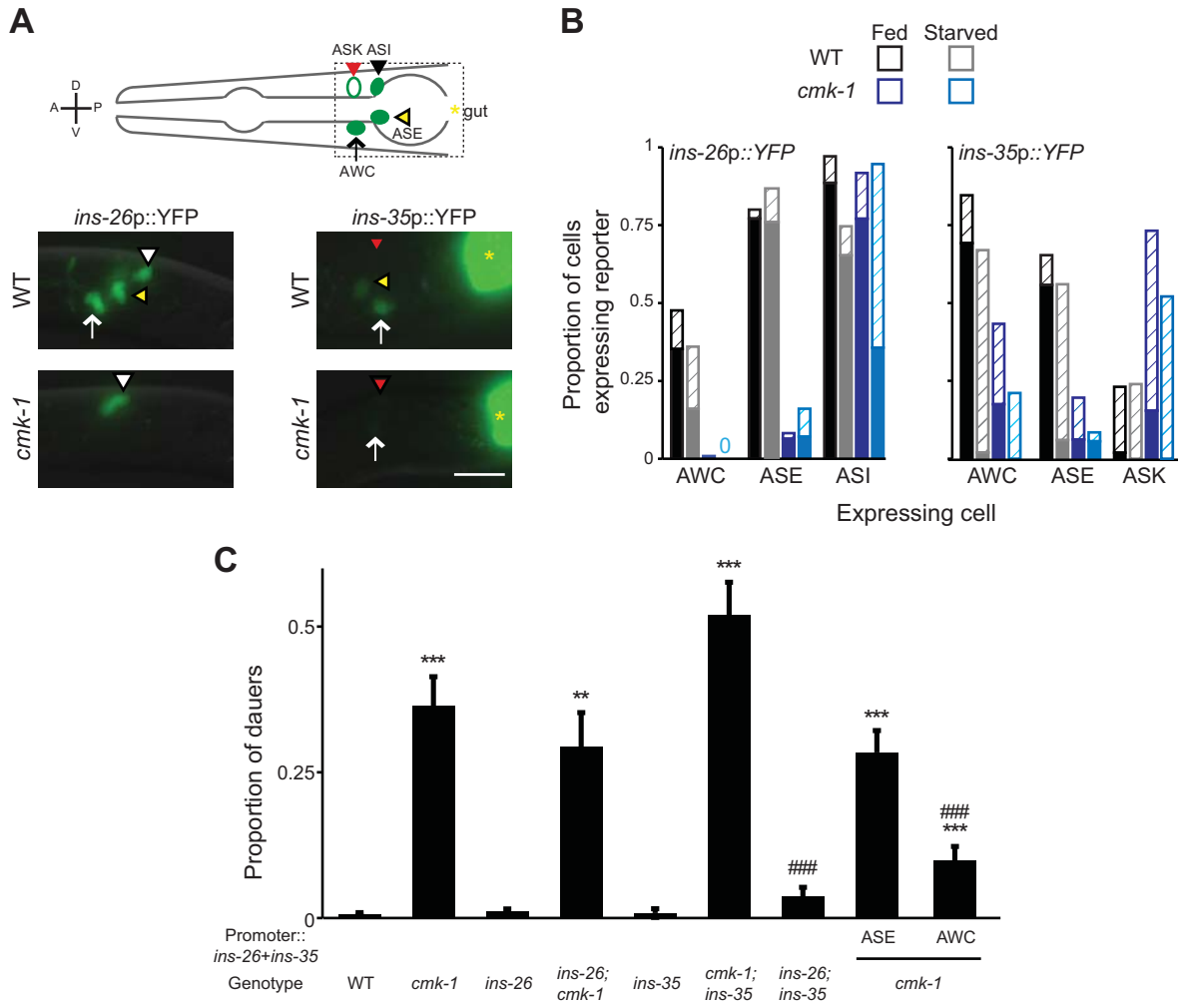
A
ASK ASI
D
A
P
V
gut
ASE
AWC
ins-26p::YFP
ins-35p::YFP
WT
cmk-1
B
Fed
Starved
WT
cmk-1
ins-26p::YFP
ins-35p::YFP
Proportion of cells expressing reporter
1
0.75
0.5
0.25
0
AWC
ASE
ASI
ASK
Expressing cell
C
Proportion of dauers
0.5
0.25
0
***
**
***
###
***
###
***
Promoter::
ins-26+ins-35
ASE
AWC
Genotype
WT
cmk-1
ins-26
ins-26; cmk-1
ins-35
cmk-1; ins-35
ins-26; ins-35
cmk-1

Figure 3.5

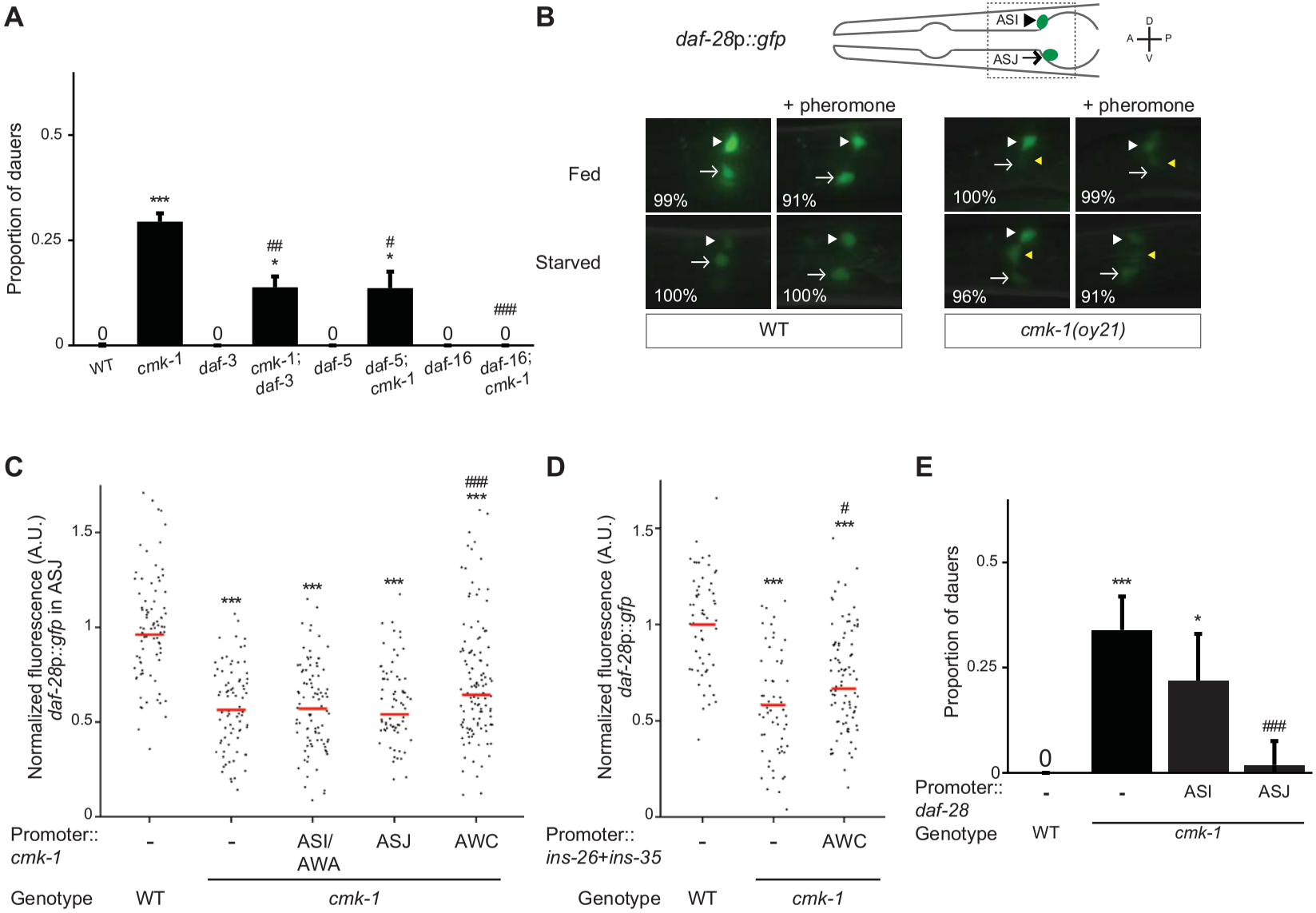
A
Proportion of dauers
0.5
0.25
0
***
##
*
#
*
###
0
0
0
0
0
0
WT
cmk-1
daf-3
cmk-1; daf-3
daf-5
daf-5; cmk-1
daf-16
daf-16; cmk-1
B
daf-28p::gfp
ASI
ASJ
D
A
P
V
+ pheromone
+ pheromone
Fed
Starved
99%
91%
100%
99%
100%
100%
96%
91%
WT
cmk-1(oy21)
C
Normalized fluorescence (A.U.)
daf-28p::gfp in ASJ
1.5
1
0.5
0
***
***
***
###
***
Promoter::
cmk-1
-
-
ASI/ AWA
ASJ
AWC
Genotype
WT
cmk-1
D
Normalized fluorescence (A.U.)
daf-28p::gfp
1.5
1
0.5
0
***
#
***
Promoter::
ins-26+ins-35
-
-
AWC
Genotype
WT
cmk-1
E
Proportion of dauers
0.5
0.25
0
***
*
###
0
Promoter::
daf-28
-
-
ASI
ASJ
Genotype
WT
cmk-1

Figure 3.6

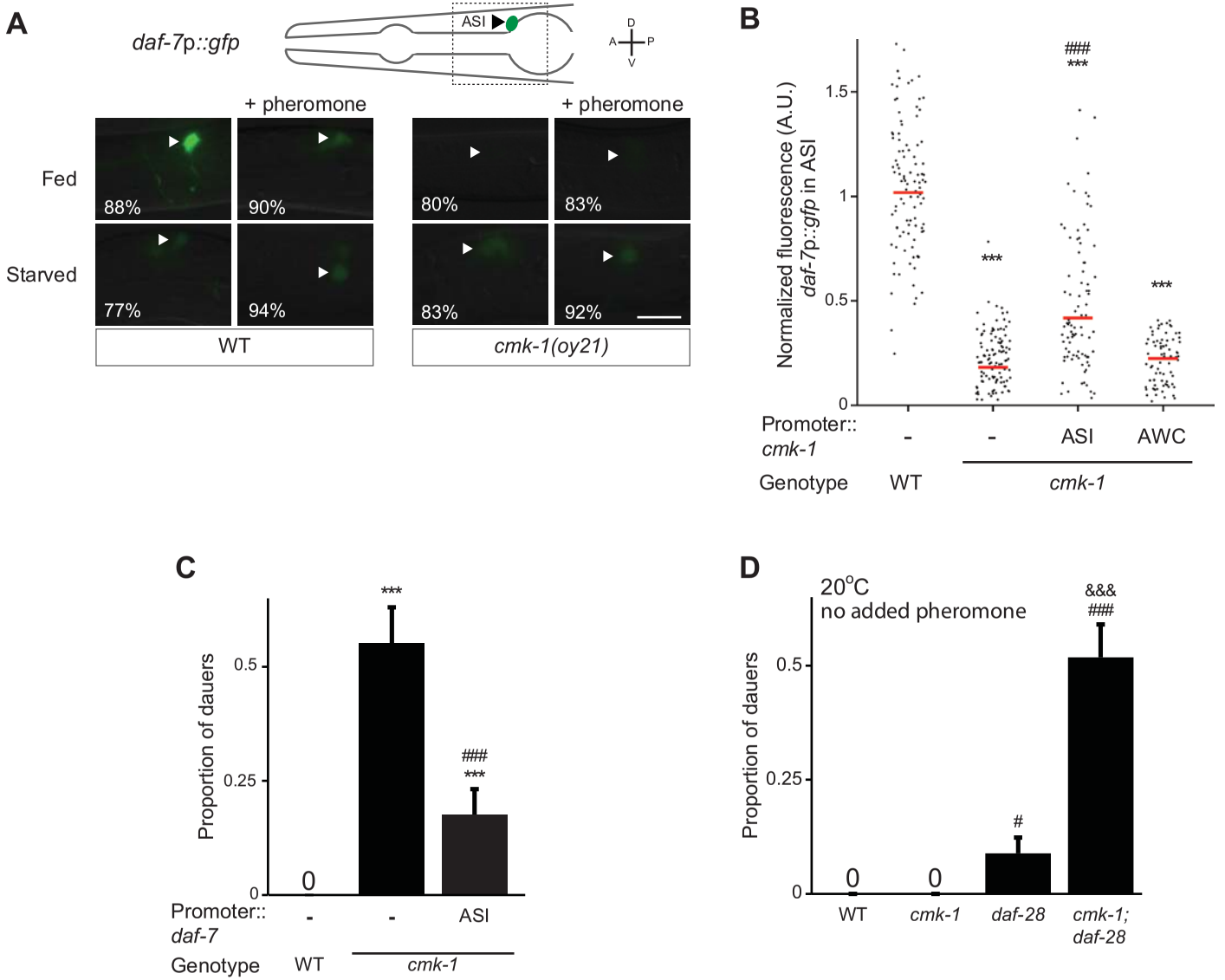
A
daf-7p::gfp
ASI
D
A
P
V
+ pheromone
+ pheromone
Fed
Starved
88%
90%
80%
83%
77%
94%
83%
92%
WT
cmk-1(oy21)
B
Normalized fluorescence (A.U.)
daf-7p::gfp in ASI
1.5
1
0.5
0
###
***
***
***
Promoter::
cmk-1
-
-
ASI
AWC
Genotype
WT
cmk-1
C
Proportion of dauers
0.5
0.25
0
***
###
***
0
Promoter::
daf-7
-
-
ASI
Genotype
WT
cmk-1
D
20°C
no added pheromone
Proportion of dauers
0.5
0.25
0
&&&
###
#
0
0
WT
cmk-1
daf-28
cmk-1;
daf-28

Figure 3.7

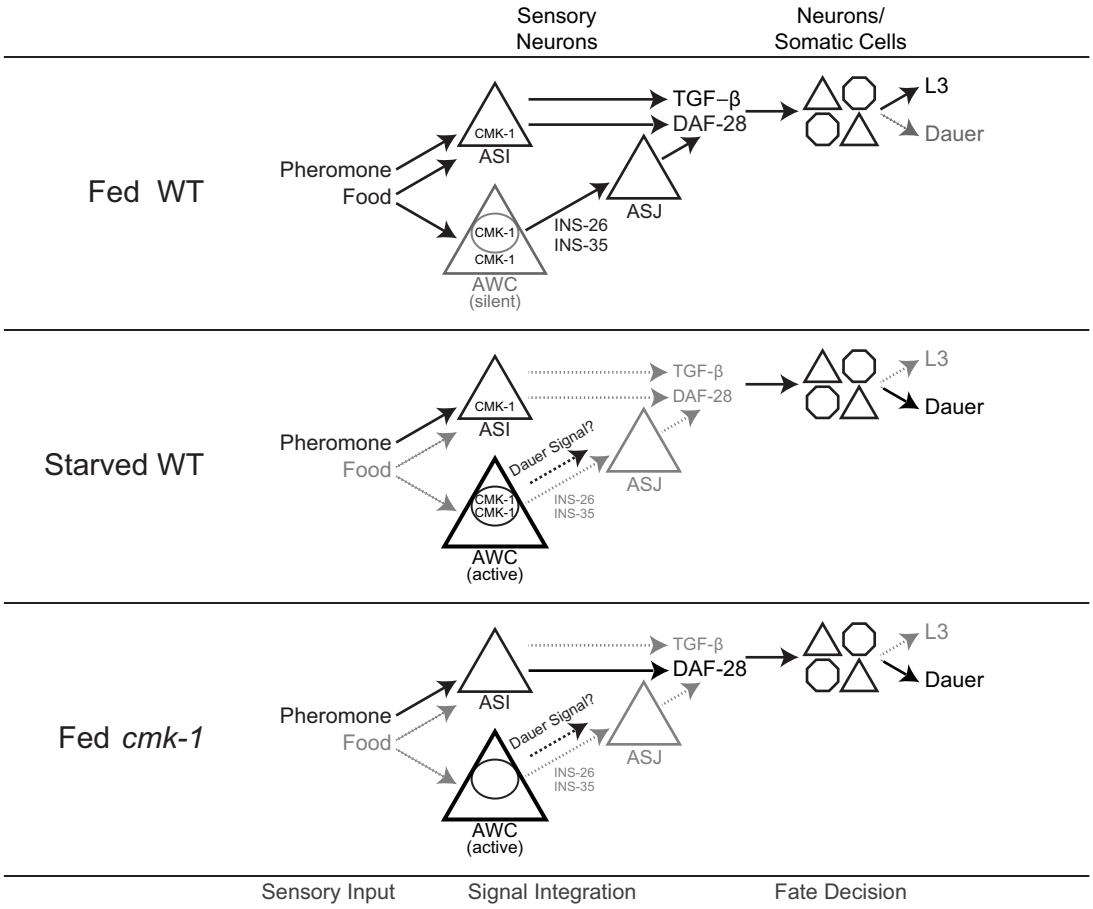
Sensory Neurons
Neurons/ Somatic Cells
Fed WT
Pheromone
Food
CMK-1
ASI
CMK-1
CMK-1
AWC
(silent)
INS-26
INS-35
ASJ
TGF–β
DAF-28
L3
Dauer
Starved WT
Pheromone
Food
CMK-1
ASI
Dauer Signal?
CMK-1
CMK-1
AWC
(active)
INS-26
INS-35
ASJ
TGF-β
DAF-28
L3
Dauer
Fed cmk-1
Pheromone
Food
ASI
Dauer Signal?
AWC
(active)
INS-26
INS-35
ASJ
TGF-β
DAF-28
L3
Dauer
Sensory Input
Signal Integration
Fate Decision

3.9 Supplemental Figure Legends

Figure S3.1. CMK-1 inhibits dauer formation in fed animals.

(A) Dauer formation in fed wild-type and *cmk-1* mutants on 80 μg live OP50 in the absence of exogenous pheromone. n>65 animals per assay; at least 12 independent trials. Errors are SEM. (B) Dauers formed by *daf-22*(*m130*) animals in the presence of 6 μM ascr#3 and the indicated amounts of heat-killed or live OP50 bacteria. Each filled circle represents one assay; n>65 animals per assay, 3 independent experiments. ** and *** indicate different from values using 160 μg of heat-killed bacteria at $P<0.01$ and 0.001, respectively (ANOVA and Games-Howell *post-hoc* test). (C, D) Dauers formed by wild-type or *cmk-1* mutants on 80 μg live OP50 and the indicated amounts of ascr#2 or icas#9. *** indicates different from wild-type at $P<0.001$ (ANOVA and Games-Howell *post-hoc* test). n>65 animals each, 3 independent experiments. Errors are SEM. (E) Egg-laying is sensitive to bacterial food in wild-type and *cmk-1*(*oy21*) mutants. Shown is the average number of eggs laid per hour in the presence or absence of live OP50 by adult animals. *** indicates different between the indicated values at $P<0.001$ (Student's t-test). n>30 animals for each condition. Errors are SEM. (F) Dauers formed by wild-type or *cmk-1*(*oy21*) mutants on 80 μg of live OP50 and 6 μM ascr#3 at 20°C. For each assay: n>65 animals each, 3 independent experiments. Errors are SEM.

Figure S3.2. *cmk-1*p::*gfp* is expressed broadly in multiple neurons.

Shown is the expression pattern of *cmk-1*p::*gfp* in an L1 larva (left panel; GFP; right panel: DIC). Note GFP expression in multiple neurons in the head and tail. Scale bar: 10 μm.

Figure S3.3. Localization of CMK-1::NLS::GFP and CMK-1::NES::GFP in AWC.

Shown is the localization of NLS::GFP or NES::GFP tagged CMK-1 protein in AWC in the indicated genetic background and conditions. Scale bar: 5 μm.

Figure S3.4. CMK-1 may also inhibit dauer-promoting signals in AWC.

Dauers formed by the indicated strains on 6 μM ascr#3 and 80 μg live OP50. Alleles used were: *cmk-1*(*oy21*) and *bli-4*(*e937*). *bli-4* and *egl-3* sense and antisense (SAS) constructs were expressed in AWC under the indicated promoters in *cmk-1* mutants. Numbers shown are from two transgenic lines each with the exception of *odr-1*p::*egl-3*(SAS). * and *** indicate different from wild-type at $P<0.05$ and 0.001, respectively; $^{\#}$, $^{\#\#}$ and $^{\#\#\#}$ indicate different from *cmk-1* at $P<0.05$, 0.01 and 0.001, respectively (ANOVA and Games-Howell *post-hoc* test). n>65 animals each; ≥3 independent experiments.

Figure S3.5. *daf-28* expression is not affected by cultivation temperature.

(Top) Schematic of worm head indicating positions of the ASI and ASJ sensory neuron cell bodies. Boxed area is shown in images below. (Below) Representative images of *daf-28*p::*gfp* in developmentally-synchronized L1 animals, grown on live OP50 and in the absence of exogenous pheromone, at the indicated temperatures. White arrowheads and arrows indicate cell bodies of ASI and ASJ, respectively. Lateral view; scale bar: 10 μm.

Table S3.1. Quantification of calcium dynamics in fed and starved wild-type and *cmk-1(oy21)* mutants.

Strain	Feeding state (n)[a]	% cells with $(\Delta F/F_0)_{max}$ >10%	% cells with $(\Delta F/F_0)_{max}$ >25%	Mean $(\Delta F/F_0)_{max}$	Maximum $(\Delta F/F_0)_{max}$
WT	Fed (22)	14	5	1.05	1.51
	Starved (12)	83	42	1.52	2.74
cmk-1 (oy21)	Fed (26)	92	58	1.84	3.37
	Starved (15)	93	87	2.13	4.20

[a]Animals were imaged immediately upon removal from food, or were starved for two hours prior to imaging. n=AWC neurons; 1 neuron was imaged per animal. Responses shown are from both left and right AWC neurons; responses from left and right neurons were similar.
WT and *cmk-1* animals were imaged together on multiple days at 20°C (see Materials and Methods).

Table S3.2. List of strains used in this work.

Strain	Genotype	Source and/or parent strains[a]	Relevant Figures (3.X, S3.X)
WT	N2 (Bristol)	CGC	1B, 1C, 1E, 2D, 3C, 4C, 5A, 5E, 6C, 6D, S1A, S1C-F, S4
PY8385	*aak-1*(*tm1944*) III	NBRP	1C
RB524	*aak-2*(*ok524*) X	CGC	1C
YT17	*crh-1*(*tz2*) III	CGC	1C
PY8386	*cmk-1*(*oy20*) IV	outcrossed from PY1237 (Satterlee et al., 2004)	1C-D, S1C-D
PY8387	*cmk-1*(*oy21*) IV	outcrossed from PY1589 (Satterlee et al., 2004)	1C-E, 2D, 3C, 4C, 5A, 5E, 6C, 6D, S1A, S1C-F, S4
DA521	*egl-4*(*ad450*) IV	CGC	1C
MT1074	*egl-4*(*n479*) IV	CGC	1C
MT6308	*eat-4*(*ky5*) III	CGC	1C
PY8388	*tph-1*(*mg280*) II	GR1321	1C
CB1112	*cat-2*(*e1112*) II	CGC	1C
SPC168	*dvIs19* [(pAF15)*gst-4*p::*gfp*::NLS] III; *skn-1*(*lax188*) IV	CGC	1C
PY8389	*hlh-30*(*tm1978*) IV	NBRP	1C
RB1588	*mxl-3*(*ok1947*) X	CGC	1C
PY8390	*cmk-1*(*oy21*) IV; Ex[*cmk-1*p::*cmk-1 unc-122*p::*dsRed*]	outcrossed from PY4672	1E
PY8391	*cmk-1*(*oy21*) IV; Ex[*sra-9*p::*cmk-1 unc-122*p::*gfp*] line 1	injected into PY8387	1E
PY8392	*cmk-1*(*oy21*) IV; Ex[*sra-9*p::*cmk-1 unc-122*p::*gfp*] line 2	injected into PY8387	1E
PY5698	*cmk-1*(*oy21*) IV; Ex[*ttx-1*p::*cmk-1 unc-122*p::*dsRed*]	injected into PY1589	1E
PY8393	*cmk-1*(*oy21*) IV; Ex[*trx-1*p::*cmk-1 unc-122*p::*gfp*] line 1	injected into PY8387	1E
PY8394	*cmk-1*(*oy21*) IV; Ex[*trx-1*p::*cmk-1 unc-122*p::*gfp*] line 2	injected into PY8387	1E
PY5399	*cmk-1*(*oy21*) IV; Ex[*gpa-4*p::*cmk-1 unc-122*p::*dsRed*]	injected into PY1589	1E
PY8395	*cmk-1*(*oy21*) IV; Ex[*ceh-36*Δp::*cmk-1 unc-122*p::*dsRed*] line 1	injected into PY8387	1E
PY8396	*cmk-1*(*oy21*) IV; Ex[*ceh-36*Δp::*cmk-1 unc-122*p::*dsRed*] line 2	injected into PY8387	1E
PY8397	*cmk-1*(*oy21*) IV; Ex[*ceh-36*Δp::*cmk-1 gpa-4*p::*cmk-1 unc-122*p::*dsRed*] line 1	injected into PY8387	1E

PY8398	*cmk-1*(*oy21*) IV; Ex[*ceh-36*Δp::*cmk-1 gpa-4*p::*cmk-1 unc-122*p::*dsRed*] line 2	injected into PY8387	1E
PY7548	Ex[*ceh-36*Δp::*GCaMP3 unc-122*p::*dsRed*]	(Beverly et al., 2011)	2A-C
PY8399	*cmk-1*(*oy21*) IV; Ex[*ceh-36*Δp::*GCaMP3 unc-122*p::*dsRed*]	PY8387, PY7548	2A-C
PY7502	*oyIs85*[*ceh-36*Δp::TU813(*recCaspase*) *ceh-36*Δp::TU814(*recCaspase*) *unc-122*p::*dsRed srtx-1*p::*gfp*]	(Beverly et al., 2011)	2D-E
PY10700	*cmk-1*(*oy21*) IV; *oyIs85*[*ceh-36*Δp::TU813(*recCaspase*) *ceh-36*Δp::TU814(*recCaspase*) *unc-122*p::*dsRed srtx-1*p::*gfp*]	PY8387, PY7502	2D
PY10701	*cmk-1*(*oy21*) IV; Ex[*ceh-36*Δp::*cmk-1*::*gfp unc-122*p::*dsRed*]	(3)	3A-B
PY8705	*cmk-1*(*oy21*) IV; Ex[*ttx-1*p::*cmk-1*::*gfp unc-122*p::*dsRed*]	(Yu et al., 2014)	3A
PY10702	*cmk-1*(*oy21*) IV; Ex[*ceh-36*Δp::*cmk-1*::NLS::*gfp unc-122*p::*gfp*] line 1	injected into PY8387	3C
PY10703	*cmk-1*(*oy21*) IV; Ex[*ceh-36*Δp::*cmk-1*::NLS::*gfp unc-122*p::*gfp*] line 2	injected into PY8387	3C
PY10704	*cmk-1*(*oy21*) IV; Ex[*ceh-36*Δp::*cmk-1*::NES::*gfp unc-122*p::*gfp*] line 1	injected into PY8387	3C
PY10705	*cmk-1*(*oy21*) IV; Ex[*ceh-36*Δp::*cmk-1*::NES::*gfp unc-122*p::*gfp*] line 2	injected into PY8387	3C
LRB50	*unc-119*(*ed9*) III; Ex[*ins-26*p::*yfp*::PEST *unc-119*+]	(Chen and Baugh, 2014)	4A-B
PY10706	*cmk-1*(*oy21*) IV; Ex[*ins-26*p::*yfp*::PEST *unc-119*+]	PY8387, LRB50	4A-B
LRB54	*unc-119*(*ed9*) III; Ex[*ins-35*p::*yfp*::PEST *unc-119*+]	(Chen and Baugh, 2014)	4A-B
PY10707	*cmk-1*(*oy21*) IV; Ex[*ins-35*p::*yfp*::PEST *unc-119*+]	PY8387, LRB54	4A-B
PY10708	*ins-26*(*tm1983*) I	NBRP	4C
PY10709	*ins-26*(*tm1983*) I; *cmk-1*(*oy21*) IV	PY8387, PY10708	4C
PY10710	*ins-35*(*ok3297*) V	outcrossed from RB2412	4C
PY10711	*cmk-1*(*oy21*) IV; *ins-35*(*ok3297*) V	PY8387, RB2412	4C
PY10712	*ins-26*(*tm1983*) I; *ins-35*(*ok3297*) V	PY10708, RB2412	4C
PY10713	*cmk-1*(*oy21*) IV; Ex[*che-1*p::*ins-26 che-1*p::*ins-35 unc-122*p::*gfp*] line 1	injected into PY8387	4C
PY10714	*cmk-1*(*oy21*) IV; Ex[*che-1*p::*ins-26 che-1*p::*ins-35 unc-122*p::*gfp*] line 2	injected into PY8387	4C
PY10715	*cmk-1*(*oy21*) IV; Ex[*trx-1*p::*ins-26 trx-1*p::*ins-35 unc-122*p::*gfp*] line 1	injected into PY8387	4C
PY10716	*cmk-1*(*oy21*) IV; Ex[*trx-1*p::*ins-26 trx-1*p::*ins-35 unc-122*p::*gfp*] line 2	injected into PY8387	4C

PY10717	*cmk-1*(*oy21*) IV; Ex[*ceh-36*Δp::*ins-26 ceh-36*Δp::*ins-35 unc-122*p::*gfp*] line 1	injected into PY8387	4C
PY10718	*cmk-1*(*oy21*) IV; Ex[*ceh-36*Δp::*ins-26 ceh-36*Δp::*ins-35 unc-122*p::*gfp*] line 2	injected into PY8387	4C
GR1311	*daf-3*(*mgDf90*) X	CGC	5A
PY10719	*cmk-1*(*oy21*) IV; *daf-3*(*mgDf90*) X	PY8387, GR1311	5A
CB1385	*daf-5*(*e1385*) II	CGC	5A
PY10720	*daf-5*(*e1385*) II; *cmk-1*(*oy21*) IV	PY8387, CB1385	5A
GR1307	*daf-16*(*mgDf50*) I	CGC	5A
PY10721	*daf-16*(*mgDf50*) I; *cmk-1*(*oy21*) IV	PY8387, GR1307	5A
GR1455	*mgIs40*[*daf-28*p::NLS::*gfp lin-15*+]	CGC	5B-D, S5
PY10722	*cmk-1*(*oy21*) IV; *mgIs40*[*daf-28*p::NLS::*gfp lin-15*+]	PY8387, GR1455	5B-D
PY10723	*cmk-1*(*oy21*) IV; *mgIs40*[*daf-28*p::NLS::*gfp lin-15*+]; Ex[*gpa-4*p::*cmk-1 unc-122*p::*dsRed*]	PY10722, PY5399	5C
PY10724	*cmk-1*(*oy21*) IV; *mgIs40*[*daf-28*p::NLS::*gfp lin-15*+]; Ex[*trx-1*p::*cmk-1 unc-122*p::*gfp*]	PY10722, PY8393	5C
PY10725	*cmk-1*(*oy21*) IV; *mgIs40*[*daf-28*p::NLS::*gfp lin-15*+]; Ex[*ceh-36*Δp::*cmk-1 unc-122*p::*dsRed*]	PY10722, PY8395	5C
PY10726	*cmk-1*(*oy21*) IV; *mgIs40*[*daf-28*p::NLS::*gfp lin-15*+]; Ex[*ceh-36*Δp::*ins-26 ceh-36*Δp::*ins-35*::SL2::*mCherry unc-122*p::*dsRed*] line 1	injected into PY10722	5D
PY10727	cmk-1(oy21) IV; *mgIs40*[*daf-28*p::NLS::*gfp lin-15*+]; Ex[*ceh-36*Δp::*ins-26 ceh-36*Δp::*ins-35*::SL2::*mCherry unc-122*p::*dsRed*] line 2	injected into PY10722	5D
PY10728	*cmk-1*(*oy21*) IV; Ex[*srg-47*p::*daf-28*(gDNA) *unc-122*p::*gfp*] line 1	injected into PY8387	5E
PY10729	*cmk-1*(*oy21*) IV; Ex[*srg-47*p::*daf-28*(gDNA) *unc-122*p::*gfp*] line 2	injected into PY8387	5E
PY10730	*cmk-1*(*oy21*) IV; Ex[*trx-1*p::*daf-28*(gDNA) *unc-122*p::*gfp*] line 1	injected into PY8387	5E
PY10731	*cmk-1*(*oy21*) IV; Ex[*trx-1*p::*daf-28*(gDNA) *unc-122*p::*gfp*] line 2	injected into PY8387	5E
FK181	*ksIs2*[*daf-7*p::*gfp rol-6*(*su1006*)]	CGC	6A-B
PY10732	*cmk-1*(*oy21*) IV; *ksIs2*[*daf-7*p::*gfp rol-6*(*su1006*)]	PY8387, FK181	6A-B
PY10733	*cmk-1*(*oy21*) IV; *ksIs2*[*daf-7*p::*gfp rol-6*(*su1006*)]; Ex[*srg-47*p::*cmk-1 unc-122*p::*dsRed*] line 1	injected into PY10732	6B

PY10734	cmk-1(oy21) IV; *ksIs2*[*daf-7*p::*gfp rol-6*(*su1006*)]; Ex[*srg-47*p::*cmk-1 unc-122*p::*dsRed*] line 2	injected into PY10732	6B
PY10735	*cmk-1*(*oy21*) IV; *ksIs2*[*daf-7*p::*gfp rol-6*(*su1006*)]; Ex[*ceh-36*Δp::*cmk-1 unc-122*p::*dsRed*]	PY10732, PY8395	6B
PY10736	*cmk-1*(*oy21*) IV; Ex[*srg-47*p::*daf-7 unc-122*p::*gfp*] line 1	injected into PY8387	6C
PY10737	*cmk-1*(*oy21*) IV; Ex[*srg-47*p::*daf-7 unc-122*p::*gfp*] line 2	injected into PY8387	6C
PY10738	*daf-28*(*tm2308*) V	NBRP	6D
PY10739	*cmk-1*(*oy21*) IV; *daf-28*(*tm2308*) V	PY8387, PY10738	6D
DR476	*daf-22*(*m130*) II	CGC	S1B
PY1991	Ex[*cmk-1*p::*gfp rol-6*(*su1006*)]	(Satterlee et al., 2004)	S2
PY10740	Ex[*ceh-36*Δp::*cmk-1*::NLS::*gfp unc-122*p::*gfp*]	injected into WT	S3A
PY10741	Ex[*ceh-36*Δp::*cmk-1*::NES::*gfp unc-122*p::*gfp*]	injected into WT	S3A
PY10742	*cmk-1*(*oy21*) IV; Ex[*ceh-36*Δp::*cmk-1*::NLS::*gfp unc-122*p::*gfp*]	injected into PY8387	S3B
PY10743	*cmk-1*(*oy21*) IV; Ex[*ceh-36*Δp::*cmk-1*::NES::*gfp unc-122*p::*gfp*]	injected into PY8387	S3B
PY10744	*bli-4*(*e937*) I; *cmk-1*(*oy21*) IV	PY8387, CB937	S4
PY10745	*cmk-1*(*oy21*) IV; Ex[*ceh-36*Δp::*bli-4*(S)::SL2::*mCherry ceh-36*Δp::*bli-4*(AS)::SL2::*mCherry unc-122*p::*gfp*] line 1	injected into PY8387	S4
PY10746	*cmk-1*(*oy21*) IV; Ex[*ceh-36*Δp::*bli-4*(S)::SL2::*mCherry ceh-36*Δp::*bli-4*(AS)::SL2::*mCherry unc-122*p::*gfp*] line 2	injected into PY8387	S4
PY10747	*cmk-1*(*oy21*) IV; Ex[*odr-1*p::*bli-4*(S)::SL2::*mCherry odr-1*p::*bli-4*(AS)::SL2::*mCherry unc-122*p::*gfp*] line 1	injected into PY8387	S4
PY10748	*cmk-1*(*oy21*) IV; Ex[*odr-1*p::*bli-4*(S)::SL2::*mCherry odr-1*p::*bli-4*(AS)::SL2::*mCherry unc-122*p::*gfp*] line 2	injected into PY8387	S4
PY10749	*cmk-1*(*oy21*) IV; Ex[*odr-3*p::*bli-4*(S)::SL2::*mCherry odr-3*p::*bli-4*(AS)::SL2::*mCherry unc-122*p::*gfp*] line 1	injected into PY8387	S4
PY10750	*cmk-1*(*oy21*) IV; Ex[*odr-3*p::*bli-4*(S)::SL2::*mCherry odr-3*p::*bli-4*(AS)::SL2::*mCherry unc-122*p::*gfp*] line 2	injected into PY8387	S4

PY10751	*cmk-1*(*oy21*) IV; Ex[*ceh-36*Δp::*egl-3*(S)::SL2::*mCherry ceh-36*Δp::*egl-3*(AS)::SL2::*mCherry unc-122*p::*gfp*] line 1	injected into PY8387	S4
PY10752	*cmk-1*(*oy21*) IV; Ex[*ceh-36*Δp::*egl-3*(S)::SL2::*mCherry ceh-36*Δp::*egl-3*(AS)::SL2::*mCherry unc-122*p::*gfp*] line 2	injected into PY8387	S4
PY10753	*cmk-1*(*oy21*) IV; Ex[*odr-1*p::*egl-3*(S) *odr-1*p::*egl-3*(AS) *unc-122*p::*gfp*]	PY8387, ZC2114 (Harris et al., 2014)	S4

[a]CGC – *Caenorhabditis* Genetics Center; NBRP – National BioResource Project

Figure S3.1

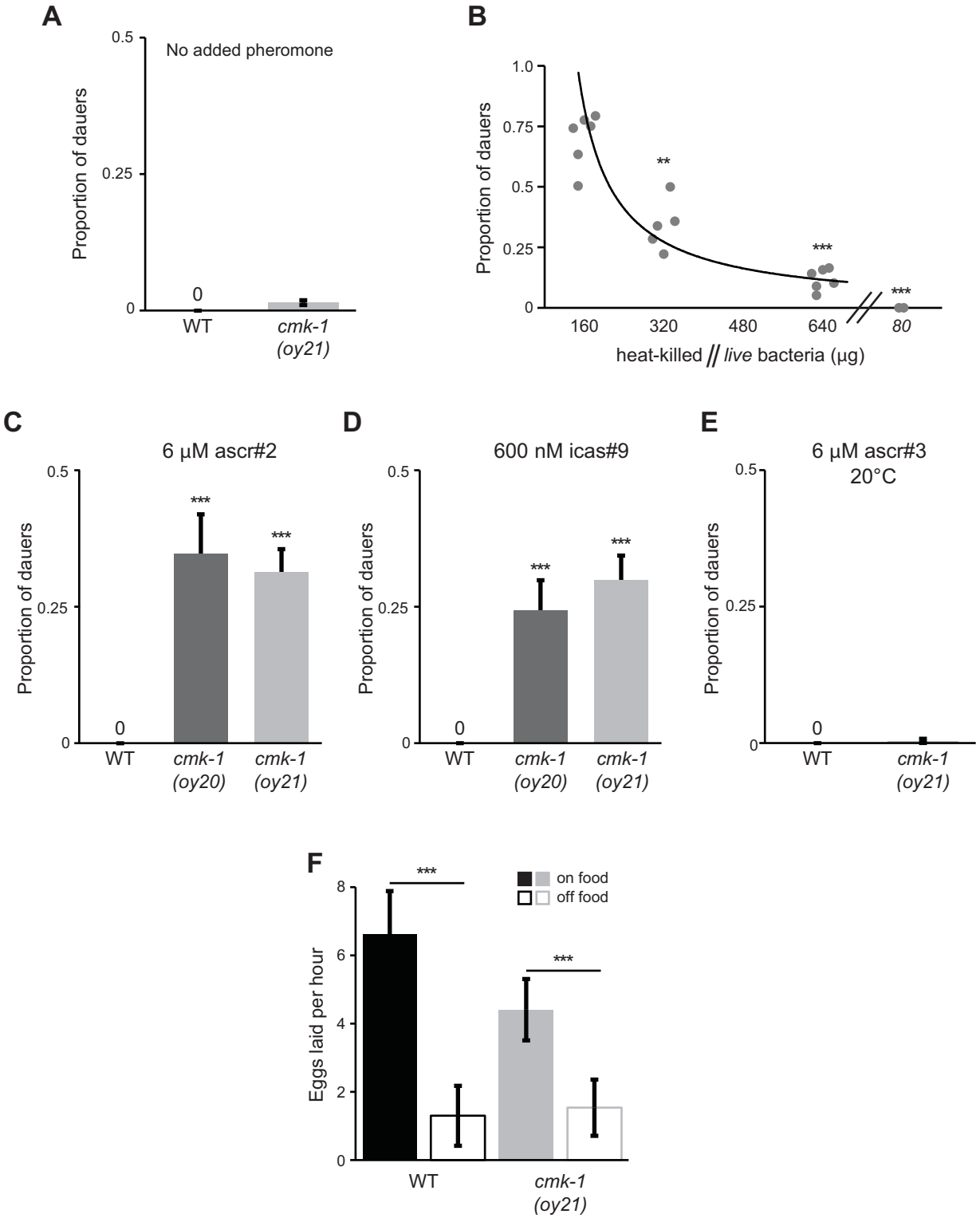
A
No added pheromone
Proportion of dauers
0.5
0.25
0
0
WT
cmk-1 (oy21)
B
Proportion of dauers
1.0
0.75
0.5
0.25
0
**
***
***
160
320
480
640
80
heat-killed // live bacteria (µg)
C
6 µM ascr#2
Proportion of dauers
0.5
0.25
0
***
***
0
WT
cmk-1 (oy20)
cmk-1 (oy21)
D
600 nM icas#9
Proportion of dauers
0.5
0.25
0
***
***
0
WT
cmk-1 (oy20)
cmk-1 (oy21)
E
6 µM ascr#3 20°C
Proportion of dauers
0.5
0.25
0
0
WT
cmk-1 (oy21)
F
***
***
on food
off food
Eggs laid per hour
8
6
4
2
0
WT
cmk-1 (oy21)

Figure S3.2

Figure S3.3

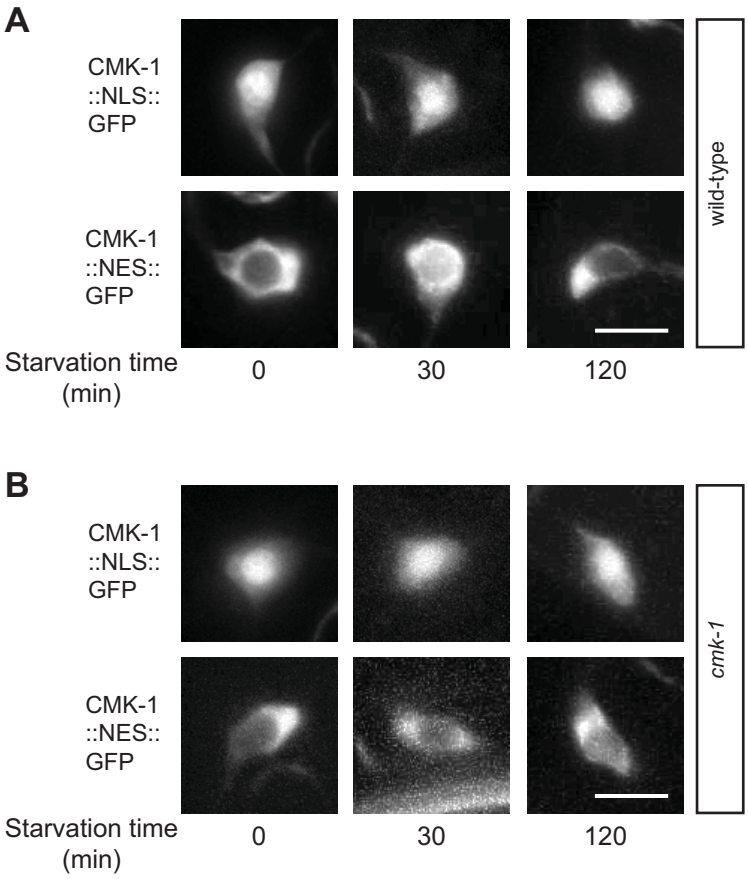
A
CMK-1
::NLS::
GFP
CMK-1
::NES::
GFP
wild-type
Starvation time
(min)
0
30
120
B
CMK-1
::NLS::
GFP
CMK-1
::NES::
GFP
cmk-1
Starvation time
(min)
0
30
120

Figure S3.4

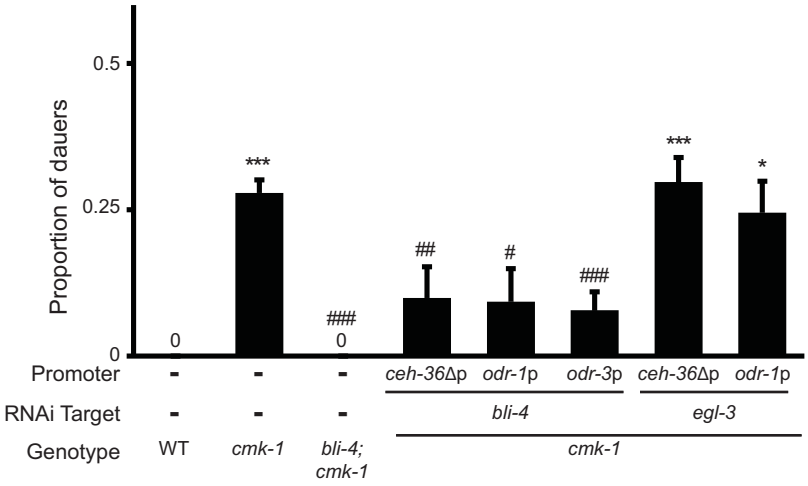
Proportion of dauers
0.5
0.25
0
***
###
##
#
###
***
*
0
0
Promoter
RNAi Target
Genotype
-
-
-
-
-
-
-
-
-
WT
cmk-1
bli-4; cmk-1
ceh-36Δp
odr-1p
odr-3p
ceh-36Δp
odr-1p
bli-4
egl-3
cmk-1

Figure S3.5

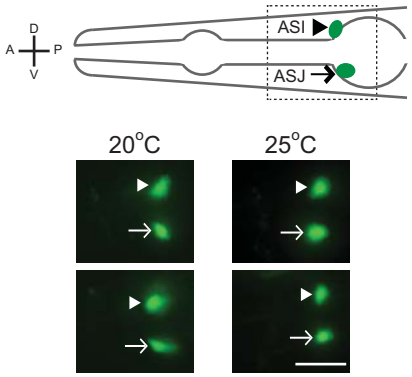

CHAPTER 4

General Discussion

4.1 Impact of this Work

In this dissertation I have described the identification of new signaling molecules (Chapter 2) and mechanisms of cellular and circuit-level regulation of endocrine signaling (Chapter 3) which integrate environmental signals to inform a critical developmental choice. Organisms must be adapted to their environments, and yet seldom are these environments stable. The evolution of polyphenism, and of reaction norms, highlight how developmental plasticity is used to compensate for environmental uncertainty (Nijhout, 2003; Simpson et al., 2011; Stearns, 1989). Such adaptations are particularly salient for small organisms with reduced homeostatic buffering capacity and for those with limited ability to disperse from unfavorable environments (Kodama-Namba et al., 2013). Just as behavioral studies have helped to provide insight into the mechanisms of sensory signal integration in acute responses and short term plasticity, studies of developmental processes will help us understand how long term integration of life history traits manifest in the neuromodulatory state (Bargmann, 2012; Bargmann and Marder, 2013; Marder, 2012; Taghert and Nitabach, 2012), and to lasting and even transgenerational effects on the epigenome of an organism (Beldade et al., 2011; Hall et al., 2010).

In Chapter 2 I sought to identify molecules which function in the signal transduction of ascarosides. Indeed I identified potential roles for several molecules and also found evidence for the function of two avoidance neurons, ADL and ASH, in the regulation for dauer formation. ADL was previously identified by laser ablation to affect dauer formation (Schackwitz et al., 1996), though no dauer signaling molecules which function specifically in ADL have been described. I have identified a role for QUI-1 in both ADL and ASH. This large protein may serve as a scaffold to stabilize sensory transduction machinery at the membrane, but has also been proposed to be involved in lipid signaling (Hilliard et al., 2004). In addition, I have

identified three members of a TTBK family that is expanded in *C. elegans* (Manning, 2005), which function to regulate dauer formation. The selective expression of these TTBKs in subsets of ciliated sensory neurons may suggest that they have a specific role in either maintaining ciliary function or in directing appropriate signaling molecules to the ciliary compartment.

In Chapter 3 I investigated the mechanism by which nutritive cues are integrated with instructive pheromone cues to modulate dauer formation. I identified for the first time a role for the AWC olfactory neurons in regulating dauer formation as well as a role for CMK-1 as a molecular integrator of feeding state. I demonstrated how feeding state is encoded in the pattern of activity of the AWC neuron and in the expression of specific ILPs which are expressed by AWC to non cell-autonomously regulate expression of the key downstream ILP DAF-28. It remains to be determined how the shuttling of CMK-1 between the cytoplasm and nucleus of AWC encodes feeding state on the molecular level. CMK-1 may function in the nucleus to activate or repress specific transcription factors which alter the expression of endocrine signals by this neuron. An alternate hypothesis is that sequestering CMK-1 in the nucleus may prevent the adaptation of membrane ion channel, thus allowing them to hyperactivate the neuron (Inoue et al., 2013). Given a similar potential role for CMK-1 in temperature integration (Satterlee et al., 2004; Schild et al., 2014; Yu et al., 2014), and the conservation of CMK-1 across taxa, these hypotheses should be explored in future research.

4.2 Integration of TGF-β and Insulin Signals

The regulation of dauer formation is controlled by parallel endocrine pathways (Hu, 2007). As has been proposed in other examples of polyphenism, it is likely that the endogenous actions of these established signaling cascades has been co-opted by the evolution of the

polyphenism (Nijhout, 2003). However, it is interesting to speculate as to their redundant and non-redundant roles. With respect to models of cancer formation a "two-hit hypothesis" was formed, proposing that safeguards are in place to prevent malignant growth (Ashley, 1969). Similar developmental controls may exist such that distinct environmental factors differentially regulate the TGF-β and insulin pathways and that dauers are formed only in the coincidence of the appropriate stimuli. It has already been proposed that the interplay between these pathways may define a sharp boundary between acceptable and unacceptable environments for reproductive growth (Schackwitz et al., 1996), but what is the integrator?

In Chapter 3 I investigated the role for CMK-1 in integrating food information into the dauer decision and observed the CMK-1 dependence of both insulin and TGF-β signals. CMK-1 is likely to function downstream of DAF-11 in this regard. Interestingly, although I demonstrated a role for CMK-1 in ASI neurons, its function in this cell type was selective to the cell-autonomous regulation of the expression of the *daf-7* TGF-β ligand, but not of the *daf-28* ILP. Instead, pheromone regulates the expression of the *daf-28* ILP in ASI in a CMK-1-independent mechanism. Indeed, the entire basis of the work in Chapter 2 was to identify molecules which might non cell-autonomously integrate pheromone signals into gene expression in ASI. It will thus be interesting to determine where and how molecules such as QUI-1 and TTBKs affect the integration of food and pheromone cues with respect to the insulin and TGF-β pathways. Furthermore, these results provide the basis for examining the role of TGF-β signaling in the expression of polyphenism in other organisms since it has thus far remained unexplored.

4.3 Future Directions

What is the Food Signal? Our ability to truly understand how sensory stimuli are integrated is contingent upon knowing what the relevant stimuli are. Our understanding of the sensory processing of ascarosides has benefitted tremendously from their chemical identification, and similar identification of the food stimulus/stimuli is required. Notably, I have identified roles for a gustatory neuron, ASI, and an olfactory neuron, AWC, in the integration of the food signal in the dauer polyphenism. Although it is easy to imagine how an olfactory neuron might alert *C. elegans* to the presence of food it is more difficult to foresee how this stimulus can be anything more than correlated with the nutritional value of food. Instead, the role of the gustatory neuron may be to directly sense the nutritive value of the food source, perhaps via the detection of sugars or amino acids. However, in mammals, both the nutritive and hedonic values of food are assessed and are reported via a hypothalamic circuit to modulate food seeking behavior (Chambers et al., 2013; Jennings et al., 2013; Palouzier-Paulignan et al., 2012). Thus, the role of the olfactory neuron in reporting the presence of food and/or the intrinsic feeding state is not to be disparaged (Sengupta, 2013).

In the course of this work I have also identified and established a number of molecules and processes which may be developed into tools to further interrogate sensory signaling mechanisms. Broadly expressed molecules with conserved functions such as CHE-12 (Bacaj et al., 2008) and MACO-1 (Arellano-Carbajal et al., 2011) may be used to establish the necessity and sufficiency of specific cells types, and the associated pathways in the detection and integration of environmental stimuli. Though we typically think of sensory responses in an acute way, the dauer developmental decision is integrated over hours and likely relies robust operation of signal transduction cascades for the duration of the period. Thus, molecules like MACO-1

might ensure the proper function of the circuit by providing a steady supply of the appropriate ion channels to synapses and CHE-12 may function similarly, instead in the cilium. In addition, redundant and non-redundant functions among TTBKs should be explored; identifying their substrate(s) will also be of great importance. Given the implication of human TTBKs in neurodegenerative disease there lies the potential to exploit the tools afforded by *C. elegans* to benefit human health (Goetz et al., 2012; Liachko et al., 2014; Sato et al., 2006).

REFERENCES

Ailion, M., and Thomas, J.H. (2000). Dauer formation induced by high temperatures in Caenorhabditis elegans. Genetics *156*, 1047-1067.
Albert, P.S., Brown, S.J., and Riddle, D.L. (1981). Sensory control of dauer larva formation in Caenorhabditis elegans. The Journal of comparative neurology *198*, 435-451.
Albert, P.S., and Riddle, D.L. (1988). Mutants of Caenorhabditis elegans that form dauer-like larvae. Developmental biology *126*, 270-293.
Alcedo, J., and Kenyon, C. (2004). Regulation of C. elegans longevity by specific gustatory and olfactory neurons. Neuron *41*, 45-55.
Antebi, A., Culotti, J.G., and Hedgecock, E.M. (1998). daf-12 regulates developmental age and the dauer alternative in Caenorhabditis elegans. Development *125*, 1191-1205.
Antebi, A., Yeh, W.H., Tait, D., Hedgecock, E.M., and Riddle, D.L. (2000). daf-12 encodes a nuclear receptor that regulates the dauer diapause and developmental age in C. elegans. Genes & development *14*, 1512-1527.
Apfeld, J., O'Connor, G., McDonagh, T., DiStefano, P.S., and Curtis, R. (2004). The AMP-activated protein kinase AAK-2 links energy levels and insulin-like signals to lifespan in C. elegans. Genes & development *18*, 3004-3009.
Arellano-Carbajal, F., Briseno-Roa, L., Couto, A., Cheung, B.H., Labouesse, M., and de Bono, M. (2011). Macoilin, a conserved nervous system-specific ER membrane protein that regulates neuronal excitability. PLoS genetics *7*, e1001341.
Ashley, D.J. (1969). The two "hit" and multiple "hit" theories of carcinogenesis. British journal of cancer *23*, 313-328.
Avery, L. (1993). The genetics of feeding in Caenorhabditis elegans. Genetics *133*, 897-917.
Avery, L. (2014). A model of the effect of uncertainty on the C elegans L2/L2d decision. PloS one *9*, e100580.
Bacaj, T., Lu, Y., and Shaham, S. (2008). The conserved proteins CHE-12 and DYF-11 are required for sensory cilium function in Caenorhabditis elegans. Genetics *178*, 989-1002.
Bargmann, C.I. (2006). Chemosensation in C. elegans. WormBook : the online review of C elegans biology, 1-29.
Bargmann, C.I. (2012). Beyond the connectome: how neuromodulators shape neural circuits. BioEssays : news and reviews in molecular, cellular and developmental biology *34*, 458-465.
Bargmann, C.I., Hartwieg, E., and Horvitz, H.R. (1993). Odorant-selective genes and neurons mediate olfaction in C. elegans. Cell *74*, 515-527.
Bargmann, C.I., and Horvitz, H.R. (1991). Control of larval development by chemosensory neurons in Caenorhabditis elegans. Science *251*, 1243-1246.
Bargmann, C.I., and Marder, E. (2013). From the connectome to brain function. Nature methods *10*, 483-490.
Barriere, A., and Felix, M.A. (2005). High local genetic diversity and low outcrossing rate in Caenorhabditis elegans natural populations. Current biology : CB *15*, 1176-1184.
Bartelt, R.J., Schaner, A.M., and Jackson, L.L. (1985). cis-Vaccenyl acetate as an aggregation pheromone in Drosophila melanogaster. Journal of chemical ecology *11*, 1747-1756.
Baugh, L.R. (2013). To grow or not to grow: nutritional control of development during Caenorhabditis elegans L1 arrest. Genetics *194*, 539-555.
Baugh, L.R., and Sternberg, P.W. (2006). DAF-16/FOXO regulates transcription of cki-1/Cip/Kip and repression of lin-4 during C. elegans L1 arrest. Current biology : CB *16*, 780-785.

Beldade, P., Mateus, A.R., and Keller, R.A. (2011). Evolution and molecular mechanisms of adaptive developmental plasticity. Molecular ecology *20*, 1347-1363.
Bell, L.R., Stone, S., Yochem, J., Shaw, J.E., and Herman, R.K. (2006). The molecular identities of the Caenorhabditis elegans intraflagellar transport genes dyf-6, daf-10 and osm-1. Genetics *173*, 1275-1286.
Bento, G., Ogawa, A., and Sommer, R.J. (2010). Co-option of the hormone-signalling module dafachronic acid-DAF-12 in nematode evolution. Nature *466*, 494-497.
Beverly, M., Anbil, S., and Sengupta, P. (2011a). Degeneracy and neuromodulation among thermosensory neurons contribute to robust thermosensory behaviors in Caenorhabditis elegans. The Journal of neuroscience : the official journal of the Society for Neuroscience *31*, 11718-11727.
Bigelow, H., Doitsidou, M., Sarin, S., and Hobert, O. (2009). MAQGene: software to facilitate C. elegans mutant genome sequence analysis. Nature methods *6*, 549.
Birnby, D.A., Link, E.M., Vowels, J.J., Tian, H., Colacurcio, P.L., and Thomas, J.H. (2000). A transmembrane guanylyl cyclase (DAF-11) and Hsp90 (DAF-21) regulate a common set of chemosensory behaviors in caenorhabditis elegans. Genetics *155*, 85-104.
Biron, D., Wasserman, S., Thomas, J.H., Samuel, A.D., and Sengupta, P. (2008). An olfactory neuron responds stochastically to temperature and modulates Caenorhabditis elegans thermotactic behavior. Proceedings of the National Academy of Sciences of the United States of America *105*, 11002-11007.
Brenner, S. (1974). The genetics of Caenorhabditis elegans. Genetics *77*, 71-94.
Brenner, S. (2009). In the beginning was the worm. Genetics *182*, 413-415.
Butcher, R.A., Fujita, M., Schroeder, F.C., and Clardy, J. (2007a). Small-molecule pheromones that control dauer development in Caenorhabditis elegans. Nature chemical biology *3*, 420-422.
Butcher, R.A., Fujita, M., Schroeder, F.C., and Clardy, J. (2007b). Small molecule signaling of dauer formation in C. elegans. Nat Chem Biol *3*, 420-422.
Butcher, R.A., Ragains, J.R., and Clardy, J. (2009a). An indole-containing dauer pheromone component with unusual dauer inhibitory activity at higher concentrations. Organic letters *11*, 3100-3103.
Butcher, R.A., Ragains, J.R., Kim, E., and Clardy, J. (2008). A potent dauer pheromone component in Caenorhabditis elegans that acts synergistically with other components. Proceedings of the National Academy of Sciences of the United States of America *105*, 14288-14292.
Butcher, R.A., Ragains, J.R., Li, W., Ruvkun, G., Clardy, J., and Mak, H.Y. (2009b). Biosynthesis of the Caenorhabditis elegans dauer pheromone. Proceedings of the National Academy of Sciences of the United States of America *106*, 1875-1879.
Cassada, R.C., and Russell, R.L. (1975). The dauerlarva, a post-embryonic developmental variant of the nematode Caenorhabditis elegans. Developmental biology *46*, 326-342.
Castaneda, L.E., Figueroa, C.C., Bacigalupe, L.D., and Nespolo, R.F. (2010). Effects of wing polyphenism, aphid genotype and host plant chemistry on energy metabolism of the grain aphid, Sitobion avenae. Journal of insect physiology *56*, 1920-1924.
Chalasani, S.H., Chronis, N., Tsunozaki, M., Gray, J.M., Ramot, D., Goodman, M.B., and Bargmann, C.I. (2007). Dissecting a neural circuit for food-seeking behavior in Caenorhabditis elegans. Nature *450*, 63-70.

Chambers, A.P., Sandoval, D.A., and Seeley, R.J. (2013). Integration of satiety signals by the central nervous system. Current biology : CB *23*, R379-388.
Chang, A.J., Chronis, N., Karow, D.S., Marletta, M.A., and Bargmann, C.I. (2006). A distributed chemosensory circuit for oxygen preference in C. elegans. PLoS biology *4*, e274.
Chelur, D.S., and Chalfie, M. (2007). Targeted cell killing by reconstituted caspases. Proceedings of the National Academy of Sciences of the United States of America *104*, 2283-2288.
Chen, Y., and Baugh, L.R. (2014). Ins-4 and daf-28 function redundantly to regulate C. elegans L1 arrest. Developmental biology *394*, 314-326.
Chen, Z., Hendricks, M., Cornils, A., Maier, W., Alcedo, J., and Zhang, Y. (2013). Two insulin-like peptides antagonistically regulate aversive olfactory learning in C. elegans. Neuron *77*, 572-585.
Chute, C.D., and Srinivasan, J. (2014). Chemical mating cues in C. elegans. Seminars in cell & developmental biology *33*, 18-24.
Coburn, C.M., and Bargmann, C.I. (1996). A putative cyclic nucleotide-gated channel is required for sensory development and function in C. elegans. Neuron *17*, 695-706.
Colbert, H.A., Smith, T.L., and Bargmann, C.I. (1997). OSM-9, a novel protein with structural similarity to channels, is required for olfaction, mechanosensation, and olfactory adaptation in Caenorhabditis elegans. The Journal of neuroscience : the official journal of the Society for Neuroscience *17*, 8259-8269.
Collet, J., Spike, C.A., Lundquist, E.A., Shaw, J.E., and Herman, R.K. (1998). Analysis of osm-6, a gene that affects sensory cilium structure and sensory neuron function in Caenorhabditis elegans. Genetics *148*, 187-200.
Cornils, A., Gloeck, M., Chen, Z., Zhang, Y., and Alcedo, J. (2011). Specific insulin-like peptides encode sensory information to regulate distinct developmental processes. Development *138*, 1183-1193.
Cui, M., Cohen, M.L., Teng, C., and Han, M. (2013). The tumor suppressor Rb critically regulates starvation-induced stress response in C. elegans. Current biology : CB *23*, 975-980.
Cunningham, K.A., Hua, Z., Srinivasan, S., Liu, J., Lee, B.H., Edwards, R.H., and Ashrafi, K. (2012). AMP-activated kinase links serotonergic signaling to glutamate release for regulation of feeding behavior in C. elegans. Cell metabolism *16*, 113-121.
da Graca, L.S., Zimmerman, K.K., Mitchell, M.C., Kozhan-Gorodetska, M., Sekiewicz, K., Morales, Y., and Patterson, G.I. (2004). DAF-5 is a Ski oncoprotein homolog that functions in a neuronal TGF beta pathway to regulate C. elegans dauer development. Development *131*, 435-446.
Daniels, S.A., Ailion, M., Thomas, J.H., and Sengupta, P. (2000). egl-4 acts through a transforming growth factor-beta/SMAD pathway in Caenorhabditis elegans to regulate multiple neuronal circuits in response to sensory cues. Genetics *156*, 123-141.
de Bono, M., Tobin, D.M., Davis, M.W., Avery, L., and Bargmann, C.I. (2002). Social feeding in Caenorhabditis elegans is induced by neurons that detect aversive stimuli. Nature *419*, 899-903.
Dorman, J.B., Albinder, B., Shroyer, T., and Kenyon, C. (1995). The age-1 and daf-2 genes function in a common pathway to control the lifespan of Caenorhabditis elegans. Genetics *141*, 1399-1406.

Dusenbery, D.B. (1980). Chemotactic Behavior of Mutants of the Nematode Caenorhabditis elegans that are Defective in Osmotic Avoidance. Journal of Comparative Physiology *137*, 93-96.
Edison, A.S. (2009). Caenorhabditis elegans pheromones regulate multiple complex behaviors. Current opinion in neurobiology *19*, 378-388.
Emerson, K.J., Bradshaw, W.E., and Holzapfel, C.M. (2009). Complications of complexity: integrating environmental, genetic and hormonal control of insect diapause. Trends in genetics : TIG *25*, 217-225.
Emlen, D.J. (1994). Environmental-control of Horn Length Dimorphism in the Beetle Onthophagus acuminatus (Coleoptera, Scarabaeidae). Proc R Soc B-Biol Sci *256*, 131-136.
Erion, R., and Sehgal, A. (2013). Regulation of insect behavior via the insulin-signaling pathway. Frontiers in physiology *4*, 353.
Erkut, C., Penkov, S., Fahmy, K., and Kurzchalia, T.V. (2012). How worms survive desiccation: Trehalose pro water. Worm *1*, 61-65.
Erkut, C., Penkov, S., Khesbak, H., Vorkel, D., Verbavatz, J.M., Fahmy, K., and Kurzchalia, T.V. (2011). Trehalose renders the dauer larva of Caenorhabditis elegans resistant to extreme desiccation. Current biology : CB *21*, 1331-1336.
Estevez, M., Attisano, L., Wrana, J.L., Albert, P.S., Massague, J., and Riddle, D.L. (1993). The daf-4 gene encodes a bone morphogenetic protein receptor controlling C. elegans dauer larva development. Nature *365*, 644-649.
Evans, J.D., and Wheeler, D.E. (2001). Gene expression and the evolution of insect polyphenisms. BioEssays : news and reviews in molecular, cellular and developmental biology *23*, 62-68.
Ezcurra, M., Tanizawa, Y., Swoboda, P., and Schafer, W.R. (2011). Food sensitizes C. elegans avoidance behaviours through acute dopamine signalling. The EMBO journal *30*, 1110-1122.
Fay, D. (2006a). Genetic mapping and manipulation: chapter 2--Two-point mapping with genetic markers. WormBook : the online review of C elegans biology, 1-6.
Fay, D. (2006b). Genetic mapping and manipulation: chapter 3--Three-point mapping with genetic markers. WormBook : the online review of C elegans biology, 1-7.
Felix, M.A., and Duveau, F. (2012). Population dynamics and habitat sharing of natural populations of Caenorhabditis elegans and C. briggsae. BMC biology *10*, 59.
Fernandes de Abreu, D.A., Caballero, A., Fardel, P., Stroustrup, N., Chen, Z., Lee, K., Keyes, W.D., Nash, Z.M., Lopez-Moyado, I.F., Vaggi, F.*, et al.* (2014). An insulin-to-insulin regulatory network orchestrates phenotypic specificity in development and physiology. PLoS genetics *10*, e1004225.
Fielenbach, N., and Antebi, A. (2008). C. elegans dauer formation and the molecular basis of plasticity. Genes & development *22*, 2149-2165.
Fukuyama, M., Rougvie, A.E., and Rothman, J.H. (2006). C. elegans DAF-18/PTEN mediates nutrient-dependent arrest of cell cycle and growth in the germline. Current biology : CB *16*, 773-779.
Gallagher, T., Kim, J., Oldenbroek, M., Kerr, R., and You, Y.J. (2013). ASI regulates satiety quiescence in C. elegans. The Journal of neuroscience : the official journal of the Society for Neuroscience *33*, 9716-9724.
Gallo, M., and Riddle, D.L. (2009). Effects of a Caenorhabditis elegans dauer pheromone ascaroside on physiology and signal transduction pathways. Journal of chemical ecology *35*, 272-279.

Gems, D., Sutton, A.J., Sundermeyer, M.L., Albert, P.S., King, K.V., Edgley, M.L., Larsen, P.L., and Riddle, D.L. (1998). Two pleiotropic classes of daf-2 mutation affect larval arrest, adult behavior, reproduction and longevity in Caenorhabditis elegans. Genetics *150*, 129-155.

Georgi, L.L., Albert, P.S., and Riddle, D.L. (1990). daf-1, a C. elegans gene controlling dauer larva development, encodes a novel receptor protein kinase. Cell *61*, 635-645.

Gerisch, B., and Antebi, A. (2004). Hormonal signals produced by DAF-9/cytochrome P450 regulate C. elegans dauer diapause in response to environmental cues. Development *131*, 1765-1776.

Gerisch, B., Rottiers, V., Li, D., Motola, D.L., Cummins, C.L., Lehrach, H., Mangelsdorf, D.J., and Antebi, A. (2007). A bile acid-like steroid modulates Caenorhabditis elegans lifespan through nuclear receptor signaling. Proceedings of the National Academy of Sciences of the United States of America *104*, 5014-5019.

Gerisch, B., Weitzel, C., Kober-Eisermann, C., Rottiers, V., and Antebi, A. (2001). A hormonal signaling pathway influencing C. elegans metabolism, reproductive development, and life span. Developmental cell *1*, 841-851.

Gil, E.B., Malone Link, E., Liu, L.X., Johnson, C.D., and Lees, J.A. (1999). Regulation of the insulin-like developmental pathway of Caenorhabditis elegans by a homolog of the PTEN tumor suppressor gene. Proceedings of the National Academy of Sciences of the United States of America *96*, 2925-2930.

Gluckman, P.D., Hanson, M.A., and Beedle, A.S. (2007). Early life events and their consequences for later disease: a life history and evolutionary perspective. American journal of human biology : the official journal of the Human Biology Council *19*, 1-19.

Goetz, S.C., Liem, K.F., Jr., and Anderson, K.V. (2012). The spinocerebellar ataxia-associated gene Tau tubulin kinase 2 controls the initiation of ciliogenesis. Cell *151*, 847-858.

Golden, J.W., and Riddle, D.L. (1982). A pheromone influences larval development in the nematode Caenorhabditis elegans. Science *218*, 578-580.

Golden, J.W., and Riddle, D.L. (1984a). ACaenorhabditis elegans dauer-inducing pheromone and an antagonistic component of the food supply. Journal of chemical ecology *10*, 1265-1280.

Golden, J.W., and Riddle, D.L. (1984b). A Caenorhabditis elegans dauer-inducing pheromone and an antagonistic component of the food supply. Journal of chemical ecology *10*, 1265-1280.

Golden, J.W., and Riddle, D.L. (1984c). The Caenorhabditis elegans dauer larva: developmental effects of pheromone, food, and temperature. Developmental biology *102*, 368-378.

Golden, J.W., and Riddle, D.L. (1984d). A pheromone-induced developmental switch in Caenorhabditis elegans: Temperature-sensitive mutants reveal a wild-type temperature-dependent process. Proceedings of the National Academy of Sciences of the United States of America *81*, 819-823.

Golden, J.W., and Riddle, D.L. (1985). A gene affecting production of the Caenorhabditis elegans dauer-inducing pheromone. Molecular & general genetics : MGG *198*, 534-536.

Gordus, A., Pokala, N., Levy, S., Flavell, S.W., and Bargmann, C.I. (2015). Feedback from Network States Generates Variability in a Probabilistic Olfactory Circuit. Cell.

Gottlieb, S., and Ruvkun, G. (1994). daf-2, daf-16 and daf-23: genetically interacting genes controlling Dauer formation in Caenorhabditis elegans. Genetics *137*, 107-120.

Greene, E. (1989). A diet-induced developmental polymorphism in a caterpillar. Science *243*, 643-646.

Grozinger, C.M., Fischer, P., and Hampton, J.E. (2007). Uncoupling primer and releaser responses to pheromone in honey bees. Die Naturwissenschaften *94*, 375-379.
Ha, H.I., Hendricks, M., Shen, Y., Gabel, C.V., Fang-Yen, C., Qin, Y., Colon-Ramos, D., Shen, K., Samuel, A.D., and Zhang, Y. (2010). Functional organization of a neural network for aversive olfactory learning in Caenorhabditis elegans. Neuron 68, 1173-1186.
Hahn, D.A., and Denlinger, D.L. (2011). Energetics of insect diapause. Annual review of entomology *56*, 103-121.
Hall, S.E., Beverly, M., Russ, C., Nusbaum, C., and Sengupta, P. (2010). A cellular memory of developmental history generates phenotypic diversity in C. elegans. Current biology : CB *20*, 149-155.
Hansen, I.A., Attardo, G.M., Rodriguez, S.D., and Drake, L.L. (2014). Four-way regulation of mosquito yolk protein precursor genes by juvenile hormone-, ecdysone-, nutrient-, and insulin-like peptide signaling pathways. Frontiers in physiology *5*, 103.
Harris, G., Shen, Y., Ha, H., Donato, A., Wallis, S., Zhang, X., and Zhang, Y. (2014). Dissecting the signaling mechanisms underlying recognition and preference of food odors. The Journal of neuroscience : the official journal of the Society for Neuroscience *34*, 9389-9403.
Hart, A.C., Kass, J., Shapiro, J.E., and Kaplan, J.M. (1999). Distinct signaling pathways mediate touch and osmosensory responses in a polymodal sensory neuron. The Journal of neuroscience : the official journal of the Society for Neuroscience *19*, 1952-1958.
He, J., Ma, L., Kim, S., Schwartz, J., Santilli, M., Wood, C., Durnin, M.H., and Yu, C.R. (2010). Distinct signals conveyed by pheromone concentrations to the mouse vomeronasal organ. The Journal of neuroscience : the official journal of the Society for Neuroscience *30*, 7473-7483.
Hilliard, M.A., Apicella, A.J., Kerr, R., Suzuki, H., Bazzicalupo, P., and Schafer, W.R. (2005). In vivo imaging of C. elegans ASH neurons: cellular response and adaptation to chemical repellents. The EMBO journal *24*, 63-72.
Hilliard, M.A., Bergamasco, C., Arbucci, S., Plasterk, R.H., and Bazzicalupo, P. (2004). Worms taste bitter: ASH neurons, QUI-1, GPA-3 and ODR-3 mediate quinine avoidance in Caenorhabditis elegans. The EMBO journal *23*, 1101-1111.
Hills, T., Brockie, P.J., and Maricq, A.V. (2004). Dopamine and glutamate control area-restricted search behavior in Caenorhabditis elegans. The Journal of neuroscience : the official journal of the Society for Neuroscience *24*, 1217-1225.
Hobert, O. (2002). PCR fusion-based approach to create reporter gene constructs for expression analysis in transgenic C. elegans. BioTechniques *32*, 728-730.
Holman, L. (2010). Queen pheromones: The chemical crown governing insect social life. Communicative & integrative biology *3*, 558-560.
Hong, Y., Roy, R., and Ambros, V. (1998). Developmental regulation of a cyclin-dependent kinase inhibitor controls postembryonic cell cycle progression in Caenorhabditis elegans. Development *125*, 3585-3597.
Hu, P.J. (2007). Dauer. WormBook : the online review of C elegans biology, 1-19.
Hung, W.L., Wang, Y., Chitturi, J., and Zhen, M. (2014). A Caenorhabditis elegans developmental decision requires insulin signaling-mediated neuron-intestine communication. Development *141*, 1767-1779.
Iino, Y., and Yoshida, K. (2009). Parallel use of two behavioral mechanisms for chemotaxis in Caenorhabditis elegans. The Journal of neuroscience : the official journal of the Society for Neuroscience *29*, 5370-5380.

Inoue, A., Sawatari, E., Hisamoto, N., Kitazono, T., Teramoto, T., Fujiwara, M., Matsumoto, K., and Ishihara, T. (2013). Forgetting in C. elegans is accelerated by neuronal communication via the TIR-1/JNK-1 pathway. Cell reports *3*, 808-819.

Inoue, T., and Thomas, J.H. (2000a). Suppressors of transforming growth factor-beta pathway mutants in the Caenorhabditis elegans dauer formation pathway. Genetics *156*, 1035-1046.

Inoue, T., and Thomas, J.H. (2000b). Targets of TGF-beta signaling in Caenorhabditis elegans dauer formation. Developmental biology *217*, 192-204.

Jang, H., Kim, K., Neal, S.J., Macosko, E., Kim, D., Butcher, R.A., Zeiger, D.M., Bargmann, C.I., and Sengupta, P. (2012a). Neuromodulatory state and sex specify alternative behaviors through antagonistic synaptic pathways in C. elegans. Neuron *75*, 585-592.

Jang, H., Kim, K., Neal, S.J., Macosko, E.Z., Kim, D., Butcher, R.A., Zeiger, D.M., Bargmann, C.I., and Sengupta, P. (2012b). Neuromodulatory state and sex specify alternative behaviors through antagonistic synaptic pathways in C. elegans. . Neuron *In press*.

Jansen, G., Thijssen, K.L., Werner, P., van der Horst, M., Hazendonk, E., and Plasterk, R.H. (1999). The complete family of genes encoding G proteins of Caenorhabditis elegans. Nature genetics *21*, 414-419.

Jennings, J.H., Rizzi, G., Stamatakis, A.M., Ung, R.L., and Stuber, G.D. (2013). The inhibitory circuit architecture of the lateral hypothalamus orchestrates feeding. Science *341*, 1517-1521.

Jeong, P.Y., Jung, M., Yim, Y.H., Kim, H., Park, M., Hong, E., Lee, W., Kim, Y.H., Kim, K., and Paik, Y.K. (2005). Chemical structure and biological activity of the Caenorhabditis elegans dauer-inducing pheromone. Nature *433*, 541-545.

Jia, K., Albert, P.S., and Riddle, D.L. (2002). DAF-9, a cytochrome P450 regulating C. elegans larval development and adult longevity. Development *129*, 221-231.

Jia, K., Chen, D., and Riddle, D.L. (2004). The TOR pathway interacts with the insulin signaling pathway to regulate C. elegans larval development, metabolism and life span. Development *131*, 3897-3906.

Joo, H.J., Kim, K.Y., Yim, Y.H., Jin, Y.X., Kim, H., Kim, M.Y., and Paik, Y.K. (2010). Contribution of the peroxisomal acox gene to the dynamic balance of daumone production in Caenorhabditis elegans. The Journal of biological chemistry *285*, 29319-29325.

Jyotaki, M., Shigemura, N., and Ninomiya, Y. (2010). Modulation of sweet taste sensitivity by orexigenic and anorexigenic factors. Endocrine journal *57*, 467-475.

Kamakura, M. (2011). Royalactin induces queen differentiation in honeybees. Nature *473*, 478-483.

Kang, C., and Avery, L. (2009). Systemic regulation of starvation response in Caenorhabditis elegans. Genes & development *23*, 12-17.

Kaplan, J.M., and Horvitz, H.R. (1993). A dual mechanosensory and chemosensory neuron in Caenorhabditis elegans. Proceedings of the National Academy of Sciences of the United States of America *90*, 2227-2231.

Karlson, P., and Luscher, M. (1959). Pheromones': a new term for a class of biologically active substances. Nature *183*, 55-56.

Kasuga, H., Fukuyama, M., Kitazawa, A., Kontani, K., and Katada, T. (2013). The microRNA miR-235 couples blast-cell quiescence to the nutritional state. Nature *497*, 503-506.

Kato, S., Xu, Y., Cho, C.E., Abbott, L.F., and Bargmann, C.I. (2014). Temporal responses of C. elegans chemosensory neurons are preserved in behavioral dynamics. Neuron *81*, 616-628.

Kaul, T.K., Reis Rodrigues, P., Ogungbe, I.V., Kapahi, P., and Gill, M.S. (2014). Bacterial fatty acids enhance recovery from the dauer larva in Caenorhabditis elegans. PloS one *9*, e86979.

Kenyon, C., Chang, J., Gensch, E., Rudner, A., and Tabtiang, R. (1993). A C. elegans mutant that lives twice as long as wild type. Nature *366*, 461-464.
Kim, K., Sato, K., Shibuya, M., Zeiger, D.M., Butcher, R.A., Ragains, J.R., Clardy, J., Touhara, K., and Sengupta, P. (2009). Two chemoreceptors mediate developmental effects of dauer pheromone in C. elegans. Science *326*, 994-998.
Kimura, K.D., Tissenbaum, H.A., Liu, Y., and Ruvkun, G. (1997). daf-2, an insulin receptor-like gene that regulates longevity and diapause in Caenorhabditis elegans. Science *277*, 942-946.
Kimura, Y., Corcoran, E.E., Eto, K., Gengyo-Ando, K., Muramatsu, M.A., Kobayashi, R., Freedman, J.H., Mitani, S., Hagiwara, M., Means, A.R.*, et al.* (2002). A CaMK cascade activates CRE-mediated transcription in neurons of Caenorhabditis elegans. EMBO reports *3*, 962-966.
Klass, M., and Hirsh, D. (1976). Non-ageing developmental variant of Caenorhabditis elegans. Nature *260*, 523-525.
Kodama-Namba, E., Fenk, L.A., Bretscher, A.J., Gross, E., Busch, K.E., and de Bono, M. (2013). Cross-modulation of homeostatic responses to temperature, oxygen and carbon dioxide in C. elegans. PLoS genetics *9*, e1004011.
Komatsu, H., Mori, I., Rhee, J.S., Akaike, N., and Ohshima, Y. (1996). Mutations in a cyclic nucleotide-gated channel lead to abnormal thermosensation and chemosensation in C. elegans. Neuron *17*, 707-718.
Kostal, V. (2006). Eco-physiological phases of insect diapause. Journal of insect physiology *52*, 113-127.
Koyama, T., Mendes, C.C., and Mirth, C.K. (2013). Mechanisms regulating nutrition-dependent developmental plasticity through organ-specific effects in insects. Frontiers in physiology *4*, 263.
Larsen, P.L., Albert, P.S., and Riddle, D.L. (1995). Genes that regulate both development and longevity in Caenorhabditis elegans. Genetics *139*, 1567-1583.
Lavine, L., Gotoh, H., Brent, C.S., Dworkin, I., and Emlen, D.J. (2015). Exaggerated trait growth in insects. Annual review of entomology *60*, 453-472.
Le Conte, Y., Mohammedi, A., and Robinson, G.E. (2001). Primer effects of a brood pheromone on honeybee behavioural development. Proceedings Biological sciences / The Royal Society *268*, 163-168.
Lee, J., Kim, K.Y., Joo, H.J., Kim, H., Jeong, P.Y., and Paik, Y.K. (2011). Methods for evaluating the Caenorhabditis elegans dauer state: standard dauer-formation assay using synthetic daumones and proteomic analysis of O-GlcNAc modifications. Methods in cell biology *106*, 445-460.
Leinwand, S.G., and Chalasani, S.H. (2013). Neuropeptide signaling remodels chemosensory circuit composition in Caenorhabditis elegans. Nature neuroscience *16*, 1461-1467.
Li, C., and Kim, K. (2010). Neuropeptide gene families in Caenorhabditis elegans. Advances in experimental medicine and biology *692*, 98-137.
Li, Q., and Liberles, S.D. (2015). Aversion and attraction through olfaction. Current biology : CB *25*, R120-129.
Li, W., Kennedy, S.G., and Ruvkun, G. (2003). daf-28 encodes a C. elegans insulin superfamily member that is regulated by environmental cues and acts in the DAF-2 signaling pathway. Genes & development *17*, 844-858.

Li, Z., Li, Y., Yi, Y., Huang, W., Yang, S., Niu, W., Zhang, L., Xu, Z., Qu, A., Wu, Z., *et al.* (2012). Dissecting a central flip-flop circuit that integrates contradictory sensory cues in C. elegans feeding regulation. Nature communications *3*, 776.

Liachko, N.F., McMillan, P.J., Guthrie, C.R., Bird, T.D., Leverenz, J.B., and Kraemer, B.C. (2013). CDC7 inhibition blocks pathological TDP-43 phosphorylation and neurodegeneration. Annals of neurology *74*, 39-52.

Liachko, N.F., McMillan, P.J., Strovas, T.J., Loomis, E., Greenup, L., Murrell, J.R., Ghetti, B., Raskind, M.A., Montine, T.J., Bird, T.D., *et al.* (2014). The tau tubulin kinases TTBK1/2 promote accumulation of pathological TDP-43. PLoS genetics *10*, e1004803.

Libbrecht, R., Corona, M., Wende, F., Azevedo, D.O., Serrao, J.E., and Keller, L. (2013). Interplay between insulin signaling, juvenile hormone, and vitellogenin regulates maternal effects on polyphenism in ants. Proceedings of the National Academy of Sciences of the United States of America *110*, 11050-11055.

Liu, T., Zimmerman, K.K., and Patterson, G.I. (2004). Regulation of signaling genes by TGFbeta during entry into dauer diapause in C. elegans. BMC developmental biology *4*, 11.

Lochrie, M.A., Mendel, J.E., Sternberg, P.W., and Simon, M.I. (1991). Homologous and unique G protein alpha subunits in the nematode Caenorhabditis elegans. Cell regulation *2*, 135-154.

Long, X., Spycher, C., Han, Z.S., Rose, A.M., Muller, F., and Avruch, J. (2002). TOR deficiency in C. elegans causes developmental arrest and intestinal atrophy by inhibition of mRNA translation. Current biology : CB *12*, 1448-1461.

Ludewig, A.H., Kober-Eisermann, C., Weitzel, C., Bethke, A., Neubert, K., Gerisch, B., Hutter, H., and Antebi, A. (2004). A novel nuclear receptor/coregulator complex controls C. elegans lipid metabolism, larval development, and aging. Genes & development *18*, 2120-2133.

Ludewig, A.H., and Schroeder, F.C. (2013). Ascaroside signaling in C. elegans. WormBook : the online review of C elegans biology, 1-22.

Luo, L., Wen, Q., Ren, J., Hendricks, M., Gershow, M., Qin, Y., Greenwood, J., Soucy, E.R., Klein, M., Smith-Parker, H.K., *et al.* (2014). Dynamic encoding of perception, memory, and movement in a C. elegans chemotaxis circuit. Neuron *82*, 1115-1128.

MacNeil, L.T., Watson, E., Arda, H.E., Zhu, L.J., and Walhout, A.J. (2013). Diet-induced developmental acceleration independent of TOR and insulin in C. elegans. Cell *153*, 240-252.

Macosko, E.Z., Pokala, N., Feinberg, E.H., Chalasani, S.H., Butcher, R.A., Clardy, J., and Bargmann, C.I. (2009). A hub-and-spoke circuit drives pheromone attraction and social behaviour in C. elegans. Nature *458*, 1171-1175.

Magner, D.B., and Antebi, A. (2008). Caenorhabditis elegans nuclear receptors: insights into life traits. Trends in endocrinology and metabolism: TEM *19*, 153-160.

Maisonnasse, A., Alaux, C., Beslay, D., Crauser, D., Gines, C., Plettner, E., and Le Conte, Y. (2010). New insights into honey bee (Apis mellifera) pheromone communication. Is the queen mandibular pheromone alone in colony regulation? Frontiers in zoology *7*, 18.

Malone, E.A., Inoue, T., and Thomas, J.H. (1996). Genetic analysis of the roles of daf-28 and age-1 in regulating Caenorhabditis elegans dauer formation. Genetics *143*, 1193-1205.

Malone, E.A., and Thomas, J.H. (1994). A screen for nonconditional dauer-constitutive mutations in Caenorhabditis elegans. Genetics *136*, 879-886.

Manning, G. (2005). Genomic overview of protein kinases. WormBook : the online review of C elegans biology, 1-19.

Marder, E. (2012). Neuromodulation of neuronal circuits: back to the future. Neuron *76*, 1-11.

Massague, J., Seoane, J., and Wotton, D. (2005). Smad transcription factors. Genes & development *19*, 2783-2810.
Matsunaga, Y., Gengyo-Ando, K., Mitani, S., Iwasaki, T., and Kawano, T. (2012). Physiological function, expression pattern, and transcriptional regulation of a Caenorhabditis elegans insulin-like peptide, INS-18. Biochemical and biophysical research communications *423*, 478-483.
Mayr, E. (1963). Animal species and evolution (Cambridge: Belknap Press of Harvard University Press).
McGrath, P.T., Xu, Y., Ailion, M., Garrison, J.L., Butcher, R.A., and Bargmann, C.I. (2011). Parallel evolution of domesticated Caenorhabditis species targets pheromone receptor genes. Nature *477*, 321-325.
Meisel, J.D., Panda, O., Mahanti, P., Schroeder, F.C., and Kim, D.H. (2014). Chemosensation of bacterial secondary metabolites modulates neuroendocrine signaling and behavior of C. elegans. Cell *159*, 267-280.
Mello, C.C., Kramer, J.M., Stinchcomb, D., and Ambros, V. (1991). Efficient gene transfer in C.elegans: extrachromosomal maintenance and integration of transforming sequences. The EMBO journal *10*, 3959-3970.
Michener, C.D. (1961). Social Polymorphism in Hymenoptera. Paper presented at: Symp R Entomol Soc Lond.
Mihaylova, V.T., Borland, C.Z., Manjarrez, L., Stern, M.J., and Sun, H. (1999). The PTEN tumor suppressor homolog in Caenorhabditis elegans regulates longevity and dauer formation in an insulin receptor-like signaling pathway. Proceedings of the National Academy of Sciences of the United States of America *96*, 7427-7432.
Minevich, G., Park, D.S., Blankenberg, D., Poole, R.J., and Hobert, O. (2012). CloudMap: a cloud-based pipeline for analysis of mutant genome sequences. Genetics *192*, 1249-1269.
Mirth, C.K., Tang, H.Y., Makohon-Moore, S.C., Salhadar, S., Gokhale, R.H., Warner, R.D., Koyama, T., Riddiford, L.M., and Shingleton, A.W. (2014). Juvenile hormone regulates body size and perturbs insulin signaling in Drosophila. Proceedings of the National Academy of Sciences of the United States of America *111*, 7018-7023.
Moczek, A.P., Sultan, S., Foster, S., Ledon-Rettig, C., Dworkin, I., Nijhout, H.F., Abouheif, E., and Pfennig, D.W. (2011). The role of developmental plasticity in evolutionary innovation. Proceedings Biological sciences / The Royal Society *278*, 2705-2713.
Morehouse, N.I., Mandon, N., Christides, J.P., Body, M., Bimbard, G., and Casas, J. (2013). Seasonal selection and resource dynamics in a seasonally polyphenic butterfly. Journal of evolutionary biology *26*, 175-185.
Morris, J.Z., Tissenbaum, H.A., and Ruvkun, G. (1996). A phosphatidylinositol-3-OH kinase family member regulating longevity and diapause in Caenorhabditis elegans. Nature *382*, 536-539.
Motola, D.L., Cummins, C.L., Rottiers, V., Sharma, K.K., Li, T., Li, Y., Suino-Powell, K., Xu, H.E., Auchus, R.J., Antebi, A.*, et al.* (2006). Identification of ligands for DAF-12 that govern dauer formation and reproduction in C. elegans. Cell *124*, 1209-1223.
Murakami, M., Koga, M., and Ohshima, Y. (2001). DAF-7/TGF-beta expression required for the normal larval development in C. elegans is controlled by a presumed guanylyl cyclase DAF-11. Mechanisms of development *109*, 27-35.
Murphy, C.T., and Hu, P.J. (2013). Insulin/insulin-like growth factor signaling in C. elegans. WormBook : the online review of C elegans biology, 1-43.

Mutti, N.S., Dolezal, A.G., Wolschin, F., Mutti, J.S., Gill, K.S., and Amdam, G.V. (2011). IRS and TOR nutrient-signaling pathways act via juvenile hormone to influence honey bee caste fate. The Journal of experimental biology *214*, 3977-3984.
Nakai, J., Ohkura, M., and Imoto, K. (2001). A high signal-to-noise Ca(2+) probe composed of a single green fluorescent protein. Nature biotechnology *19*, 137-141.
Narasimhan, S.D., Yen, K., Bansal, A., Kwon, E.S., Padmanabhan, S., and Tissenbaum, H.A. (2011). PDP-1 links the TGF-beta and IIS pathways to regulate longevity, development, and metabolism. PLoS genetics *7*, e1001377.
Narbonne, P., and Roy, R. (2009). Caenorhabditis elegans dauers need LKB1/AMPK to ration lipid reserves and ensure long-term survival. Nature *457*, 210-214.
Neal, S.J., Kim, K., and Sengupta, P. (2013). Quantitative assessment of pheromone-induced Dauer formation in Caenorhabditis elegans. Methods in molecular biology *1068*, 273-283.
Nechipurenko, I.V., Doroquez, D.B., and Sengupta, P. (2013). Primary cilia and dendritic spines: different but similar signaling compartments. Molecules and cells *36*, 288-303.
Nijhout, H.F. (2003). Development and evolution of adaptive polyphenisms. Evolution & development *5*, 9-18.
Nolan, K.M., Sarafi-Reinach, T.R., Horne, J.G., Saffer, A.M., and Sengupta, P. (2002). The DAF-7 TGF-beta signaling pathway regulates chemosensory receptor gene expression in C. elegans. Genes & development *16*, 3061-3073.
Nylin, S. (2013). Induction of diapause and seasonal morphs in butterflies and other insects: knowns, unknowns and the challenge of integration. Physiological entomology *38*, 96-104.
O'Rourke, E.J., and Ruvkun, G. (2013). MXL-3 and HLH-30 transcriptionally link lipolysis and autophagy to nutrient availability. Nature cell biology *15*, 668-676.
Ogawa, A., Bento, G., Bartelmes, G., Dieterich, C., and Sommer, R.J. (2011). Pristionchus pacificus daf-16 is essential for dauer formation but dispensable for mouth form dimorphism. Development *138*, 1281-1284.
Ogg, S., Paradis, S., Gottlieb, S., Patterson, G.I., Lee, L., Tissenbaum, H.A., and Ruvkun, G. (1997). The Fork head transcription factor DAF-16 transduces insulin-like metabolic and longevity signals in C. elegans. Nature *389*, 994-999.
Ogg, S., and Ruvkun, G. (1998). The C. elegans PTEN homolog, DAF-18, acts in the insulin receptor-like metabolic signaling pathway. Molecular cell *2*, 887-893.
Ohba, K., and Ishibashi, N. (1982). A Factor Inducing Dauer Juvenile Formation in Caenorhabditis-Elegans. Nematologica *28*, 318-325.
Ohnishi, N., Kuhara, A., Nakamura, F., Okochi, Y., and Mori, I. (2011). Bidirectional regulation of thermotaxis by glutamate transmissions in Caenorhabditis elegans. The EMBO journal *30*, 1376-1388.
Opienska-Blauth, J., Madecka-Borkowska, I., and Borkowski, T. (1952). Comparative studies on the metabolism of lactose, glucose and galactose in liquid cultures of E. coli. Nature *169*, 798-799.
Orth, J.D., Conrad, T.M., Na, J., Lerman, J.A., Nam, H., Feist, A.M., and Palsson, B.O. (2011). A comprehensive genome-scale reconstruction of Escherichia coli metabolism--2011. Molecular systems biology *7*, 535.
Ortiz, C.O., Etchberger, J.F., Posy, S.L., Frokjaer-Jensen, C., Lockery, S., Honig, B., and Hobert, O. (2006). Searching for neuronal left/right asymmetry: genomewide analysis of nematode receptor-type guanylyl cyclases. Genetics *173*, 131-149.

Paek, J., Lo, J.Y., Narasimhan, S.D., Nguyen, T.N., Glover-Cutter, K., Robida-Stubbs, S., Suzuki, T., Yamamoto, M., Blackwell, T.K., and Curran, S.P. (2012). Mitochondrial SKN-1/Nrf mediates a conserved starvation response. Cell metabolism *16*, 526-537.

Palouzier-Paulignan, B., Lacroix, M.C., Aime, P., Baly, C., Caillol, M., Congar, P., Julliard, A.K., Tucker, K., and Fadool, D.A. (2012). Olfaction under metabolic influences. Chemical senses *37*, 769-797.

Paradis, S., and Ruvkun, G. (1998). Caenorhabditis elegans Akt/PKB transduces insulin receptor-like signals from AGE-1 PI3 kinase to the DAF-16 transcription factor. Genes & development *12*, 2488-2498.

Park, D., Estevez, A., and Riddle, D.L. (2010). Antagonistic Smad transcription factors control the dauer/non-dauer switch in C. elegans. Development *137*, 477-485.

Park, D., Jones, K.L., Lee, H., Snutch, T.P., Taubert, S., and Riddle, D.L. (2012a). Repression of a potassium channel by nuclear hormone receptor and TGF-beta signaling modulates insulin signaling in Caenorhabditis elegans. PLoS genetics *8*, e1002519.

Park, D., O'Doherty, I., Somvanshi, R.K., Bethke, A., Schroeder, F.C., Kumar, U., and Riddle, D.L. (2012b). Interaction of structure-specific and promiscuous G-protein-coupled receptors mediates small-molecule signaling in Caenorhabditis elegans. Proceedings of the National Academy of Sciences of the United States of America *109*, 9917-9922.

Patterson, G.I., Koweek, A., Wong, A., Liu, Y., and Ruvkun, G. (1997). The DAF-3 Smad protein antagonizes TGF-beta-related receptor signaling in the Caenorhabditis elegans dauer pathway. Genes & development *11*, 2679-2690.

Peckol, E.L., Troemel, E.R., and Bargmann, C.I. (2001). Sensory experience and sensory activity regulate chemosensory receptor gene expression in Caenorhabditis elegans. Proceedings of the National Academy of Sciences of the United States of America *98*, 11032-11038.

Perens, E.A., and Shaham, S. (2005). C. elegans daf-6 encodes a patched-related protein required for lumen formation. Developmental cell *8*, 893-906.

Perkins, L.A., Hedgecock, E.M., Thomson, J.N., and Culotti, J.G. (1986). Mutant sensory cilia in the nematode Caenorhabditis elegans. Developmental biology *117*, 456-487.

Pfennig, D.W. (1992). Proximate and functional causes of polyphenism in an anuran tadpole. Funct Ecol *6*.

Pfennig, D.W., Wund, M.A., Snell-Rood, E.C., Cruickshank, T., Schlichting, C.D., and Moczek, A.P. (2010). Phenotypic plasticity's impacts on diversification and speciation. Trends in ecology & evolution *25*, 459-467.

Pierce, S.B., Costa, M., Wisotzkey, R., Devadhar, S., Homburger, S.A., Buchman, A.R., Ferguson, K.C., Heller, J., Platt, D.M., Pasquinelli, A.A.*, et al.* (2001). Regulation of DAF-2 receptor signaling by human insulin and ins-1, a member of the unusually large and diverse C. elegans insulin gene family. Genes & development *15*, 672-686.

Pool, A.H., and Scott, K. (2014). Feeding regulation in Drosophila. Current opinion in neurobiology *29*, 57-63.

Pungaliya, C., Srinivasan, J., Fox, B.W., Malik, R.U., Ludewig, A.H., Sternberg, P.W., and Schroeder, F.C. (2009). A shortcut to identifying small molecule signals that regulate behavior and development in Caenorhabditis elegans. Proceedings of the National Academy of Sciences of the United States of America *106*, 7708-7713.

Qi, H., Yao, C., Cai, W., Girton, J., Johansen, K.M., and Johansen, J. (2009). Asator, a tau-tubulin kinase homolog in Drosophila localizes to the mitotic spindle. Developmental

dynamics : an official publication of the American Association of Anatomists *238*, 3248-3256.
Rechavi, O., Houri-Ze'evi, L., Anava, S., Goh, W.S., Kerk, S.Y., Hannon, G.J., and Hobert, O. (2014). Starvation-induced transgenerational inheritance of small RNAs in C. elegans. Cell *158*, 277-287.
Ren, P., Lim, C.S., Johnsen, R., Albert, P.S., Pilgrim, D., and Riddle, D.L. (1996). Control of C. elegans larval development by neuronal expression of a TGF-beta homolog. Science *274*, 1389-1391.
Riddle, D.L., Swanson, M.M., and Albert, P.S. (1981). Interacting genes in nematode dauer larva formation. Nature *290*, 668-671.
Riera, C.E., and Dillin, A. (2015). Tipping the metabolic scales towards increased longevity in mammals. Nature cell biology *17*, 196-203.
Ritter, A.D., Shen, Y., Fuxman Bass, J., Jeyaraj, S., Deplancke, B., Mukhopadhyay, A., Xu, J., Driscoll, M., Tissenbaum, H.A., and Walhout, A.J. (2013). Complex expression dynamics and robustness in C. elegans insulin networks. Genome research *23*, 954-965.
Rogers, C., Persson, A., Cheung, B., and de Bono, M. (2006). Behavioral motifs and neural pathways coordinating O2 responses and aggregation in C. elegans. Current biology : CB *16*, 649-659.
Ryan, D.A., Miller, R.M., Lee, K., Neal, S.J., Fagan, K.A., Sengupta, P., and Portman, D.S. (2014). Sex, age, and hunger regulate behavioral prioritization through dynamic modulation of chemoreceptor expression. Current biology : CB *24*, 2509-2517.
Sambongi, Y., Nagae, T., Liu, Y., Yoshimizu, T., Takeda, K., Wada, Y., and Futai, M. (1999). Sensing of cadmium and copper ions by externally exposed ADL, ASE, and ASH neurons elicits avoidance response in Caenorhabditis elegans. Neuroreport *10*, 753-757.
Sarin, S., Bertrand, V., Bigelow, H., Boyanov, A., Doitsidou, M., Poole, R.J., Narula, S., and Hobert, O. (2010). Analysis of multiple ethyl methanesulfonate-mutagenized Caenorhabditis elegans strains by whole-genome sequencing. Genetics *185*, 417-430.
Sato, A., Sokabe, T., Kashio, M., Yasukochi, Y., Tominaga, M., and Shiomi, K. (2014). Embryonic thermosensitive TRPA1 determines transgenerational diapause phenotype of the silkworm, Bombyx mori. Proceedings of the National Academy of Sciences of the United States of America *111*, E1249-1255.
Sato, S., Cerny, R.L., Buescher, J.L., and Ikezu, T. (2006). Tau-tubulin kinase 1 (TTBK1), a neuron-specific tau kinase candidate, is involved in tau phosphorylation and aggregation. Journal of neurochemistry *98*, 1573-1584.
Satoh, Y., Sato, H., Kunitomo, H., Fei, X., Hashimoto, K., and Iino, Y. (2014). Regulation of experience-dependent bidirectional chemotaxis by a neural circuit switch in Caenorhabditis elegans. The Journal of neuroscience : the official journal of the Society for Neuroscience *34*, 15631-15637.
Satterlee, J.S., Ryu, W.S., and Sengupta, P. (2004). The CMK-1 CaMKI and the TAX-4 Cyclic nucleotide-gated channel regulate thermosensory neuron gene expression and function in C. elegans. Current biology : CB *14*, 62-68.
Sawin, E.R., Ranganathan, R., and Horvitz, H.R. (2000). C. elegans locomotory rate is modulated by the environment through a dopaminergic pathway and by experience through a serotonergic pathway. Neuron *26*, 619-631.
Schackwitz, W.S., Inoue, T., and Thomas, J.H. (1996). Chemosensory neurons function in parallel to mediate a pheromone response in C. elegans. Neuron *17*, 719-728.

Schaedel, O.N., Gerisch, B., Antebi, A., and Sternberg, P.W. (2012). Hormonal signal amplification mediates environmental conditions during development and controls an irreversible commitment to adulthood. PLoS biology *10*, e1001306.
Schild, L.C., Zbinden, L., Bell, H.W., Yu, Y.V., Sengupta, P., Goodman, M.B., and Glauser, D.A. (2014a). The balance between cytoplasmic and nuclear CaM kinase-1 signaling controls the operating range of noxious heat avoidance. Neuron *84*, 983-996.
Schindler, A.J., Baugh, L.R., and Sherwood, D.R. (2014). Identification of late larval stage developmental checkpoints in Caenorhabditis elegans regulated by insulin/IGF and steroid hormone signaling pathways. PLoS genetics *10*, e1004426.
Schroeder, F.C. (2006). Small molecule signaling in Caenorhabditis elegans. ACS chemical biology *1*, 198-200.
Schroeder, F.C. (2015). Modular assembly of primary metabolic building blocks: a chemical language in C. elegans. Chemistry & biology *22*, 7-16.
Schroeder, N.E., Androwski, R.J., Rashid, A., Lee, H., Lee, J., and Barr, M.M. (2013). Dauer-specific dendrite arborization in C. elegans is regulated by KPC-1/Furin. Current biology : CB *23*, 1527-1535.
Sengupta, P. (2013). The belly rules the nose: feeding state-dependent modulation of peripheral chemosensory responses. Current opinion in neurobiology *23*, 68-75.
Sharma, K.K., Wang, Z., Motola, D.L., Cummins, C.L., Mangelsdorf, D.J., and Auchus, R.J. (2009). Synthesis and activity of dafachronic acid ligands for the C. elegans DAF-12 nuclear hormone receptor. Molecular endocrinology *23*, 640-648.
Shaw, W.M., Luo, S., Landis, J., Ashraf, J., and Murphy, C.T. (2007). The C. elegans TGF-beta Dauer pathway regulates longevity via insulin signaling. Current biology : CB *17*, 1635-1645.
Shinkai, Y., Yamamoto, Y., Fujiwara, M., Tabata, T., Murayama, T., Hirotsu, T., Ikeda, D.D., Tsunozaki, M., Iino, Y., Bargmann, C.I*., et al.* (2011). Behavioral choice between conflicting alternatives is regulated by a receptor guanylyl cyclase, GCY-28, and a receptor tyrosine kinase, SCD-2, in AIA interneurons of Caenorhabditis elegans. The Journal of neuroscience : the official journal of the Society for Neuroscience *31*, 3007-3015.
Sim, C., and Denlinger, D.L. (2009). A shut-down in expression of an insulin-like peptide, ILP-1, halts ovarian maturation during the overwintering diapause of the mosquito Culex pipiens. Insect molecular biology *18*, 325-332.
Sim, C., and Denlinger, D.L. (2013). Insulin signaling and the regulation of insect diapause. Frontiers in physiology *4*, 189.
Sim, C., Kang, D.S., Kim, S., Bai, X., and Denlinger, D.L. (2015). Identification of FOXO targets that generate diverse features of the diapause phenotype in the mosquito Culex pipiens. Proceedings of the National Academy of Sciences of the United States of America.
Simpson, S.J., Sword, G.A., and Lo, N. (2011). Polyphenism in insects. Current biology : CB *21*, R738-749.
Snow, M.I., and Larsen, P.L. (2000). Structure and expression of daf-12: a nuclear hormone receptor with three isoforms that are involved in development and aging in Caenorhabditis elegans. Biochimica et biophysica acta *1494*, 104-116.
Sokolchik, I., Tanabe, T., Baldi, P.F., and Sze, J.Y. (2005). Polymodal sensory function of the Caenorhabditis elegans OCR-2 channel arises from distinct intrinsic determinants within the protein and is selectively conserved in mammalian TRPV proteins. The Journal of neuroscience : the official journal of the Society for Neuroscience *25*, 1015-1023.

Srinivasan, J., Kaplan, F., Ajredini, R., Zachariah, C., Alborn, H.T., Teal, P.E., Malik, R.U., Edison, A.S., Sternberg, P.W., and Schroeder, F.C. (2008). A blend of small molecules regulates both mating and development in Caenorhabditis elegans. Nature *454*, 1115-1118.
Starich, T.A., Herman, R.K., Kari, C.K., Yeh, W.H., Schackwitz, W.S., Schuyler, M.W., Collet, J., Thomas, J.H., and Riddle, D.L. (1995). Mutations affecting the chemosensory neurons of Caenorhabditis elegans. Genetics *139*, 171-188.
Stearns, S.C. (1989). The Evolutionary Significance of Phenotypic Plasticity - Phenotypic Sources of Variation Among Organisms can be Described by Developmental Developmental Switches and Reaction Norms. Bioscience *39*, 436-445.
Suo, S., Culotti, J.G., and Van Tol, H.H. (2009). Dopamine counteracts octopamine signalling in a neural circuit mediating food response in C. elegans. The EMBO journal *28*, 2437-2448.
Suo, S., and Ishiura, S. (2013). Dopamine modulates acetylcholine release via octopamine and CREB signaling in Caenorhabditis elegans. PloS one *8*, e72578.
Suo, S., Kimura, Y., and Van Tol, H.H. (2006). Starvation induces cAMP response element-binding protein-dependent gene expression through octopamine-Gq signaling in Caenorhabditis elegans. The Journal of neuroscience : the official journal of the Society for Neuroscience *26*, 10082-10090.
Suzuki, H., Thiele, T.R., Faumont, S., Ezcurra, M., Lockery, S.R., and Schafer, W.R. (2008). Functional asymmetry in Caenorhabditis elegans taste neurons and its computational role in chemotaxis. Nature *454*, 114-117.
Swanson, M.M., and Riddle, D.L. (1981). Critical periods in the development of the Caenorhabditis elegans dauer larva. Developmental biology *84*, 27-40.
Swoboda, P., Adler, H.T., and Thomas, J.H. (2000). The RFX-type transcription factor DAF-19 regulates sensory neuron cilium formation in C. elegans. Molecular cell *5*, 411-421.
Taghert, P.H., and Nitabach, M.N. (2012). Peptide neuromodulation in invertebrate model systems. Neuron *76*, 82-97.
Takahashi, M., Tomizawa, K., Sato, K., Ohtake, A., and Omori, A. (1995). A novel tau-tubulin kinase from bovine brain. FEBS letters *372*, 59-64.
Tanaka, S., Harano, K., and Nishide, Y. (2012). Re-examination of the roles of environmental factors in the control of body-color polyphenism in solitarious nymphs of the desert locust Schistocerca gregaria with special reference to substrate color and humidity. Journal of insect physiology *58*, 89-101.
Tennessen, J.M., Opperman, K.J., and Rougvie, A.E. (2010). The C. elegans developmental timing protein LIN-42 regulates diapause in response to environmental cues. Development *137*, 3501-3511.
Thatcher, J.D., Haun, C., and Okkema, P.G. (1999). The DAF-3 Smad binds DNA and represses gene expression in the Caenorhabditis elegans pharynx. Development *126*, 97-107.
Thevenaz, P., Ruttimann, U.E., and Unser, M. (1998). A pyramid approach to subpixel registration based on intensity. IEEE transactions on image processing : a publication of the IEEE Signal Processing Society *7*, 27-41.
Thomas, J.H., Birnby, D.A., and Vowels, J.J. (1993). Evidence for parallel processing of sensory information controlling dauer formation in Caenorhabditis elegans. Genetics *134*, 1105-1117.
Thomas, J.H., and Robertson, H.M. (2008). The Caenorhabditis chemoreceptor gene families. BMC biology *6*, 42.
Thummel, C.S. (2001). Molecular mechanisms of developmental timing in C. elegans and Drosophila. Developmental cell *1*, 453-465.

Touhara, K., and Vosshall, L.B. (2009). Sensing odorants and pheromones with chemosensory receptors. Annual review of physiology *71*, 307-332.
Vergoz, V., McQuillan, H.J., Geddes, L.H., Pullar, K., Nicholson, B.J., Paulin, M.G., and Mercer, A.R. (2009). Peripheral modulation of worker bee responses to queen mandibular pheromone. Proceedings of the National Academy of Sciences of the United States of America *106*, 20930-20935.
Vowels, J.J., and Thomas, J.H. (1992). Genetic analysis of chemosensory control of dauer formation in Caenorhabditis elegans. Genetics *130*, 105-123.
Vowels, J.J., and Thomas, J.H. (1994). Multiple chemosensory defects in daf-11 and daf-21 mutants of Caenorhabditis elegans. Genetics *138*, 303-316.
Wang, L., and Anderson, D.J. (2010). Identification of an aggression-promoting pheromone and its receptor neurons in Drosophila. Nature *463*, 227-231.
Wang, L., Han, X., Mehren, J., Hiroi, M., Billeter, J.C., Miyamoto, T., Amrein, H., Levine, J.D., and Anderson, D.J. (2011). Hierarchical chemosensory regulation of male-male social interactions in Drosophila. Nature neuroscience *14*, 757-762.
Ward, S., Thomson, N., White, J.G., and Brenner, S. (1975). Electron microscopical reconstruction of the anterior sensory anatomy of the nematode Caenorhabditis elegans.?2UU. The Journal of comparative neurology *160*, 313-337.
Ware, R.W., Clark, D., Crossland, K., and Russell, R.L. (1975). Nerve Ring of Nematode Caenorhabditis elegans - Sensory Input and Motor Output. J Comp Neurol *162*, 71-110.
Watanabe, D., Gotoh, H., Miura, T., and Maekawa, K. (2014). Social interactions affecting caste development through physiological actions in termites. Frontiers in physiology *5*, 127.
Wheeler, D.E. (1986). Developmental and physiological determinants of caste in social hymenoptera- evolutionary implications. Am Nat *128*, 13-34.
Wheeler, D.E., Buck, N., and Evans, J.D. (2006). Expression of insulin pathway genes during the period of caste determination in the honey bee, Apis mellifera. Insect molecular biology *15*, 597-602.
White, J.G., Southgate, E., Thomson, J.N., and Brenner, S. (1986). The structure of the nervous system of the nematode Caenorhabditis elegans. Philosophical transactions of the Royal Society of London Series B, Biological sciences *314*, 1-340.
Wilson, E.O. (1971). The insect societies (Cambridge, Mass.: Belknap Press of Harvard University Press).
Wyatt, T.D. (2003). Peromones and Animal Behaviour: Communication by Smell and Taste, 1 edn (Cambridge: Cambridge University Press).
Yamashita, O. (1996). Diapause hormone of the silkworm, Bombyx mori: Structure, gene expression and function. Journal of insect physiology *42*, 669-679.
You, Y.J., Kim, J., Raizen, D.M., and Avery, L. (2008). Insulin, cGMP, and TGF-beta signals regulate food intake and quiescence in C. elegans: a model for satiety. Cell metabolism *7*, 249-257.
Yu, S., Avery, L., Baude, E., and Garbers, D.L. (1997). Guanylyl cyclase expression in specific sensory neurons: a new family of chemosensory receptors. Proceedings of the National Academy of Sciences of the United States of America *94*, 3384-3387.
Yu, Y.V., Bell, H.W., Glauser, D.A., Van Hooser, S.D., Goodman, M.B., and Sengupta, P. (2014). CaMKI-dependent regulation of sensory gene expression mediates experience-dependent plasticity in the operating range of a thermosensory neuron. Neuron *84*, 919-926.

Zhang, X., Feng, L., Chinta, S., Singh, P., Wang, Y., Nunnery, J.K., and Butcher, R.A. (2015). Acyl-CoA oxidase complexes control the chemical message produced by Caenorhabditis elegans. Proceedings of the National Academy of Sciences of the United States of America.
Zhang, X., Noguez, J.H., Zhou, Y., and Butcher, R.A. (2013). Analysis of ascarosides from Caenorhabditis elegans using mass spectrometry and NMR spectroscopy. Methods in molecular biology *1068*, 71-92.
Zhang, X., and Zhang, Y. (2009). Neural-immune communication in Caenorhabditis elegans. Cell host & microbe *5*, 425-429.
Zwaal, R.R., Mendel, J.E., Sternberg, P.W., and Plasterk, R.H. (1997). Two neuronal G proteins are involved in chemosensation of the Caenorhabditis elegans Dauer-inducing pheromone. Genetics *145*, 715-727.

APPENDIX 1

Quantitative Assessment of Pheromone-Induced Dauer Formation in *Caenorhabditis elegans*

This work is published (Neal et al., 2013).

Chapter 20

Quantitative Assessment of Pheromone-Induced Dauer Formation in *Caenorhabditis elegans*

Scott J. Neal, Kyuhyung Kim, and Piali Sengupta

Abstract

Environmental conditions experienced during early larval stages dictate the developmental trajectory of the nematode *C. elegans*. Favorable conditions such as low population density, abundant food, and lower temperatures allow reproductive growth, while stressful conditions promote entry of second-stage (L2) larvae into the alternate dauer developmental stage. Population density is signaled by the concentration and composition of a complex mixture of small molecules that is produced by all stages of animals, and is collectively referred to as dauer pheromone; pheromone concentration is a major trigger for dauer formation. Here, we describe a quantitative dauer formation assay that provides a measure of the potency of single or mixtures of pheromone components in regulating this critical developmental decision.

Key words Dauer larva, Ascaroside, *C. elegans*, Pheromone

1 Introduction

C. elegans can develop via one of the two alternative developmental pathways [1]. This developmental decision is regulated by environmental cues experienced during early larval stages. Exposure of L1 larvae to overcrowding, high temperatures, and low food abundance causes them to develop as pre-dauer L2d larvae; continued stressful conditions result in irreversible commitment to the long-lived and stress-resistant alternative third larval stage called the dauer stage [2–5]. When conditions improve, dauer larvae molt and resume reproductive growth [6]. Conversely, favorable conditions promote continuous reproductive growth. Genetic analyses of mutants that fail to form dauers under stressful conditions, or enter into the dauer stage regardless of environmental cues, have identified the signaling pathways underlying the dauer developmental decision [7–13]. In brief, environmental cues sensed by sensory neurons regulate TGF-β and insulin signaling. These signals in turn regulate the production of steroid hormones and signaling via the DAF-12 nuclear hormone receptor. Hormone-bound

Kazushige Touhara (ed.), *Pheromone Signaling: Methods and Protocols*, Methods in Molecular Biology, vol. 1068,
DOI 10.1007/978-1-62703-619-1_20,

DAF-12 promotes reproductive growth, whereas unliganded DAF-12 promotes dauer arrest (reviewed in [11, 13]).

A major trigger for dauer formation is a complex mixture of small molecules called ascarosides that are produced by all stages of animals, and whose concentration serves as a measure of local population density [2, 4, 14–20]. The role of secreted/excreted molecules in regulating dauer formation was demonstrated by showing that conditioned medium from wild-type worms was sufficient to induce dauer formation in well-fed larvae [2]. This chapter describes an assay in which the ability of partially purified conditioned medium, called crude pheromone (*see* Chapter 6), or chemically synthesized pure ascarosides, to induce dauer formation is assessed. Since food levels and ambient temperature significantly modulate the efficacy of pheromone-induced dauer formation [3, 4, 21], this assay is designed to carefully control for environmental variables so as to provide a reproducible quantification of the efficiency of single or mixtures of ascarosides in inducing dauer entry. A variation of this assay has been described [22].

2 Materials

Prepare all solutions using Milli-Q or equivalent (≥18 MΩ) ultrapure water. Use reagent-grade ethanol (≥99.5 %) for reconstituting and diluting synthetic pheromones. All other materials should be of molecular biology grade or better. This protocol assumes basic knowledge of standard *C. elegans* husbandry.

1. Dissecting microscope, heat block, 20 °C incubator, 25 °C incubator, water bath.
2. *E. coli* strain OP50, grown on Luria-Bertani (LB) medium.
3. 1 M potassium phosphate buffer pH 6.0: ~1:3 1 M K_2HPO_4:1 M KH_2PO_4, titrate with 1 M K_2HPO_4 to desired pH.
4. S-basal buffer: 0.1 M NaCl, 50 mM potassium phosphate buffer pH 6.0.
5. 5 mg/mL cholesterol in 95 % ethanol.
6. Dauer formation assay agar: 50 mM NaCl, 1.7 % Noble agar (*see* **Note 1**), 1 mM $CaCl_2$, 1 mM $MgSO_4$, 25 mM potassium phosphate buffer pH 6.0, 5 μg/mL cholesterol.
7. Crude and/or synthetic pheromone (*see* Chapter 6).

3 Methods

3.1 Overview of Assay Timeline

This protocol involves multiple steps that are carried out on several independent days. In this protocol, it is important to be considerate of sources of biological variation which might compromise assay

results. For instance, there is increasing evidence of transgenerational inheritance of epigenetic information which may influence the results of behavioral or developmental assays [23–26]. It is thus important to control the developmental history of the parent animals that will contribute the embryos for the assay. Typically, worms should be maintained under well-fed conditions at 20 °C (*see* **Note 2**) for at least three generations prior to the assay. An overall summary of the protocol is shown in Fig. 1.

1. On day 1, pick five mid-L4-stage larvae to a fresh OP50-seeded nematode growth medium (NGM) plate around midday. Culture the worms at 20 °C. This parental plate should have at least 100 fairly synchronous well-fed L4 larvae on day 4.
2. On day 4, pick the required number of mid- to late-L4 larvae to fresh 60 mm OP50-seeded NGM plates; on day 5, five young adults will be required for each assay plate. Care must be taken not to induce crowding; typically no more than 70 L4 larvae should be subcultured to the same plate in order to minimize their exposure to endogenous pheromone. Culture these animals overnight at 20 °C in preparation for the assay.
3. Also on day 4, prepare the dauer agar assay plates and inoculate the OP50 culture for the heat-killed food source (Subheadings 3.3 and 3.4, respectively).
4. On day 5, apply the heat-killed OP50 cultures to the assay plates. Transfer five young adult animals to each assay plate and collect eggs (Subheading 3.5).
5. Incubate the assay plates at 25 °C and quantify dauer formation on day 8 or 9 (Subheading 3.6).

3.2 Preparation of Crude or Synthetic Pheromone

The methodology for preparation of crude pheromone is addressed elsewhere in this volume (*see* Chapter 6). Purification and synthesis of individual ascarosides have been described [14–20]. Crude or synthetic pheromones can be stably stored dry at −20 °C with some exceptions. For instance, PABA-C7 (ascr#8) [18] is less stable and is, therefore, stored at −80 °C. For use, dilutions of crude pheromone are made in water or 50:50 water:ethanol and may either be mixed with the molten assay agar or spread on the surface of the assay plate. Synthetic pheromones may be reconstituted at low millimolar concentrations in either dimethyl sulfoxide or ethanol. These solutions are stored at −20 °C and should be diluted in the original solvent when testing multiple concentrations in a dauer formation assay so as to keep the concentration of solvent constant in all assay plates. Our standard practice is to use ethanol as the solvent though in limited testing we have not observed any differences between the two solvents in this assay.

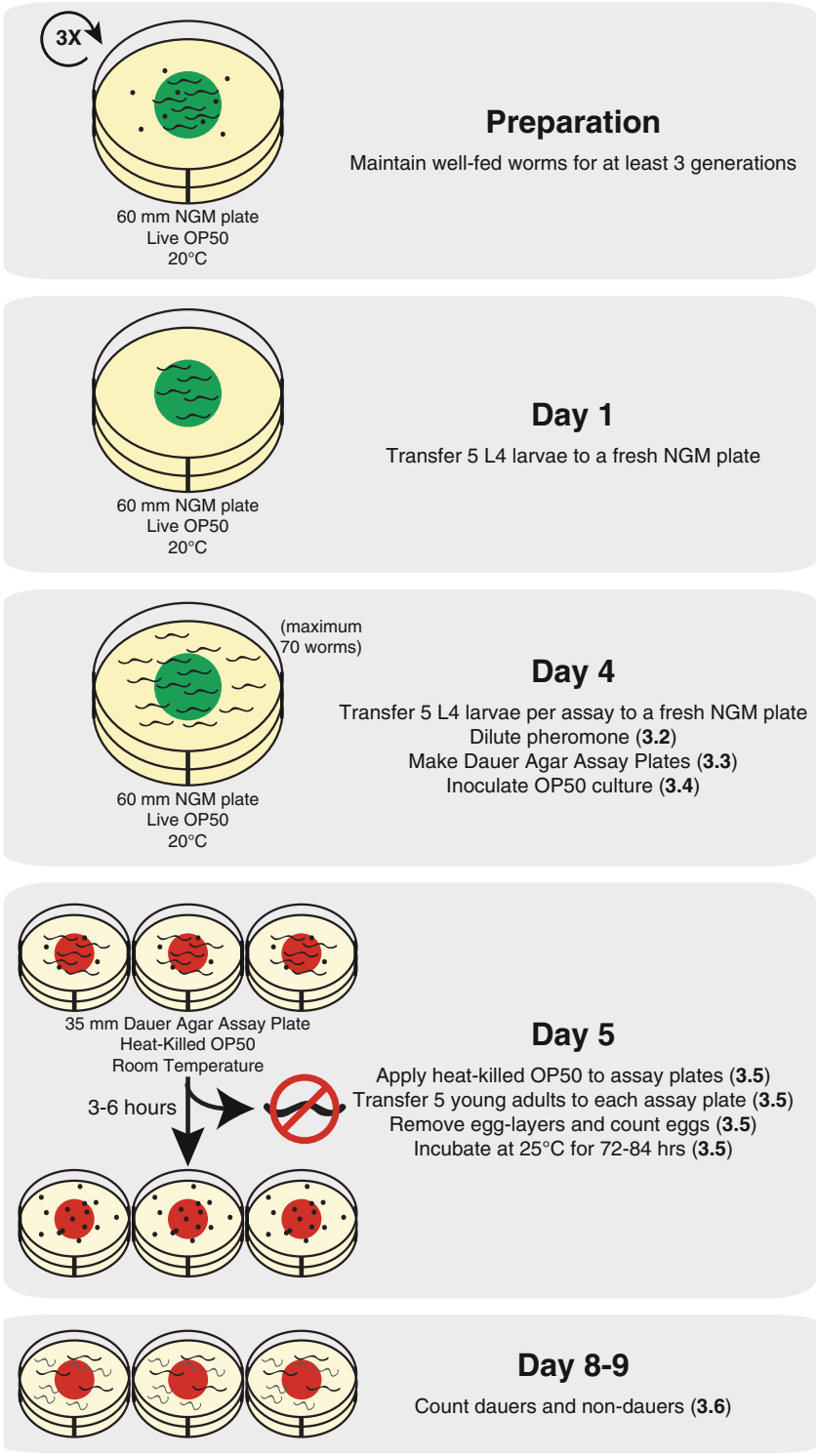

Fig. 1 Overview of the timeline and individual steps in the described protocol. *Numbers* in parentheses refer to the respective sections in Subheading 3 as described in the text. *Green* and *red* bacterial spots indicate live and heat-killed OP50 bacteria, respectively

3.3 Preparation of Dauer Agar Assay Plates

Use sterile technique throughout this procedure. Be sure to prepare sufficient agar for all assay plates while allowing for some loss due to evaporation and pipetting error. 3 mL of dauer assay agar is required per 35 mm assay plate (*see* **Note 3**).

1. In a clean, autoclave-safe bottle add (per 100 mL) 0.3 g NaCl, 1.7 g Noble agar, and an autoclave-safe stir bar. Add 100 mL of MilliQ H_2O and autoclave for 20 min on a liquid cycle. Tighten the cap and cool the sterilized solution to 60 °C in a water bath.
2. Place the cooled media on a stir plate and add (per 100 mL) 100 µL 1 M $CaCl_2$, 100 µL 1 M $MgSO_4$, 2.5 mL 1 M potassium phosphate buffer pH 6.0, and 100 µL 5 mg/mL cholesterol in 95 % ethanol. Stirring should be sufficient to mix in the cholesterol while avoiding bubbles or frothing.
3. Pheromone solutions should be prepared immediately before plate pouring, and for consistency should be prepared as a master mix. For each plate combine 6 µL of appropriately diluted pheromone in solvent (or solvent alone) with 94 µL of sterile MilliQ water. Array the empty 35 mm assay plates on a flat surface (*see* **Note 4**) and transfer 100 µL of the above pheromone master mix to the center of the empty plate.
4. Dispense 3 mL of assay agar into the pheromone-containing plates (*see* **Note 5**), and allow them to set overnight on the bench at room temperature (*see* **Note 6**). Ensure that there are no bubbles in the agar.

3.4 Preparation of Heat-Killed OP50

Although pheromone-induced dauer formation can be significantly suppressed by the presence of bacterial food, food is necessary to bypass the starvation-induced arrest at the L1 larval stage [27]. The typical food source used in most *C. elegans* laboratories is the *E. coli* strain OP50. Fresh cultures of OP50 may continue to grow on standard NGM plates, and this self-renewing food source suppresses dauer formation; therefore, either heat-killed or streptomycin-killed bacteria are used. For best results, OP50 should be freshly streaked onto an LB plate from a glycerol stock of the strain.

1. Inoculate a single OP50 colony into 35 mL of LB broth in a 50 mL conical tube. With the lid slightly loosened, grow the culture to stationary phase overnight at 37 °C with 225 rpm shaking.
2. Pre-weigh an appropriate number (generally 2–4) of 1.5 mL tubes to establish their tare weights. Transfer 1.45 mL of overnight culture into each tube and spin for 1 min at 8,000 × *g*. Discard the supernatant and transfer an additional 1.45 mL of overnight culture to the tube. Spin for 1 min at 8,000 × *g* and

aspirate the supernatant carefully. Spin the pellet for 1 min at maximum speed (≥13,000 × *g*) and carefully aspirate any supernatant with a pipette. Spin the pellet for 2 min at maximum speed and remove any final traces of supernatant with a P10 or a P20 pipetman.

3. Weight the tube and determine the pellet weight; the expected mass is between 8 and 10 mg. Fully resuspend the pellet to a concentration of 8 mg/mL in S-basal + 5 μg/mL cholesterol.
4. Heat-kill the bacteria by incubating in a heat block at 95 °C for 30 min with vortexing at 10-min intervals. Cool by placing at 4 °C for at least 30 min before use.
5. This reagent is best prepared fresh on the day of or the day before the assay (store overnight at 4 °C), but may also be kept for at most 1 week at 4 °C. Always vortex the bacterial suspension before use.

3.5 Setting Up the Assay

1. On the day of the assay, pipette 20 μL of fresh 8 mg/mL heat-killed OP50 (Subheading 3.4) onto the center of the assay agar. Care should be taken at all stages of this protocol not to pierce the surface of the assay agar to prevent animals from burrowing (*see* **Note 7**).
2. Briefly dry the food spot by incubating the plates in the fume hood; do not offset the lids, even if they are not vented (*see* **Note 8**). The plates are ready once the spot has completely dried and when there is no condensation on the lid. It generally takes 20–30 min for the food spot to dry fully. If a fume hood is not available the plates will dry on the bench but will require more time to do so.
3. Carefully transfer (*see* **Note 9**) five young adult hermaphrodites to each assay plate to begin the egg laying process (*see* **Note 10**). It is essential that only minimal live bacteria are transferred to the assay plates (*see* **Note 11**).
4. Allow the worms to lay approximately 75 eggs on each plate at room temperature. About 65–85 eggs are sufficient, although more consistent results are achieved with 75 eggs. Wild-type worms that have been correctly staged should lay sufficient eggs in about 3 h. It is useful to check the plates after the first hour and to return worms that have moved off the food back to the bacterial spot. When sufficient eggs are present on the plate, remove the adult worms and discard them. Be certain that all five adults are accounted for and removed, even those that may have begun to desiccate on the plate walls and those that may have burrowed (*see* **Note 7**).

5. Count the number of eggs on the plate and remove any eggs in excess of 85 (*see* **Note 12**); do not remove any of the heat-killed OP50 in this process.
6. Invert the plates in a loosely sealed plastic container and place them in a 25 °C incubator (*see* **Note 13**) for 72–84 h.

3.6 Scoring the Assay

The scoring of dauers can be subjective to untrained observers. Many physical hallmarks of true dauer larvae are not readily visible under a standard dissection microscope, and the use of a compound microscope is not compatible with large-scale experiments. Since true dauer larvae are resistant to 1 % sodium dodecyl sulfate (SDS) [1, 28], SDS selection can be used to identify dauers. However, it is difficult to accurately count all dauer larvae present on SDS-flooded plates, and we do not routinely perform this procedure. With some practice, the size, movement, body posture, and gut refraction phenotypes of dauer larvae [1, 10, 12, 29] can be readily used to discriminate them from non-dauer animals. In reporting the results from any assay it is important to state whether worms exhibiting pre-dauer arrest or characteristics of partial dauers are being excluded. Under the described conditions, it is atypical to observe either pre-dauer arrest or partial dauers in wild-type worms but the prevalence of such animals may be increased in some mutant backgrounds.

1. Remove the plates from the incubator and inspect them using a dissecting microscope. Provided with sufficient heat-killed food, wild-type worms will develop from embryo to late L4 stage within 72 h at the assay temperature of 25 °C. In a properly executed assay, 0–10 % of wild-type worms should arrest as dauers under negative control or "no-pheromone" conditions. When characterizing dauer formation in non-wild-type worms, it is important to allow sufficient time for their development, which might proceed at a slower rate than in wild-type worms. Therefore, the assay is routinely scored 84 h after egg laying. This additional time has no effect on the results for wild-type worms since dauers remain arrested and animals that have bypassed the dauer pathway remain easily distinguishable. If scoring at 84 h, ignore any next-generation L1 larvae that may have hatched.
2. Count the number of dauer larvae and the number of young adult worms on the plate. The counting process is simplified by drawing a grid on the base of the plate. Note that some worms may be burrowed into the agar and that dauers may be present on the sidewalls of the plate.
3. Compare the number of worms counted to the number of eggs recorded on day 5. In wild-type worms, at least 95 % of eggs should hatch and develop normally. Discard data from

plates with significant contamination and from those with too many (>85) or too few (<65) worms.

4. The number of dauers is presented as a proportion of the total number of worms (dauers and adults) on the plate, and is correlated with the log of the concentration of pheromone in the assay plate. A complete dataset should consist of replicate data from at least three independent experiments performed on different days.

4 Notes

1. Noble agar increases the rate of dauer formation by about 10 % and gives more consistent results. The concentration of agar may be increased up to 2 % to suppress burrowing behavior (*see* **Note 7**), although this may affect the baseline rate of dauer formation.
2. Culturing animals at 20 °C is optimal for growth and fecundity, especially for mutant strains with compromised health. We have not observed any quantitative differences in wild-type dauer formation rates when the parental worms are cultured at 20 °C versus 25 °C.
3. Depending on the actual dimensions of the Petri plates used, it might be necessary to increase the volume of assay agar in order to fully cover the bottom surface of the plate. To achieve consistent results the agar must evenly cover the bottom surface of the plate. However, if the agar is too thin it may dry excessively or crack over the course of the assay. Remember to adjust the pheromone volume to maintain the desired concentration.
4. It is useful to array the assay plates on a small flat tray to facilitate their movement from the bench to the fume hood when it is time to dry the food spots.
5. When dispensing the molten agar on top of the 100 μL of pheromone in the assay plate it is not necessary to stir or swirl the media. The mixing that occurs during dispensation is sufficient to distribute the pheromone throughout the medium. Swirling the cooling medium tends to leave a meniscus of dried agar around the plate, allowing worms to crawl up the sidewalls and eventually desiccate.
6. Plates should be prepared by mid-afternoon and be given 16–18 h to dry completely on the bench. There should be no condensation on the lid when the assay is started. If the assay plates are too humid the egg-laying worms tend to move off the food and crawl up the wall of the plate and/or burrow (*see* **Note 7**).

7. If an egg-laying worm burrows into the agar it does not have access to the food on the surface and will typically lay fewer eggs. Eggs laid in the agar are also difficult to see and count and will develop abnormally with respect to this assay. Extensive burrowing on a plate also typically coincides with reduced rates of dauer formation. Occasionally an egg-laying worm will burrow into the agar and must be removed prior to counting the eggs. Briefly vortexing or tapping the plate will sometimes draw the worm to the surface. The worm should only be extracted/dug from the plate as a last resort since the damage to the agar will encourage the larvae to burrow as well.
8. It is not advisable to offset the lids of the assay plates to expedite drying. This may lead to dust particles landing on the plate and increases in fungal contamination. Overdrying of the plates may lead to cracking of the agar and will cause the worms to burrow (*see* **Note 7**).
9. The shape of the tip of the platinum wire used to transfer worms is important in this assay—it must not scratch or gouge the assay agar surface during transfer and it must also carry over minimal live bacteria (*see* **Note 11**). A smoothed spatula-shaped wire tip is useful since this allows worms to be scooped from underneath without the use of bacterial "glue." This is also useful when the egg-laying worms must be removed from the assay plate without removing significant amounts of the heat-killed bacteria.
10. The use of five gravid hermaphrodites in this assay is intended to allow the correct number of embryos to be deposited on a plate in a reasonable time frame in order to have a growth-synchronized brood. Using varying number of egg-layers will affect the assay in two ways: it will affect the amount of food that is consumed prior to the hatch of the brood and it will alter the concentration of endogenous pheromone. Also note that extended egg-laying sessions may result in the earliest-laid embryos hatching before the eggs are counted.
11. Live OP50 is more attractive to egg-laying worms than the heat-killed OP50. Eggs will tend to be tightly clustered in patches of live food whereas they are normally more randomly distributed on plates featuring only heat-killed food. Live food is a potent suppressor of dauer formation in this assay and will negatively impact results.
12. Care should be taken to only count fertilized eggs when assessing the number of embryos on each assay plate. One-day-old adult wild-type worms will lay few if any unfertilized oocytes whereas some mutant strains will lay many. Since population density is an important factor in this assay as is the concentration of available food, it is important that the correct number

of L1 larvae hatch on each assay plate. Inspect the full surface of the plate, including around the edges of the agar, when counting fertilized eggs.

13. Temperature significantly modulates dauer formation and must be carefully controlled. A sensitive thermometer should be used to calibrate the 25 °C incubator and in addition, the placement of assay plates within the incubator should be consistent. Since humidity affects dauer formation to some extent, care should also be taken to house the plates in similar containers and to not overly stack the assay plates within the container. Natural convection incubators are used as opposed to forced-air incubators.

Acknowledgments

Funding for this work was provided by the National Science Foundation (IOS 0842452 and IOS 1256488 to P.S.), the Human Frontiers Science Program (RGY0042/2010 to P.S.), and the DGIST Convergence Science Center Program of the Ministry of Education, Science and Technology (11-BD-04 to K.K.). S.J.N. was supported by a postgraduate scholarship (PGS-D3) from the Natural Sciences and Engineering Research Council of Canada and by the Brandeis National Committee.

References

1. Cassada RC, Russell RL (1975) The dauer larva, a post-embryonic developmental variant of the nematode *Caenorhabditis elegans*. Dev Biol 46:326–342
2. Golden JW, Riddle DL (1982) A pheromone influences larval development in the nematode *Caenorhabditis elegans*. Science 218:578–580
3. Golden JW, Riddle DL (1984) The *Caenorhabditis elegans* dauer larva: developmental effects of pheromone, food, and temperature. Dev Biol 102:368–378
4. Golden JW, Riddle DL (1984) A *Caenorhabditis elegans* dauer-inducing pheromone and an antagonistic component of the food supply. J Chem Ecol 10:1265–1280
5. Schaedel ON, Gerisch B, Antebi A, Sternberg PW (2012) Hormonal signal amplification mediates environmental conditions during development and controls an irreversible commitment to adulthood. PLoS Biol 10(4):e1001306
6. Klass M, Hirsh D (1976) Non-ageing developmental variant of *Caenorhabditis elegans*. Nature 260:523–525
7. Riddle DL, Swanson MM, Albert PS (1981) Interacting genes in nematode dauer larva formation. Nature 290:668–671
8. Thomas JH, Birnby DA, Vowels JJ (1993) Evidence for parallel processing of sensory information controlling dauer formation in *Caenorhabditis elegans*. Genetics 134: 1105–1117
9. Vowels JJ, Thomas JH (1992) Genetic analysis of chemosensory control of dauer formation in *Caenorhabditis elegans*. Genetics 130: 105–123
10. Riddle DL, Albert PS (1997) Genetic and environmental regulation of dauer larva development. In: Riddle DS, Blumenthal T, Meyer BJ, Priess JR (eds) *C. elegans* II. Cold Spring Harbor Press, Cold Spring Harbor, Plainview, NY, pp 739–768
11. Hu PJ (2007) Dauer. WormBook:1–19. http://www.wormbook.org/chapters/www_dauer/dauer.html
12. Albert PS, Riddle DL (1988) Mutants of *Caenorhabditis elegans* that form dauer-like larvae. Dev Biol 126:270–293

13. Fielenbach N, Antebi A (2008) *C. elegans* dauer formation and the molecular basis of plasticity. Genes Dev 22:2149–2165
14. Butcher RA, Fujita M, Schroeder FC, Clardy J (2007) Small molecule signaling of dauer formation in *C. elegans*. Nat Chem Biol 3:420–422
15. Butcher RA, Ragains JR, Kim E, Clardy J (2008) A potent dauer pheromone component in *Caenorhabditis elegans* that acts synergistically with other components. Proc Natl Acad Sci U S A 105:14288–14292
16. Butcher RA, Ragains JR, Clardy J (2009) An indole-containing dauer pheromone component with unusual dauer inhibitory activity at higher concentrations. Org Lett 11:3100–3103
17. Srinivasan J, von Reuss SH, Bose N, Zaslaver A, Mahanti P, Ho MC, O'Doherty OG, Edison AS, Sternberg PW, Schroeder FC (2012) A modular library of small molecule signals regulates social behaviors in *Caenorhabditis elegans*. PLoS Biol 10:e1001237
18. Pungaliya C, Srinivasan J, Fox BW, Malik RU, Ludewig AH, Sternberg PW, Schroeder FC (2009) A shortcut to identifying small molecule signals that regulate behavior and development in *Caenorhabditis elegans*. Proc Natl Acad Sci U S A 106:7708–7713
19. Jeong PY, Jung M, Yim YH, Kim H, Park M, Hong E, Lee W, Kim YH, Kim K, Paik YK (2005) Chemical structure and biological activity of the *Caenorhabditis elegans* dauer-inducing pheromone. Nature 433:541–545
20. von Reuss SH, Bose N, Srinivasan J, Yim JJ, Judkins JC, Sternberg PW, Schroeder FC (2012) Comparative metabolomics reveals biogenesis of ascarosides, a modular library of small-molecule signals in *C. elegans*. J Am Chem Soc 134:1817–1824
21. Ailion M, Thomas JH (2000) Dauer formation induced by high temperatures in *Caenorhabditis elegans*. Genetics 156: 1047–1067
22. Lee J, Kim KY, Joo HJ, Kim H, Jeong PY, Paik YK (2011) Methods for evaluating the *Caenorhabditis elegans* dauer state: standard dauer-formation assay using synthetic daumones and proteomic analysis of O-GlcNAc modifications. Methods Cell Biol 106:445–460
23. Gu SG, Pak J, Guang S, Maniar JM, Kennedy S, Fire A (2012) Amplification of siRNA in *Caenorhabditis elegans* generates a transgenerational sequence-targeted histone H3 lysine 9 methylation footprint. Nat Genet 44:157–164
24. Rechavi O, Minevich G, Hobert O (2011) Transgenerational inheritance of an acquired small RNA-based antiviral response in *C. elegans*. Cell 147:1248–1256
25. Greer EL, Maures TJ, Ucar D, Hauswirth AG, Mancini E, Lim JP, Benayoun BA, Shi Y, Brunet A (2011) Transgenerational epigenetic inheritance of longevity in *Caenorhabditis elegans*. Nature 479:365–371
26. Katz DJ, Edwards TM, Reinke V, Kelly WG (2009) A *C. elegans* LSD1 demethylase contributes to germline immortality by reprogramming epigenetic memory. Cell 137:308–320
27. Johnson TE, Mitchell DH, Kline S, Kemal R, Foy J (1984) Arresting development arrests aging in the nematode *Caenorhabditis elegans*. Mech Ageing Dev 28:23–40
28. Swanson MM, Riddle DL (1981) Critical periods in the development of the *Caenorhabditis elegans* dauer larva. Dev Biol 84:27–40
29. Popham JD, Webster JM (1979) Aspects of the fine structure of the dauer larva of the nematode *Caenorhabditis elegans*. Can J Zool 57:794–800

APPENDIX 2

Neuromodulatory State and Sex Specify Alternative Behaviors through Antagonistic Synaptic Pathways in *C. elegans*

This work is published (Jang et al., 2012).

Neuron
Report

Neuromodulatory State and Sex Specify Alternative Behaviors through Antagonistic Synaptic Pathways in *C. elegans*

Heeun Jang,[1,6] Kyuhyung Kim,[2,4,6,*] Scott J. Neal,[2] Evan Macosko,[1] Dongshin Kim,[3] Rebecca A. Butcher,[5] Danna M. Zeiger,[2] Cornelia I. Bargmann,[1,*] and Piali Sengupta[2,*]
[1]Howard Hughes Medical Institute and Laboratory of Neural Circuits and Behavior, The Rockefeller University, New York, NY 10065, USA
[2]Department of Biology and National Center for Behavioral Genomics
[3]Department of Physics
Brandeis University, Waltham, MA 02454, USA
[4]Department of Brain Science, Daegu Gyeongbuk Institute of Science and Technology (DGIST), Daegu 711-873, Korea
[5]Department of Chemistry, University of Florida, Gainesville, FL 32611, USA
[6]These authors contributed equally to this work
*Correspondence: khkim@dgist.ac.kr (K.K.), cori@rockefeller.edu (C.I.B.), sengupta@brandeis.edu (P.S.)
http://dx.doi.org/10.1016/j.neuron.2012.06.034

SUMMARY

Pheromone responses are highly context dependent. For example, the *C. elegans* pheromone ascaroside C9 (ascr#3) is repulsive to wild-type hermaphrodites, attractive to wild-type males, and usually neutral to "social" hermaphrodites with reduced activity of the *npr-1* neuropeptide receptor gene. We show here that these distinct behavioral responses arise from overlapping push-pull circuits driven by two classes of pheromone-sensing neurons. The ADL sensory neurons detect C9 and, in wild-type hermaphrodites, drive C9 repulsion through their chemical synapses. In *npr-1* mutant hermaphrodites, C9 repulsion is reduced by the recruitment of a gap junction circuit that antagonizes ADL chemical synapses. In males, ADL sensory responses are diminished; in addition, a second pheromone-sensing neuron, ASK, antagonizes C9 repulsion. The additive effects of these antagonistic circuit elements generate attractive, repulsive, or neutral pheromone responses. Neuronal modulation by circuit state and sex, and flexibility in synaptic output pathways, may permit small circuits to maximize their adaptive behavioral outputs.

INTRODUCTION

Connectomics, the description of neuronal circuits based on anatomically defined synapses, is an ongoing venture in neuroscience (White et al., 1986; Lichtman and Denk, 2011). A question that is unanswered by such studies is the extent to which these synapses are functionally, as opposed to anatomically, stable in their properties. In many animals, pheromone detection results in behaviors that are highly sensitive to context (Wyatt, 2003). Here, we examine circuits for pheromone-dependent behaviors and show that a small set of common sensory inputs can give rise to multiple behavioral outputs through flexible circuit interactions.

The nematode worm *Caenorhabditis elegans* releases a pheromone mixture composed of derivatives of the dideoxysugar ascarylose (ascarosides), each of which has characteristic effects on development and behavior (Edison, 2009; Srinivasan et al., 2012). Two pheromones that have been characterized in multiple assays are C3 (ascr#5; asc ωC3) and C9 (ascr#3; asc ΔC9) ascarosides. C3 and C9 potently regulate larval entry into and exit from the alternate dauer developmental stage (Butcher et al., 2007, 2008; Kim et al., 2009) and also elicit a variety of behavioral effects in adults. Adult wild-type males accumulate in low concentrations of C9, suggesting a role in sex attraction (Srinivasan et al., 2008). Hermaphrodites with low-activity alleles of the *npr-1* neuropeptide receptor gene (henceforth "*npr-1*") are weakly attracted to ascaroside mixtures of C3 and C9 but not to either single compound alone (Macosko et al., 2009). Hermaphrodites from the standard laboratory strain N2 (henceforth "wild-type") strongly avoid C9 alone or together with C3 (Srinivasan et al., 2008; Macosko et al., 2009). The differential pheromone response in hermaphrodites correlates with aggregation behaviors: social *npr-1* animals usually aggregate into groups on food, consistent with attraction to pheromones, whereas solitary wild-type animals rarely aggregate (de Bono and Bargmann, 1998). The *npr-1* genotype appears to be a surrogate for a stress-related behavioral state, as aggregation and other *npr-1*-associated behaviors are stimulated regardless of genotype by stressful conditions (de Bono et al., 2002; Rogers et al., 2006). Thus, pheromone responses in *C. elegans* depend on sex and neuromodulatory state.

The bilateral pair of ASK sensory neurons acts with different partners in different pheromone responses. In dauer formation, ascaroside pheromones are sensed by ASK and ASI sensory

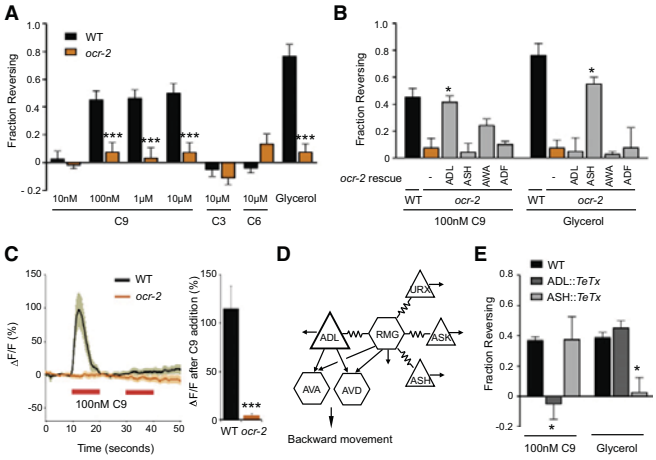

Figure 1. ADL Sensory Neurons Mediate C9 Avoidance

(A) Wild-type hermaphrodites avoid C9 in the drop test assay, but *ocr-2(ak47)* mutants do not. Assays were performed in the absence of food. *** indicates responses different from wild-type at $p < 0.001$. n = 20–100 animals each. See Figure S1A for assays on food and Figure S1B for behaviors of *osm-9* mutants. (B) *ocr-2* acts in ADL to mediate C9 avoidance. Assays were performed in the absence of food. * indicates responses different from *ocr-2* at $p < 0.05$. n = 20–100 animals each. *ocr-2* expression in AWA showed a trend toward rescue, but *odr-7* mutants with developmental defects in the AWA neurons (Sengupta et al., 1994) responded normally to C9 (Figure S1C). (C) C9-induced pheromone responses in ADL. (Left) Intracellular Ca^{2+} dynamics in GCaMP3-expressing ADL neurons in wild-type and *ocr-2(ak47)* hermaphrodites upon addition of pulses of 100 nM C9 (red horizontal bars). $n \geq 10$ neurons each. Shading around lines represents SEM. (Right) Average peak percentage changes in fluorescence upon addition of the first pulse of C9. * indicates amplitude different from wild-type at $p < 0.001$. Also see Figure S1D. (D) ADL has chemical synapses onto AVA and AVD command interneurons and is electrically coupled with the RMG hub-and-spoke circuit (adapted from White et al., 1986). Triangles represent sensory neurons and hexagons represent interneurons. Additional synapses (not shown) are indicated by arrows. (E) C9 avoidance requires ADL chemical synapses. Avoidance assays in the presence of food. * indicates responses different from wild-type at $p < 0.05$. n = 20–80 animals each. Error bars in all panels represent standard error of the mean (SEM).

neurons (Hu, 2007; Kim et al., 2009). In adult males, attraction to hermaphrodite pheromones requires ASK and the male-specific CEM sensory neurons (Srinivasan et al., 2008). In *npr-1* hermaphrodites, the ASK neurons sense pheromones and promote aggregation by cooperating with URX, ASH, and ADL sensory neurons, all of which are connected by gap junctions to the RMG inter/motorneurons in a hub-and-spoke circuit (White et al., 1986; de Bono et al., 2002; Macosko et al., 2009). The integrated input from spoke sensory neurons drives synaptic outputs from RMG and ASK to promote aggregation (Macosko et al., 2009). In wild-type animals, high NPR-1 activity in RMG inhibits this circuit (Macosko et al., 2009).

Wild-type hermaphrodites are repelled by ascarosides (Srinivasan et al., 2008; Macosko et al., 2009) but the underlying circuit mechanisms are unknown. Here we ask how repulsion from pheromones is mediated and how repulsion is transformed into neutral or attractive pheromone responses in males and in *npr-1* mutants. We find that the ADL sensory neurons promote repulsion from C9 in a sex- and *npr-1* state-dependent manner and that alternative pheromone-dependent behaviors rely differentially upon antagonistic activities of ADL chemical synapses, the RMG gap junction circuit, and ASK. Our results describe a mechanism by which overlapping, flexible circuits allow animals to integrate pheromone signals with sex and neuromodulatory state to generate a biologically appropriate behavioral response.

RESULTS

ADL Neurons Detect the Repulsive Pheromone Ascaroside C9

To identify neurons responsible for pheromone avoidance behavior, we first examined the acute responses of wild-type hermaphrodites to individual ascarosides using the drop-test assay (Hilliard et al., 2002). In this assay, a chemical diluted in buffer is presented to an animal that is moving forward, and reversal responses are compared to those to buffer alone (see Experimental Procedures). Using this behavioral response, we found that wild-type hermaphrodites specifically avoided nanomolar concentrations of ascaroside C9, but not ascarosides C3 or C6 (Figure 1A). These responses were enhanced in the presence of food, resulting in a ~10-fold increase in sensitivity (Figure S1A available online).

The neurons required for C9 avoidance were identified by examining sensory transduction mutants. *C. elegans* detects many chemical repellents with ciliated sensory neurons that signal through OSM-9 and OCR-2 TRPV channels (Bargmann, 2006). We found that both *osm-9* and *ocr-2* mutants exhibited strong defects in C9 avoidance (Figure 1A and Figure S1B). These two genes are coexpressed in four classes of head sensory neurons (Colbert et al., 1997; Tobin et al., 2002), which were individually tested for transgenic rescue of the *ocr-2* behavioral defect. The C9 avoidance defects were rescued upon expression of *ocr-2* in ADL, but not in other neurons (Figure 1B; also see Figure S1C). In control experiments, *ocr-2* expression in ADL did not rescue avoidance of high-osmotic-strength glycerol, a sensory response characteristic of ASH neurons (Bargmann, 2006) (Figure 1B). These results indicate that OCR-2 acts in the ADL neurons to mediate C9 avoidance.

To ask whether ADL responds to C9, we expressed the genetically encoded calcium (Ca^{2+}) sensor GCaMP3 (Tian et al., 2009) in ADL neurons and monitored intracellular Ca^{2+} dynamics in response to C9. A pulse of 100 nM C9 induced a rapid, transient increase in ADL intracellular Ca^{2+} levels (Figure 1C). ADL Ca^{2+} transients adapted quickly, returning to baseline within 10 s of C9 addition, and recovering ~120 s later (Figure 1C and data not shown). The response to C9 was abolished in *ocr-2* mutants

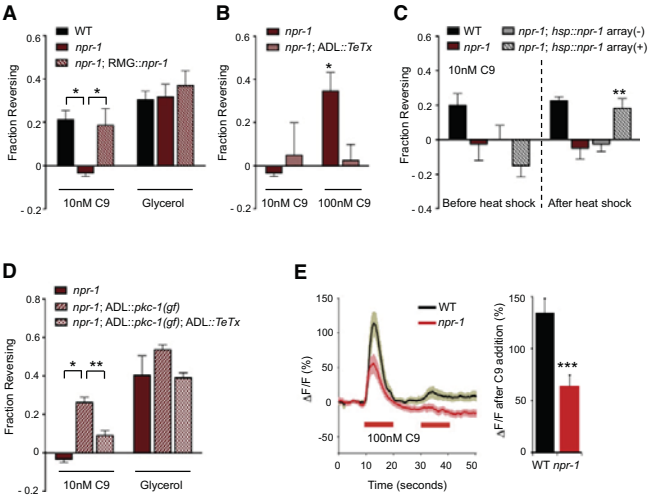

Figure 2. Reducing NPR-1 Activity in RMG Antagonizes ADL Chemical Synapses

(A) *npr-1* animals show decreased C9 avoidance. Avoidance assays in the presence of food. * indicates responses different from values indicated by brackets at $p < 0.05$. n = 40–100 animals each. (B) ADL chemical synapses can drive C9 avoidance in *npr-1*. Avoidance assays in the presence of food. * indicates responses different from wild-type at $p < 0.05$. n = 40–100 animals each. (C) Heat shock-driven expression of *npr-1* in adults rescues C9 avoidance in *npr-1* animals. ** indicates responses different from those of the same animals before heat shock at $p < 0.01$. Array(-) indicates animals from the *hsp16.2::npr-1*-expressing transgenic strain that have lost the extrachromosomal array, sibling controls for array(+) transgenic animals. Behavioral assays were performed in the presence of food before and immediately after heat shock at 33°C for 30 min. n = 40–60 animals each. (D) Strengthening ADL chemical synapses enhances C9 avoidance in *npr-1*. Avoidance assays in the presence of food. * and ** indicate responses different from values indicated by brackets at $p < 0.05$ and $p < 0.01$, respectively. n = 40–100 animals each. Also see Figure S2A. (E) (Left) Changes in GCaMP fluorescence in response to C9 in ADL neurons of wild-type and *npr-1(ad609)* hermaphrodites. Wild-type and all experimental conditions (see Figure 4C and Experimental Procedures) were examined together on multiple days. n = 12 neurons each. Shading around lines represents SEM. (Right) Average peak percentage changes in fluorescence upon addition of C9. *** indicates responses different from wild-type at $p < 0.001$. Also see Figures S2B and S2C. Error bars in all panels represent SEM.

that disrupt the sensory TRPV channel (Figure 1C). The ascaroside-evoked Ca^{2+} transients matched the behavioral results showing ADL-specific, chemically selective responses: ASH neurons did not respond to C9 or other ascarosides with Ca^{2+} transients, and no changes in Ca^{2+} dynamics were observed in the ADL neurons upon addition of C3 and C6 ascarosides (Figure S1D).

The anatomical wiring diagram of *C. elegans* hermaphrodites indicates that the ADL neurons are connected by chemical synapses to the AVA and AVD backward command interneurons, as well as other neurons (Figure 1D) (Chalfie et al., 1985; White et al., 1986). In addition, ADL neurons are spoke neurons connected by gap junctions to the RMG hub-and-spoke circuit that promotes aggregation (Figure 1D) (Macosko et al., 2009). In the simplest model, ADL-mediated avoidance behavior could be driven by synaptic output of the ADL neurons and activation of the backward command interneurons. To examine this possibility, we inhibited ADL chemical synapses by cell-specific expression of the tetanus toxin light chain (TeTx) that cleaves the synaptic vesicle protein synaptobrevin (Schiavo et al., 1992). Blocking synaptic transmission in ADL significantly suppressed C9 avoidance responses (Figure 1E), but not osmotic avoidance behavior mediated by the ASH neurons. Conversely, expression of similar transgenes in ASH blocked high-osmolarity glycerol avoidance but did not affect C9 avoidance (Figure 1E). Thus, the ADL neurons drive C9 avoidance through their chemical synapses.

Reducing *npr-1* Activity in the RMG Hub-and-Spoke Circuit Suppresses C9 Avoidance

npr-1 animals show reduced avoidance of repulsive pheromones in accumulation assays (Macosko et al., 2009), consistent with their increased aggregation behaviors. As the aggregation behaviors are most prominent on food (de Bono and Bargmann, 1998; de Bono et al., 2002), we included food when comparing *npr-1* and wild-type responses to C9. *npr-1* mutants did not avoid 10 nM C9 in the drop test, although they avoided higher concentrations (Figures 2A and 2B). High-osmolarity glycerol avoidance was unaffected by *npr-1* (Figure 2A). Silencing ADL synaptic output by TeTx expression in *npr-1* mutants did not further affect their behavioral responses to 10 nM C9, but reduced their avoidance of 100 nM C9 (Figure 2B). These results suggest that ADL chemical synapses can drive C9 avoidance in *npr-1* animals, but with reduced sensitivity compared to wild-type.

Previous studies have indicated that the ADL neurons promote aggregation in *npr-1* mutants, in apparent contradiction to their role in C9 avoidance in wild-type (de Bono et al., 2002). A possible explanation of this paradox is provided by the proposed circuit for aggregation, which involves gap junctions between ADL and RMG neurons rather than ADL chemical synapses (Figure 1D) (White et al., 1986; Macosko et al., 2009). Aggregation through the RMG circuit is inhibited by *npr-1* expression in RMG (Macosko et al., 2009). We hypothesized that this gap junction circuit might antagonize or inactivate C9 avoidance mediated by ADL chemical synapses. Indeed, the C9 avoidance defects in *npr-1* animals were fully rescued by a transgene expressing an *npr-1* cDNA in RMG (Figure 2A), indicating that NPR-1 acts in RMG to enhance C9 avoidance behaviors initiated by ADL.

To determine whether NPR-1 acts during development to affect connectivity, or in adults to regulate circuit function, we asked whether expression of NPR-1 during the adult stage could rescue C9 avoidance in *npr-1* animals. An *npr-1* cDNA

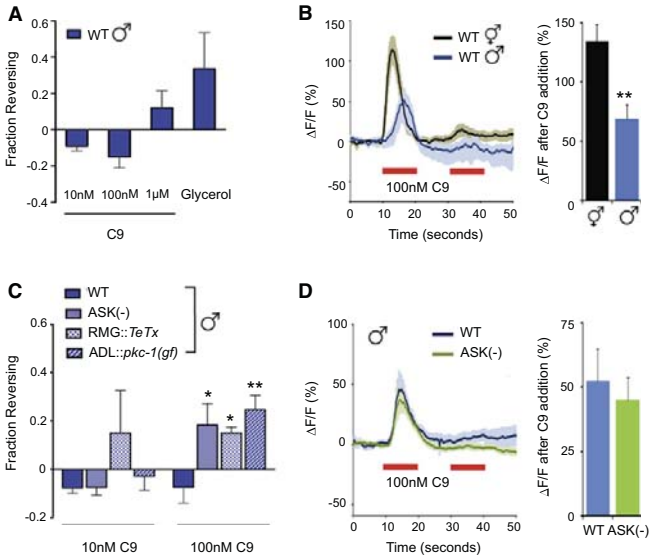

Figure 3. ASK Antagonism of ADL Decreases C9 Avoidance in Males

(A) Wild-type males do not avoid C9. Avoidance assays were performed in the presence of food. n = 20–70 animals each. (B) (Left) Changes in intracellular fluorescence in GCaMP3-expressing ADL neurons of wild-type hermaphrodites and males upon addition of 100 nM C9. n ≥ 12 neurons each. Shading around the lines represents SEM. (Right) Average peak percentage change in fluorescence upon C9 addition. ** indicates responses different from wild-type at $p < 0.01$. Also see Figures S3A and S3B. (C) ASK and RMG antagonize ADL in wild-type males. Avoidance of C9 in the presence of food. * and ** indicate responses different from wild-type at $p < 0.05$ and $p < 0.01$, respectively. n = 20–120 animals each. Also see Figure S3C. (D) C9 responses in wild-type male ADL neurons are unaffected by ASK ablation. Ca^{2+} transients upon C9 addition (red horizontal bar) in ADL in wild-type and ASK-ablated animals. n ≥ 10 neurons each. Error bars in all panels represent SEM.

expressed under a heat shock promoter (Coates and de Bono, 2002) restored C9 avoidance fully after 30 min of heat shock (Figure 2C), suggesting that NPR-1 acts acutely to regulate neuronal responses and circuit output.

The model that *npr-1* in RMG antagonizes ADL chemical synapses predicts that increased ADL synaptic function might restore avoidance. To test this prediction, we used an ADL-specific promoter to drive *pkc-1(gf)*, a constitutively active protein kinase C isoform that enhances neuronal synaptic output (Okochi et al., 2005; Sieburth et al., 2007; Tsunozaki et al., 2008; Macosko et al., 2009). Expression of *pkc-1(gf)* in ADL enhanced C9 avoidance in *npr-1* animals (Figure 2D), and blocking ADL chemical synapses with TeTx eliminated C9 avoidance in the *pkc-1(gf)* strain (Figure 2D). Expression of *pkc-1(gf)* in ADL neurons of wild-type animals had little effect on C9 avoidance (Figure S2A). These results suggest that strengthening ADL chemical synapses can override the effect of the *npr-1* mutation.

ADL Ca^{2+} transients were slightly but significantly reduced in amplitude in *npr-1* as compared to wild-type animals (Figures 2E and S2B). Two results suggest that this small change in amplitude is due to indirect effects of RMG on ADL. First, ADL Ca^{2+} responses were rescued by expressing *npr-1* under a promoter that is expressed in RMG (as well as a few other neurons) but not in ADL (Figure S2B). Second, the effect of *npr-1* on ADL Ca^{2+} responses was reversed in animals mutant for *unc-9*, which encodes a gap junction subunit that is broadly expressed in muscles and neurons (Liu et al., 2006; Starich et al., 2009) (Figure S2C). This observation suggests that gap junctions are required for NPR-1 to affect ADL, as predicted by the hub-and-spoke model. However, *unc-9* has stronger effects on ADL Ca^{2+} responses than *npr-1* (Figure S2C) and acts at multiple sites, so it may have either direct or indirect effects on ADL. In summary, *npr-1* has a strong effect on C9 avoidance behavior that is mediated by RMG and an indirect effect on ADL Ca^{2+} responses. Our results suggest that *npr-1* functions primarily by changing activity of the RMG gap junction circuit relative to ADL chemical synapses, and not solely by changing ADL sensory properties.

Reduced ADL C9 Responses and ADL-ASK Antagonism Abolish C9 Avoidance in Wild-Type Males

Unlike wild-type hermaphrodites, wild-type *C. elegans* males accumulate in low concentrations of C9, a behavior that requires the ASK neurons and the male-specific CEM sensory neurons (Srinivasan et al., 2008). In agreement with this result, we found that wild-type males did not avoid either 10 nM or 100 nM C9 in the drop test, although they exhibited robust avoidance of high-osmolarity glycerol (Figure 3A).

This sexually dimorphic behavioral response to C9 was accompanied by sexually dimorphic Ca^{2+} responses in ADL neurons. C9-induced Ca^{2+} transients in male ADL neurons were delayed by several seconds and reduced in amplitude compared to responses in hermaphrodites (Figures 3B, Figure S3A). Because slow changes in neuronal responses are often associated with neuropeptide signaling, we investigated ADL C9 responses in *egl-3* and *egl-21* mutants, which lack processed neuropeptides (Kass et al., 2001; Jacob and Kaplan, 2003). Both males and hermaphrodites showed sex-appropriate ADL Ca^{2+} transients in neuropeptide mutant backgrounds (Figure S3A), suggesting that classical neuropeptide signaling is not essential for this sexual dimorphism. Thus, altered male behaviors are associated with decreased and delayed pheromone signaling by the ADL neurons, which might or might not be intrinsic to ADL.

We next probed the roles of other sexually dimorphic neurons in C9 avoidance. The male-specific CEM sensory neurons are required for male accumulation at low C9 concentrations (Srinivasan et al., 2008), but were not central to C9 avoidance: sex-appropriate behaviors to C9 were observed both in males lacking CEM neurons (*ceh-30(lf)*) and in hermaphrodites

with ectopic CEM neurons (*ceh-30(gf)*) (Schwartz and Horvitz, 2007) (Figure S3B). The ASK neurons are pheromone-sensing neurons that participate in the RMG gap junction circuit (Macosko et al., 2009) (Figure 1D), and these neurons are functionally dimorphic between males and hermaphrodites (Srinivasan et al., 2008, 2012). Males whose ASK neurons were killed with a mouse caspase gene (Kim et al., 2009) exhibited significant avoidance of 100 nM C9, unlike wild-type males (Figure 3C). Ablation of ASK had little effect on wild-type hermaphrodite C9 avoidance (Figure S3C). Thus, ASK effectively antagonizes ADL-mediated C9 avoidance in wild-type males, but not in wild-type hermaphrodites. ASK ablation did not affect C9-induced Ca^{2+} transients in male ADL neurons (Figure 3D), suggesting that ASK acts at a circuit level to suppress C9 avoidance.

Reasoning by analogy to the *npr-1* circuit, we asked whether synaptic output of the RMG gap junction circuit antagonizes C9 avoidance in males. Indeed, expression of TeTx in the RMG neurons led to robust C9 avoidance behavior in wild-type males (Figure 3C). Expression of *pkc-1(gf)* in ADL also led to C9 avoidance, indicating that a strongly activated ADL neuron can drive repulsion in males (Figure 3C), as it can in *npr-1* hermaphrodites (Figure 2D). These results suggest that ADL has a latent ability to drive C9 avoidance in males, but this activity is inhibited by ASK and RMG.

Male Sexual Identity and *npr-1* Have Additive Effects on C9 Responses

Both males and *npr-1* hermaphrodites have decreased C9 avoidance (compare Figures 2A and 3A), and males also resemble *npr-1* hermaphrodites in their avoidance of high oxygen, their rapid movement on food, and their propensity to aggregate (Figures S4A and S4B). Despite this similarity, behavioral analysis of *npr-1* males suggests that *npr-1* mutations and male sex have independent effects on C9 responses. First, in *npr-1* males C9 failed to induce reversals as it did in *npr-1* hermaphrodites and wild-type males, but instead suppressed spontaneous reversals (Figure 4A). Based on the biased random walk model for *C. elegans* chemotaxis, the suppression of reversals suggests that *npr-1* males are attracted to C9 (Pierce-Shimomura et al., 1999; Luo et al., 2008). The suppression of reversals was eliminated by each of the genetic manipulations that increased C9 repulsion in wild-type males: killing ASK with the caspase transgene, reducing RMG synaptic output with TeTx, or enhancing ADL output with *pkc-1(gf)* (Figure 4B). Like other effects of *npr-1*, the effect on males was rescued by *npr-1* expression in RMG neurons (Figure 4B) and was rapidly reversed after acute expression of *npr-1* in adults (Figure S4C).

Additive effects of *npr-1* and male sex were also observed in Ca^{2+} imaging. The majority of ADL neurons in *npr-1* mutant males failed to modulate Ca^{2+} after C9 addition (Figure 4C, right panel). This reduction in ADL Ca^{2+} responses exceeded that of wild-type males or *npr-1* hermaphrodites, even considering only the small subset of *npr-1* males that did modulate ADL Ca^{2+} in response to C9 (Figure 4C, left panel).

The strong reduction in ADL Ca^{2+} transients might explain the loss of C9 avoidance in *npr-1* males but would not predict the appearance of the new behavior of C9 attraction (strictly speaking, reversal suppression). Therefore, we sought another sensory neuron that enhances C9 attraction in *npr-1* males. ASK was a plausible candidate to drive C9 attraction based on the behavioral analysis (Figure 4B), so we asked whether its pheromone sensitivity was altered by *npr-1*. Indeed, ASK neurons showed much stronger C9-evoked Ca^{2+} transients in *npr-1* males than in wild-type males (Figure 4D). A similar enhancement of ASK responses was present in *npr-1* hermaphrodites, whose C9 avoidance is also antagonized by ASK (Figures 4D and S3C).

Together, these results indicate that *npr-1* males have enhanced ASK C9 responses and decreased ADL C9 responses compared to wild-type males and that these changes drive attraction to C9 through RMG chemical synapses. Circuit changes driving sexually dimorphic and NPR-1-dependent C9 pheromone responses are summarized in Figure 4E.

Pheromone Blends Are Integrated by the RMG Circuit

The results described above suggest that antagonism between repulsive signaling from ADL chemical synapses and attractive signaling mediated by ASK and the RMG gap junction circuit determine whether C9 is repulsive, neutral, or attractive. We considered what this might mean for the pheromone-dependent behaviors of *npr-1* hermaphrodites, which are weakly attracted to mixtures of ascarosides, including C9 and C3, but not to either C3 or C9 alone (Srinivasan et al., 2008; Macosko et al., 2009). By analogy with the detection of pheromone blends in other animals (Kaissling, 1996), synergistic attraction to ascaroside blends could result from cooperation of multiple pheromone-sensing neurons. Hermaphrodite ASK neurons detect C3 at nanomolar concentrations (Kim et al., 2009), and ASK pheromone responses are stronger in *npr-1* than in wild-type hermaphrodites (Macosko et al., 2009). If antagonism between ASK and ADL applies to pheromone blends, C3 detection by ASK should suppress repulsion to C9 detected by ADL. To address this hypothesis, we used the drop-test assay to detect behavioral interactions between pheromones.

In agreement with the observation that C3 is not highly attractive or repulsive on its own (Macosko et al., 2009), C3 did not induce or suppress reversals in wild-type or *npr-1* hermaphrodites (Figure 4F). However, C3 did modify the response to C9 in *npr-1* hermaphrodites, suppressing their avoidance of 100 nM C9 almost to baseline levels (Figure 4F). No suppression was observed in wild-type hermaphrodites, indicating that the interaction depends on *npr-1* and the gap junction circuit. Genetic ablation of the ASK neurons in *npr-1* hermaphrodites abolished the interaction between C3 and C9 (Figure 4F). These results support the model that ASK suppresses ADL-mediated avoidance and additionally are consistent with a circuit that can evaluate pheromone blends, so that the combination of C3 detected by ASK and C9 detected by ADL is less repulsive than C9 alone.

DISCUSSION

Sex and NPR-1 neuropeptide signaling converge on a common neural circuit to regulate behavioral responses to the ascaroside C9. In each case, alternative behaviors are initiated by the ADL and ASK sensory neurons, but specific behavioral

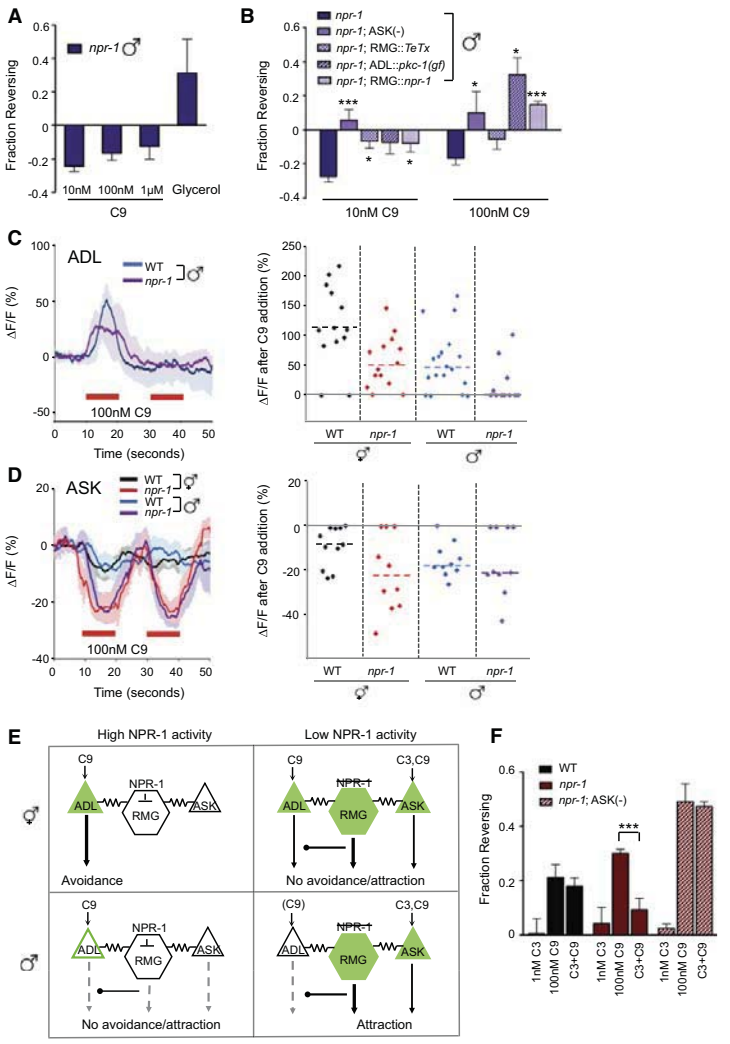

Figure 4. Masculinization and NPR-1 Exert Additive Effects on a Common Circuit

(A) Spontaneous reversals are suppressed by C9 in *npr-1* males. Avoidance assays were performed in the presence of food. n = 30–120 animals each. Responses to 10 nM and 1 μM C9 are different from those of wild-type males at $p < 0.01$ (see Figure 3A). Also see Figure S4. (B) C9-induced suppression of spontaneous reversals in *npr-1* males is eliminated by circuit manipulations that enhance C9 avoidance. * and *** indicate responses different from *npr-1* at $p < 0.05$ and $p < 0.001$, respectively. n = 40–120 animals each. (C) (Left) Intracellular Ca^{2+} dynamics in GCaMP-expressing ADL neurons of wild-type and *npr-1(ad609)* males in response to 100 nM C9. Only animals with positive responses were included in the averages at left: n = 14 (of 17) neurons for wild-type males and n = 4 (of 11) neurons for *npr-1* males. Shading around the lines represents SEM. (Right) Scatter plot showing peak percentage changes in fluorescence in individual ADL neurons of animals of the indicated genotypes in response to a pulse of 100 nM C9. Data are included from Figure 2E for comparison. Dotted lines indicate the median. ADL neurons that failed to exhibit significant changes in fluorescence: 14% in wild-type hermaphrodites (n = 14); 14% in *npr-1* hermaphrodites (n = 14); 12% in wild-type males (n = 17) and 64% in *npr-1* males (n = 11). (D) ASK responses to C9 are enhanced in *npr-1* mutants. (Left) Intracellular Ca^{2+} dynamics in GCaMP3-expressing ASK neurons (Macosko et al., 2009) of wild-type and *npr-1(ad609)* males and hermaphrodites in response to 100 nM C9 (red horizontal bars). Only animals with quantifiable changes were included in these averages; n ≥ 6 neurons for each. Shading around lines represents SEM. (Right) Scatter plot showing peak percentage changes in fluorescence in individual ASK neurons of animals of the indicated genotypes in response to a pulse of 100 nM C9. Dotted lines indicate the median. (E) Inferred activities of ADL, ASK, and RMG neurons in animals of different sex and *npr-1* genotype. High NPR-1 activity inhibits RMG. C9 responses are high in ADL and low in ASK in wild-type hermaphrodites; ADL drives C9 avoidance via its chemical synapses. In males, ASK C9 responses remain low and ADL C9 responses are decreased due to sexual dimorphism. ASK and the RMG circuit antagonize ADL output to further reduce ADL-driven C9 avoidance. In *npr-1* animals, ASK C9 responses are increased in both males and hermaphrodites, and ADL C9 responses are significantly decreased in *npr-1* males. ASK and RMG antagonize ADL chemical synapses and decrease avoidance (hermaphrodites) or promote attraction (males). (F) Integration of pheromone blend information in *npr-1* hermaphrodites requires ASK. Assays were performed in the presence of food. *** indicates responses different from values indicated by brackets at $p < 0.001$. n = 60–80 animals each. Error bars in all panels represent SEM.

outcomes are determined by antagonism between ADL chemical synapses that promote repulsion and the RMG gap junction circuit that promotes attraction. These two antagonistic elements form a push-pull circuit motif, in which a single sensory input can give rise to opposite behaviors (Figure 4E). On the repulsive arm of the circuit, wild-type hermaphrodites avoid C9 through ADL chemical synapses, whose predicted targets include the backward command interneurons. Although this effect is diminished in *npr-1* mutants and males, all genotypes retain a covert ability to avoid C9. On the attractive arm, the RMG gap junction circuit suppresses C9 avoidance via RMG chemical synapses, which converge with ADL chemical synapses on the command interneurons (see Figure 1D). NPR-1 inhibits RMG through unknown molecular mechanisms; in one model, it could close the RMG gap junctions to disengage the entire hub-and-spoke circuit. The ASK neurons also sense C9 and drive attractive behavioral responses more strongly in males, in *npr-1* mutants, or in the presence of C3.

ASK and ADL form gap junctions with RMG; both behavioral results and functional imaging indicate that RMG potentiates ASK signaling and inhibits ADL signaling (Macosko et al., 2009, and this work). The attractive arm of the circuit dominates in *npr-1* males, which have minimal C9 responses in ADL, strong C9 responses in ASK, and the ability to propagate these changes through the RMG circuit.

It is likely that the alternative circuits in wild-type and *npr-1* mutants are representative of alternative neuromodulatory states that exist in all genotypes to differing degrees. The behaviors of *npr-1* animals resemble the behaviors of wild-type animals under metabolic or crowding stress, and conversely, *npr-1* animals placed in low-oxygen environments behave like wild-type animals in most respects (de Bono et al., 2002; Rogers et al., 2006). The differential modulation of ADL chemical synapses and gap junctions in overlapping circuits by *npr-1* is reminiscent of the flexible circuit states of crustacean stomach central pattern generators and vertebrate spinal cord motor circuits, which are also controlled by neuromodulatory inputs (Dickinson et al., 1990; Grillner, 2006). In males, sexual dimorphism in sensory neuron responses and circuit properties further expand this behavioral flexibility.

The RMG hub-and-spoke circuit has both similarities to and differences from the recently described RIH hub-and-spoke circuit for mechanosensation (Chatzigeorgiou and Schafer, 2011). A central hub neuron coordinates responses via gap junctions in both circuits, but RIH appears to facilitate the transfer of mechanosensory information through the circuit (Chatzigeorgiou and Schafer, 2011), whereas RMG antagonizes ADL synaptic output while facilitating ASK synaptic output, generating a consensus behavior that can be distinct from that generated by either sensory neuron. Thus, a common network motif can perform distinct computations in ways that are not evident solely from anatomical wiring diagrams.

Pheromone blends with defined concentrations of individual pheromone components elicit sex- and context-specific behaviors in many organisms (Kaissling, 1996; Slessor et al., 1988; Wyatt, 2003). The RMG circuit coordinates sensory responses via gap junctions to generate coherent responses to specific pheromones and pheromone blends. Spoke sensory neurons in the RMG circuit also respond to nonpheromone cues (Bargmann, 2006), allowing the circuit to integrate pheromones with other environmental signals. At the same time, each sensory neuron also has other outputs; for example, ASK can promote attraction to indole ascarosides via its chemical synapses in an RMG-independent manner (Srinivasan et al., 2012), and ADL alone can drive repulsion. These results reveal a multifunctional, multiplexed sensory circuit, whose compact structure integrates external context with internal states to generate a variety of adaptive behaviors.

EXPERIMENTAL PROCEDURES

Detailed protocols are listed in Supplemental Experimental Procedures.

Behavioral Assays

The drop test was performed essentially as previously described (Hilliard et al., 2002). "Fraction reversing" represents (fraction of animals reversing in 4 s to pheromone) – (fraction reversing in 4 s to buffer).

Ca^{2+} Imaging

Ca^{2+} imaging experiments were performed as previously described (Kim et al., 2009; Macosko et al., 2009) using microfluidic devices custom-designed to restrain adult hermaphrodites (Chalasani et al., 2007) or adult males (this study) (Microfluidics Facility, Brandeis Materials Research Science and Engineering Center).

SUPPLEMENTAL INFORMATION

Supplemental Information includes four figures and Supplemental Experimental Procedures and can be found with this article online at http://dx.doi.org/10.1016/j.neuron.2012.06.034.

ACKNOWLEDGMENTS

We are grateful to Eugene Kim and Andrew Gordus for assistance with ADL imaging experiments and analysis, the *Caenorhabditis* Genetics Center for strains, and Eve Marder for discussion. This work was supported by the NSF (IOS 0542372, P.S.; DMR-0820492, D.K. [MRSEC program]), the HFSP (RGY0042- P.S.), the NIH (core grant P30 NS45713 to the Brandeis Biology Department; F31 DC011467, D.M.Z.; R00 GM87533, R.A.B.), the DGIST MIREBrain and Convergence Science Center (12-BD-0403) and Basic Science Research Program (2012009385) of the Ministry of Education, Science and Technology, Korea (K.K.), the Natural Sciences and Engineering Research Council of Canada (PGS-D3), and the Brandeis National Committee (S.J.N.), a gift from the Jensam Foundation (C.I.B.), and the Howard Hughes Medical Institute (C.I.B.). C.I.B. is an Investigator of the Howard Hughes Medical Institute. Author contributions: H.J., K.K., S.J.N., and D.M.Z. performed the experiments; E.M., D.K. and R.B. provided reagents; H.J., K.K., C.I.B., and P.S. analyzed and interpreted data; C.I.B. and P.S. wrote the manuscript.

Accepted: June 26, 2012
Published: August 22, 2012

REFERENCES

Bargmann, C.I. (2006). Chemosensation in *C. elegans*. *WormBook*, ed. The *C. elegans* Research Community, WormBook, http://dx.doi.org/10.1895/wormbook.1.144.1, http://www.wormbook.org.

Butcher, R.A., Fujita, M., Schroeder, F.C., and Clardy, J. (2007). Small-molecule pheromones that control dauer development in *Caenorhabditis elegans*. Nat. Chem. Biol. *3*, 420–422.

Butcher, R.A., Ragains, J.R., Kim, E., and Clardy, J. (2008). A potent dauer pheromone component in *Caenorhabditis elegans* that acts synergistically with other components. Proc. Natl. Acad. Sci. USA *105*, 14288–14292.

Chalasani, S.H., Chronis, N., Tsunozaki, M., Gray, J.M., Ramot, D., Goodman, M.B., and Bargmann, C.I. (2007). Dissecting a circuit for olfactory behaviour in *Caenorhabditis elegans*. Nature *450*, 63–70.

Chalfie, M., Sulston, J.E., White, J.G., Southgate, E., Thomson, J.N., and Brenner, S. (1985). The neural circuit for touch sensitivity in *Caenorhabditis elegans*. J. Neurosci. *5*, 956–964.

Chatzigeorgiou, M., and Schafer, W.R. (2011). Lateral facilitation between primary mechanosensory neurons controls nose touch perception in *C. elegans*. Neuron *70*, 299–309.

Coates, J.C., and de Bono, M. (2002). Antagonistic pathways in neurons exposed to body fluid regulate social feeding in *Caenorhabditis elegans*. Nature *419*, 925–929.

Colbert, H.A., Smith, T.L., and Bargmann, C.I. (1997). OSM-9, a novel protein with structural similarity to channels, is required for olfaction, mechanosensation, and olfactory adaptation in *Caenorhabditis elegans*. J. Neurosci. *17*, 8259–8269.

de Bono, M., and Bargmann, C.I. (1998). Natural variation in a neuropeptide Y receptor homolog modifies social behavior and food response in *C. elegans*. Cell *94*, 679–689.

de Bono, M., Tobin, D.M., Davis, M.W., Avery, L., and Bargmann, C.I. (2002). Social feeding in *Caenorhabditis elegans* is induced by neurons that detect aversive stimuli. Nature *419*, 899–903.

Dickinson, P.S., Mecsas, C., and Marder, E. (1990). Neuropeptide fusion of two motor-pattern generator circuits. Nature *344*, 155–158.

Edison, A.S. (2009). *Caenorhabditis elegans* pheromones regulate multiple complex behaviors. Curr. Opin. Neurobiol. *19*, 378–388.

Grillner, S. (2006). Biological pattern generation: the cellular and computational logic of networks in motion. Neuron *52*, 751–766.

Hilliard, M.A., Bargmann, C.I., and Bazzicalupo, P. (2002). *C. elegans* responds to chemical repellents by integrating sensory inputs from the head and the tail. Curr. Biol. *12*, 730–734.

Hu, P.J. (2007). Dauer. *WormBook*, ed. The *C. elegans* Research Community, WormBook, http://dx.doi.org/10.1895/wormbook.1.144.1, http://www.wormbook.org.

Jacob, T.C., and Kaplan, J.M. (2003). The EGL-21 carboxypeptidase E facilitates acetylcholine release at *Caenorhabditis elegans* neuromuscular junctions. J. Neurosci. *23*, 2122–2130.

Kaissling, K.E. (1996). Peripheral mechanisms of pheromone reception in moths. Chem. Senses *21*, 257–268.

Kass, J., Jacob, T.C., Kim, P., and Kaplan, J.M. (2001). The EGL-3 proprotein convertase regulates mechanosensory responses of *Caenorhabditis elegans*. J. Neurosci. *21*, 9265–9272.

Kim, K., Sato, K., Shibuya, M., Zeiger, D.M., Butcher, R.A., Ragains, J.R., Clardy, J., Touhara, K., and Sengupta, P. (2009). Two chemoreceptors mediate developmental effects of dauer pheromone in *C. elegans*. Science *326*, 994–998.

Lichtman, J.W., and Denk, W. (2011). The big and the small: challenges of imaging the brain's circuits. Science *334*, 618–623.

Liu, Q., Chen, B., Gaier, E., Joshi, J., and Wang, Z.W. (2006). Low conductance gap junctions mediate specific electrical coupling in body-wall muscle cells of *Caenorhabditis elegans*. J. Biol. Chem. *281*, 7881–7889.

Luo, L., Gabel, C.V., Ha, H.I., Zhang, Y., and Samuel, A.D. (2008). Olfactory behavior of swimming *C. elegans* analyzed by measuring motile responses to temporal variations of odorants. J. Neurophysiol. *99*, 2617–2625.

Macosko, E.Z., Pokala, N., Feinberg, E.H., Chalasani, S.H., Butcher, R.A., Clardy, J., and Bargmann, C.I. (2009). A hub-and-spoke circuit drives pheromone attraction and social behaviour in *C. elegans*. Nature *458*, 1171–1175.

Okochi, Y., Kimura, K.D., Ohta, A., and Mori, I. (2005). Diverse regulation of sensory signaling by *C. elegans* nPKC-epsilon/eta TTX-4. EMBO J. *24*, 2127–2137.

Pierce-Shimomura, J.T., Morse, T.M., and Lockery, S.R. (1999). The fundamental role of pirouettes in *Caenorhabditis elegans* chemotaxis. J. Neurosci. *19*, 9557–9569.

Rogers, C., Persson, A., Cheung, B., and de Bono, M. (2006). Behavioral motifs and neural pathways coordinating O_2 responses and aggregation in *C. elegans*. Curr. Biol. *16*, 649–659.

Schiavo, G., Benfenati, F., Poulain, B., Rossetto, O., Polverino de Laureto, P., DasGupta, B.R., and Montecucco, C. (1992). Tetanus and botulinum-B neurotoxins block neurotransmitter release by proteolytic cleavage of synaptobrevin. Nature *359*, 832–835.

Schwartz, H.T., and Horvitz, H.R. (2007). The *C. elegans* protein CEH-30 protects male-specific neurons from apoptosis independently of the Bcl-2 homolog CED-9. Genes Dev. *21*, 3181–3194.

Sengupta, P., Colbert, H.A., and Bargmann, C.I. (1994). The *C. elegans* gene *odr-7* encodes an olfactory-specific member of the nuclear receptor superfamily. Cell *79*, 971–980.

Sieburth, D., Madison, J.M., and Kaplan, J.M. (2007). PKC-1 regulates secretion of neuropeptides. Nat. Neurosci. *10*, 49–57.

Slessor, K.N., Kaminski, L.A., King, G.G.S., Borden, J.H., and Winston, M.L. (1988). Semiochemical basis of the retinue response to queen honey bees. Nature *332*, 354–356.

Srinivasan, J., Kaplan, F., Ajredini, R., Zachariah, C., Alborn, H.T., Teal, P.E., Malik, R.U., Edison, A.S., Sternberg, P.W., and Schroeder, F.C. (2008). A blend of small molecules regulates both mating and development in *Caenorhabditis elegans*. Nature *454*, 1115–1118.

Srinivasan, J., von Reuss, S.H., Bose, N., Zaslaver, A., Mahanti, P., Ho, M.C., O'Doherty, O.G., Edison, A.S., Sternberg, P.W., and Schroeder, F.C. (2012). A modular library of small molecule signals regulates social behaviors in *Caenorhabditis elegans*. PLoS Biol. *10*, e1001237.

Starich, T.A., Xu, J., Skerrett, I.M., Nicholson, B.J., and Shaw, J.E. (2009). Interactions between innexins UNC-7 and UNC-9 mediate electrical synapse specificity in the *Caenorhabditis elegans* locomotory nervous system. Neural Dev. *4*, 16.

Tian, L., Hires, S.A., Mao, T., Huber, D., Chiappe, M.E., Chalasani, S.H., Petreanu, L., Akerboom, J., McKinney, S.A., Schreiter, E.R., et al. (2009). Imaging neural activity in worms, flies and mice with improved GCaMP calcium indicators. Nat. Methods *6*, 875–881.

Tobin, D., Madsen, D., Kahn-Kirby, A., Peckol, E., Moulder, G., Barstead, R., Maricq, A., and Bargmann, C.I. (2002). Combinatorial expression of TRPV channel proteins defines their sensory functions and subcellular localization in *C. elegans* neurons. Neuron *35*, 307–318.

Tsunozaki, M., Chalasani, S.H., and Bargmann, C.I. (2008). A behavioral switch: cGMP and PKC signaling in olfactory neurons reverses odor preference in *C. elegans*. Neuron *59*, 959–971.

White, J.G., Southgate, E., Thomson, J.N., and Brenner, S. (1986). The structure of the nervous system of the nematode *Caenorhabditis elegans*. Philos. Trans. R. Soc. Lond. B Biol. Sci. *314*, 1–340.

Wyatt, T.S. (2003). Pheromones and Animal Behavior:Communication by Smell and Taste (Cambridge: Cambridge University Press).

Neuron, Volume *75*

Supplemental Information

Neuromodulatory State and Sex Specify Alternative Behaviors through Antagonistic Synaptic Pathways in *C. elegans*

Heeun Jang, Kyuhyung Kim, Scott J. Neal, Evan Macosko, Dongshin Kim, Rebecca A. Butcher, Danna M. Zeiger, Cornelia I. Bargmann, and Piali Sengupta

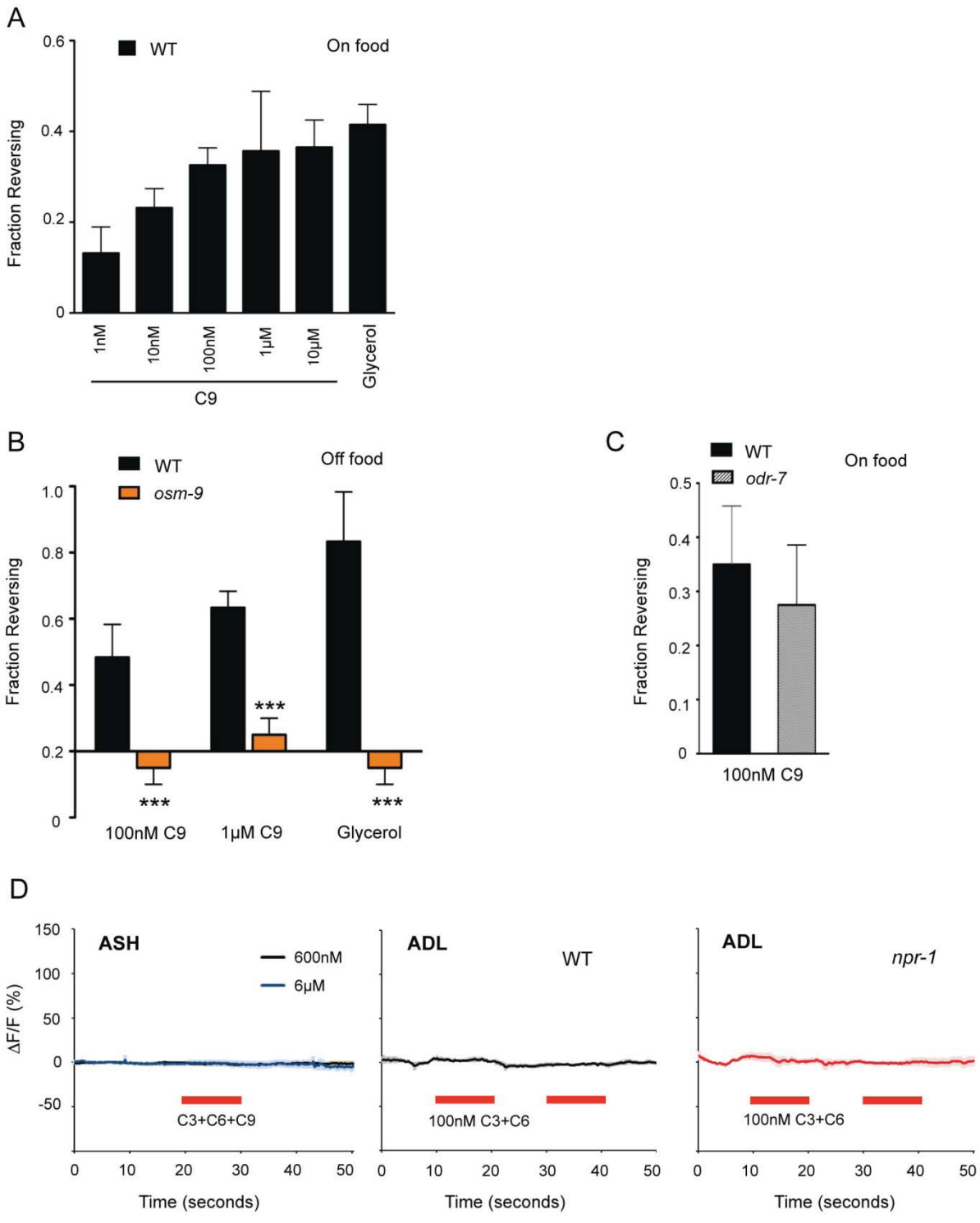

Jang, Kim et al
Figure S1

Figure S1 related to Figure 1. Characterization of C9 avoidance.

A. C9 avoidance at low nanomolar concentrations is enhanced in the presence of food (Compare with Figure 1A).

B. C9 avoidance is abolished in *osm-9(ky10)* mutants. Assays were performed in the absence of food. *** indicates responses different from wild type at $P< 0.001$. Error bars are the SEM. n=20-40 animals each.

C. *odr-7(ky4)* mutants avoid C9. Error bars are the SEM. n=40 animals each.

D. No Ca^{2+} transients are observed in G-CaMP-expressing ASH neurons (left) upon addition of mixtures of 600 nM or 6 μM each C3, C6 and C9 (red horizontal bar), or in ADL neurons of wild-type or *npr-1* hermaphrodites (middle and right) upon addition of a mixture of 100 nM C3 and C6 (red bars). n≥6 neurons each. Shading around the lines represents SEM.

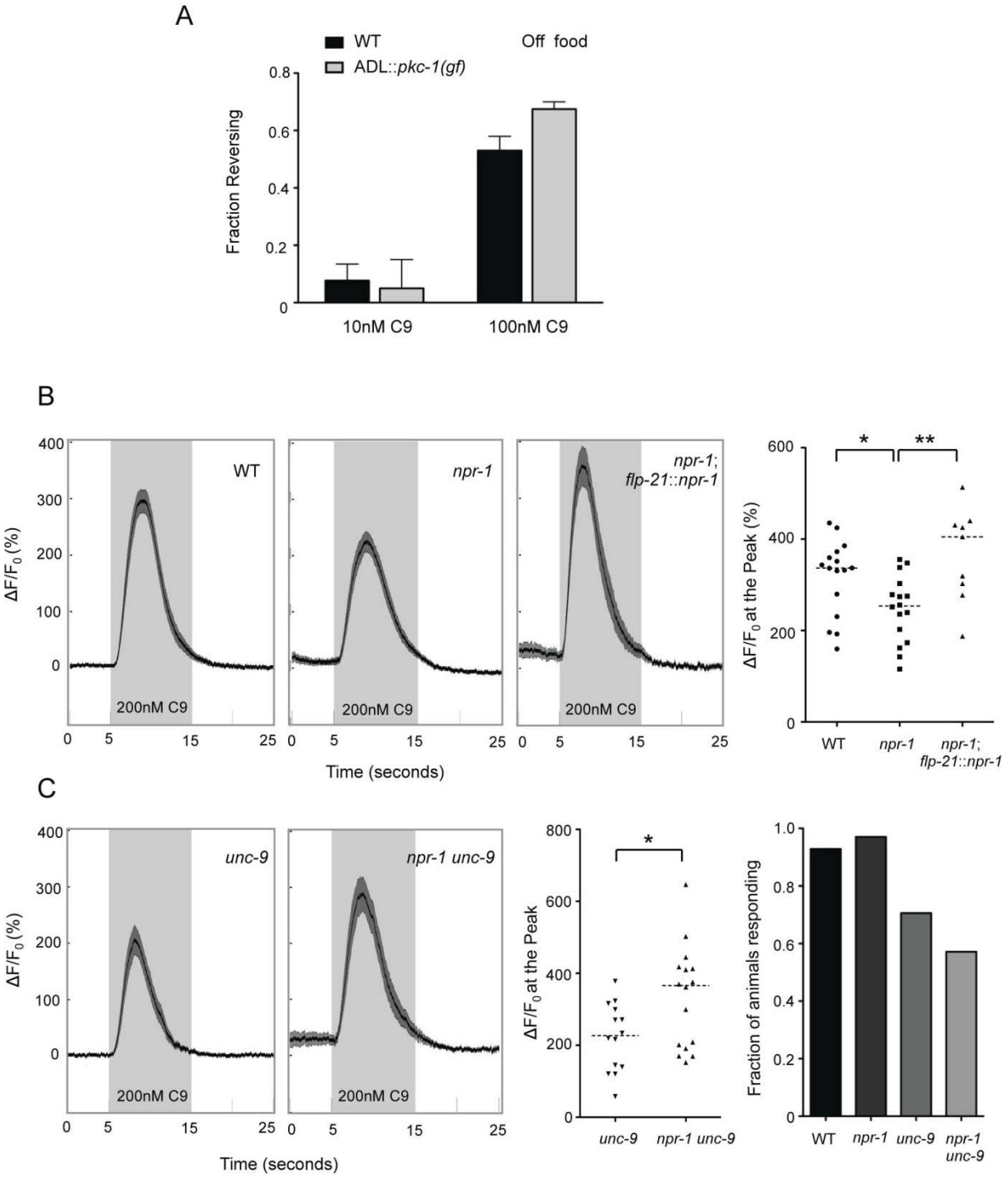

Jang, Kim et al
Figure S2

Figure S2 related to Figure. 2. NPR-1 acts in RMG to modulate ADL C9 responses.

A. *pkc-1(gf)* does not significantly enhance C9 avoidance in wild-type animals in the absence of food (compare *npr-1; pkc-1(gf)* in Figure 2D) or in the presence of food (data not shown). Error bars are the SEM. n=20-100 animals each.

B. *npr-1* expression in RMG restores ADL C9 responses. Wild-type *npr-1* cDNA was expressed from a 4.1 kb *flp-21* promoter fragment that drives expression in RMG and other neurons, but not in ADL (Macosko et al., 2009). The scatter plot represents the percentage change in fluorescence at the peak of 200 nM C9-induced Ca^{2+} responses in ADL neurons. Shading around the lines represents SEM. * and ** indicate responses different from values indicated by brackets at $P<0.05$ and 0.01, respectively. Dotted horizontal lines indicate the median. n≥9 neurons each.

C. *unc-9* is required for the *npr-1*-dependent reduction in ADL C9 responses. The scatter plot represents the percentage change in fluorescence at the peak of 200 nM C9-induced Ca^{2+} responses in ADL neurons of the indicated genotypes. The *unc-9(e101)* allele was used. Dotted horizontal lines indicate the median response. * indicates responses different from values indicated by the bracket at $P<0.05$; note that the direction of change is reversed relative to Figure S2B. Right panel, proportion of ADL neurons that respond to C9 with Ca^{2+} transients; note increased failure rate in *unc-9* mutants. n≥14 neurons each.

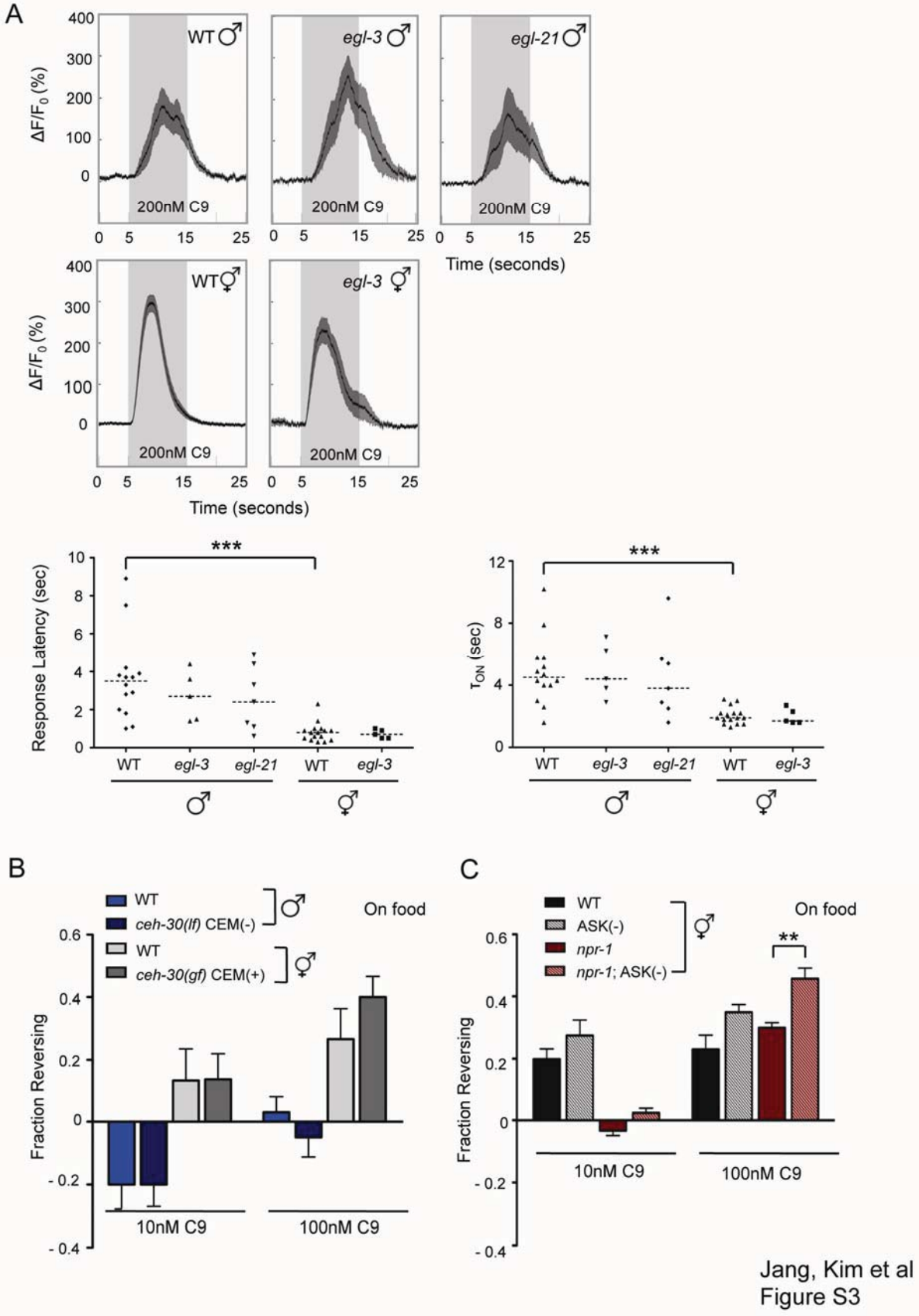

Jang, Kim et al
Figure S3

Figure S3 related to Figure 3. Male responses to C9.

A. C9-induced Ca^{2+} transients in male ADL neurons have increased response latency, which is not dependent on classical neuropeptides. Scatter plots show response latencies (left) and time to half maximum response (τ_{ON}, right) of 200 nM C9-induced Ca^{2+} responses in ADL neurons of males and hermaphrodites of the indicated genotypes. Wild-type males and mutant males with defects in neuropeptide processing exhibit similar C9-induced Ca^{2+} dynamics; the same is true for hermaphrodites. Dotted horizontal lines indicate the median response. Alleles used were *egl-3(ok979)* and *egl-21(n476)*. WT males and WT hermaphrodites are different at $P<0.001$ as indicated by asterisks. No significant difference is observed within males of different genotypes or within hermaphrodites of different genotypes (ANOVA with Tukey test for multiple comparisons). n≥5 neurons each. We were unable to examine the effects of blocking classical neurotransmission on ADL C9 responses using the synaptic vesicle exocytosis mutant *unc-13* (Richmond et al., 1999), because expression of GCaMP3 driven by multiple independent ADL promoters was downregulated in *unc-13* mutants (data not shown).

B. Male-specific CEM sensory neurons do not affect C9 avoidance in the drop test. CEM neurons normally survive in males and die in hermaphrodites, but CEM neurons die in *ceh-30(n4289lf)* males and survive in *ceh-30(n3714gf)* hermaphrodites (Schwartz and Horvitz, 2007). Responses of mutants are not significantly different from the wild-type responses of the same sex. Assays were performed in the presence of food. Error bars are the SEM. n=40-80 animals each.

C. ASK ablation enhances avoidance of 100 nM C9 in *npr-1* hermaphrodites. Assays were performed in the presence of food. ** indicates responses different from non-ablated control at $P<0.01$. Error bars are the SEM. n=40-120 animals each.

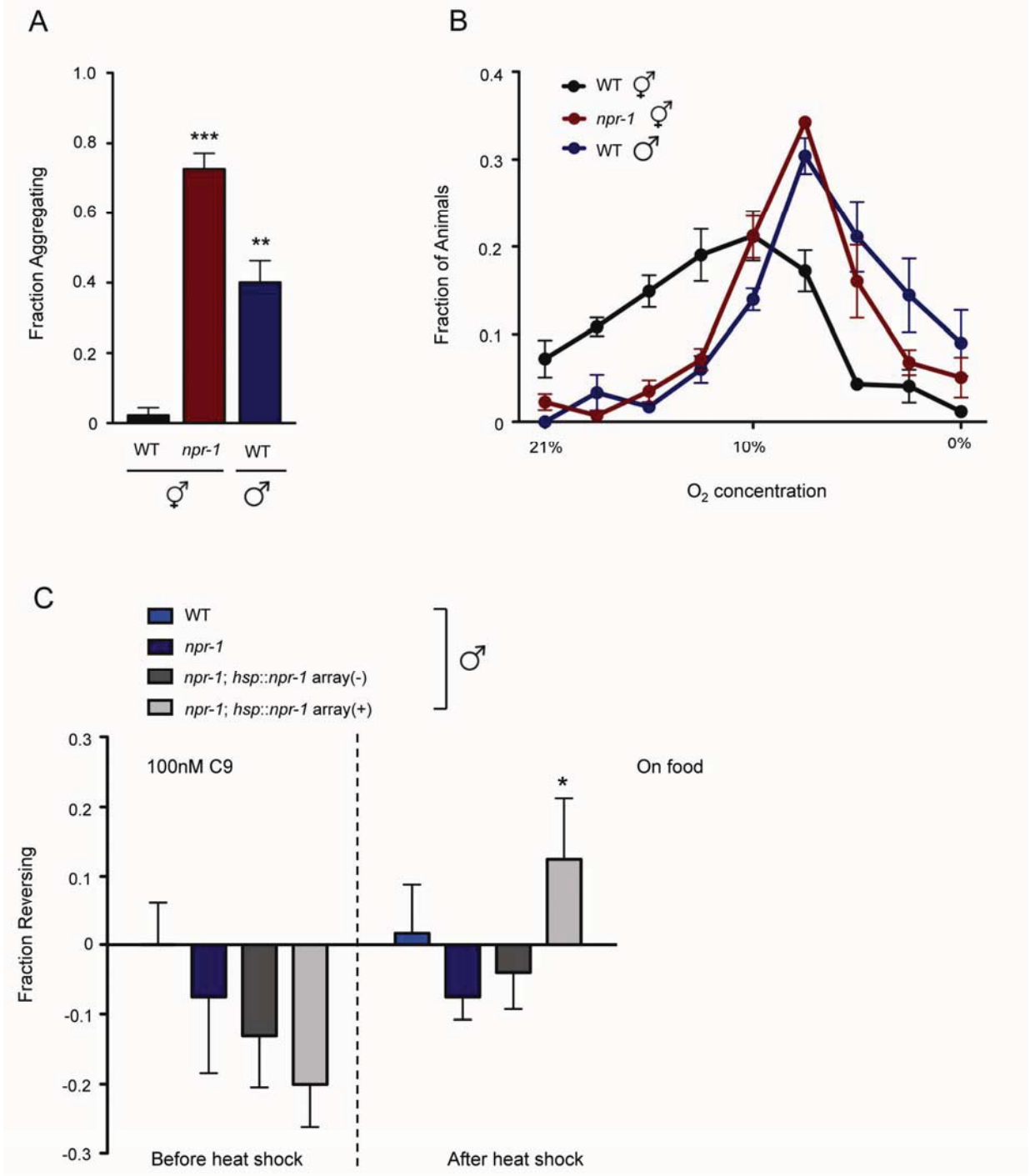

Jang, Kim et al
Figure S4

Figure S4 related to Figure 4. Wild-type males and *npr-1* hermaphrodites exhibit similar aggregation (**A**) and oxygen preference (**B**) behaviors. Aggregation was scored as the percentage of animals touching two or more animals with at least 50% of their body length (de Bono and Bargmann, 1998). 60 animals per assay, n≥3 assays each. ** and *** indicate different from wild-type hermaphrodites at $P<0.01$ and 0.001, respectively. Aerotaxis assays show the distribution of populations of animals in linear oxygen gradients in the presence of food as described (Chang et al., 2006). Hyperoxia avoidance of wild-type hermaphrodites is significantly different from wild-type males or *npr-1* hermaphrodites ($P<0.01$ by ANOVA with Tukey test for multiple comparisons). Responses of wild-type males and *npr-1* hermaphrodites are not significantly different. **C**. Heat shock-driven expression of *npr-1* during the adult stage rescues the C9 avoidance defect of *npr-1* male animals. * indicates responses different from the responses of the same genotype before heat shock at $P<0.05$. Array(-) indicates animals from the *hsp16.2::npr-1*-expressing transgenic strain that have lost the extrachromosomal array, which represent sibling controls for the array(+) animals. Behavioral assays were performed in the presence of food before or immediately after heat-shock at 33˚C for 30 minutes. Error bars are the SEM. n=40-60 animals each.

SUPPLEMENTAL EXPERIMENTAL PROCEDURES

Strains

The wild-type strain used was *C. elegans* variety Bristol strain N2. Alleles used were *ocr-2(ak47), osm-9(ky10)* and *npr-1(ad609)*. Strains expressing *npr-1* or tetanus toxin light chain (TeTx) in RMG were generated using the Cre/*Lox* system as described previously (Macosko et al., 2009). For genetic ablation of ASK, a strain with stably integrated *sra-9*p::m*CaspaseI* was used (*qrIs2*: a gift of Ryuzo Shingai) (Kim et al., 2009). For the heat shock rescue of *npr-1*, a strain with the *hsp-16.2* heat-inducible promoter driving the expression of wild-type *npr-1* cDNA was used (a gift of Mario de Bono) (Coates and de Bono, 2002). Transgenic strains were generated by injecting the experimental plasmid at 30-50 ng/µl together with *unc-122*::*dsRed or unc-122::gfp* as the coinjection marker.

Behavioral assays

20-30 young adult worms grown at 20˚C were transferred to an unseeded NGM plate followed by transfer to assay plates with or without food. Assays were performed in the presence of bacterial food, except for assays in Figures 1A, 1B, S1B and S2A, which were performed in the absence of food. For drop tests in the presence of food, NGM plates were uniformly seeded with OP50 bacteria the day before the assay and grown overnight at 37˚C, followed by incubation at room temperature for at least one hour prior to the assay. For tests in the absence of food, care was taken that no food was transferred to the unseeded assay plate. After 30-60 minutes on the assay plate, a drop of M13 buffer with dissolved pheromone or other chemicals was delivered to individual young adult

worms moving forward using glass capillaries. Responses were scored as reversals if animals initiated backward movements longer than half their body length within 4 seconds. Most reversals initiated immediately and were followed by omega turns. Typically, 10-15% of animals reversed in response to buffer in the absence of food, and 30% in the presence of food. All assays were performed at room temperature on at least two different days. All genotypes were also assayed for their ability to reverse in response to 2M glycerol dissolved in water.

Statistical analysis was conducted by comparing the effect sizes of different genotypes, stimuli, and interactions by ANOVA with post-hoc corrections for multiple comparisons. Effect sizes (shown in figures as fraction reversing) represent the increase or decrease in fraction of animals reversing in response to pheromone, compared to the fraction reversing in response to buffer alone.

For heat shock experiments, animals were assayed for their behavior in the drop test in the presence of food (before heat shock), transferred to a new assay plate with food and incubated at 33˚C for 30 minutes. After heat shock, the assay plate was removed to room temperature, and animals were immediately re-assayed for their behavior in the drop test.

Molecular Biology

1 kb of sequences upstream of *sre-1* was used to drive ADL-specific expression of *pkc-1(gf), TeTx*, and *GCaMP3*. Plasmids driving *ocr-2* genomic DNA under cell-specific promoters were described previously (de Bono et al., 2002). *pkc-1(gf)* and *TeTx* plasmids were described previously (Macosko et al., 2009).

Ca^{2+} imaging

Ca^{2+} imaging experiments were performed using custom-designed microfluidics devices as described (Kim et al., 2009; Macosko et al., 2009; Chalasani et al., 2010). To image males, microfluidic imaging chambers with modified dimensions were used (channel height=25 μm; channel width for body=60 μm, channel width for nose=22 μm). Imaging was performed on an Olympus BX52WI microscope with a 40X objective and a CCD camera (Hamamatsu). Images were processed and analyzed using OpenLab 4.0 software (Improvision), ImageJ (NIH), and custom-written MATLAB (The Mathworks) scripts.

GCaMP3 (Tian et al., 2009) was expressed specifically in the ADL neurons under the *sre-1* promoter, and the behavioral responses of the transgenic strain expressing this construct were verified prior to use in imaging experiments. The same transgenic array expressing *GCaMP3* was examined in wild type and *npr-1* mutant backgrounds. For quantification of fluorescence changes, the cell body area of an ADL neuron was selected as the region of interest and a similar sized area near the cell body was selected as the background. To ensure that fluorescence measurements were performed within the linear dynamic range, only images exhibiting less than 1,000 average fluorescence intensity units in the region of interest and background were used for further analysis. Average fluorescence intensities in the first 5 seconds of imaging were used for normalization. In all cases, control and test genotypes were interleaved over several days of imaging. Animals were pre-exposed to near-UV light for 1 min prior to initiation of imaging; pre-exposure did not affect Ca^{2+} responses in the ADL neurons. *osm-10::GCaMP2.2b-*

expressing transgenic worms were used for ASH imaging, and animals were pre-exposed to near-UV light for 3 min before imaging. The ASH neurons in these animals responded robustly to 10 mM $CuSO_4$ (Sambongi et al., 1999). ASK responses were imaged using animals expressing *sra-9::GCaMP2.2b* (Kim et al., 2009).

SUPPLEMENTAL REFERENCES

Chalasani, S.H., Kato, S., Albrecht, D.R., Nakagawa, T., Abbott, L.F., and Bargmann, C.I. (2010). Neuropeptide feedback modifies odor-evoked dynamics in *Caenorhabditis elegans* olfactory neurons. Nat. Neurosci. *13*, 615-621.

Chang, A.J., Chronis, N., Karow, D.S., Marletta, M.A., and Bargmann, C.I. (2006). A distributed chemosensory circuit for oxygen preference in *C. elegans*. PLoS Biol. *4*, e274.

Coates, J.C., and de Bono, M. (2002). Antagonistic pathways in neurons exposed to body fluid regulate social feeding in *Caenorhabditis elegans*. Nature *419*, 925-929.

de Bono, M., and Bargmann, C.I. (1998). Natural variation in a neuropeptide Y receptor homolog modifies social behavior and food response in *C. elegans*. Cell *94*, 679-689.

de Bono, M., Tobin, D.M., Davis, M.W., Avery, L., and Bargmann, C.I. (2002). Social feeding in *Caenorhabditis elegans* is induced by neurons that detect aversive stimuli. Nature *419*, 899-903.

Kim, K., Sato, K., Shibuya, M., Zeiger, D.M., Butcher, R.A., Ragains, J.R., Clardy, J., Touhara, K., and Sengupta, P. (2009). Two chemoreceptors mediate developmental effects of dauer pheromone in *C. elegans*. Science *326*, 994-998.

Macosko, E.Z., Pokala, N., Feinberg, E.H., Chalasani, S.H., Butcher, R.A., Clardy, J., and Bargmann, C.I. (2009). A hub-and-spoke circuit drives pheromone attraction and social behavior in *C. elegans*. Nature *458*, 1171-1175.

Richmond, J.E., Davis, W.S., and Jorgensen, E.M. (1999). UNC-13 is required for synaptic vesicle fusion in *C. elegans*. Nat. Neurosci. *2*, 959-964.

Sambongi, Y., Nagae, T., Liu, Y., Yoshimizu, T., Takeda, K., Wada, Y., and Futai, M. (1999). Sensing of cadmium and copper ions by externally exposed ADL, ASE, and ASH neurons elicits avoidance response in *Caenorhabditis elegans*. Neuroreport *10*, 753-757.

Schwartz, H.T., and Horvitz, H.R. (2007). The C. elegans protein CEH-30 protects male-specific neurons from apoptosis independently of the Bcl-2 homolog CED-9. Genes Dev. *21*, 3181-3194.

Tian, L., Hires, S.A., Mao, T., Huber, D., Chiappe, M.E., Chalasani, S.H., Petreanu, L., Akerboom, J., McKinney, S.A., Schreiter, E.R.*, et al.* (2009). Imaging neural activity in worms, flies and mice with improved GCaMP calcium indicators. Nat. Methods *6*, 875-881.

APPENDIX 3

Sex, Age, and Hunger Regulate Behavioral Prioritization through Dynamic Modulation of Chemoreceptor Expression

This work is published (Ryan et al., 2014).

Current Biology 24, 2509–2517, November 3, 2014 ©2014 Elsevier Ltd All rights reserved http://dx.doi.org/10.1016/j.cub.2014.09.032

Article

Sex, Age, and Hunger Regulate Behavioral Prioritization through Dynamic Modulation of Chemoreceptor Expression

Deborah A. Ryan,[1] Renee M. Miller,[1,2] KyungHwa Lee,[1,4] Scott J. Neal,[3] Kelli A. Fagan,[1] Piali Sengupta,[3] and Douglas S. Portman[1,*]

[1]Center for Neural Development and Disease, Department of Biomedical Genetics, School of Medicine and Dentistry, University of Rochester Medical Center, Rochester, NY 14642, USA

[2]Department of Brain and Cognitive Sciences, University of Rochester, Rochester, NY 14642, USA

[3]Department of Biology, National Center for Behavioral Genomics, Brandeis University, Waltham, MA 02454, USA

Summary

Background: Adaptive behavioral prioritization requires flexible outputs from fixed neural circuits. In *C. elegans*, the prioritization of feeding versus mate searching depends on biological sex (males will abandon food to search for mates, whereas hermaphrodites will not) as well as developmental stage and feeding status. Previously, we found that males are less attracted than hermaphrodites to the food-associated odorant diacetyl, suggesting that sensory modulation may contribute to behavioral prioritization.

Results: We show that somatic sex acts cell autonomously to reconfigure the olfactory circuit by regulating a key chemoreceptor, *odr-10*, in the AWA neurons. Moreover, we find that *odr-10* has a significant role in food detection, the regulation of which contributes to sex differences in behavioral prioritization. Overexpression of *odr-10* increases male food attraction and decreases off-food exploration; conversely, loss of *odr-10* impairs food taxis in both sexes. In larvae, both sexes prioritize feeding over exploration; correspondingly, the sexes have equal *odr-10* expression and food attraction. Food deprivation, which transiently favors feeding over exploration in adult males, increases male food attraction by activating *odr-10* expression. Furthermore, the weak expression of *odr-10* in well-fed adult males has important adaptive value, allowing males to efficiently locate mates in a patchy food environment.

Conclusions: We find that modulated expression of a single chemoreceptor plays a key role in naturally occurring variation in the prioritization of feeding and exploration. The convergence of three independent regulatory inputs—somatic sex, age, and feeding status—on chemoreceptor expression highlights sensory function as a key source of plasticity in neural circuits.

Introduction

Animals constantly integrate internal and external information to guide the prioritization of innate behavioral programs [1]. For example, prioritizing feeding is appropriate when nutritional demands are high but might be maladaptive in a well-fed animal that is vulnerable to predation. Although long-term changes in behavioral choice can emerge from structural modifications to neural circuitry, dynamic behavioral changes involve functional remodeling of circuits by neuromodulatory signals [2]. Central neurons that govern behavioral programs are known to be important regulators of this state-dependent plasticity. In addition, recent studies have found that sensory systems are also subject to extensive modulation [3], indicating that behavioral plasticity may rely on distributed changes to multiple levels of neural circuits [4]. However, the relative importance of sensory plasticity, the mechanisms by which it is implemented, and its significance for behavioral prioritization are not well understood.

Food availability and nutritional state are pervasive modulators of behavioral prioritization. Interestingly, studies in several systems have highlighted the importance of sensory systems as the targets of nutrition-dependent neural plasticity. In the medicinal leech, feeding animals disregard otherwise noxious stimuli as a result of presynaptic inhibition of mechanosensory cells by serotonin [5]. Similarly, monoamines and insulin-like signaling modulate sensory behavior as a function of food availability in *C. elegans* [6, 7]. In *Drosophila*, food deprivation brings about increased sensitivity to nutrients through peptidergic and dopaminergic modulation of olfactory and gustatory function [8, 9], whereas in mammals, ghrelin, leptin, insulin, and endocannabinoids modulate olfactory sensitivity in response to feeding status [10–12].

Biological sex also has a central role in regulating behavioral state. Recent work in several systems has shown that sex-specific modulation of shared circuits is likely to underlie many of these differences [13]. In *C. elegans*, sex differences in chemosensory behavior are regulated at least in part through functional modulation of common circuitry [14–16], and in *Drosophila*, regulation of homologous circuits underlies sex differences in aspects of pheromone response and courtship behavior [17, 18]. Even in rodents, sex differences in sensory function may contribute to sex-typical patterns of sexual behavior [19, 20]. However, the mechanisms whereby sexual state modulates neural circuit function remain generally unknown [21], and the integration of sexual state with other internal cues is not well understood.

The *C. elegans* nervous system, despite its anatomical simplicity, is subject to extensive functional modulation [22]. This species features two sexes, a self-fertile hermaphrodite (essentially, a modified somatic female) and a male. Each sex exhibits sex-specific behaviors (e.g., egg laying and copulation); additionally, shared behaviors such as olfaction [14], locomotion [23], associative learning [24], and exploration [25] also exhibit sex differences [26]. In particular, whereas a small food patch will efficiently retain an adult hermaphrodite, solitary adult males will frequently leave food to explore their environment. Because this exploration is suppressed by the presence of a mate, it is considered a mate-searching behavior [25]. This behavioral choice also depends on developmental stage (sexually immature larval males do not engage in mate searching) and feeding status (transient starvation leads to the temporary reprioritization of feeding over mate-searching behavior) [25]. Although input from male-specific neurons and peptide signals

[4]Present address: Sophie Davis School of Biomedical Education, The City College of New York, New York, NY 10031, USA

*Correspondence: douglas.portman@rochester.edu

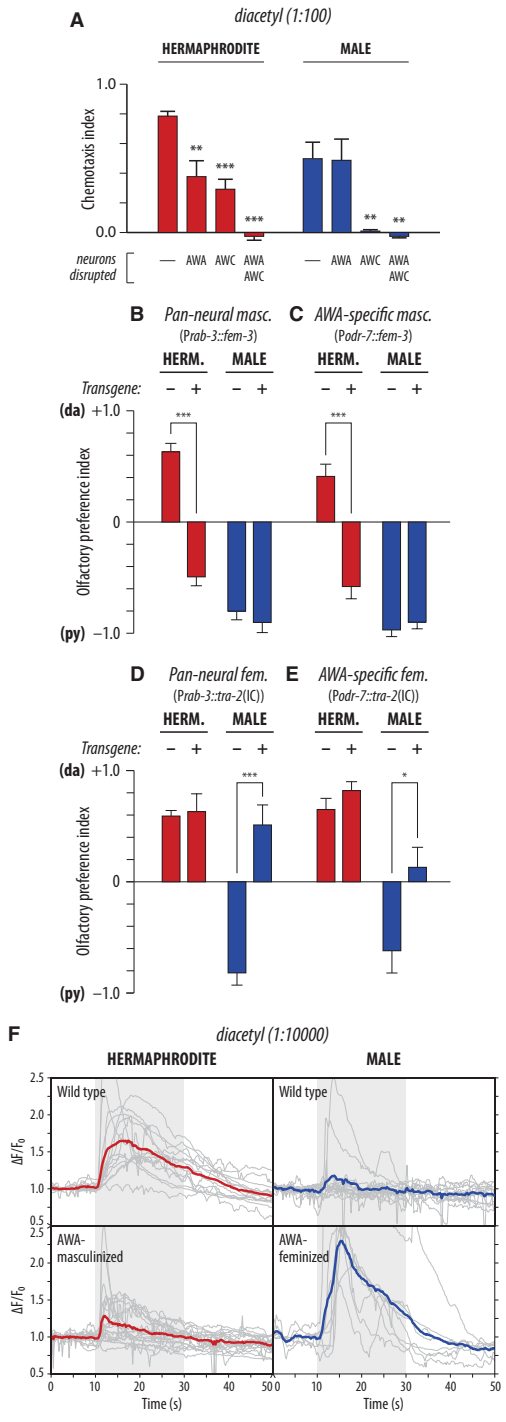

Figure 1. Genetic Sex Acts in AWA to Modulate Sensory Function

(A) Attraction of hermaphrodites (red) and males (blue) to diacetyl (1:100). Mutations in *odr-7* and *ceh-36* were used to disrupt the function of AWA and AWC, respectively [32, 33]. Four independent experiments were performed for a total of n = 275, 296, 219, 117, 205, 236, 102, and 116 in each group (left to right). One-way ANOVA with Bonferroni correction was used; asterisks indicate post hoc comparisons with controls (**p < 0.01, ***p < 0.001). Error bars indicate SEM.

(B–E) Diacetyl-pyrazine olfactory preference [14] in wild-type and transgenic hermaphrodites (red) and males (blue). +1 indicates a strong preference for diacetyl (da), whereas 0 indicates no preference, and −1 indicates a strong preference for pyrazine (py). The plus sign (+) indicates the presence of sex-reversal transgenes. Groups were compared with unpaired, two-tailed t tests; asterisks indicate statistically significant comparisons with wild-type controls. Error bars indicate SEM.

(B) Pan-neural masculinization (P*rab-3::fem-3*) (data from [14]). Five independent experiments were performed for a total of n = 188, 175, 205, and 190 responders in each group (left to right) (hermaphrodites: p < 0.0001; males: p = 0.42).

(C) AWA-specific masculinization (P*odr-7::fem-3*). Seven independent experiments were performed for a total of n = 231, 82, 298, and 44 responders per group (left to right) (hermaphrodites: p < 0.0001; males: p = 0.19).

(D) Pan-neural feminization (P*rab-3::tra-2(IC)*). Five independent experiments were performed for a total of n = 321, 178, 245, and 111 responders per group (left to right) (hermaphrodites: p = 0.81; males: p = 0.0002).

(E) AWA-specific feminization (P*odr-7::tra-2(IC)*). Four independent experiments were performed for a total of n = 95, 81, 84, and 52 responders per group (left to right) (hermaphrodites: p = 0.23; males: p = 0.032).

(F) Imaging of calcium transients evoked by diacetyl (1:10,000) in AWA using P*gpa-4::GCaMP3* in wild-type and transgenic hermaphrodites and males. Gray shading indicates the diacetyl pulse. Individual recordings are shown in gray; the average $\Delta F/F_0$ across the population is superimposed in red (hermaphrodites) or blue (males).

See also Figure S1.

are important for generating the male exploratory drive [27, 28], the neural effectors of this feeding versus exploration decision are unknown, as are the mechanisms by which multiple internal variables modulate this decision.

Previously, we found strong sex differences in attraction to diacetyl [14], an olfactory stimulus proposed to represent a food signal [29]. Here, we show that these behavioral differences arise from cell-autonomous regulation of the diacetyl receptor ODR-10 [30] by the *C. elegans* sex determination hierarchy. Moreover, we find that the downregulation of *odr-10* in adult males facilitates exploration over feeding. *odr-10* expression is also regulated by developmental and nutritional signals that influence male behavioral prioritization, and upregulation of *odr-10* in males by starvation is necessary for starvation-induced increase in food attraction. Together, these results identify a neural and genetic mechanism that guides adaptive behavioral prioritization through the dynamic modulation of chemoreceptor expression and sensory function.

Results

Genetic Sex Modulates Sensory Response in the AWA Olfactory Neurons

C. elegans adults exhibit pronounced sex differences in olfactory behavior. Whereas some stimuli, such as pyrazine and 2-butanone, elicit strong attraction in both sexes, attraction to the odorant diacetyl is much stronger in hermaphrodites than in males [14]. To understand the neural basis for this difference, we asked whether both sexes use the same circuitry to detect diacetyl. In hermaphrodites, this compound is sensed primarily by the AWA olfactory neuron pair [29], with a secondary contribution at high concentration from the AWC neurons [31]. However, the weak attraction of males to diacetyl depended only on AWC: genetic ablation of AWA function [32] had no effect on male diacetyl attraction, whereas genetic ablation of AWC [33] eliminated it (Figure 1A).

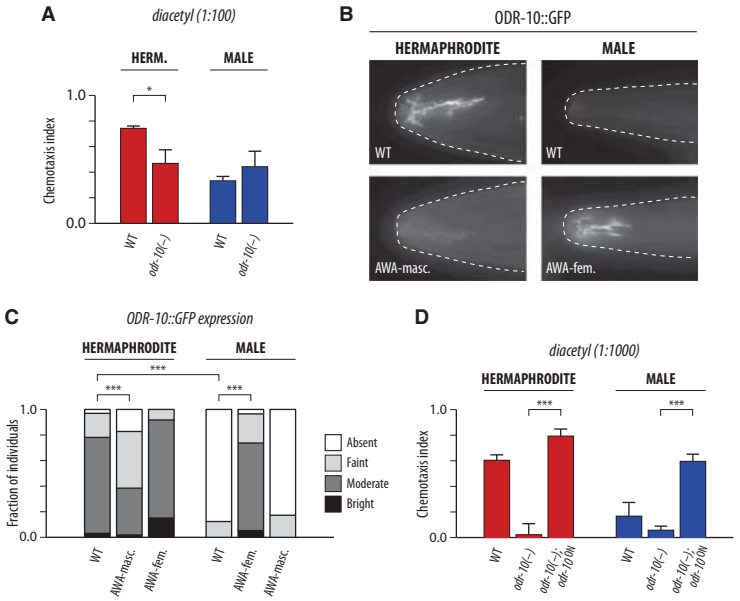

Figure 2. The Diacetyl Chemoreceptor ODR-10 Is Regulated by AWA Genetic Sex

(A) Chemotaxis to diacetyl (1:100) in wild-type and *odr-10(ky225)* hermaphrodites (red) and males (blue). Four independent experiments were performed with a total of n = 113, 183, 96, and 97 per group (left to right). Unpaired two-tailed t tests were employed to determine significance; asterisks indicate comparisons with wild-type controls (hermaphrodites: p = 0.044; males: p = 0.42). Error bars indicate SEM.

(B) Representative examples of ODR-10::GFP (*kyIs53*) fluorescence in a wild-type hermaphrodite, wild-type male, AWA-masculinized (P*gpa-4Δ6::fem-3*) hermaphrodite, and AWA-feminized (P*gpa-4Δ6::tra-2(IC)*) male. All images were acquired using the same illumination intensity and exposure time. White dashes indicate the outline of the body.

(C) Quantitation of ODR-10::GFP expression. Fluorescence intensity was binned into four categories, as indicated with the investigator blinded to genotype. Experiments were performed on a total of n = 96, 52, 73, 97, 57, and 52 animals per group (left to right) over the course of at least four independent sessions. Kruskal-Wallis with Dunn's multiple comparisons tests were used to determine significance (***p < 0.001).

(D) Diacetyl (1:1,000) chemotaxis in hermaphrodites (red) and males (blue), comparing wild-type adults to *odr-10(ky225)* mutants (*odr-10(–)*) and *odr-10(ky225)* mutants carrying P*gpa-4Δ6::odr-10(+)* (*odr-10*^{ON}). Four independent experiments were performed for a total of n = 124, 131, 97, 119, 120, and 104 in each group (left to right). Two-way ANOVA with Tukey's multiple comparisons tests were employed to determine significance; asterisks indicate post-test comparisons with *odr-10* mutants (***p < 0.001). Error bars indicate SEM.

See also Figure S2.

AWA is not simply dormant in males because this neuron is essential for pyrazine attraction in both sexes (Figure S1A available online). Thus, genetic sex functionally reconfigures the diacetyl circuit, such that hermaphrodites rely on two sensory neurons to sense this compound, whereas males use only one.

To determine how genetic sex modulates the olfactory circuit, we took advantage of the strong sex difference in the response of *C. elegans* adults to opposing sources of diacetyl and pyrazine [14]. Previously, we used sexually mosaic animals to show that this sex difference was a function of the sexual state of the nervous system [14]. Pan-neural genetic masculinization via expression of FEM-3 [34], a specific inhibitor of the master feminizing factor TRA-1 [35], strongly masculinized olfactory behavior [23] (Figure 1B). To determine whether genetic sex acts in the AWA neurons themselves, we expressed FEM-3 in these cells using an AWA-specific promoter [32]; this resulted in strongly masculinized olfactory behavior (Figure 1C). To genetically feminize the male nervous system, we used TRA-2^{IC} [34], a specific activator of TRA-1. Both pan-neural and AWA-specific TRA-2^{IC} expression significantly feminized male olfactory behavior (Figures 1D and 1E). AWA sex reversal also significantly sex reversed diacetyl attraction in single-odorant assays (Figure S1B). Thus, sex differences in diacetyl attraction stem, at least in part, from the cell-autonomous modulation of AWA by sexual state.

We recorded diacetyl-evoked activity in AWA by using the calcium sensor GCaMP3 [36] to ask whether sexual state regulates AWA physiology. In hermaphrodites, diacetyl triggered a robust, transient calcium increase in AWA (Figures 1F and S1C). However, most (8 out of 10) males exhibited no detectable response to diacetyl (Figures 1F and S1C). Again, AWA-specific sex reversal largely reversed this response: AWA-masculinized hermaphrodites had significantly reduced calcium transients, whereas AWA feminization enabled strong diacetyl responses in all males tested (Figures 1F and S1C). Together, these results indicate that the genetic sex of AWA acts cell autonomously to determine its sensory properties.

Sensory Behavior Is Modulated by Sexual Regulation of the Diacetyl Chemoreceptor ODR-10

In hermaphrodites, the diacetyl sensitivity of AWA (but not AWC) is conferred by ODR-10, a seven-transmembrane chemoreceptor that localizes to AWA's sensory cilia and is thought to directly bind diacetyl [30]. Consistent with the diacetyl insensitivity of AWA in males, *odr-10(ky225)* null mutant males had no defect in diacetyl attraction (Figure 2A). Therefore, we examined *odr-10* expression using the translational GFP reporter *kyIs53* [30]. As expected, we observed clear ODR-10::GFP expression in nearly all adult hermaphrodites; however, expression was undetectable in most adult males (Figures 2B and 2C), indicating that *odr-10* may be a target of sexual regulation. To rule out potential artifacts arising from the X linkage of *kyIs53*, we generated *fsEx295*, an extrachromosomal, fosmid-based ODR-10::GFP transgene. *fsEx295* hermaphrodites showed strong, AWA-specific expression, whereas expression in males was very weak (Figure S2A). With both reporters, GFP expression remained AWA specific in unusual males in which it was detectable. By quantitative RT-PCR (qRT-PCR), we found that *odr-10* mRNA abundance was roughly 6-fold lower in males than in hermaphrodites (Figure S2B). Further, expression of a transcriptional P*odr-10::GFP* reporter (*kyIs37*) [30] was significantly higher in

hermaphrodites than in males (Figure S2C), indicating that the sexual regulation of *odr-10* occurs primarily at the transcriptional level.

This sex difference in *odr-10* expression depended largely on AWA genetic sex. AWA-specific masculinization resulted in a significant decrease in hermaphrodite ODR-10::GFP expression, whereas AWA feminization was sufficient to bring about hermaphrodite-like expression levels in males (Figures 2B and 2C). Because the effects of AWA masculinization on *odr-10* expression are incomplete, non-cell-autonomous signals might be important for the full extent of sex differences in AWA. Nevertheless, these results indicate that the genetic sex of AWA influences sensory behavior by regulating chemoreceptor expression.

To determine whether providing *odr-10* function would be sufficient to allow males to respond to diacetyl, we expressed wild-type *odr-10* under the control of P*gpa-4Δ6*, an AWA-specific promoter that shows no significant sex differences (see Figure S5 below). This transgene ("*odr-10*^{ON}") rescued diacetyl attraction in *odr-10* mutant hermaphrodites; moreover, *odr-10*^{ON} conferred robust diacetyl attraction in males (Figure 2D). Thus, plasticity in *odr-10* expression is both necessary and sufficient to generate sex differences in diacetyl chemotaxis.

Sexual Regulation of AWA and *odr-10* Modulates Feeding Behavior

Diacetyl is produced by a variety of microorganisms, including lactic acid bacteria, some of which are known to be suitable food sources for *C. elegans* [37]. Thus, diacetyl attraction in *C. elegans* is thought to reflect an innate food-seeking drive [29]. Given the propensity of *C. elegans* males to spontaneously leave food to search for mates [25], we hypothesized that the low expression of *odr-10* in males might help promote exploratory behavior by attenuating the perception of food.

To test this possibility, we first used the food-leaving assay [25]. We found that *odr-10*^{ON} males and AWA-feminized males exhibited significantly reduced food-leaving behavior (Figures 3A and 3B). Conversely, *odr-10(ky225)* null mutant hermaphrodites showed significantly increased off-food exploration (Figure 3C). Consistent with the low expression of *odr-10* in wild-type adult males, *odr-10(ky225)* males exhibited no increase in food leaving (Figure 3D). Notably, both *odr-10*^{ON} and AWA-feminized males continued to exhibit significant exploratory behavior, indicating that other male-specific exploratory drives [27, 28] likely act in parallel with AWA modulation. Together, these results demonstrate that AWA and *odr-10* are important regulators of male behavioral prioritization.

These results also indicated that ODR-10 may have a substantial role in food detection. To test this more directly, we placed single animals 3 cm from a small patch of *E. coli* OP50, the standard *C. elegans* laboratory diet, and measured their latency to arrive at the food. Wild-type adult hermaphrodites migrated to the food patch with a median latency of roughly 30 min. In contrast, males took significantly longer (Figure 3E): fewer than 50% of males located the food within 60 min, even though their locomotor speed is significantly higher than that of hermaphrodites [23]. Thus, males are less attracted to food than hermaphrodites, indicating that the reduced perception of food could be an important component of sexually motivated male exploration.

Several findings indicated that *odr-10* has an important role in sex differences in food attraction. First, we found that equalization of *odr-10* expression with the *odr-10*^{ON} transgene eliminated sex differences in food attraction (Figure 3F). Consistent with this, *odr-10(ky225)* hermaphrodites showed significantly reduced food attraction (Figure 3G) but had no change in body-bend frequency (Figure S3A). Unexpectedly, *odr-10(ky225)* males also had marked defects in food taxis (Figures 3G and S4A), indicating that the low level of *odr-10* expression in males is still important for behavior. Notably, a sex difference in food taxis persists in *odr-10(ky225)* animals (Figure 3G, $p < 0.001$), suggesting that other food-detection mechanisms (e.g., [38–40]) also differ by sex.

Supporting these interpretations, we obtained similar results using *odr-10(ky32)*, an independently isolated *odr-10* allele (Figures S3B and S3C). *odr-10* was also important for the detection of *E. coli* HT115, a strain distantly related to OP50 (Figure S3D). *odr-10* mutants exhibited normal chemotaxis to pyrazine (Figures S3E and S3F), butanone, and 2,3-pentanedione [30], ruling out general sensory defects. Neuron-specific [41] *odr-10(RNAi)* beginning in L3–L4 larvae impaired both diacetyl and food attraction (Figures S3G and S3H), indicating that these sensory phenotypes do not result from an early developmental function of *odr-10*.

To further characterize the role of *odr-10* in food-search behavior, we tracked the position of individuals at 7 min intervals during the course of the food-search assay. Whereas most wild-type animals reached the food within the first few intervals, *odr-10* mutants exhibited relatively undirected locomotion and remained near the start point, reminiscent of the area-restricted search behavior that *C. elegans* exhibits upon removal from food [42] (Figure S4A). To find out whether the apparent defects of *odr-10* mutants in the food-search assay might simply be secondary to reduced exploration, we determined the orientation of worm movement with respect to the food spot during each 7 min interval and binned these according to the distance from the food at the beginning of that interval. We found that most wild-type animals moved toward the food at essentially all regions of the plate (Figure S4B). However, *odr-10* mutants exhibited significantly less food-biased locomotion, particularly in regions farther from the food (Figure S4B). Together, these results indicate that *odr-10* mutants have specific defects in the ability to sense food-derived chemical cues.

We also found that the genetic sex of AWA was important for sex differences in feeding behavior: AWA-specific masculinization significantly increased hermaphrodites' latency to find food without an effect on locomotion rate (Figures 3H and S3I). However, the reciprocal manipulation, AWA-specific feminization, did not detectably increase the efficiency of male food-search behavior (Figures 3H and S3J). Although the reasons for this are unclear, this result might indicate that feminization disrupts other properties of AWA that are important for food detection in males. It also suggests that the sexual state of AWA acts in parallel with exploratory drives promoted by the male tail sensory rays and PDF neuropeptide signaling [27, 28] to determine the animal's behavioral program.

Age and Feeding Status Also Converge on *odr-10*

Behavioral prioritization in *C. elegans* males is also regulated by developmental stage and feeding status: larval males do not exhibit food-leaving behavior, and starved adult males transiently reprioritize feeding over exploration [25]. Therefore, we asked whether these aspects of internal state might also regulate *odr-10*. We found that sex differences in *odr-10* expression during development correlated with behavioral prioritization: L3 larval males and hermaphrodites expressed roughly equal levels of ODR-10::GFP, with sex differences

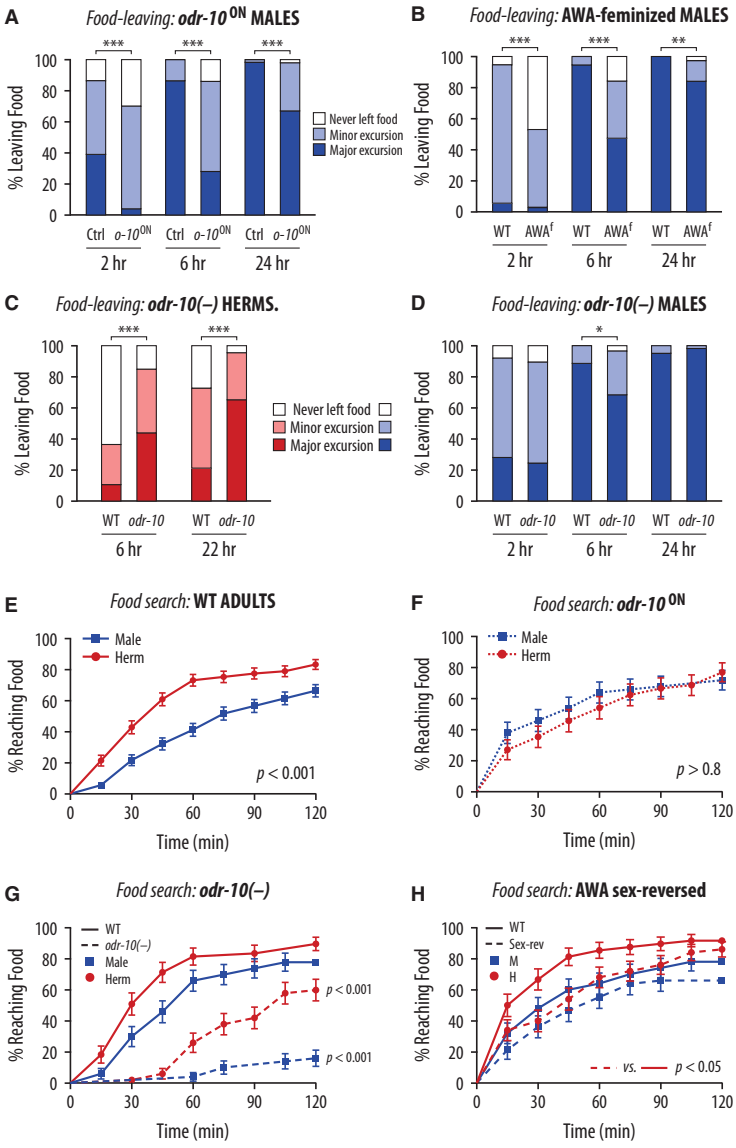

Figure 3. *odr-10* Regulates Behavioral Prioritization

(A–D) Food-leaving behavior of animals of the indicated sex and genotype. "Ctrl" indicates control animals (P*gpa-4Δ6::GFP*), "*o-10*^{ON}" indicates *odr-10*^{ON}, and "AWA^{f}" indicates AWA-feminized (P*gpa-4Δ6::tra-2(IC)*) males. Individuals were placed on a small food spot, and track patterns were scored at the indicated times. "Never left food" indicates the absence of tracks outside the food spot. "Minor excursion" indicates that tracks were observed not beyond 1 cm from the food. "Major excursion" indicates the presence of tracks past the 1 cm boundary. Each data point shows data pooled from 37–50 animals, tested over 3–4 separate days. Asterisks indicate statistically significant differences compared to control or wild type by chi-square test (***p < 0.001; **p < 0.01; *p < 0.05).

(E) Food-search behavior in adult hermaphrodites (red, n = 140) and males (blue, n = 143). Data are pooled from 12 assays. p < 0.001.

(F) Food-search behavior of *odr-10(ky225)*; *Ex [Pgpa-4Δ6::odr-10(+)]* males and hermaphrodites (blue, n = 50 and red, n = 48, respectively). Assays were performed for five independent sessions, with at least eight animals per group. p > 0.05.

(G) Food-search behavior of wild-type and *odr-10(ky225)* null mutants. Assays were performed for five independent sessions; n = 49 or 50 for each group. p < 0.001 for wild-type versus *odr-10(ky225)* in each sex.

(H) Food-search behavior of wild-type and AWA-specific sex-reversed strains (P*gpa-4Δ6::fem-3* hermaphrodites and P*gpa-4Δ6::tra-2(IC)* males). Assays were performed for four independent sessions; n = 47–50 for each group. p < 0.05 for wild-type versus AWA-masculinized hermaphrodites. p > 0.05 for wild-type versus AWA-feminized males.

Error bars in (F)–(H) indicate SE. See also Figures S3 and S4.

beginning to appear in L4, but not manifesting fully until adulthood (Figure 4A). Correspondingly, we observed no sex differences in the ability of L3 animals to locate food or chemotax to diacetyl (Figures 4B and 4C). Together, this suggests that *odr-10* contributes to age-dependent changes in behavioral choice.

With respect to nutritional status, we found that 18 hr of food deprivation significantly increased ODR-10::GFP expression in males, although it had no detectable effect in adult hermaphrodites (Figure 5A). Starvation induced only a slight decrease in expression of the control marker P*gpa-4Δ6::GFP* in both sexes, confirming the specificity of this effect (Figure S5). Moreover, food deprivation did not influence food search in hermaphrodites but significantly increased its efficiency in males (Figure 5C). This increase was completely dependent on *odr-10* because food deprivation had no effect on the behavior of *odr-10* mutant males (Figure 5D). Finally, the starvation-induced increase in *odr-10* expression was reversible: after refeeding starved males for 24 hr, ODR-10::GFP fluorescence returned to levels found in continuously fed animals (Figure 5B). Together, these findings establish *odr-10* as a regulatory node that integrates genetic sex, developmental stage, and metabolic demands to influence feeding behavior.

Adult-Specific Repression of *odr-10* Is Important for Male Reproductive Fitness

To determine whether the low expression of *odr-10* in well-fed adult males is an adaptation that promotes mate searching over feeding, we examined reproductive fitness in a setting in which males were required to navigate through a patchy food environment in order to mate (Figure 6A). Individual males were placed on small food patches around the edge of a 10 cm culture plate, and four paralyzed adult hermaphrodites were placed on a small food patch at the center. Between the males

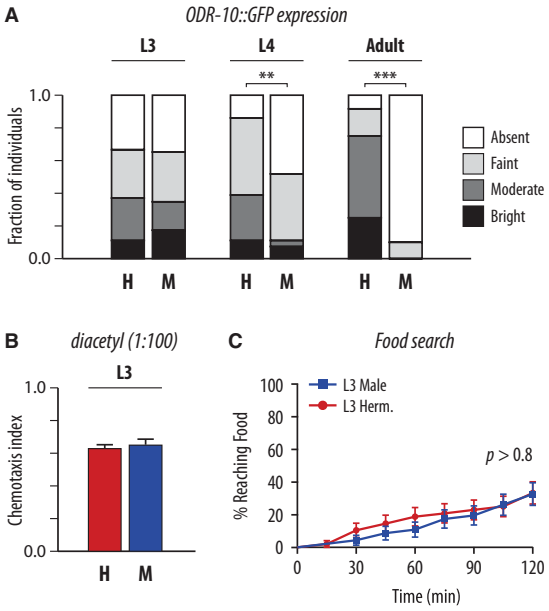

Figure 4. *odr-10* Expression and Chemosensory Behavior Are Sexually Isomorphic in Larvae

(A) ODR-10::GFP (*kyIs53*) fluorescence binned into four groups in L3 (hermaphrodite: n = 27; male: n = 23), L4 (hermaphrodite: n = 36; male: n = 27), and adult animals (hermaphrodite: n = 12; male: n = 20). Data were collected during two independent sessions and analyzed by Mann-Whitney tests (L3 hermaphrodite versus male: p = 0.87; L4: p = 0.0020; adult: p < 0.0001).

(B) Diacetyl (1:100) chemotaxis in L3 animals (hermaphrodites: red, n = 127; males: blue, n = 134). Data are pooled from four independent experiments. p > 0.05 by unpaired, two-tailed t test. Error bars indicate SEM.

(C) Food-search behavior in L3 animals (hermaphrodites: red, n = 48; males: blue, n = 46). Data are pooled from three independent experiments. p = 0.87 by log rank (Mantel-Cox) test. Error bars indicate SE.

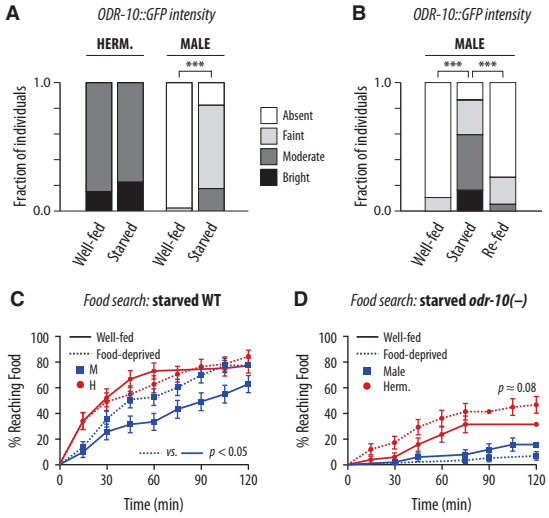

Figure 5. Starvation Transiently Upregulates *odr-10* to Increase Male Food Attraction

(A) ODR-10::GFP (*kyIs53*, n = 40 per group). Animals were removed from food 18–24 hr before imaging. Data were collected during at least two independent sessions. ***p < 0.001 by Mann-Whitney test.

(B) ODR-10::GFP fluorescence in well-fed (n = 19), starved (n = 37), and refed (n = 38) adult males, binned into four groups by intensity. Experiments were performed over the course of 4 days, and data were analyzed by Kruskal-Wallis with Dunn's multiple comparisons test (***p < 0.0001 in post-test comparisons).

(C and D) Data were analyzed as in Figures 3E–3H.

(C) Food-search behavior in well-fed (solid red line, n = 49) and starved (dotted red line, n = 52) wild-type adult hermaphrodites (p = 0.84) and in well-fed (solid blue line, n = 50) and starved (dotted blue line, n = 58) wild-type adult males (p = 0.043).

(D) Food-search behavior in well-fed (solid red line, n = 50) and starved (dotted red line, n = 57) *odr-10(ky225)* adult hermaphrodites (p = 0.084) and in well-fed (solid blue line, n = 50) and starved (dotted blue line, n = 57) *odr-10(ky225)* adult males (p = 0.14).

Error bars indicate SE. See also Figure S5.

and the hermaphrodites was a "barrier" ring of food. Control (P*gpa-4Δ6::GFP*) and *odr-10*^{ON} males were placed in alternating spots at the edge of the plate and allowed to feed, explore, and mate for 18 hr. Two days later, the paternity of cross-progeny was scored to determine male reproductive fitness. We found that *odr-10*^{ON} males sired far fewer progeny than their control competitors did (Figure 6B). To control for potential effects of *odr-10*^{ON} on copulatory behavior itself, we carried out parallel experiments in which males were placed directly in the center spot along with hermaphrodites. In this setting, *odr-10*^{ON} males sired nearly as many progeny as control males (Figure 6B); the small advantage of control males in this assay may indicate an unexpected requirement for AWA in male mating behavior. Together, these results indicate that the impaired fitness of *odr-10*^{ON} males in the foraging versus mating setting results primarily from a hermaphrodite-like prioritization of feeding over exploration.

To evaluate this interpretation, we tracked the position of individual males in the behavioral arena over several hours. Whereas many control males migrated to the center mating spot during this time, nearly all *odr-10*^{ON} males remained in the peripheral spots or in the barrier ring (Figure 6C). This reduced exploratory behavior was not a consequence of reduced locomotor speed because on-food body-bend rate did not differ significantly between control and *odr-10*^{ON} males (Figure S3J). Reduced exploration was also unlikely to result from reduced attraction to hermaphrodites because *odr-10*^{ON} had no effect on male attraction to hermaphrodite-conditioned media (Figure S6). Thus, increasing *odr-10* expression in adult males is sufficient to shift behavioral prioritization away from mate searching and toward feeding. AWA feminization had similar effects on male behavior: these animals exhibited significantly less exploratory behavior than control males did, although their locomotor rate was unaffected (Figures 6D and S3L). Thus, the repression of *odr-10* in adult males has important adaptive value for reproductive fitness, allowing animals to prioritize sexually motivated exploration over feeding.

Discussion

In order to generate flexible behaviors, fixed neural circuits must integrate multiple internal states. Here, we find that genetic sex, developmental stage, and feeding status regulate the adaptive prioritization of *C. elegans* behavior through dynamic modulation of food sensitivity of a single pair of sensory

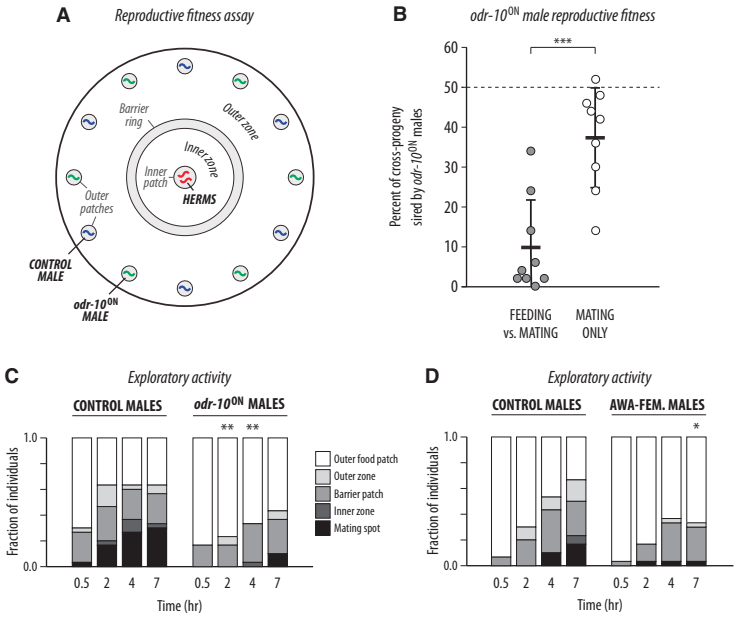

Figure 6. *odr-10* Downregulation Optimizes Male Reproductive Fitness

(A) The reproductive fitness assay. Twelve small food patches were placed at the edge of a 9 cm culture plate; control (P*gpa-4Δ6::GFP*) and *odr-10*^{ON} males were placed in alternating spots. In the center, four paralyzed *unc-31* adult hermaphrodites were placed in a small food spot. A ring-shaped barrier food patch was seeded in between the center spot and the peripheral spots. Males were allowed to feed, explore, and mate for 18 hr and were then removed from the plate. Two days later, the paternity of cross-progeny was determined using genetic markers.

(B) Relative male reproductive fitness. The relative reproductive fitness of *odr-10*^{ON} males was defined as the fraction of total cross-progeny that they sired. "Feeding vs. Mating" indicates that males were placed at the peripheral spots at the beginning of the assay. "Mating Only" indicates that males were placed at the center spot along with the *unc-31* hermaphrodites; in this case, exploration was not necessary for males to find mates. Two independent experiments were performed with a total of nine plates per group. Each plate contained six *odr-10*^{ON} and six control males, and the paternity of >50 cross-progeny was scored for each plate. The difference in *odr-10*^{ON} male reproductive fitness between the "Feeding vs. Mating" and "Mating Only" conditions was evaluated using an unpaired two-tailed t test ($p = 0.0002$). Error bars indicate SD.

(C) Exploratory behavior of control (P*gpa-4Δ6::GFP*) (n = 30) and *odr-10*^{ON} (n = 30) males. The positions of individual males on the assay plate were scored at the indicated intervals. The behavior of control and *odr-10*^{ON} males was compared with Mann-Whitney tests (2 hr: $p = 0.0012$; 4 hr: $p = 0.0038$).

(D) Exploratory behavior of control (P*gpa-4Δ6::GFP*) (n = 30) and AWA-feminized (P*gpa-4Δ6::tra-2(IC)*) (n = 30) males. The behavior of control and AWA-feminized males was compared with Mann-Whitney tests (7 hr: $p = 0.012$).

See also Figure S6.

neurons. Furthermore, this modulation occurs through regulation of a single key chemoreceptor, ODR-10. Our results provide important support for the idea that changes in behavioral choice can be mediated not only by the modulation of central circuits but also by the tuning of sensory function itself. In several systems, sensory neuron physiology has been shown to be plastic, particularly in response to food or feeding behavior [3]. In these cases, presynaptic modulation alters the excitability or synaptic output of sensory neurons to alter chemosensory responses. In contrast, our findings identify dynamic chemoreceptor expression as an additional mechanism by which such presynaptic changes can occur. Indeed, previous studies have found that chemoreceptor expression in *C. elegans* is regulated by internal and external cues [43, 44]; however, the functional significance of this regulation has been unclear. This level of plasticity may be particularly valuable in *C. elegans*: because chemosensory neurons in this species respond to many stimuli and express many candidate chemoreceptors [45], dynamic chemoreceptor expression can provide a degree of specificity beyond modulation of the entire neuron. Interestingly, chemoreceptors in other systems are also regulated by feeding status and developmental stage [3], indicating that similar mechanisms could also play key roles in sensory and behavioral plasticity in more-complex organisms.

At first glance, modulation of chemoreceptor expression seems quite distinct from the synaptic modulation mechanisms that are hallmarks of circuit plasticity [2]. However, an important feature of this plasticity, particularly in long-term potentiation and long-term depression paradigms, is the regulated expression and localization of neurotransmitter receptors, including both ionotropic and metabotropic receptors. Like chemoreceptors, the latter of these are G-protein-coupled receptors. Because the sensory endings of chemosensory neurons have intriguing structural and functional similarities to postsynaptic specializations [46], it is possible that regulated chemoreceptor expression employs mechanisms that are also important for modulating postsynaptic function. Indeed, it may be that this "zeroth" sensory synapse, in which environmental signals substitute for neurotransmitters, is subject to as much plasticity as any other.

To our knowledge, these findings represent the first identification of a food-associated chemoreceptor in *C. elegans*. Although the role of *odr-10* in attraction to diacetyl has been extensively studied, a function for this receptor in food detection has not been described. Our results show that the loss of *odr-10* function significantly compromises food-search behavior in both sexes without more generally disrupting sensory behavior. Although ODR-10 is known to directly recognize diacetyl, behavioral and imaging experiments suggest that ODR-10 can also detect other compounds [47, 48]. This implies that diacetyl or another ODR-10 ligand is produced by *E. coli* and that this signal is an important cue by which *C. elegans* detects food. Interestingly, *odr-10* is under significant purifying selection [49], suggesting that stability in its function is important for fitness. In hermaphrodites, significant food attraction is still intact in *odr-10* null mutants, consistent with findings that other sensory neurons have important roles in food detection (e.g., [38–40]). Interestingly, we find that loss

of *odr-10* has more severe consequences for male behavior, suggesting that *odr-10*-independent food detection is less robust in males than in hermaphrodites. This may reflect a need for the male to devote significant chemosensory resources to the detection of sex pheromones, a signal less important for hermaphrodites themselves. Indeed, AWA has been implicated in the male response to factors secreted by hermaphrodites [15].

In adult males, tonic signals from the rays (sex-specific tail sensilla) are thought to activate the male exploratory drive [27], as are modulatory signals transduced by the PDFR-1 neuropeptide receptor [28]. One interesting possibility is that male-specific downregulation of *odr-10* acts in parallel with this mechanism, allowing the efficient release of exploratory behavior that is driven by male-specific signals. However, it is also possible that *odr-10* has a role in implementing the exploratory state downstream of the rays and/or PDFR-1 signaling.

Notably, our findings reveal that *odr-10* expression is regulated by developmental stage and feeding state, in addition to genetic sex. These three mechanisms might converge on *odr-10* independently; alternatively, there could be interaction between these signals upstream of *odr-10*. Because AWA-specific manipulation of TRA-1A, the master regulator of somatic sex in *C. elegans*, is sufficient to alter *odr-10* expression, genetic sex acts cell autonomously to regulate this sex difference. However, TRA-1A is unlikely to regulate *odr-10* directly because this factor is thought to be a transcriptional repressor [35], and no strong matches to the TRA-1A consensus binding site exist in the vicinity of *odr-10* [50]. Thus, one or more unknown factors likely act downstream of TRA-1 to regulate *odr-10*. With regard to regulation by feeding state, monoamines appear to be dispensable for *odr-10* regulation (data not shown). Other potential candidates for this signal could be insulins, other neuropeptides, or the TGFβ-family ligand DAF-7. Developmental signals that control the timing of *odr-10* downregulation in males are unlikely to be driven by signals from the gonad [14]. However, heterochronic genes, which mediate the larval-to-adult transition in somatic tissues, may play a role in this process. Understanding how these multiple dimensions of internal state regulate *odr-10* remains an important area for future work.

In humans, many studies have found superior olfactory acuity in females [51]. Human olfactory perception is also strongly influenced by nutritional state: classic studies show that a previously attractive odor becomes less appealing after caloric intake [52]. Thus, state-dependent behavioral prioritization through modulation of the perception and hedonic value of olfactory stimuli is likely to be a common theme across species [53]. Our results indicate that regulation of chemoreceptor expression itself could be an important mechanism by which this occurs. Sex differences in the AWA neurons also provide an outstanding opportunity to understand how the genetically encoded sexual state of the specific neurons influence their development and function, a mechanism that is emerging as a critical dimension of neural plasticity throughout the animal kingdom [21].

Experimental Procedures

C. elegans Strains

Strains used are shown in Table S1. Except where noted otherwise, all strains contained *him-5(e1490)* to increase the production of males by self-fertilization.

GFP Quantitation

One-day-old adults (sex segregated as L4 larvae) were mounted on 4% agarose pads in levamisole solution; epifluorescence was observed using a 63× PlanApo objective on a Zeiss Axioplan. Because sensory cilia are complex 3D structures, computer-aided quantitation of fluorescence intensity was not feasible. With the investigator blinded to genotype, GFP intensity in the AWA sensory cilia (or throughout the cell, for the P*odr-10*::*GFP* reporter) was qualitatively assessed using the following rating scale: absent (0), faint (1), moderate (2), or bright (3). Nonparametric tests were used to compare groups (see Supplemental Experimental Procedures).

Behavioral Assays

Odortaxis and olfactory preference assays were carried out as described [14, 29], except that worms within 2 cm of the odorant were scored as responders. To assay food-search behavior, we placed animals 3 cm from a spot of *E. coli* OP50, and their positions were scored at 15 min intervals (see Supplemental Experimental Procedures). Curves were generated with the Kaplan-Meier method and compared using the log rank (Mantel-Cox) test. Food-leaving assays were carried out as described [25], with behavior scored using three categories (see legend for Figure 3). Investigators were blinded to genotype; statistical significance was assessed using the chi-square test. Body-bend analysis was carried out as previously described, with minor modifications (see Supplemental Experimental Procedures). The reproductive fitness assay is described in the Results; further details can be found in Supplemental Experimental Procedures.

Supplemental Information

Supplemental Information includes Supplemental Experimental Procedures, six figures, and one table and can be found with this article online at http://dx.doi.org/10.1016/j.cub.2014.09.032.

Acknowledgments

We thank Eugene Kim for help with starvation experiments, and we thank current and former members of the D.S.P. laboratory, particularly Jessica Bennett, Adam Mason, and William Mowrey, for discussion and insights. We thank Dorothy Heyer and Helene McMurray for help with qPCR. Some strains used in these studies were provided by the *Caenorhabditis* Genetics Center, which is funded by the NIH Office of Research Infrastructure Programs (P40 OD010440). Funding for this work was provided by the NIH (R01 GM086456 to D.S.P.), the National Science Foundation (IOS 0920024 to D.S.P. and IOS 1256488 to P.S.), the Human Frontiers Science Program (RGY0042/2010-C to P.S.), and NAAR/Autism Speaks (78a2r to D.S.P.). During part of this project, D.A.R. was supported by NIH T32 ES007026. S.J.N. was supported by a postgraduate scholarship (PGS-D3) from the Natural Sciences and Engineering Research Council of Canada and by the Brandeis National Committee.

Received: April 11, 2014
Revised: August 4, 2014
Accepted: September 11, 2014
Published: October 16, 2014

References

1. McFarland, D.J. (1977). Decision making in animals. Nature *269*, 15–21.
2. Marder, E. (2012). Neuromodulation of neuronal circuits: back to the future. Neuron *76*, 1–11.
3. Sengupta, P. (2013). The belly rules the nose: feeding state-dependent modulation of peripheral chemosensory responses. Curr. Opin. Neurobiol. *23*, 68–75.
4. Palmer, C.R., and Kristan, W.B., Jr. (2011). Contextual modulation of behavioral choice. Curr. Opin. Neurobiol. *21*, 520–526.
5. Gaudry, Q., and Kristan, W.B., Jr. (2009). Behavioral choice by presynaptic inhibition of tactile sensory terminals. Nat. Neurosci. *12*, 1450–1457.
6. Tomioka, M., Adachi, T., Suzuki, H., Kunitomo, H., Schafer, W.R., and Iino, Y. (2006). The insulin/PI 3-kinase pathway regulates salt chemotaxis learning in Caenorhabditis elegans. Neuron *51*, 613–625.
7. Kindt, K.S., Quast, K.B., Giles, A.C., De, S., Hendrey, D., Nicastro, I., Rankin, C.H., and Schafer, W.R. (2007). Dopamine mediates context-dependent modulation of sensory plasticity in C. elegans. Neuron *55*, 662–676.

8. Root, C.M., Ko, K.I., Jafari, A., and Wang, J.W. (2011). Presynaptic facilitation by neuropeptide signaling mediates odor-driven food search. Cell *145*, 133–144.
9. Inagaki, H.K., Ben-Tabou de-Leon, S., Wong, A.M., Jagadish, S., Ishimoto, H., Barnea, G., Kitamoto, T., Axel, R., and Anderson, D.J. (2012). Visualizing neuromodulation in vivo: TANGO-mapping of dopamine signaling reveals appetite control of sugar sensing. Cell *148*, 583–595.
10. Savigner, A., Duchamp-Viret, P., Grosmaitre, X., Chaput, M., Garcia, S., Ma, M., and Palouzier-Paulignan, B. (2009). Modulation of spontaneous and odorant-evoked activity of rat olfactory sensory neurons by two anorectic peptides, insulin and leptin. J. Neurophysiol. *101*, 2898–2906.
11. Tong, J., Mannea, E., Aimé, P., Pfluger, P.T., Yi, C.X., Castaneda, T.R., Davis, H.W., Ren, X., Pixley, S., Benoit, S., et al. (2011). Ghrelin enhances olfactory sensitivity and exploratory sniffing in rodents and humans. J. Neurosci. *31*, 5841–5846.
12. Soria-Gómez, E., Bellocchio, L., Reguero, L., Lepousez, G., Martin, C., Bendahmane, M., Ruehle, S., Remmers, F., Desprez, T., Matias, I., et al. (2014). The endocannabinoid system controls food intake via olfactory processes. Nat. Neurosci. *17*, 407–415.
13. Mowrey, W.R., and Portman, D.S. (2012). Sex differences in behavioral decision-making and the modulation of shared neural circuits. Biol Sex Differ *3*, 8.
14. Lee, K., and Portman, D.S. (2007). Neural sex modifies the function of a C. elegans sensory circuit. Curr. Biol. *17*, 1858–1863.
15. White, J.Q., Nicholas, T.J., Gritton, J., Truong, L., Davidson, E.R., and Jorgensen, E.M. (2007). The sensory circuitry for sexual attraction in C. elegans males. Curr. Biol. *17*, 1847–1857.
16. Jang, H., Kim, K., Neal, S.J., Macosko, E., Kim, D., Butcher, R.A., Zeiger, D.M., Bargmann, C.I., and Sengupta, P. (2012). Neuromodulatory state and sex specify alternative behaviors through antagonistic synaptic pathways in C. elegans. Neuron *75*, 585–592.
17. Clyne, J.D., and Miesenböck, G. (2008). Sex-specific control and tuning of the pattern generator for courtship song in Drosophila. Cell *133*, 354–363.
18. Ruta, V., Datta, S.R., Vasconcelos, M.L., Freeland, J., Looger, L.L., and Axel, R. (2010). A dimorphic pheromone circuit in Drosophila from sensory input to descending output. Nature *468*, 686–690.
19. Stowers, L., Holy, T.E., Meister, M., Dulac, C., and Koentges, G. (2002). Loss of sex discrimination and male-male aggression in mice deficient for TRP2. Science *295*, 1493–1500.
20. Kimchi, T., Xu, J., and Dulac, C. (2007). A functional circuit underlying male sexual behaviour in the female mouse brain. Nature *448*, 1009–1014.
21. McCarthy, M.M., and Arnold, A.P. (2011). Reframing sexual differentiation of the brain. Nat. Neurosci. *14*, 677–683.
22. Bargmann, C.I. (2012). Beyond the connectome: how neuromodulators shape neural circuits. Bioessays *34*, 458–465.
23. Mowrey, W.R., Bennett, J.R., and Portman, D.S. (2014). Distributed effects of biological sex define sex-typical motor behavior in Caenorhabditis elegans. J. Neurosci. *34*, 1579–1591.
24. Sakai, N., Iwata, R., Yokoi, S., Butcher, R.A., Clardy, J., Tomioka, M., and Iino, Y. (2013). A sexually conditioned switch of chemosensory behavior in C. elegans. PLoS ONE *8*, e68676.
25. Lipton, J., Kleemann, G., Ghosh, R., Lints, R., and Emmons, S.W. (2004). Mate searching in Caenorhabditis elegans: a genetic model for sex drive in a simple invertebrate. J. Neurosci. *24*, 7427–7434.
26. Fagan, K.A., and Portman, D.S. (2014). Sexual modulation of neural circuits and behavior in Caenorhabditis elegans. Semin. Cell Dev. Biol. *33*, 3–9.
27. Barrios, A., Nurrish, S., and Emmons, S.W. (2008). Sensory regulation of C. elegans male mate-searching behavior. Curr. Biol. *18*, 1865–1871.
28. Barrios, A., Ghosh, R., Fang, C., Emmons, S.W., and Barr, M.M. (2012). PDF-1 neuropeptide signaling modulates a neural circuit for mate-searching behavior in C. elegans. Nat. Neurosci. *15*, 1675–1682.
29. Bargmann, C.I., Hartwieg, E., and Horvitz, H.R. (1993). Odorant-selective genes and neurons mediate olfaction in C. elegans. Cell *74*, 515–527.
30. Sengupta, P., Chou, J.H., and Bargmann, C.I. (1996). odr-10 encodes a seven transmembrane domain olfactory receptor required for responses to the odorant diacetyl. Cell *84*, 899–909.
31. Chou, J.H., Bargmann, C.I., and Sengupta, P. (2001). The Caenorhabditis elegans odr-2 gene encodes a novel Ly-6-related protein required for olfaction. Genetics *157*, 211–224.
32. Sengupta, P., Colbert, H.A., and Bargmann, C.I. (1994). The C. elegans gene odr-7 encodes an olfactory-specific member of the nuclear receptor superfamily. Cell *79*, 971–980.
33. Lanjuin, A., VanHoven, M.K., Bargmann, C.I., Thompson, J.K., and Sengupta, P. (2003). Otx/otd homeobox genes specify distinct sensory neuron identities in C. elegans. Dev. Cell *5*, 621–633.
34. Mehra, A., Gaudet, J., Heck, L., Kuwabara, P.E., and Spence, A.M. (1999). Negative regulation of male development in Caenorhabditis elegans by a protein-protein interaction between TRA-2A and FEM-3. Genes Dev. *13*, 1453–1463.
35. Zarkower, D., and Hodgkin, J. (1992). Molecular analysis of the C. elegans sex-determining gene tra-1: a gene encoding two zinc finger proteins. Cell *70*, 237–249.
36. Tian, L., Hires, S.A., Mao, T., Huber, D., Chiappe, M.E., Chalasani, S.H., Petreanu, L., Akerboom, J., McKinney, S.A., Schreiter, E.R., et al. (2009). Imaging neural activity in worms, flies and mice with improved GCaMP calcium indicators. Nat. Methods *6*, 875–881.
37. Ikeda, T., Yasui, C., Hoshino, K., Arikawa, K., and Nishikawa, Y. (2007). Influence of lactic acid bacteria on longevity of Caenorhabditis elegans and host defense against salmonella enterica serovar enteritidis. Appl. Environ. Microbiol. *73*, 6404–6409.
38. Bargmann, C.I., and Horvitz, H.R. (1991). Control of larval development by chemosensory neurons in Caenorhabditis elegans. Science *251*, 1243–1246.
39. Gray, J.M., Hill, J.J., and Bargmann, C.I. (2005). A circuit for navigation in Caenorhabditis elegans. Proc. Natl. Acad. Sci. USA *102*, 3184–3191.
40. Gallagher, T., Kim, J., Oldenbroek, M., Kerr, R., and You, Y.J. (2013). ASI regulates satiety quiescence in C. elegans. J. Neurosci. *33*, 9716–9724.
41. Calixto, A., Chelur, D., Topalidou, I., Chen, X., and Chalfie, M. (2010). Enhanced neuronal RNAi in C. elegans using SID-1. Nat. Methods *7*, 554–559.
42. Hills, T., Brockie, P.J., and Maricq, A.V. (2004). Dopamine and glutamate control area-restricted search behavior in Caenorhabditis elegans. J. Neurosci. *24*, 1217–1225.
43. Peckol, E.L., Troemel, E.R., and Bargmann, C.I. (2001). Sensory experience and sensory activity regulate chemosensory receptor gene expression in Caenorhabditis elegans. Proc. Natl. Acad. Sci. USA *98*, 11032–11038.
44. Lanjuin, A., and Sengupta, P. (2002). Regulation of chemosensory receptor expression and sensory signaling by the KIN-29 Ser/Thr kinase. Neuron *33*, 369–381.
45. Bargmann, C.I. (2006). Chemosensation in C. elegans. WormBook, 1–29.
46. Shaham, S. (2010). Chemosensory organs as models of neuronal synapses. Nat. Rev. Neurosci. *11*, 212–217.
47. Troemel, E.R., Kimmel, B.E., and Bargmann, C.I. (1997). Reprogramming chemotaxis responses: sensory neurons define olfactory preferences in *C. elegans*. Cell *91*, 161–169.
48. Larsch, J., Ventimiglia, D., Bargmann, C.I., and Albrecht, D.R. (2013). High-throughput imaging of neuronal activity in Caenorhabditis elegans. Proc. Natl. Acad. Sci. USA *110*, E4266–E4273.
49. Jovelin, R., Dunham, J.P., Sung, F.S., and Phillips, P.C. (2009). High nucleotide divergence in developmental regulatory genes contrasts with the structural elements of olfactory pathways in caenorhabditis. Genetics *181*, 1387–1397.
50. Berkseth, M., Ikegami, K., Arur, S., Lieb, J.D., and Zarkower, D. (2013). TRA-1 ChIP-seq reveals regulators of sexual differentiation and multilevel feedback in nematode sex determination. Proc. Natl. Acad. Sci. USA *110*, 16033–16038.
51. Doty, R.L., and Cameron, E.L. (2009). Sex differences and reproductive hormone influences on human odor perception. Physiol. Behav. *97*, 213–228.
52. Cabanac, M. (1971). Physiological role of pleasure. Science *173*, 1103–1107.
53. Palouzier-Paulignan, B., Lacroix, M.C., Aimé, P., Baly, C., Caillol, M., Congar, P., Julliard, A.K., Tucker, K., and Fadool, D.A. (2012). Olfaction under metabolic influences. Chem. Senses *37*, 769–797.

Current Biology, Volume *24*

Supplemental Information

Sex, Age, and Hunger Regulate Behavioral Prioritization through Dynamic Modulation of Chemoreceptor Expression

Deborah A. Ryan, Renee M. Miller, KyungHwa Lee, Scott Neal, Kelli A. Fagan, Piali Sengupta, and Douglas S. Portman

Figure S1

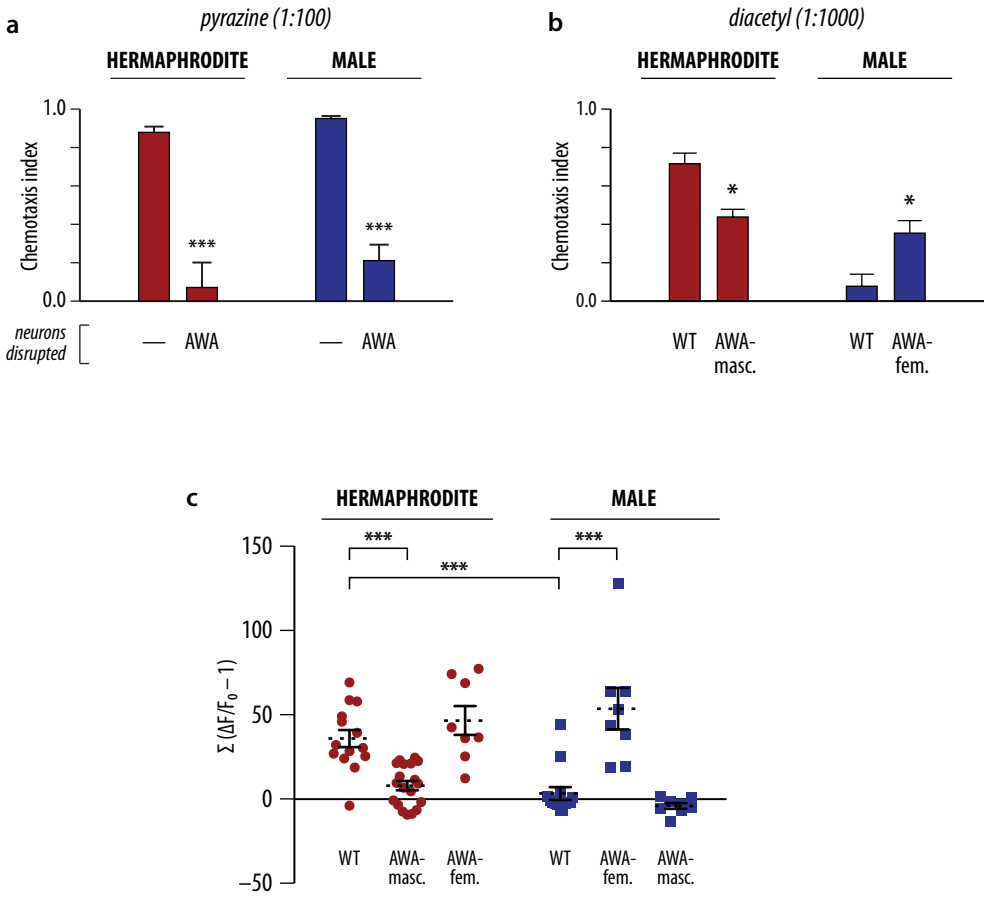
a
pyrazine (1:100)
HERMAPHRODITE
MALE
Chemotaxis index
1.0
0.0
***
***
neurons disrupted
AWA
AWA
b
diacetyl (1:1000)
HERMAPHRODITE
MALE
Chemotaxis index
1.0
0.0
*
*
WT
AWA-masc.
WT
AWA-fem.
c
HERMAPHRODITE
MALE
150
100
50
0
−50
Σ (ΔF/F0 − 1)
***
***
***
WT
AWA-masc.
AWA-fem.
WT
AWA-fem.
AWA-masc.

Figure S2

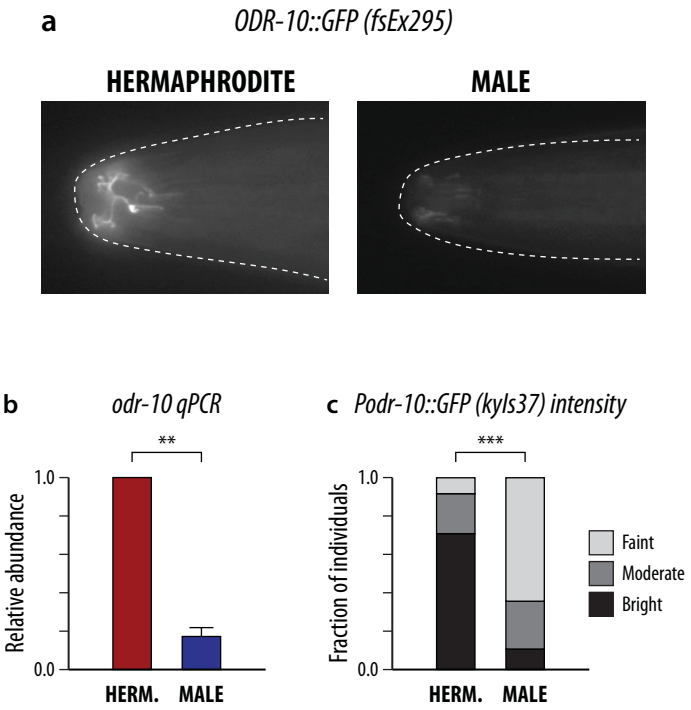
a
ODR-10::GFP (fsEx295)
HERMAPHRODITE
MALE
b
odr-10 qPCR
**
1.0
0.0
Relative abundance
HERM.
MALE
c
Podr-10::GFP (kyIs37) intensity
***
1.0
0.0
Fraction of individuals
Faint
Moderate
Bright
HERM.
MALE

Figure S3

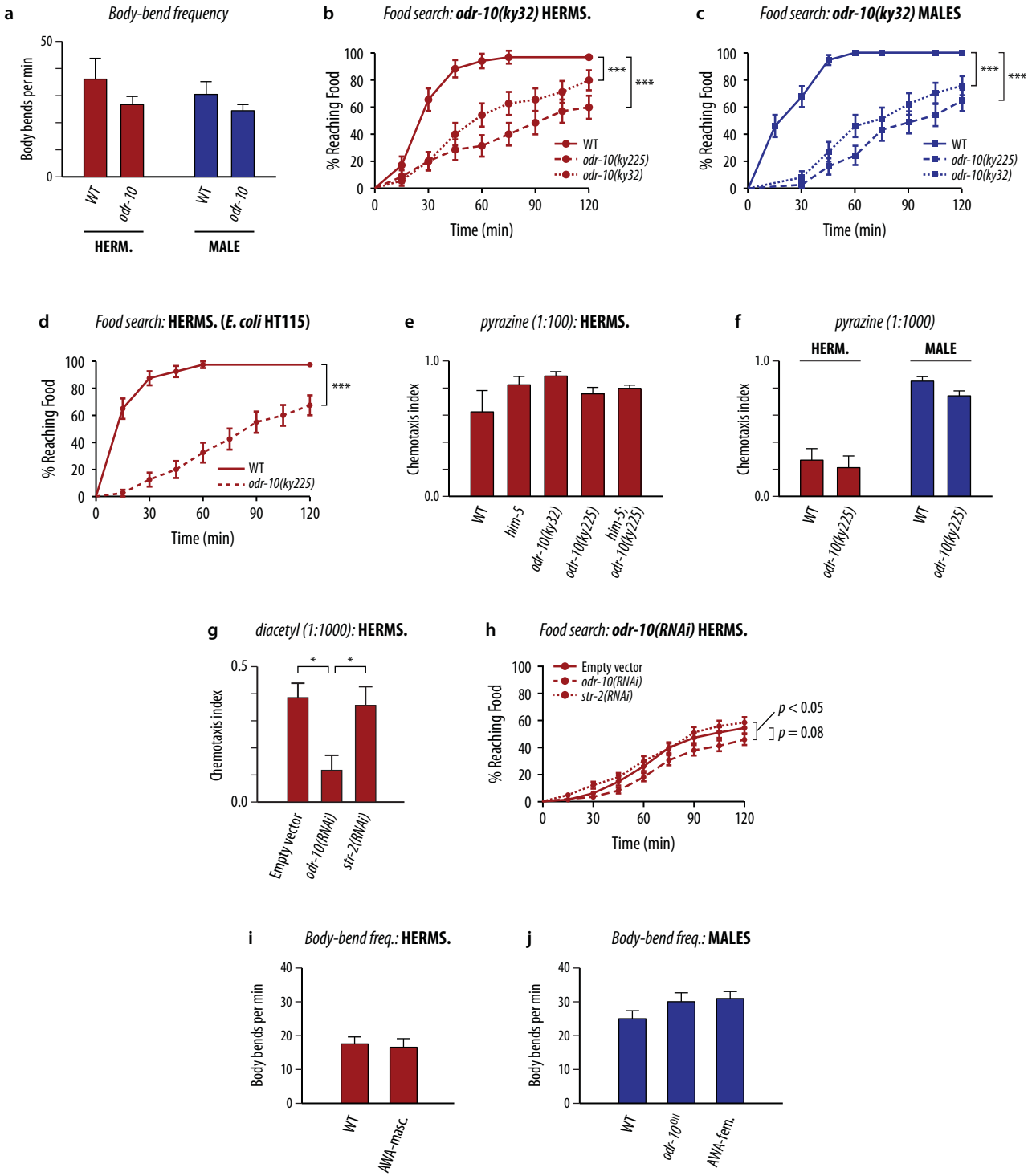
a
Body-bend frequency
Body bends per min
50
0
WT
odr-10
WT
odr-10
HERM.
MALE
b
Food search: odr-10(ky32) HERMS.
% Reaching Food
100
80
60
40
20
0
0
30
60
90
120
Time (min)
***
***
WT
odr-10(ky225)
odr-10(ky32)
c
Food search: odr-10(ky32) MALES
% Reaching Food
Time (min)
***
***
WT
odr-10(ky225)
odr-10(ky32)
d
Food search: HERMS. (E. coli HT115)
% Reaching Food
Time (min)
***
WT
odr-10(ky225)
e
pyrazine (1:100): HERMS.
Chemotaxis index
1.0
0.0
WT
him-5
odr-10(ky32)
odr-10(ky225)
him-5; odr-10(ky225)
f
pyrazine (1:1000)
HERM.
MALE
Chemotaxis index
1.0
0.0
WT
odr-10(ky225)
WT
odr-10(ky225)
g
diacetyl (1:1000): HERMS.
Chemotaxis index
0.5
0.0
*
*
Empty vector
odr-10(RNAi)
str-2(RNAi)
h
Food search: odr-10(RNAi) HERMS.
% Reaching Food
Time (min)
Empty vector
odr-10(RNAi)
str-2(RNAi)
p < 0.05
p = 0.08
i
Body-bend freq.: HERMS.
Body bends per min
40
30
20
10
0
WT
AWA-masc.
j
Body-bend freq.: MALES
Body bends per min
40
30
20
10
0
WT
odr-10ON
AWA-fem.

Figure S4

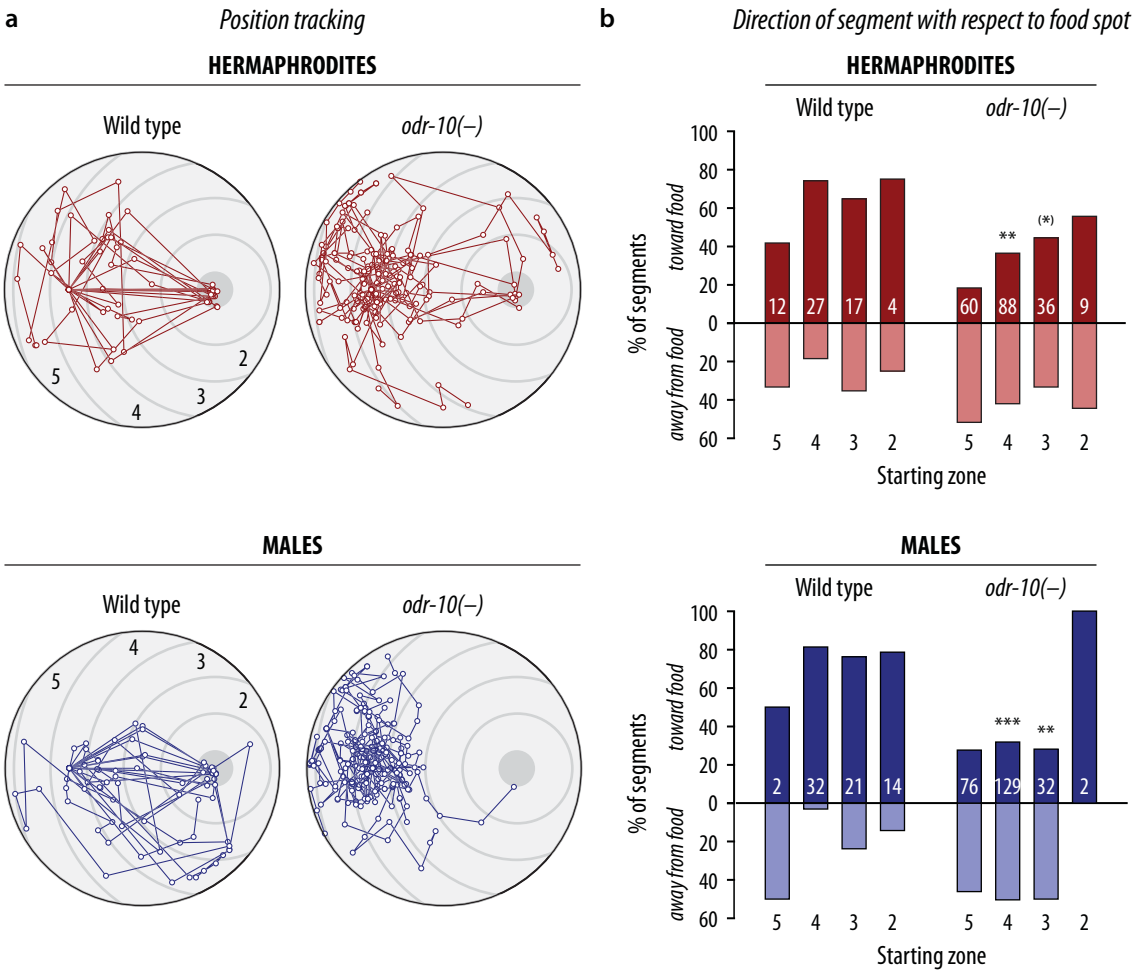
a
Position tracking
HERMAPHRODITES
Wild type
odr-10(–)
5
4
3
2
MALES
Wild type
odr-10(–)
5
4
3
2
b
Direction of segment with respect to food spot
HERMAPHRODITES
Wild type
odr-10(–)
% of segments
toward food
away from food
100
80
60
40
20
0
20
40
60
12
27
17
4
60
88
36
9
**
(*)
5 4 3 2 5 4 3 2
Starting zone
MALES
Wild type
odr-10(–)
% of segments
toward food
away from food
2
32
21
14
76
129
32
2
***
**
5 4 3 2 5 4 3 2
Starting zone

Figure S5

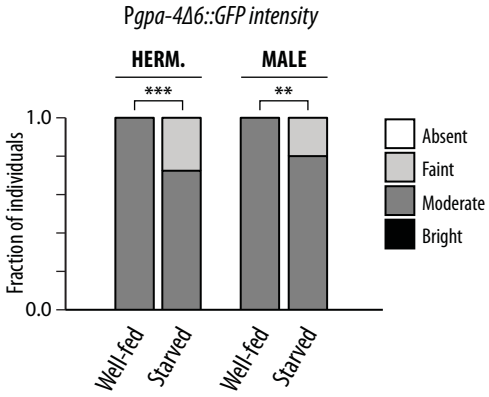
Pgpa-4Δ6::GFP intensity
HERM.
MALE
***
**
1.0
0.0
Fraction of individuals
Absent
Faint
Moderate
Bright
Well-fed
Starved
Well-fed
Starved

Figure S6

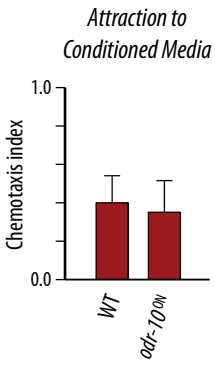
Attraction to
Conditioned Media
1.0
0.0
Chemotaxis index
WT
odr-10 ON

SUPPLEMENTAL FIGURE LEGENDS

Fig. S1. Supplement to Fig. 1, The neural architecture of diacetyl attraction differs by sex. (a) Chemotaxis of wild type and *odr-7* mutant hermaphrodites and males to pyrazine (1:100). Five independent experiments were performed for a total of $n = 259$, 252, 270 and 251 in each group (left to right). Asterisks indicate *odr-7* vs. WT p values by unpaired two-tailed t-tests (hermaphrodites $p = 0.0004$; males $p < 0.0001$); error bars indicate SEM. **(b)** Chemotaxis to 1:1000 diacetyl for wild-type ($n = 119$) and AWA-masculinized (P*gpa-4*Δ*6::fem-3(+)*) ($n = 111$) hermaphrodites (red) and wild-type ($n = 79$) and AWA-feminized (P*gpa-4*Δ*6::tra-2(IC)*) ($n = 70$) males (blue). Data are pooled from three independent experiments. Asterisks indicate $p < 0.05$ for WT vs. sex-reversed by unpaired two-tailed t-tests (hermaphrodites $p = 0.015$, males $p = 0.036$). Error bars are SEM. **(c)** Total calcium response, calculated by summing $\Delta F/F_0$ above the baseline during the period of diacetyl stimulation. Wild-type and transgenic hermaphrodites are shown on the left; wild-type and transgenic males on the right. Data were collected over the course of three independent sessions with a total of $n = 14$, 19, 8, 14, 8 and 8 animals per group, from left to right. Statistical significance was determined using a one-way ANOVA with Bonferroni's multiple comparisons test. Asterisks indicate post-test comparisons with wild-type controls; ***$p<0.001$. Error bars indicate SD.

Fig. S2. Supplement to Fig. 2, The diacetyl chemoreceptor ODR-10 is regulated by AWA genetic sex. (a) Expression of the ODR-10::GFP fosmid reporter *fsEx295* is sexually dimorphic. Panels show representative examples of head fluorescence in an

fsEx295 adult hermaphrodite (left) and male (right). All images were acquired using the same illumination intensity and exposure time. Dashed lines indicate the outline of the body. More than 50 animals per group were examined, demonstrating similar results. **(b)** Relative abundance of *odr-10* mRNA in wild-type adult males (blue) relative to wild-type adult hermaphrodites (red). *odr-10* levels were normalized using two control mRNAs (see Supplemental Experimental Procedures). Three independent experiments were performed in which at least 200 animals were collected for each sample. Asterisks indicate significant differences by one-sample t-test ($p = 0.003$). Error bars indicate SEM. **(c)** Quantitation of P*odr-10::GFP* (*kyIs37*) expression. Fluorescence intensity was scored qualitatively using four categories (absent, faint, moderate and bright) with investigator blinded to genotype. Comparison of hermaphrodites ($n = 24$) vs. males ($n = 28$) was done by Mann-Whitney test; $***p < 10^{-5}$.

Figure S3. Supplement to Fig. 3, *odr-10* is a critical regulator of food-search behavior. (a) Off-food body-bend frequencies of wild-type ($n = 7$) and *odr-10(ky225)* ($n = 10$) hermaphrodites (red) and wild-type ($n = 10$) and *odr-10(ky225)* ($n = 10$) males (blue). Data were analyzed by unpaired two-tailed t-tests with no significant differences identified (hermaphrodites $p = 0.27$; males $p = 0.26$). Error bars indicate SEM. **(b)** Food-search behavior of wild-type (solid line), *odr-10(ky225)* (dashed line) and *odr-10(ky32)* (dotted line) hermaphrodites. $n = 37$ for all genotypes. $***p < 0.001$ by Mantel-Cox test. **(c)** Food-search behavior of wild-type (solid line), *odr-10(ky225)* (dashed line) and *odr-10(ky32)* (dotted line) males. $n \geq 37$ for all genotypes. $***p < 0.001$ by Mantel-Cox test. **(d)** Food-search behavior of wild-type (solid line, $n = 40$) and *odr-10(ky225)* (dashed

line, $n = 40$) hermaphrodites to *E. coli* HT115 in the standard food-search assay. $p <$ 0.0001 by Mantel-Cox text. **(e)** Chemotaxis to pyrazine (1:100) by hermaphrodites of the indicated genotypes. In this experiment, only the strains indicated contained the *him-5(e1490)* mutation. Experiments were performed on a total of $n = 138$, 142, 143, 150 and 133 animals (left to right). One-way ANOVA and Bonferroni's multiple comparison tests were used to determine significance. **(f)** Chemotaxis to pyrazine (1:1000) by *him-5* ($n =$ 119 hermaphrodites, 121 males) and *him-5; odr-10(ky225)* ($n = 162$ hermaphrodites, 143 males) hermaphrodites (left, red) and males (right, blue). Data were analyzed by unpaired two-tailed t-tests. In (e) and (f), no significant differences in behavior ($p < 0.05$) were identified. **(g)** Chemotaxis to diacetyl (1:1000) by control ("empty vector"), *odr-10(RNAi)*, and *str-2(RNAi)* hermaphrodites. *him-5(e1490)* was not present in the background of these strains. RNAi was delivered by bacterial feeding starting at the late L3 or early L4 stage (see Supplemental Experimental Procedures). *str-2*, a putative chemoreceptor expressed in one of the two AWC neurons, was used as a negative control. Each group represents data from at least 121 animals. Data were analyzed by unpaired two-tailed t-tests ($*p < 0.05$). **(h)** Food-search behavior of control ("empty vector"), *odr-10(RNAi)*, and *str-2(RNAi)* hermaphrodites. *him-5(e1490)* was not present in the background of these strains. By Mantel-Cox, $p = 0.081$ for *odr-10(RNAi) vs.* empty vector; $p = 0.012$ for *odr-10(RNAi) vs. str-2(RNAi)*. **(i)** On-food body-bend frequencies of wild-type ($n = 12$) and AWA-masculinized (P*gpa-4Δ6::fem-3(+)*) ($n = 11$) hermaphrodites. Data were analyzed by unpaired two-tailed t-test ($p = 0.76$). **(j)** On-food body-bend frequencies of control (P*gpa-4Δ6::GFP*), *odr-10*^{ON} (P*gpa-4Δ6::odr-10(+)*),

and AWA-feminized (P*gpa-4Δ6::tra-2(IC)*) males (n = 11 animals in each group). Data were analyzed by one-way ANOVA (p = 0.18). In (i) and (j), error bars indicate SEM.

Figure S4. Supplement to Fig. 3, *odr-10* is a critical regulator of food-search behavior. (a) Position-tracking of wild-type (left) and *odr-10(ky225)* (right) hermaphrodites (above; red) and males (below; blue) in the food-search assay. n = 20 animals for each group. Open circles represent the positions of animals at seven-minute intervals. Solid lines join the start and end points of each interval. The shaded circle at the right side of each diagram indicates the food spot. Gray lines and numbers indicate zones of distance from the food: zone 2, 1.6 ± 0.4 cm to center of food spot; zone 3, 2.4 ± 0.8 cm; zone 4, 3.2 ± 0.4 cm (animals start the assay in the center of this zone); and zone 5, 4.0 ± 0.4 cm. **(b)** Histogram of the orientation of each segment with respect to the food spot as a function of the starting zone. Segment orientation was binned into one of three groups: toward food (orientation 0° ± 60° with respect to a straight line from the start of the segment to the center of the food); away from food (180° ± 60°); and neutral (90° ± 30° and –90° ± 30°). Only the toward-food (above the x-axis) and away-from-food (below the x-axis) segments are shown. Numbers indicate the number of segments that began in the indicated zone. Wild-type (left) and *odr-10(ky225)* (right) data are shown for hermaphrodites (above; red) and males (below; blue). Fisher's exact test was used to compare the distribution frequencies for each zone between wild-type and *odr-10(ky225)* mutants. ***$p < 0.001$; **$p < 0.01$; *$p < 0.05$; $^{(*)}p < 0.1$.

Figure S5. Supplement to Fig. 5, Starvation transiently upregulates *odr-10* to increase male food attraction. P*gpa-4*Δ*6::GFP* (*oyIs61*; n = ~30 per group) fluorescence in well-fed and starved hermaphrodites and males, binned into four groups by intensity. Animals were removed from food 18 to 24 hr before imaging. Asterisks indicate ***$p < 0.001$, **$p < 0.01$ by Mann-Whitney non-parametric two-tailed t-test.

Figure S6. Supplement to Fig. 6, Male reproductive fitness depends on the adult-specific downregulation of *odr-10* expression. Attraction to hermaphrodite-conditioned media by wild-type (n = 40) and *odr-10*^{ON} males (n = 40) (see Supplemental Experimental Procedures). No significant difference between genotypes was detected by two-tailed t-test.

SUPPLEMENTAL TABLE

Table 1. Strains used.

CX32	*odr-10(ky32)* X
CX3410	*odr-10(ky225)* X
DA509	*unc-31(e928)* IV
PY6554	*oyEx6554[Pgpa-4::GCaMP3]*
PY8356	*fsEx421[Pgpa-4Δ6::fem-3(+)::SL2::mCherry + Pelt-2::GFP]; oyEx6554 [Pgpa-4::GCaMP3]*
PY8358	*fsEx420[Pgpa-4Δ6::tra-2(IC)::SL2::mCherry + Pelt-2::GFP]; oyEx6554 [Pgpa-4::GCaMP3]*
TU3401	*uIs69[Pmyo-2p::mCherry + Punc-119::sid-1] sid-1(pk3321) V*
UR223	*him-5(e1490)* V*; odr-7(ky4)* X
UR236	*him-5(e1490) fsIs15[Prab-3::fem-3(+)::SL2::mCherry + Punc-122::GFP]* V
UR249	*him-5(e1490)* V*; fsEx187[Prab-3::tra-2(IC)::SL2::mCherry + Punc-122::GFP]*
UR406	*him-5(e1490)* V*; odr-10(ky225)* X
UR460	*him-5(e1490)* V*; kyIs53[odr-10::GFP]* X
UR487	*him-5(e1490)* V*; ceh-36(ky640)* X
UR489	*kyIs37[Podr-10::GFP]* II; *him-5(e1490)* V; *Ex[Podr-7::mCherry]*
UR546	*him-5(e1490)* V*; fsEx202[Podr-7::fem-3(+)::SL2::mCherry + Punc-122::GFP]*
UR547	*him-5(e1490)* V*; fsEx204[Podr-7::tra-2(IC)::SL2::mCherry + Punc-122::GFP]*
UR773	*pha-1(e2123)* III*; him-5*(e1490) V*; fsEx295[ODR-10::GFP fosmid + pBx1]*
UR833	*him-5(e1490)* V*; odr-10(ky225)* X*; fsEx400[Pgpa-4Δ::odr-10(+)::SL2::mCherry + Punc-122::GFP]*
UR849	*him-5(e1490)* V*; oyIs61[Pgpa-4Δ6::GFP]*
UR883	*him-5(e1490)* V*; fsEx420[Pgpa-4Δ6::tra-2(IC)::SL2::mCherry + Pelt-2::GFP]*
UR884	*him-5(e1490)* V*; fsEx421[Pgpa-4Δ6::fem-3(+)::SL2::mCherry + Pelt-2::GFP]*
UR911	*him-5(e1490)* V*; fsEx400[Pgpa-4Δ6::odr-10(+)::SL2::mCherry + Punc-122::GFP]*
UR917	*him-5(e1490)* V*; kyIs53* X*; fsEx420[Pgpa-4Δ6::tra-2(IC)::SL2::mCherry + Pelt-2::GFP]*
UR918	*him-5(e1490)* V*; kyIs53* X*; fsEx421[Pgpa-4Δ6::fem-3(+)::SL2::mCherry + Pelt-2::GFP]*

SUPPLEMENTAL EXPERIMENTAL PROCEDURES

Transgenes

The Multisite Gateway Cloning system (Invitrogen) was used to produce transgenes driving expression of *fem-3(+)* or *tra-2(IC)* for neural masculinization and feminization, respectively [S1, S2]. AWA-specific expression was achieved using the P*odr-7* promoter [S3] or P*gpa-4*Δ*6*, a 1674-bp fragment derived from the *gpa-4* promoter that contains sequences –2873 to –1 with respect to the *gpa-4* ATG, with a deletion from –1235 to –127, inclusive (K. Kim, pers. comm.). Transgenic animals were generated using standard techniques [S4], injecting 25 ng/µl of the sex reversal construct of interest with 180 ng/µl of a coelomocyte-specific GFP reporter gene (*Punc-122::GFP*) or 100 ng/µl of a intestine-specific GFP reporter gene (P*elt-2::GFP*). To create the ODR-10::GFP reporter *fsEx295*, fosmid recombineering [S5] was used to insert an in-frame GFP cassette at the C-terminal end of the *odr-10* open-reading frame in fosmid WRM0636dA02, obtained from Source BioScience (Nottingham, UK). The *odr-10*^{ON} transgene P*gpa-4*Δ*6::odr-10(+)* was generated by placing the *odr-10* gDNA, SL2::mCherry and the *unc-54* 3′ UTR downstream of P*gpa-4*Δ*6* using Multisite Gateway Cloning.

Behavioral assays

Chemotaxis. Single-odorant chemotaxis assays were carried out as previously described [S6], except that worms within a 2-cm radius of the odorant spot were scored as responders. Investigators were not blinded to experimental conditions. The mean chemotaxis index and standard error was obtained by calculating weighted averages of at least three assays using STATA release 11. Diacetyl–pyrazine preference was assayed using the previously described olfactory preference assay [S1].

To produce hermaphrodite-conditioned media for the experiment shown in Fig. S6, 40 adult hermaphrodites were incubated in 80 µl of M9 buffer for two hours at room temperature. The assay was carried out on a standard 6-cm NGM plate containing a 3 x 3 cm lawn of *E. coli* OP50 grown overnight. The bacterial lawn was divided into four quadrants, each containing four 1 µl drops of M9 or hermaphrodite-conditioned media placed evenly in opposing quadrants. Ten WT or *odr-10*^{ON} adult males were placed at the center of the lawn (a ring with a radius of 0.25 cm that did not contain any M9 or conditioned media). After 90 min, the number of worms in each quadrant were counted. Chemotaxis index was calculated as (number of animals in conditioned media quadrants – number in control quadrants) / total number of animals. Each data point represents the mean from four assays. Error bars represent SEM. Data were analyzed using an unpaired Student's t-test; no significant difference was found.

Food-search. To assay food-search behavior, assay plates (6 cm plastic culture plates containing 4 ml of 1.5% agar with 6 mM potassium phosphate pH 6.0, 1 mM $MgSO_4$, and 1 mM $CaCl_2$) were prepared the day of the assay. A fresh *E. coli* culture was started the night before and grown to an OD_{600} of 2.5. A 7 µl drop of the *E. coli*

suspension was placed 3.2 cm from the starting location and allowed to dry. One-day old adults (sex-segregated as L4 larvae) were transferred from culture plates to an unseeded plate to remove traces of food and then immediately transferred to the starting location on the assay plate. Plates were checked at 15-min intervals for 120 min and the time at which each worm reached the food spot was recorded. Due to the objective nature of the data investigators were not blinded to experimental conditions. Each data point typically represents five replicates using roughly ten worms of each genotype for each replicate. Animals that failed to reach the food after assay completion received a censored score of 120 min. Survival fractions and curves were generated with the Kaplan-Meier method and compared using the log-rank (Mantel-Cox) test.

Food-leaving. Food-leaving assays were carried out as described [S7], except that exploratory behavior was scored using three categories: no exploration (*i.e.,* animals never left the food spot); minor exploration (tracks were present off of the food spot, but not beyond 1 cm away); and major exploration (tracks extended beyond 1 cm away from the food spot). Investigators were blinded to genotype. Statistical significance was assessed using the Chi-square test, as categorical data are not normally distributed.

Reproductive fitness. To measure reproductive fitness, 10 cm NGM plates were seeded with *E. coli* OP50 the night before the experiment began in the following configuration: a 15 µl "mating spot" was placed at the center; a "barrier patch" was created by spreading together twelve 3 µl spots, each placed 2 cm from the center; and twelve 3 µl "outer food patches" were spaced equally around the perimeter of the plate,

3.5 cm from the center (see Fig. 6a). Animals were picked as L4 larvae to sex-segregated holding plates the afternoon before the assay. Four *unc-31(e928)* hermaphrodites were placed at the center mating spot, and control (*Pgpa-4Δ6::GFP*) and *odr-10*^{ON} (*Pgpa-4Δ6::odr-10(+)*) males were placed in alternating outer food patches at the start of the assay. Males were removed from the plate after 18 hrs. After 48-50 hr, representative populations of non-Unc male cross-progeny (≥ 50 animals) were picked (blinded to genotype) and scored for their paternity using GFP fluorescence. To control for mating ability, a control experiment was performed in which all worms were placed together in the center mating spot at the beginning of the experiment.

In separate experiments for Figs. 6c and d, the experimental setup was the same, but the location of each male was tracked over the course of 7 hours. Data obtained in these experiments were subjected to non-parametric analysis because they are not normally distributed. The investigator performing the location-tracking experiments was not blinded to genotype, as the experimental design does not allow this.

Body-bend frequency. Body bend analyses were performed as previously described [S8] with slight modification. Briefly, animals were picked as L4 larvae to sex-segregated holding plates the day before the assay. For on-food assays, animals were placed on a thin lawn of *E. coli* OP50; off-food assays were performed on unseeded assay plates. Locomotion was observed over the course of 3 minutes with the investigator blinded to genotype. A body bend was counted every time the section of the worm just posterior to the pharynx reached a maximum in the opposite direction of the previous

bend. Data from 7 to 12 worms per group were averaged and represented as bends per minute.

Calcium imaging

The experimental methods for calcium imaging using microfluidic devices have been described elsewhere [S9]. Briefly, strains expressing P*gpa-4*::GCaMP3 [S10] (expressed in AWA and ASI) were used. One-day old adult worms were positioned in custom-made microfluidic devices designed to accommodate either male [S11] or hermaphrodite [S12] worms, and were imaged using an Olympus BX52WI microscope with a 40x oil objective and a Hamamatsu Orca CCD camera. Image sequences were collected at 4 Hz using Volocity software (Improvision), image stacks were aligned using the ImageJ stackreg plugin using the rigid body setting [S13] to correct for minor movement artifacts and the data were analyzed using custom MATLAB scripts (The Mathworks).

Animals expressing the reporter array were preselected at the L4 larval stage and maintained overnight at 20°C. The same transgenic reporter array was considered across all genetic test conditions. Individual worms were carefully removed from the food patch and positioned in the microfluidic device and were pre-exposed to near-UV light for 1 minute prior to the assay. Animals were exposed to a 20 s pulse of diacetyl (Sigma-Aldrich), diluted 10^4-fold in S-basal buffer, beginning at the 10 s mark of the 1 min acquisition. For quantification of the GCaMP signal, the cell body of the AWA neuron was identified by position and morphology, relative to ASI, and was selected as the

region of interest (ROI), while an equivalent area of the frame was used to calculate the background signal. Data were not considered when the orientation of the worm led to the superimposition of the two cell bodies. Background-subtracted average fluorescence intensities for the ROI were normalized to baseline fluorescence, defined as the mean background-subtracted fluorescence of the ROI from frames 3-15 (pre-stimulus). In all cases, control and test animals were interleaved within an imaging session, and results were collected across a minimum of three independent sessions.

RNA isolation and Quantitative RT-PCR

One-day old adult males and hermaphrodites were collected and flash frozen. After cuticle disruption, total RNA was isolated using the RNeasy plus Mini kit (Qiagen) and samples were treated with DNase I (Invitrogen). cDNA was generated with the SuperScript III First-Strand Synthesis System (Invitrogen) using oligo(dT) according to manufacturer protocols. Quantitative RT-PCR was performed on a Bio-Rad MyiQ2 icycler with iQ SYBR Green Supermix (BioRad) using 2 μl of cDNA with reactions in triplicate. Cycling conditions were: 1 cycle of 95°C for 5 min; 45 cycles of 95°C for 30 s, 60°C for 30 s, and 72°C for 45 s, followed by melting curve analysis to verify product specificity. Standard curves were generated for each primer using 3 serial dilutions of cDNA to determine an efficiency estimate for each run. Threshold cycles (Ct) were determined by the Bio-Rad iQ5 optical system software, which were used with efficiency estimates to calculate relative *odr-10* gene expression by the Pfaffl analysis method [S14]. Two reference genes, *cdc-42* and Y45F10D.4, were used for normalization [S15]

and male *odr-10* expression was determined relative to hermaphrodite levels. A one sample t-test was performed to compare the mean of male *odr-10* expression to the hypothetical value of 1 (no change from hermaphrodite levels).

RNA interference

RNA interference was carried out using the bacterial feeding method using the pan-neural *sid-1* expression strain TU3401 [S16]. Animals were placed on control (empty vector) or RNAi plates as late L3/early L4 larvae. Behavioral assays were carried out on young adult animals.

Statistical analysis

Statistical analyses were performed using GraphPad Prism 5 and 6 (and, where noted, STATA release 11). Sample size calculations were not performed, but sample sizes used are comparable to experiments performed previously in the literature. Statistical tests employed are indicated in each figure legend and/or above. Unless otherwise noted, asterisks denote p values as follows: * $p < 0.05$, ** $p < 0.01$, *** $p < 0.001$.

SUPPLEMENTAL REFERENCES

S1. Lee, K., and Portman, D. (2007). Neural sex modifies the function of a C. elegans sensory circuit. Curr Biol *17*, 1858-1863.

S2. Mowrey, W.R., Bennett, J.R., and Portman, D.S. (2014). Distributed Effects of Biological Sex Define Sex-Typical Motor Behavior in Caenorhabditis elegans. J Neurosci *34*, 1579-1591.

S3. Sengupta, P., Colbert, H.A., and Bargmann, C.I. (1994). The C. elegans gene odr-7 encodes an olfactory-specific member of the nuclear receptor superfamily. Cell *79*, 971-980.

S4. Mello, C.C., and Fire, A. (1995). DNA transformation. In *Caenorhabditis elegans*: Modern biological analysis of an organism, H.F. Epstein and D.C. Shakes, eds. (San Diego: Academic Press).

S5. Tursun, B., Cochella, L., Carrera, I., and Hobert, O. (2009). A toolkit and robust pipeline for the generation of fosmid-based reporter genes in C. elegans. PLoS One *4*, e4625.

S6. Bargmann, C.I., Hartwieg, E., and Horvitz, H.R. (1993). Odorant-selective genes and neurons mediate olfaction in C. elegans. Cell *74*, 515-527.

S7. Lipton, J., Kleemann, G., Ghosh, R., Lints, R., and Emmons, S.W. (2004). Mate searching in Caenorhabditis elegans: a genetic model for sex drive in a simple invertebrate. J Neurosci *24*, 7427-7434.

S8. Hart, A. (2005). Behavior. WormBook.

S9. Kim, K., Sato, K., Shibuya, M., Zeiger, D.M., Butcher, R.A., Ragains, J.R., Clardy, J., Touhara, K., and Sengupta, P. (2009). Two chemoreceptors mediate developmental effects of dauer pheromone in C. elegans. Science *326*, 994-998.

S10. Tian, L., Hires, S.A., Mao, T., Huber, D., Chiappe, M.E., Chalasani, S.H., Petreanu, L., Akerboom, J., McKinney, S.A., Schreiter, E.R., et al. (2009). Imaging neural activity in worms, flies and mice with improved GCaMP calcium indicators. Nat Methods *6*, 875-881.

S11. Jang, H., Kim, K., Neal, S.J., Macosko, E., Kim, D., Butcher, R.A., Zeiger, D.M., Bargmann, C.I., and Sengupta, P. (2012). Neuromodulatory State and Sex Specify Alternative Behaviors through Antagonistic Synaptic Pathways in C. elegans. Neuron *75*, 585-592.

S12. Chalasani, S.H., Kato, S., Albrecht, D.R., Nakagawa, T., Abbott, L.F., and Bargmann, C.I. (2010). Neuropeptide feedback modifies odor-evoked dynamics in Caenorhabditis elegans olfactory neurons. Nat Neurosci *13*, 615-621.

S13. Thévenaz, P., Ruttimann, U.E., and Unser, M. (1998). A pyramid approach to subpixel registration based on intensity. IEEE Trans Image Process *7*, 27-41.

S14. Pfaffl, M.W. (2001). A new mathematical model for relative quantification in real-time RT-PCR. Nucleic Acids Res *29*, e45.

S15. Hoogewijs, D., Houthoofd, K., Matthijssens, F., Vandesompele, J., and Vanfleteren, J.R. (2008). Selection and validation of a set of reliable reference genes for quantitative sod gene expression analysis in C. elegans. BMC molecular biology *9*, 9.

S16. Calixto, A., Chelur, D., Topalidou, I., Chen, X., and Chalfie, M. (2010). Enhanced neuronal RNAi in C. elegans using SID-1. Nature methods *7*, 554-559.